TABLE DES MATIÈRES

LISTE DES FIGURES

CHAPITRE 1

CHAPITRE 2

CHAPITRE 3

CHAPITRE 4

LISTE DES TABLEAUX

CHAPITRE 1

CHAPITRE 2

CHAPITRE 4

LISTE DES ANNEXES

CHAPITRE 1

1. INTRODUCTION

1.1. PROBLÉMATIQUE GÉNÉRALE

1.1.1. FORMATION DES SULFURES MASSIFS VOLCANOGÈNES

Les gisements de type sulfures massifs volcanogènes (SMV) sont des amas massif polymétallique (Cu, Zn, Pb, Au, Ag) dont les processus de mise en place sont bien documentés (ex: Franklin et al., 1981; Herzig and Hannington, 1995; Ohmoto, 1996; Franklin et al., 2005). Ce type de minéralisation se forme en contexte sous-marin en extension. Il résulte de la circulation d'eau de mer au travers d'un empilement volcanique et/ou sédimentaire. La minéralisation est contrôlée par trois principaux facteurs : (1) un apport illimité en eau, (2) une perméabilité structurale permettant la circulation et (3) une source de chaleur sous jacente pour mettre en convection l'eau de mer. Dans le modèle classique, deux parties sont reconnues dans les gisements de SMV (Figure 1.1): 1) une partie concordante constituée de la lentille minéralisée et de ses équivalents latéraux et 2) une partie discordante représentant la zone d'alimentation de la lentille, constituée de filonnets de sulfures communément appelés la zone de *stockwork*. Deux processus de minéralisation sont reconnus pour la formation de ces gisements : 1) augmentation du volume de la lentille par croissance, effondrement, sédimentation et renouvellement de cheminées de sulfures sur le plancher océanique (Hannington et al., 2005) et/ou 2) par remplacement de séquences poreuses et perméables (Doyle and Allen, 2003). Les processus d'accumulation par exhalation sont marginaux dans la croissance des édifices

(Rona, 1984). Ils possèdent cependant une importance de premier ordre pour l'exploration puisqu'ils représentent l'équivalent latéral syngénétique du monticule de sulfures. Appelés exhalites, ces horizons marquent un hiatus dans le volcanisme. Le mélange entre l'eau de mer et les fluides hydrothermaux émis par les évents engendre la précipitation d'un panache de particules siliceuses et métalliques qui couvrent communément une surface importante. Ce nuage va inévitablement conduire à une anomalie géochimique dans les sédiments du plancher océanique. Ainsi, de par le lien étroit (temporel et spatial) entre ces unités et les lentilles minéralisées, ils représentent des niveaux particulièrement intéressants pour comprendre l'évolution des systèmes hydrothermaux, mais aussi pour l'exploration des SMV. Ils sont d'ailleurs largement étudiés depuis près de quarante ans (ex: Ridler, 1971).

1.1.2. LES TUFFITES: ÉQUIVALENTS LATERAUX DES MINERALISATIONS

À ce jour, il n'existe pas réellement de classification pour définir les équivalents latéraux aux lentilles SMV. Aussi, « Exhalites tuffacées » (Kalogeropoulos and Scott, 1989), « sédiments métallifères » (Hrischeva and Scott, 2007), « cherts » (Leistel et al., 1997), « tuffites » (Liaghat and MacLean, 1992), et « formation de fer » (Peter and Goodfellow, 1996) sont autant de termes utilisés dans la littérature pour définir des niveaux lités, spatialement et temporellement associés

aux minéralisations volcanogènes. Cette vaste terminologie s'explique par la grande variabilité de leurs aspects et de leurs compositions. « Tuffites » est le qualificatif le plus employé pour décrire ces unités dans le camp de Matagami et c'est donc celui qui sera employé au fil de la thèse.

Kalogeropoulos and Scott (1983) proposent deux composantes pour former les tuffites (Figure 1.2a): 1) une composante chimique issue de la précipitation de fluides hydrothermaux (exhalite au sens strict), et 2) l'autre clastique, résultant du dépôt de particules volcaniques (cendres, lapillis, blocs). Ces deux pôles impliquent un hiatus du volcanisme qui assure un système hydrothermal efficace. Lors de la reprise de l'activité volcanique, une nouvelle coulée peut sceller l'évent hydrothermal. Cependant, le système ne meurt pas nécessairement, et peut même reprendre de la vigueur si la fracture synvolcanique nourricière est réactivée et se poursuit dans les unités sus-jacentes (télescopage). Ces fluides « tardifs » peuvent donc migrer latéralement dans la tuffite et modifier sa composition de manière significative. La présente étude tient compte de ce processus en ajoutant un troisième pôle à cette classification (Figure 1.2b). Ce nouveau pôle représente les processus d'altération hydrothermale postérieure à la formation des tuffites.

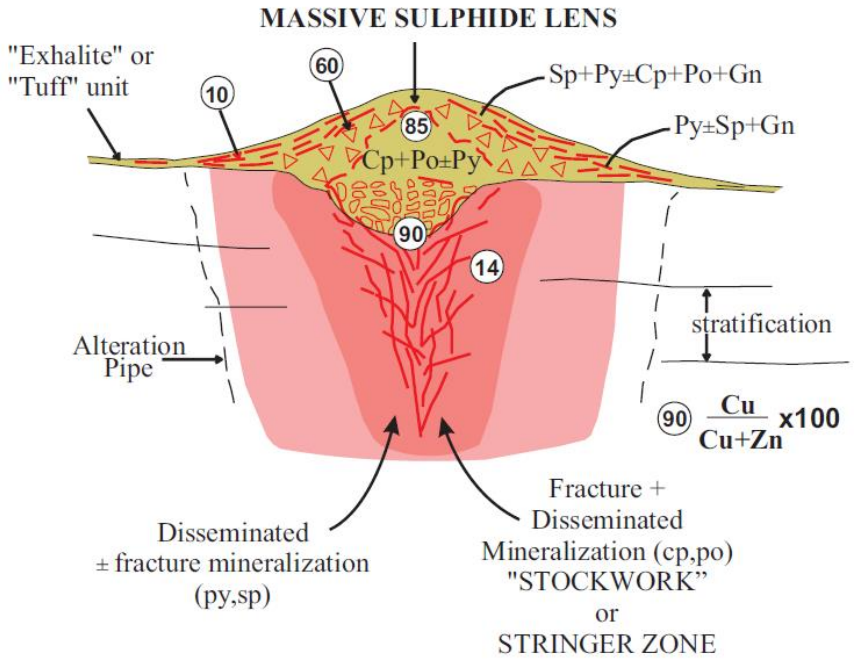

Figure 1.1: Géométrie et minéralogie classique d'un système SMV (Gibson and Kerr, 1993).

Les exemples de tuffites associées à des SMV sont nombreux. Dans cette section, 4 exemples sont présentés puis brièvement comparés : 1) le *Main Contact* en Abitibi (Québec), 2) le *Brunswick Horizon* dans le district de Bathurst (Nouveau Brunswick), 3) les cherts de la *Pyrite Belt* en Espagne et 4) le *Tetsusekiei* dans le district de Hokuroku (Japon). Ces horizons ont été choisis: 1) pour leur degré de connaissance, 2) leur répartition géographique mondiale (Figure 1.3), 3) leur association avec des minéralisations volcanogènes d'importances et 4) leur étendue dans l'échelle des temps géologiques (Archéen à Miocène).

Le Tableau 1.1 résume les caractéristiques générales de chacun des horizons, leur lien avec les minéralisations et les outils testés pour l'exploration.

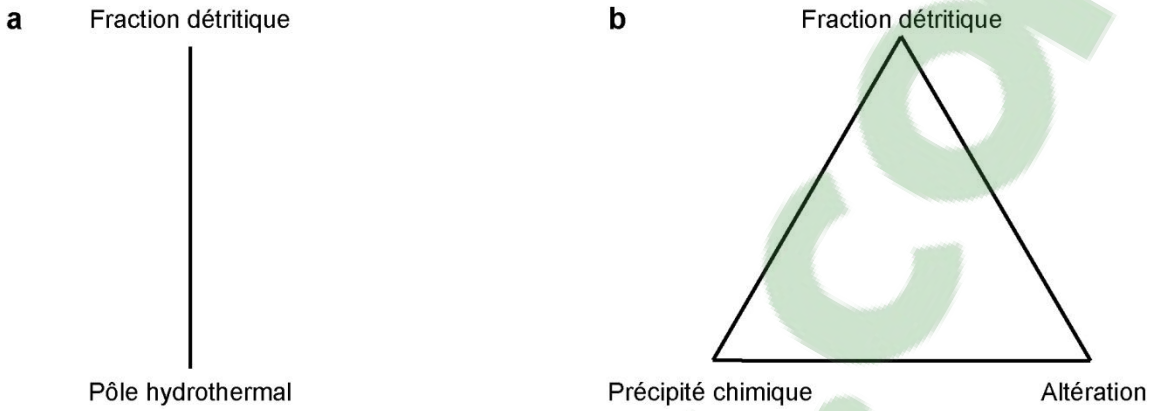

Figure 1.2: a) Classification des tuffites proposée par Kalogeropoulos et al. (1983). b) Nouvelle vision proposée pour la classification des tuffites avec l'ajout du pôle d'altération épigénétique.

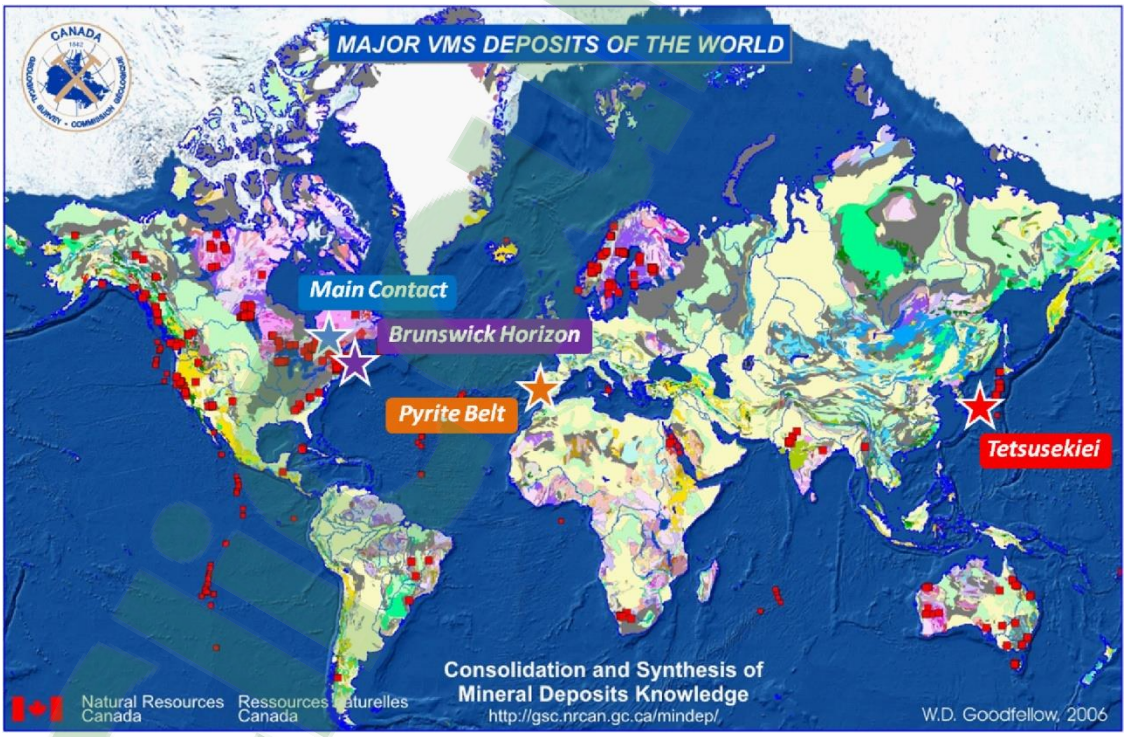

Figure 1.3: Carte de répartition des SMV dans le monde et des quatre horizons discutés dans cette étude. Modifiée de Galley et al. (2007).

Horizons - gisements		***Main Contact - Mine Millenbach***	***Brunswick Horizon - Heath Steel***	***Cherts - Pyrite belt***	***Tetsusekiei - Mine Fukazawa***
Âge		Archéen (2703 ± 3 Ma)	Ordovicien (~ 470 Ma)	Dévonien à Carbonifère (400 à 300 Ma)	Miocene (13 Ma)
District et Pays		Noranda (Canada): 125 Mt	Bathurst (Canada): 495 Mt	Espagne: 1575 Mt	Hokuroku (Japon): 80 Mt
Interface		Rhyolite-Andésite	Métasédiments-QFP	Volcano-sédiments	Dacite-tuf basaltique
Minéralisation		6 lentilles	5 lentilles	> 10 gisements	10 lentilles
Épaisseur		0 à 2 m – 60 cm en moyenne	3-4 m proximal 1-2 m distal	~ 10 cm	< 30 cm
Étendue		Étendu (>1.5 km) et discontinue	Continue > 12 km	Discontinue	Faible (~500 m) et discontinue
Minéraux		Qtz, ser, chl, py, po, sph, cpy	Qtz, mt, sid, chl, stil, po, py	Qtz, hem, mt, chl, carb	Qtz, hem, py, sph, chl, ser, rut,
Lien avec la minéralisation		syngénétique	syngénétique	**Épigénétique**	syngénétique
Outils pour l'exploration	Positif	Roche totale: Fe/[Fe+Mg] Minéraux: Fe/[Fe+Mg] dans chlorites Disparition Ilménite/apparition Rutile ou Sphène	variation d'épaisseur Roche totale: Fe/Mn; S; Fe/Ti; REE; *Eu et *Ce; Pb, Zn, Ag… Minéraux: Fe/Fe+Mg dans les chlorites Pyrites, Carbonates, Grenats...	~	Roche totale: Co, Ba R=___(K$_2$O+MgO) x 100__ K$_2$O+Na$_2$O+MgO+ CaO $\delta^{18}O$
	Négatif	Roche totale: REE Minéraux: Co/Ni dans pyrites	~	Roche totale: REE	Roche totale: REE
Références		Kalogeropoulos and Scott (1989); Pearson and Daigneault (2009)	Peter and Goodfellow (1996); Peter and Goodfellow (2003); Peter et al. (2003a); Peter et al. (2003b)	Barriga and Oliveira (1986); Leistel et al. (1997)	Kalogeropoulos and Scott (1983); Kalogeropoulos (1985)

Tableau 1.1: Comparaison de quatre niveaux de tuffites.

La classification des quatre tuffites dans le diagramme ternaire proposé par le projet est illustrée à la figure 1.4. L'approche utilisée repose sur la source des minéraux (Kalogeropoulos and Scott, 1983). Les études minéralogiques (Kalogeropoulos and Scott, 1983, 1989; Peter et al., 2003b) démontrent que le litage des tuffites est marqué par une alternance d'aluminosilicates, de quartz et de sulfures. Selon ces mêmes auteurs, les aluminosilicates (ex: chlorite, séricite) sont d'origine détritique alors que les sulfures et une partie du quartz, sous forme de cherts, sont d'origine chimique. Dans la vision proposée, il faut différencier ici le précipité chimique de la composante altération hydrothermale. En d'autres termes, une partie du quartz et des sulfures peut être d'origine primaire et une autre partie peut être due à des processus d'altération et de remplissage. Si le pourcentage de chaque minéral est associé avec son pôle source, le *Main Contact* se retrouve sur une ligne à mi chemin entre le pôle « détritique » et « précipité chimique », se dirigeant vers le pôle « altération ». En effet, l'importance du pôle « altération » n'est pas connue puisqu'aucune étude n'a été réalisée jusqu'à présent. Mais il est fort probable qu'une partie de la pyrite et de la chlorite soit modifiée par le métamorphisme. La même approche est utilisée pour le *Tetsusekiei*. Kalogeropoulos and Scott (1989) démontrent que la composante chimique est mieux représentée pour cet horizon que pour le *Main Contact*. En ce qui concerne le *Brunswick Horizon*, il évolue latéralement d'un faciès de formation de fer proximal à un faciès de tuf à chlorite distal. Le faciès

de formation de fer se retrouve près du pôle « précipité chimique » alors que le faciès distal de tuf à chlorite se rapproche du pôle « détritique ». Le pôle « altération » n'est pas très bien contraint, mais il est démontré que la formation de la magnétite, la pyrite et la chlorite est en partie issue de fluides tardifs probablement d'origine métamorphique (Peter et al., 2003b).

Les cherts de la *Pyrite Belt* se retrouvent proches du pôle « altération » (figure 1.4). Ces horizons étaient historiquement documentés comme syngénétiques des minéralisations SMV de l'Espagne (Barriga and Oliveira, 1986). Néanmoins, Leistel et al. (1997) ont démontré que la signature en isotope du plomb des cherts est significativement plus radiogénique que celle des sulfures massifs auxquels ils sont associés. Cet enrichissement des cherts implique qu'une source différente a participé au processus de précipitation (sediments, eau de mer…) et suggère que les cherts de la *Pyrite Belt* sont épigénétiques. Ils résultent de phénomènes d'altération à basses températures dans des séquences tuffacées. Un phénomène similaire est documenté pour expliquer la genèse des formations de fer dans le Groupe de Hunter Mine, en Abitibi (Chown et al., 2000). Il apparait donc primordial de comprendre le lien entre les tuffites et les minéralisations si des outils efficaces pour l'exploration veulent être développés. Dans le cas des cherts de la *Pyrite Belt*, aucun vecteur n'a pu être établi jusqu'à présent en raison du caractère épigénétique de ces unités.

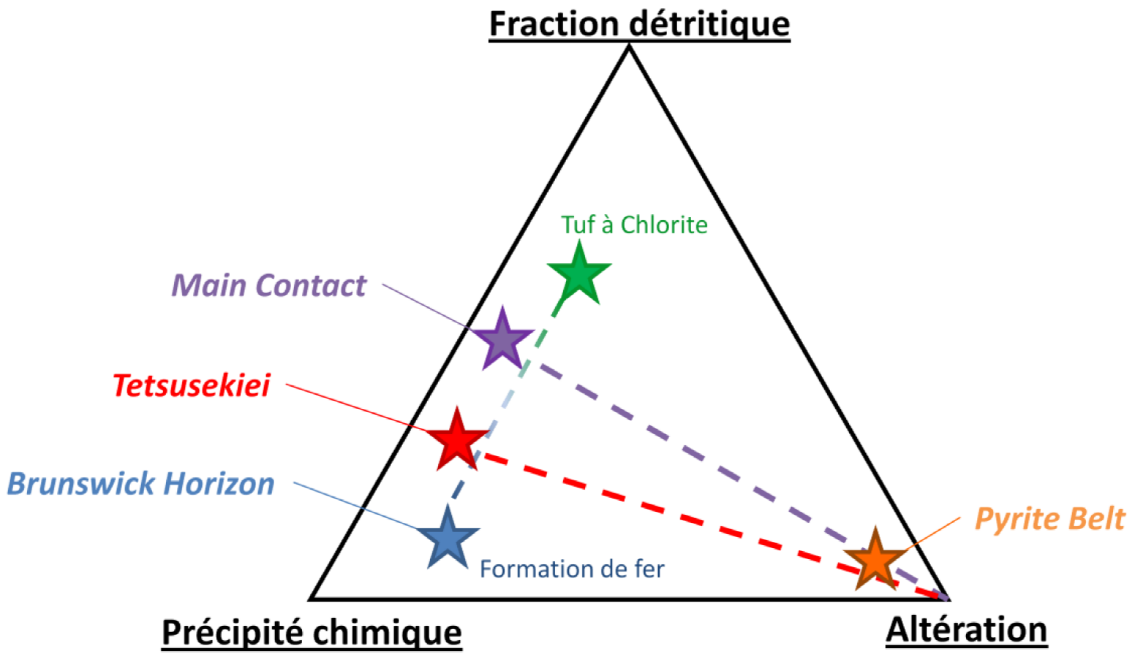

Figure 1.4: Classification des 4 niveaux de tuffites comparées. La position de ces horizons dans le diagramme ternaire repose sur la quantité et la source des minéraux présents.

1.1.3. DES OUTILS POUR L'EXPLORATION

1.1.3.1. CHIMIE DES ÉLÉMENTS MAJEURS ET MÉTAUX

L'approche la plus simple vise à regarder la chimie globale des tuffites et chercher des variations de compositions en éléments majeurs ou traces en fonction de la proximité des minéralisations. Cette méthode a fonctionné pour le *Main Contact* où Kalogeropoulos et Scott (1989) enregistrent une diminution du rapport Fe/[Fe+Mg] à proximité de la mine Millenbach (Figure 1.5). Dans le cas du *Tetsusekiei*, Kalogeropoulos and Scott (1983) et Kalogeropoulos (1985) ont observé une augmentation du Co et du Ba à proximité des 10 lentilles de la mine Fukazawa. Parallèlement, ils ont développé un indice d'altération R basé sur les éléments majeurs (Figure 1.6): $\mathrm{R} = \frac{(\mathrm{K_2O+MgO)\ x\ 100}}{\mathrm{K_2O+Na_2O+MgO+CaO}}$

1.1.3.2. CHIMIE DES ÉLÉMENTS DES TERRES RARES

La chimie des terres rares et des éléments traces, beaucoup plus fine, permet d'aller plus loin dans le développement d'outils pour l'exploration. Cette méthode n'a pas donné de résultats encourageants ni pour *le Main Contact* (Kalogeropoulos and Scott, 1989), ni pour le *Tetsusekiei* (Kalogeropoulos and Scott, 1983). Ces résultats négatifs pourraient être attribuables à l'approche utilisée puisque les variations spatiales n'ont pas été testées.

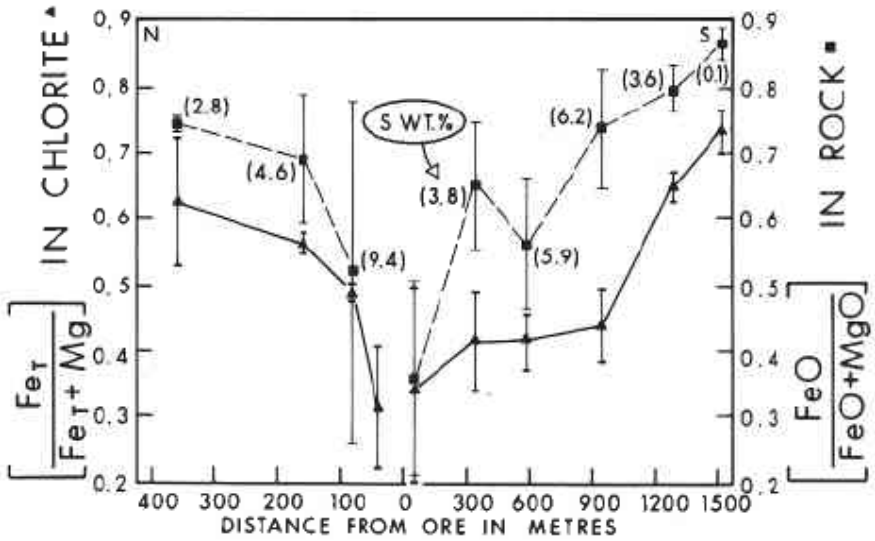

Figure 1.5: Variation du rapport Fe/[Fe+Mg] dans les chlorites et roche totale du *Main Contact* en fonction de la distance avec les zones minéralisées. Kalogeropoulos et Scott (1989).

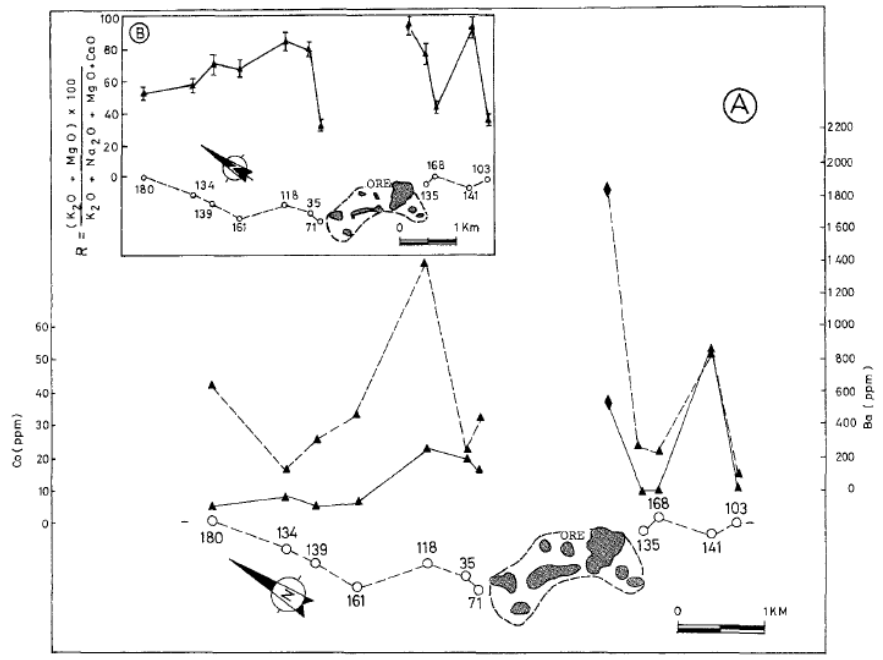

Figure 1.6: Variation du Co, du Ba et de l'indice d'altération R (en ordonné) dans le *Tetsusekiei* en fonction de l'éloignement des lentilles de la mine Fukazawa (en abscisse). Kalogeropoulos (1985).

Cependant, les connaissances sur la chimie des fluides hydrothermaux et les méthodes analytiques ont beaucoup progressées depuis. Les analyses de terres rares conduites sur le *Brunswick Horizon* démontrent des résultats particulièrement significatifs et identifient des vecteurs précis pour l'exploration (Peter et al., 2003a). Plus précisément, une forte anomalie positive en Europium (Eu) est détectée à proximité des gisements (Figure 1.7). Celle-ci caractérise la forte composante hydrothermale des tuffites à proximité des évents. Les éléments traces sont reconnus pour leur caractère immobile face aux altérations hydrothermales de type SMV (MacLean and Kranidiotis, 1987; MacLean, 1988). Néanmoins, pour comprendre cette anomalie, il faut s'attarder au comportement de cet élément et considérer sa source. L'Eu représente un cas particulier puisqu'il possède deux valences: Eu^{2+} et Eu^{3+}. L'Eu^{2+} est soluble dans les fluides réducteurs de haute température et peut donc être transporté (Sverjensky, 1984). Les plagioclases sont les grands réservoirs d'Eu, mais ils sont aussi des minéraux réactifs aux fluides de haute température. Ainsi, l'altération d'une séquence volcanique va entrainer la destruction des plagioclases et la libération d'Eu dans les fluides hydrothermaux. Cet enrichissement en Eu hydrothermal va laisser sa trace dans les produits issus de la précipitation (probablement des minéraux calciques), contenus dans les tuffites (Michard and Albarède, 1986; Douville et al., 1999; Grenne and Slack, 2005).

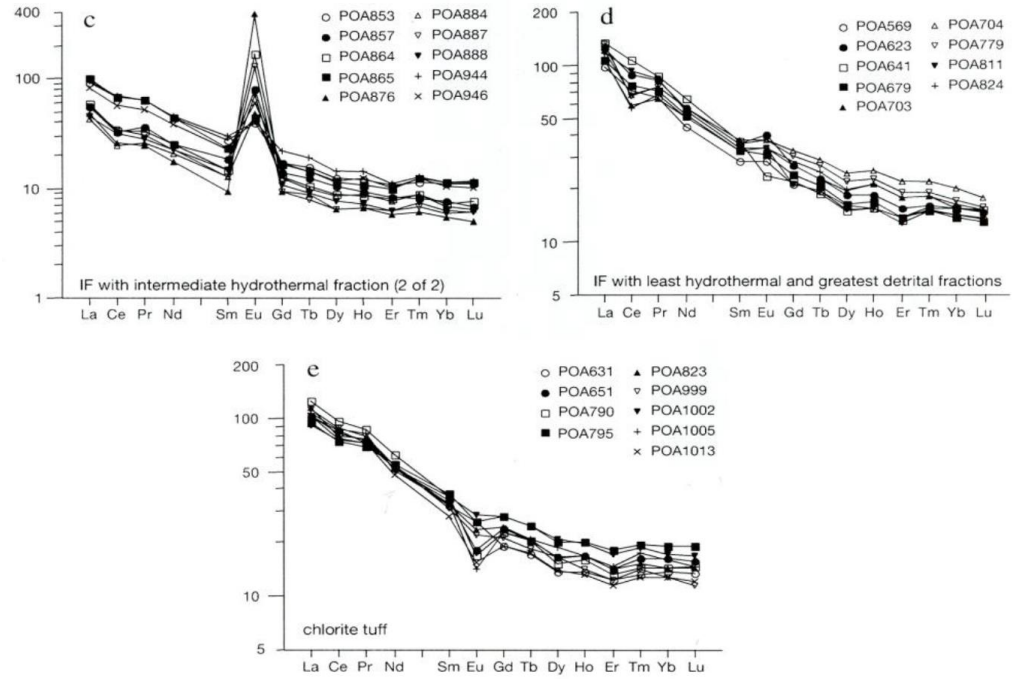

Figure 1.7 : Diagrammes de terres rares, normalisés aux chondrites (Rock, 1988) correspondants aux différents faciès du *Brunswick Horizon*. Modifiés de Peter et al., (2003a).

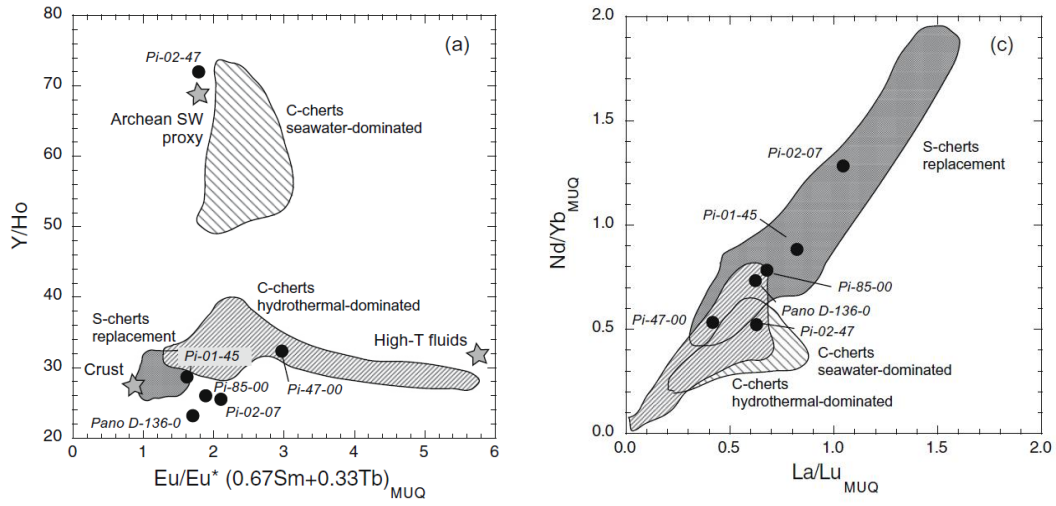

Figure 1.8 : Diagrammes binaires isolant les S-cherts et les C-cherts sur la base des éléments des terres rares. Normalisation par rapport au MUQ (Mud of Queensland, Kamber et al. (2005). Modifiés de Pinti et al. (2009).

Par ailleurs, une approche combinée isotopique, pétrographique et chimique (van den Boorn et al., 2007; Pinti et al., 2009) a permis de mettre en évidence 3 types de cherts: 1) silicification de débris volcaniques (S-cherts), 2) cherts issus de précipitation chimique (C-cherts) avec un fluide hydrothermal siliceux dominant ou 3) avec l'eau de mer dominante. Ces cherts possèdent des signatures en ETR et éléments traces qui leurs sont propres. Généralement les cherts issus de processus de remplacement sont plus riches en ETR ayant hérité de la signature en ETR de la roche originale. La figure 1.8 illustre un exemple permettant de discriminer les cherts formés par remplacement, des cherts issus d'un précipité chimique. Les possibilités de développer des outils pour l'exploration à partir de ces éléments sont considérables.

1.1.3.3. CHIMIE MINÉRALE DES PYRITES

Les analyses minéralogiques permettent de limiter la variabilité induite par les trois composantes lorsque l'origine des minéraux est connue. Un minéral sera considéré intéressant s'il présente une répartition spatiale étendue et s'il est génétiquement lié à l'hydrothermalisme. Des analyses sur minéraux ont été conduites sur la plupart de ces tuffites.

La pyrite est un minéral particulièrement étudié puisqu'il est généralement omniprésent dans les systèmes hydrothermaux et elle peut donc être utilisée pour comparer les compositions de fluides et les conditions physicochimiques de

formation, à condition que les effets de la recrystallisation métamorphique soient pris en compte. Les variations d'éléments, en particulier Ni, Co, Se, au sein des pyrites sont étudiées depuis la fin des années 1960 (Loftus-Hills and Solomon, 1967). Les analyses conduites sur les pyrites du *Main Contact* et du *Tetsusekiei* (Kalogeropoulos and Scott, 1983, 1989) ont été réalisées à la microsonde et les limites de détections sont trop hautes pour détecter les variations subtiles des éléments traces. Cependant, plusieurs études récentes démontrent un très fort potentiel pour l'exploration (ex: Large et al., 2007; Maslennikov et al., 2009) grâce à l'utilisation du LA-ICP-MS (*Laser Ablation – Inductively Coupled Plasma- Mass Spectrometry*) qui abaisse considérablement les limites de détection, permettant ainsi de réaliser de meilleures études sur la concentration, mais aussi la dristribution des éléments traces dans les minéraux. Due à l'évolution significative des limites de détections, les comparaisons avec d'anciennes données de chimie minérale sont limitées.

1.1.4. RELATIONS GENETIQUES DES TUFFITES

Le *Brunswick Horizon* se détache clairement des quatre exemples présentés puisque tous les outils testés ont fonctionné et ont conduit à la découverte de vecteurs vers les minéralisations (Figure 1.9). Ceci traduit inévitablement un synchronisme entre la mise en place de la minéralisation et celle de l'horizon. Par ailleurs, la composante de précipité chimique est probablement dominante dans

l'horizon et donc faiblement diluée par la fraction détritique, ce qui assure un signal hydrothermal fort. D'autre part, cet horizon est le seul qui est caractérisé par un épaississement (3-4 m) près des lentilles (Tableau 1.1) démontrant ainsi le lien génétique avec les évents hydrothermaux. Les autres tuffites sont des niveaux beaucoup plus fins (<2 m) et discontinus.

En ce qui concerne les cherts de la *Pyrite Belt*, ils mettent en perspective la problématique des horizons associés aux SMV. En effet, malgré le lien spatial entre les tuffites et les minéralisations, il n'existe pas toujours de lien génétique (Leistel et al. 1997). Il s'avère primordial de comprendre ce lien si des outils efficaces vers les SMV veulent être développés. Déchiffrer la source des tuffites est un défi de taille mais tout aussi important. Plus précisément, la proportion de chaque composante doit être établie afin d'isoler les composantes spécifiques dans le but de rehausser et de dégager le signal géochimique hydrothermal associé aux minéralisations. Il est démontré, par les exemples utilisés dans cette étude, que l'approche utilisée sera différente en fonction de la quantité de précipité chimique. Si la fraction chimique est dominante, des analyses de roches totales devraient permettre d'établir des vecteurs vers les minéralisations (ex: *Brunswick Horizon, Tetsusekiei*) alors que si c'est la fraction détritique qui domine, elle va diluer le signal et il devient alors plus approprié de travailler sur des minéraux dont l'origine est hydrothermale (ex: *Main Contact*).

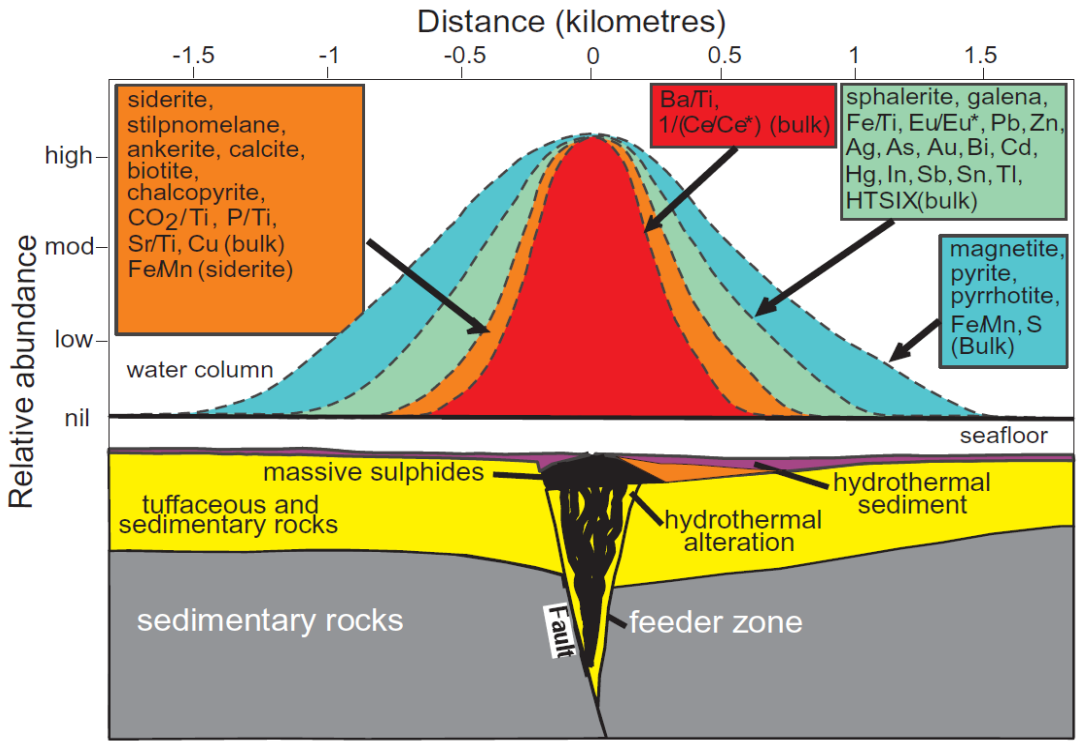

Figure 1.9: Diagramme schématique illustrant les halos géochimiques du *Brunswick Horizon* autour des lentilles minéralisées dans le camp de Bathurst. Peter et Goodfellow (2003).

1.2. PROBLÉMATIQUE SPÉCIFIQUE: LE CAS DE MATAGAMI

1.2.1. GÉOLOGIE RÉGIONALE

Avec plus de 80 gisements de SMV, la Sous-province d'Abitibi représente l'une des plus prolifiques ceintures de roches vertes au monde en ce qui concerne les minéralisations volcanogènes classiques (Card, 1990; Allen and Weihed, 2002) et celles aurifères (Mercier-Langevin et al., 2011; Mercier-Langevin et al., 2014). Elle est constituée de ségments volcano-sédimentaires linéaires, d'orientation est-ouest, perforées par des plutons synvolcaniques à post-tectoniques (Figure 1.10). Globalement, l'Abitibi est interprétée comme le résultat d'accrétion de terrains volcaniques différents, formés en contexte de supra-subduction, et datés entre 2735 Ma pour le volcanisme, et 2670 Ma pour le plutonisme post tectonique (Mueller et al., 1996; Daigneault et al., 2004; Mueller et al., 2009). La ceinture de l'Abitibi est divisée en deux zones, la Zone Volcanique Nord (ZVN) et la Zone Volcanique Sud (ZVS) (Chown et al., 1992). Ces zones sont séparées par deux grands couloirs de déformation, eux aussi d'orientation Est-Ouest : la faille de Porcupine-Destor-Manneville qui sépare les ZVN et ZVS, et la faille de Cadillac-Larder Lake qui constitue la bordure sud de la ZVS. Le camp de Matagami est situé dans le Nord de la ZVN.

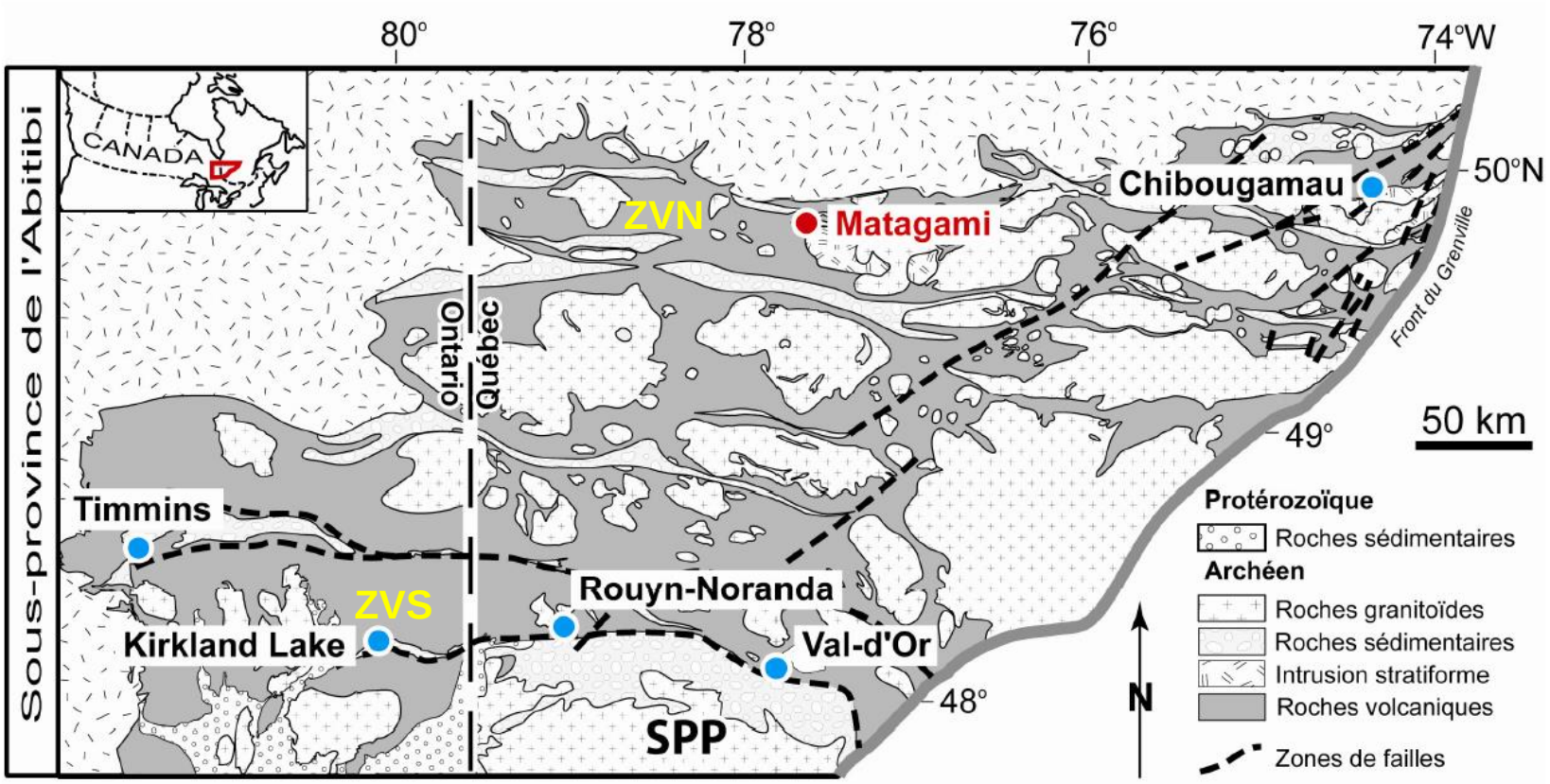

Figure 1.10: Position du camp de Matagami dans l'Abitibi. Modifiée de Mueller et Donaldson (1992).

1.2.2. GÉOLOGIE DU CAMP DE MATAGAMI

Plus de 50 Mt de minerai ont été extraites dans le camp de Matagami depuis le début des années 1960, ce qui en fait l'un des plus importants districts de SMV de l'Abitibi. Il a fait l'objet de nombreuses études (Jenney, 1961; Sharpe, 1968; Roberts, 1975; Beaudry and Gaucher, 1986; Piché et al., 1990; Pilote et al. 2011). Cependant, sa compréhension est encore très limitée en partie due à la faible proportion de roches affleurantes. Les gisements de Matagami sont réputés pour leurs teneurs en zinc particulièrement élevées. Avec des teneurs en zinc de 9% en moyenne, mais pouvant atteindre ~20% (ex: Isle Dieu: Lavallière et al., 1994), les minéralisations de Matagami sont parmi les plus riches au monde. Vingt dépôts sont connus à ce jour. La moitié d'entre eux est économique et a été exploitée. Ces gisements sont pour la plupart associés à la « Tuffite Clé » (*Key Tuffite* - KT; Miller, 1960). Ils sont répartis sur trois bandes felsiques : le « Flanc Sud », le « Flanc Nord » et le « Camp Ouest » (Figure 1.11). Au début du projet doctoral, une seule mine était en exploitation (2008-2013) dans le camp de Matagami. Il s'agit de la mine Persévérance dans le Nord du « Flanc Sud ». Cependant, deux nouveaux dépôts: Bracemac et McLeod ont été découvert (Adair, 2009) et sont entrés en production en 2013. Les deux flancs sont liés entre eux par l'anticlinal de Galinée. Le lien entre le « Camp Ouest » et les deux autres bandes felsiques, quant à lui, demeure obscur. La séquence stratigraphique générale du camp de Matagami (Figure 12) proposée par Sharpe (1968), et

validée par Piché et al. (1990) est divisée en deux groupes: le Groupe de Watson et le Groupe de Wabassee. La Tuffite Clé et la plupart des zones minéralisées connues sont à l'interface de ces deux groupes. Le Groupe de Watson comprend deux sous-unités felsiques datées entre 2726,3 et 2722,4 Ma (Mortensen, 1993) : 1) une unité de dacite de 500 m d'épaisseur à la base et 2) une unité de rhyolite de près de 1500 m au sommet. Géochimiquement, selon la classification de Lesher et al. (1986) et Hart et al. (2004), ces rhyolites sont de type FIIIb (Gaboury and Pearson, 2008) et donc considérées comme particulièrement fertiles pour les minéralisations de type SMV. Le Groupe de Wabassee est essentiellement constitué de laves mafiques sur près de 3000m. Un horizon de rhyodacite, appelé « Rhyolite de Dumagami », est cependant présent dans la partie nord et la partie centrale du Flanc Sud. Ces deux groupes sont recoupés par le Complexe de la Rivière Bell (CRB), une intrusion litée de gabbro-anorthosite datée à 2724,6 Ma (Mortensen, 1993). Cette intrusion est interprétée comme étant la source thermique à l'origine des SMV (Piché et al., 1990; Maier et al., 1996; Ioannou and Spooner, 2007; Carr et al., 2008). Le métaphormisme régional est généralement de niveau schiste vert, ce qui a pu entraîner un remplacement et une recrystallisation partielle des paragenèses originales.

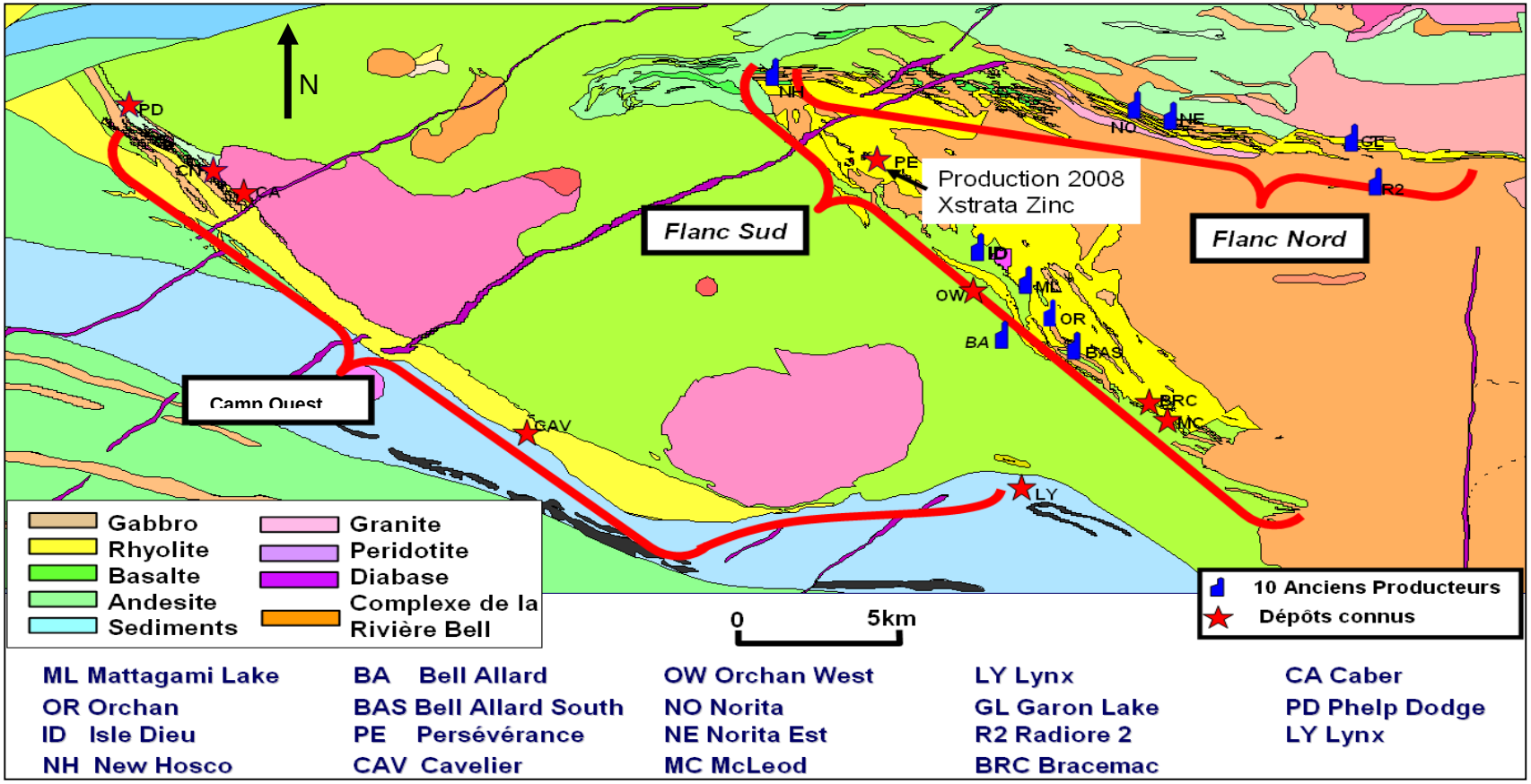

Figure 1.11: Carte géologique de la région de Matagami. Roy et Allard (2006).

1.2.3. LA TUFFITE CLÉ

La Tuffite Clé (KT) est reconnue pour être l'une des unités exhalatives les plus épaisses (0,3 à 6m), continues et étendues (>10km) en association avec des minéralisations de type SMV au Canada. Elle est le principal métallotecte utilisé pour l'exploration des SMV dans le camp de Matagami. Malgré l'importance de cet horizon et en dépit des nombreuses études réalisés sur cette unité (Sharpe, 1968; Roberts, 1975; Davidson, 1977; Costa et al., 1983; Liaghat and MacLean, 1992), le lien génétique avec les minéralisations demeure flou et les tentatives pour établir des outils géochimiques pour guider l'exploration des VMS ont été peu concluantes. Ce problème est attribuable principalement à la nature complexe de l'unité. La Tuffite Clé est une unité laminée dont la composition minérale normative a proximité du gisement de Bell Allard Sud a été estimée à: 33% de quartz, 28% de sulfures, 16% de séricite, 8% de carbonates, 6% de chlorite et 9% d'autres minéraux (Liaghat and MacLean, 1992). Selon les études antérieures, elle serait le résultat de 2 composantes principales, dont les proportions seraient variables: 1) une fraction tuffacée d'origine détritique, et 2) une composante chimique. Liaghat and MacLean (1992) ont proposé que la composante détritique résulte d'un mélange de cendres andésitiques calco-alcalines et de cendres rhyolitiques tholéitiques. Le pôle chimique s'exprime selon Davidson (1977) par la silicification, les sulfures, et les carbonates.

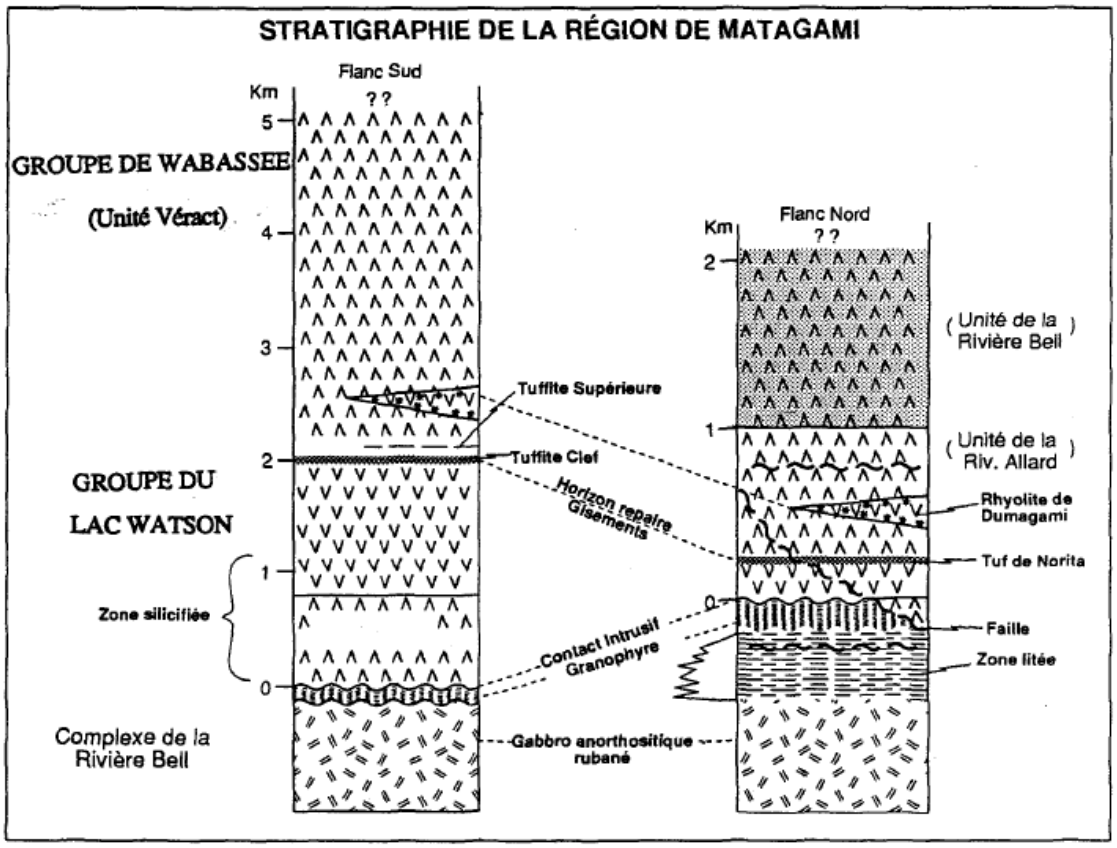

Figure 1.12: Stratigraphie générale des flancs Sud et Nord du camp de Matagami. Piché (1990).

La tuffite clé possède régionalement un bruit de fond en métaux important: 1,4% Zn, 0,1% Cu et des teneurs anomaliques en Pb, Co, Ni et Cr qui semblent s'enrichir à proximité des dépôts de même que la quantité de chert (Davidson, 1977). Ces variations sont cependant restreintes et spatialement hétérogènes.

L'hypothèse de ce projet vise à scinder le pôle chimique en deux composantes: 1) la composante précipitée et 2) la composante d'altération hydrothermale. Le pôle précipité chimique est issu des fumerolles et correspond donc à la précipitation sur le plancher océanique d'un panache métallifère et siliceux plurikilométrique. La composante d'altération hydrothermale est spatialement associée aux gisements de SMV et elle représente les processus de modification (au niveau ou sous le planché océanique) postérieur au dépôt de la Tuffite Clé. Elle correspond à la migration latérale de fluides le long de la tuffite après sa mise en place et son recouvrement par le Groupe de Wabassee. C'est cette signature qui sera ciblée ici pour dégager un meilleur signal, car elle est considérée comme découlant directement des systèmes hydrothermaux à l'origine des SMV.

L'épaisseur, la continuité et l'extension latérale de cette unité sont clairement des paramètres problématiques de la Tuffite Clé, puisqu'ils sont de loin supérieurs à ceux des autres tuffites reconnues dans le monde (Tableau 1.1). Ils tendent à suggérer un pôle détritique particulièrement dominant dans la

composition de cette unité. Cette hypothèse est soutenue par les nombreuses observations de structures sédimentaires reconnues (Davidson, 1977). L'implication directe est une dilution du pôle « précipité chimique » rendant l'utilisation de la lithogéochimie en roche totale plus difficilement utilisable et le développement d'outils pour l'exploration plus difficile. Cependant, les analyses monominéraliques prennent toutes leurs importances ici, dans le cas où des minéraux d'origine hydrothermale peuvent être identifiés et étudiés.

En résumé, la problématique concernant la Tuffite Clé de Matagami est comparable à celle de tout autre tuffite. On cherche dans un premier temps à comprendre le lien entre la Tuffite Clé et les minéralisations spatialement associées. Une fois ce lien établie, les composantes de la Tuffite Clé peuvent être décortiquées afin d'isoler le pôle hydrothermal et étudier l'évolution du système. Si le pôle hydrothermal est suffisamment présent et préservé, des outils géochimiques pour l'exploration pourront être développés. Plusieurs hypothèses de travail peuvent être proposées pour aborder le problème. Est-ce que la Tuffite Clé a enregistrée intégralement l'évolution des SMV par la précipitation de minéraux sur le planché océanique? Les minéralisations du camp de Matagami sont-elles vraiment syngénétiques? Si oui, la composante de « précipité chimique » est-elle suffisamment préservée dans l'unité pour être étudiée? A l'opposé, si les minéralisations sont épigénétiques, résultant de processus de remplacement au travers d'une unité perméables, c'est le pôle « altération » qui

retiendra l'attention. Dans ce cas, la composante altération sera-t-elle suffisante pour établir des vecteurs efficaces pour l'exploration?

1.3. OBJECTIFS

Ce projet est bâti autour de deux buts principaux: 1) étudier l'évolution d'un système hydrothermal de type SMV et 2) développer des outils géochimiques qui traduisent efficacement la signature hydrothermale des tuffites et qui permettront de guider l'exploration pour les SMV dans le camp de Matagami et ailleurs dans le monde. Afin d'atteindre ces buts, 4 objectifs ont été définis :

- Comprendre l'environnement de dépôt.
- Établir le lien entre les tuffites et les minéralisations.
- Caractériser les différentes composantes des tuffites :
    - Détritique;
    - Précipité chimique;
    - Altération.
- Développer et tester des outils pour l'exploration
    - Analyses de roche-totale/bilans de masse;
    - Analyses pyrites.

Pour atteindre ces objectifs, deux secteurs ont été travaillés en détail soit les gisements accessibles sur le flanc Sud: Bracemac-McLeod et Persévérance. Des données et des échantillons à l'échelle du camp ont aussi été recueillis, traités et intégrés dans la présente étude.

1.4. MÉTHODOLOGIE

Dans cette section, l'approche méthodologique utilisée pour accomplir tous les objectifs fixés précédemment est détaillée (Tableau 1.2).

Objectif Principal	**Objectifs spécifiques**		**Méthodes**	**Appareillage**
Développement de nouveaux outils géochimiques pour guider l'exploration des SMV le long des tuffites de Matagami	Compréhension de l'environnement de dépôt		Compilation des données des gisements	Banque de données des compagnies
			Cartographie détaillée - Echantillonnage de forages	Terrain
			Analyses pétrographiques et minéralogiques	Microscopie optique (UQAC)
			Analyses lithogéochimiques	ICP-AES et ICP-MS (INRS)
	Lien entre les tuffites et les minéralisations		Compilation des données des gisements	Banque de données des compagnies
			Interprétation des relations de recoupements	Terrain
			Comparaison des paragenèses	Microscopie optique (UQAC)
			Comparaison des signatures des pyrites dans KT et dans SMV	LA-ICP-MS (UQAC)
	Caractérisation des différentes composantes des tuffites		Détermination des paragenèses de chaque composante	Observation macroscopique et microscopique
	Détritique		Pôle détritique	ICP-AES et ICP-MS (INRS)
			Pôle hydrothermal	Roche totale: ICP-MS (INRS); Zones silicifiées versus cherts: LA-ICP-MS (UQAC); Pyrites: LA-ICP-MS (UQAC)
	Précipité Chimique		Pôle altération	
	Altération			
	Les outils	Visuel	Description détaillée de forages	Terrain
		Géochimique	Analyses roche totale / Bilan de masse	ICP-AES et ICP-MS (INRS)
			Analyses monominéraliques	Pyrites: LA-ICP-MS (UQAC)

Tableau 1.2: Objectifs versus méthodologie et appareillage.

De plus, des informations supplémentaires concernant les procédures analytiques sont fournis dans les chapitres subséquents. L'ensemble de cette méthodologie vise à développer de nouveaux outils pour l'exploration et repose donc sur plusieurs nouvelles techniques analytiques. La méthodologie employée est donc diversifiée. Les travaux sont divisés en deux parties : les travaux de terrain, et les travaux de laboratoire.

1.4.1. TRAVAUX DE TERRAIN ET ÉCHANTILLONNAGE

Les travaux de terrain ont été relativement limités puisqu'il n'y a que très peu d'affleurements. Un affleurement de Tuffite Clé a cependant été découvert au cours du projet. L'affleurement a été décapé et cartographié en détail à l'aide d'un DGPS pour obtenir le maximum d'informations et est présenté en Annexe 1. Les meilleures observations de Tuffite Clé sont réalisées de manière souterraine. Plusieurs visites de Persévérance ont permis de décrire et d'échantillonner la tuffite et observer le lien avec les roches encaissantes et la minéralisation. Le reste des observations a été réalisé en forage suivant un protocole de description et d'échantillonnage systématique des intersections de la tuffite clé et des zones minéralisées. Au moins un quart de carotte a été laissé comme témoin dans les boîtes. Les échantillons ont par la suite été utilisés pour la confection des lames minces et pour réaliser les analyses lithogéochimiques.

Les travaux de terrain permettent dans un premier temps, d'identifier les différents faciès des tuffites et d'en isoler les composantes de manière macroscopique. Une attention toute particulière a été portée sur le lien géométrique entre la Tuffite Clé et les minéralisations SMV, ainsi que les variations de faciès en fonction de l'éloignement des lentilles de sulfures afin d'essayer d'établir un outil visuel vers la minéralisation. De plus, les relations de recoupements sur la tuffite clé (avec la minéralisation et les altérations) observées en forage ou sur le terrain ont permis d'établir la chronologie des différents épisodes hydrothermaux à l'échelle d'un gisement voire même du camp.

1.4.2. TRAITEMENT ET PRÉPARATION DES ÉCHANTILLONS

Les échantillons ont été numérisés à haute résolution et nettoyés afin d'enlever les surface d'altération pour permettre d'avoir des roches fraîches pour les analyses. Deux lames minces ont été confectionnées pour chacun des échantillons. Une lame de 30 µm pour les observations pétrographiques et une lame polie de 100 µm pour les analyses de LA-ICP-MS sur les sulfures ou les cherts. Pour les analyses lithogéochimiques, les échantillons ont été réduits à une granulométrie inférieure à 75 µm à l'aide d'un broyeur à mâchoire et d'un broyeur en céramique d'alumine à l'Université du Québec à Chicoutimi ou directement envoyés au centre Eau Terre Environnement de l'INRS à Québec pour être préparés.

1.4.3. ANALYSES PÉTROGRAPHIQUES ET MINÉRALOGIQUES

Une étude pétrographique des lames minces permet de caractériser la minéralogie, la texture et les altérations des différents échantillons. Ces observations permettent d'identifier les différentes composantes de la tuffite et d'en documenter les paragenèses minérales. Cette étude permet, par la même occasion, la sélection des plages minérales de pyrites qui seront analysées pour tenter de développer des outils pour l'exploration. La même approche est utilisée pour étudier les cherts et les zones minéralisées échantillonnées. L'observation des différentes paragenèses minérales de ces zones permet de déterminer la chronologie relative des différents épisodes de minéralisations sur une base comparative.

1.4.4. ANALYSES LITHOGÉOCHIMIQUES

Les roches broyées seront utilisées pour effectuer les analyses géochimiques par *Inductively Coupled Plasma-Mass Spectrometry* (ICP-MS) et *Atomic Emission Spectrometry* (ICP-AES) afin d'obtenir les teneurs en éléments majeurs, traces et les éléments des terres rares. D'autres analyses géochimiques, réalisées par Glencore (anciennement Xstrata Zinc) sont utilisés à diverses fins dans ce projet.

Comme le pôle détritique semble dominant dans la Tuffite Clé, les analyses lithogéochimiques devrait permettre de modéliser sa composition. Dans cette

optique, les travaux de Liaghat and MacLean (1992) constituent une base très intéressante puisqu'ils identifient deux sources différentes. Il est désormais possible d'aller plus loin en modélisant un précurseur unique « non altéré » à partir de courbes de fractionnement. Celui-ci sera utilisé pour calculer des bilans de masse selon les méthodes de MacLean and Kranidiotis (1987) et (Barrett and MacLean, 1999) dans le but de déterminer des variations spatiales. Cette approche pourrait s'avérer particulièrement efficace s'il est démontré que les minéralisations sont issues de processus de remplacement le long de la Tuffite Clé.

Les résultats géochimiques permettent aussi de construire une série de diagrammes binaires et ternaires discriminant les différents sédiments métallifères (ex: Al-Fe-Mn, Fe/Ti vs Al/(Al+Fe+Mn): Boström, 1973) dans un but de caractérisation. Dans la même optique, des diagrammes multiéléments normalisés par rapport au manteau primitif (Sun and McDonough, 1989) pourront être utilisés pour confronter les différents spectres de terres rares des tuffites versus les lithologies encaissantes.

1.4.5. ANALYSES MINÉRALOGIQUES

Les analyses minéralogiques ont pour but de développer des vecteurs vers les minéralisations en limitant la variabilité induite par les trois composantes des tuffites. Les récentes études sur les cherts (van den Boorn et al., 2007; Pinti et

al., 2009) démontrent l'importance des terres rares pour identifier les processus de formation (Figure 8). Des analyses au LA-ICP-MS (UQAC) seront conduites sur les cherts de la tuffite clé afin d'obtenir la composition en terres rares de ces unités. Ces résultats seront confrontés aux classifications existantes. Ceci permettra de vérifier si les cherts sont issus de processus de précipitation chimique ou de remplacement ce qui aura de grandes conséquences sur le lien génétique entre la Tuffite Clé et les minéralisations.

Les pyrites sont, quant à elles, plus proches de l'épisode minéralisateur et sont donc à fort potentiel pour le développement d'outils de guidage, que la Tuffite Clé soit ou non syngénétique. L'étude pétrographique et minéralogique réalisée préalablement aura permis d'identifier toutes les textures de pyrites. La microsonde sera réutilisée afin de tester l'homogénéité des cristaux. C'est le LA-ICP-MS qui sera utilisé ensuite pour les analyses quantitatives des éléments traces dans les sulfures. Toutes les textures seront analysées dans le but de discriminer les pyrites synchrones à l'épisode minéralisateur. L'objectif de cette étude est quadruple: 1) obtenir la signature du cortège métallique des pyrites afin de modéliser la signature des fluides minéralisateurs, 2) comparer la signature des pyrites des zones minéralisées avec celle de la Tuffite Clé afin de tester le lien génétique entre les deux, 3) utiliser cette signature pour établir un vecteur vers les SMV, et 4) établir une chronologie relative des différents épisodes de

minéralisations sur une base comparative en utilisant les différentes signatures et textures.

1.5. FORMAT DE LA THÈSE

Cette thèse se présente sous la forme d'un recueil de trois manuscrits d'articles scientifiques. Pour chacun des manuscrits, le premier auteur est l'auteur de la thèse. Chacun de ces articles a été rédigé en anglais afin d'être publié dans des revues spécialisées internationales. Les trois articles constituent respectivement les chapitres 2, 3 et 4 de la thèse. Le premier article (Chapitre 2) a été publiés dans le journal « Mineralium Deposita » en avril 2014 et a pour titre : « The Key Tuffite, Matagami Camp, Abitibi Greenstone Belt, Canada : petrogenesis and implications for VMS formation and exploration ». L'article présente la contribution de chacune des trois composantes de la Tuffite Clé : 1) fraction détritique, 2) précipité chimique et 3) altération, autour des deux gisements accessibles au moment de cette étude : la mine Persévérance et la mine Bracemac-McLeod. Contrairement aux travaux précédents, il est clairement mis en évidence dans cette étude que la contribution exhalative est limitée, voire absente, pour les deux gisements étudiés. La minéralisation est mise en place après le dépôt de la Tuffite Clé et de la rhyolite de Bracemac sus-jacente. Suite à cette conclusion, les travaux de recherche ont été réorientés. Le pôle précipité chimique ne pouvant être utilisé pour étudier l'évolution du système hydrothermal

ou pour développer des outils de guidage vers les minéralisations, les travaux de recherche se sont concentrés sur le pôle altération de la Tuffite Clé. Dans ce premier article, le premier auteur a fait les observations sur le terrain, a réalisé les analyses au LA-ICP-MS et est responsable de l'analyse et de l'interprétation des résultats et de la rédaction de l'article. Damien Gaboury a participé à la rédaction de certaines sections, et à l'interprétation des données scientifiques, ainsi qu'aux corrections finales. Gilles Roy était responsable de l'exploration à Matagami et a donc participé à certaines observations de terrain, à la production de certaines figures ainsi qu'au processus de discussion scientifique.

Les deux articles suivants avaient pour objectifs d'étudier l'évolution des systèmes hydrothermaux de type SMV et le développement d'outils pour l'exploraiton, de manière indépendante, et à partir de la Tuffite Clé. Le deuxième article, intitulé « Evolution of a volcanogenic hydrothermal system recorded by the behaviour of LREE and Eu: Case study of the Key Tuffite at Bracemac-McLeod deposits, Matagami, Canada », a été publié en décembre 2014 dans la revue « Ore Geology Reviews ». Cet article traite du comportement des Terres Rares (REE) face aux altérations hydrothermales. Plus spécifiquement, les REE légères et l'Europium, mobiles sous certaines conditions, ont permis de reconstruire l'évolution du système hydrothermal à Bracemac-McLeod. Dans cet article, le premier auteur a fait les observations sur le terrain, a réalisé les analyses au LA-ICP-MS et est responsable de l'analyse des résultats et de la rédaction de l'article.

Damien Gaboury a contribué aux discussions scientifiques et partiellement à la rédaction, et aux corrections. Gilles Roy a contribué à la production de certaines figures ainsi qu'au processus de discussion scientifique et de corrections.

Finalement, le troisième article, intitulé «Deciphering the hydrothermal evolution of a VMS system using trace elements in pyrite by laser ablation ICP-MS: an example from the Bracemac-McLeod deposits, Abitibi, Canada and implications for exploration » a été soumis en décembre 2014 dans la revue « Economic Geology». Comme le précédant, cet article visait à étudier l'évolution du système minéralisateur, mais cette fois-ci sur la base de la chimie des sulfures, principalement des pyrites, car les sulfures sont des témoins directs de l'évènement minéralisateur. Dans cet article, le premier auteur a fait les observations macro et microscopiques, a réalisé les analyses au LA-ICP-MS et est responsable de l'analyse et de l'interprétation des résultats et de la rédaction de l'article. Damien Gaboury a participé à la validation de l'article, par le biais de discussions en cours de traitement des résultats, et de commentaires lors de la rédaction du manuscrit.

Les arguments développés dans les chapitres 2 à 4 sont résumés et restructurés au sein d'une discussion générale (Chapitre 5) dans le but d'intégrer d'une manière cohérente les différents aspects du projet de doctorat, depuis la genèse de la Tuffite Clé et des minéralisations, jusqu'aux implications du projet, autant sur le plan académique qu'économique (exploration minérale).

Enfin, le manuscrit en annexe intitulé « Behaviour of Europium in the Key Tuffite around the Bracemac-McLeod deposit: A new geochemical tool to assist VMS exploration in the Matagami mining camp, Quebec, Canada » a été rédigé à la suite de la remise du prix Julian Boldy en 2011. Ce prix est remis tous les deux ans par la division des gîtes minéraux (Mineral Deposit Division) de l'Association Géologique du Canada (AGC). Ce prix s'accompagnait de la publication des travaux dans le magazine « The Gangue ». Malheureusement, le magazine n'a pas été publié depuis 2012 et le manuscrit n'est donc jamais sorti.

1.6. RÉFÉRENCES

Adair, R., 2009, Technical report on the resource calculation for the Bracemac-McLeod discoveries, Matagami Project, Québec: Vancouver, Canada, Donner Metals Ltd., National Instrument 43-101 Report, filled on April 3, 2009, at http://www.sedar.com, p. 194.

Allen, R. L., and Weihed, P., 2002, Global comparisons of volcanic-associated massive sulphide districts: Geological Society, London, Special Publications, v. 204, p. 13-37.

Barrett, T. J., and MacLean, W. H., 1999, Volcanic sequences, lithogeochemistry, and hydrothermal alteration in some bimodal volcanic-associated massive sulfide systems, *in* Barrie, C. T., and Hannington, M. D., eds., Reviews in Economic Geology 8, 8, p. 101-131.

Barriga, F. J. A. S., and Oliveira, J. T., 1986, Geochemical study of cherts, jaspers and manganese ores from the Iberian Pyrite Belt: Maleo Boletim Informativo Sociedade Geológica de Portugal, v. 2, p. 11.

Beaudry, C., and Gaucher, E., 1986, Cartographie géologique dans la région de Matagami: Québec., Ministère de l'énergie et des Ressources, Rapport MB 86-32, p. 147.

Boström, K., 1973, The origin of ferromanganoan active ridge sediments: Stockholm Contributions in Geology, v. 27, p. 149-243.

Card, K. D., 1990, A review of the Superior Province of the Canadian Shield, a product of Archean accretion: Precambrian Research, v. 48, p. 99-156.

Carr, P. M., Cathles, L. M., and Barrie, C. T., 2008, On the size and spacing of volcanogenic massive sulfide deposits within a district with application to the Matagami district, Quebec: Economic Geology, v. 103, p. 1395-1409.

Chown, E. H., Daigneault, R., Mueller, W. U., and Mortensen, J. K., 1992, Tectonic evolution of the Northern Volcanic Zone, Abitibi belt, Quebec: Canadian Journal of Earth Sciences, v. 29, p. 2211-2225.

Chown, E. H., N'dah, E., and Mueller, W. U., 2000, The relation between iron-formation and low temperature hydrothermal alteration in an Archean volcanic environment: Precambrian Research, v. 101, p. 263-275.

Costa, U. R., Barnett, R. L., and Kerrich, R., 1983, The Mattagami Lake Mine Archean Zn-Cu sulfide deposit, Quebec; hydrothermal coprecipitation of talc and sulfides in a sea-floor brine pool; evidence from geochemistry, 18 O/ 16 O, and mineral chemistry: Economic Geology, v. 78, p. 1144-1203.

Daigneault, R., Mueller, W. U., and Chown, E. H., 2004, Abitibi greenstone belt plate tectonics: the diachronous history of arc development, accretion and collision, *in* Eriksson, P. G., Altermann, W., Nelson, D. R., Mueller, W. U., Catuneau, O., and Strand, K., eds., Developments in Precambrian Geology/Tempos of events in Precambrian time, 12: Amsterdam, Elsevier, p. 88-103.

Davidson, A. J., 1977, Petrography and chemistry of the Key Tuffite at Bell Allard, Matagami, Quebec, McGill University, 131 p.

Douville, E., Bienvenu, P., Charlou, J. L., Donval, J. P., Fouquet, Y., Appriou, P., and Gamo, T., 1999, Yttrium and rare earth elements in fluids from various deep-sea hydrothermal systems: Geochimica et Cosmochimica Acta, v. 63, p. 627-643.

Doyle, M. G., and Allen, R. L., 2003, Subsea-floor replacement in volcanic-hosted massive sulfide deposits: Ore Geology Reviews, v. 23, p. 183-222.

Franklin, J. M., Gibson, H. L., Jonasson, I. R., and Galley, A. G., 2005, Volcanogenic massive sulfide deposits: Economic Geology 100th anniversary volume, v. 98, p. 523-560.

Franklin, J. M., Sangster, D. F., and Lydon, J. W., 1981, Volcanic-associated massive sulfide deposits: Economic Geology 75th Anniversary Volume, p. 485-627.

Gaboury, D., and Pearson, V., 2008, Rhyolite geochemical signatures and association with volcanogenic massive sulfide deposits: Examples from the Abitibi Belt, Canada: Economic Geology, v. 103, p. 1531-1562.

Galley, A. G., Hannington, M. D., and Jonasson, I. R., 2007, Volcanogenic massive sulphide deposits: Mineral Deposits of Canada: A Synthesis of Major Deposit-Types, District Metallogeny, the Evolution of Geological Provinces, and Exploration Methods: Geological Association of Canada, Mineral Deposits Division, Special Publication, v. 5, p. 141-161.

Gibson, H. L., and Kerr, D. J., 1993, Giant volcanic-associated massive sulphide deposits: with emphasis on Archean examples: Economic Geology Special Publication 2, p. 319-348.

Grenne, T., and Slack, J. F., 2005, Geochemistry of jasper beds from the Ordovician Løkken Ophiolite, Norway: origin of proximal and distal siliceous exhalites: Economic Geology, v. 100, p. 1511-1527.

Hannington, M. D., de Ronde, C. D. J., and Petersen, S., 2005, Sea-floor tectonics and submarine hydrothermal systems, *in* Hedenquist, J. W., Thompson, J. F. H., Goldfarb, R. J., and Richards, J. P., eds., Economic Geology 100th anniversary volume: Littelton, Colorado, USA, Society of Economic Geologists, p. 111-141.

Hart, T. R., Gibson, H. L., and Lesher, C. M., 2004, Trace element geochemistry and petrogenesis of felsic volcanic rocks associated with volcanic massive Cu-Zn-Pb sulfide deposits: Economic Geology, v. 99, p. 1003-1013.

Herzig, P. M., and Hannington, M. D., 1995, Polymetallic massive sulfides at the modern seafloor a review: Ore Geology Reviews, v. 10, p. 95-115.

Hrischeva, E., and Scott, S. D., 2007, Geochemistry and morphology of metalliferous sediments and oxyhydroxides from the Endeavour segment,

Juan de Fuca Ridge: Geochimica et Cosmochimica Acta, v. 71, p. 3476-3497.

Ioannou, S. E., and Spooner, E. T. C., 2007, Fracture analysis of a volcanogenic massive sulfide-related hydrothermal cracking zone, Upper Bell River Complex, Matagami, Quebec: application of permeability tensor theory: Economic Geology, v. 102, p. 667-690.

Jenney, C. P., 1961, Geology and ore deposits of the Mattagami area, Quebec: Economic Geology, v. 56, p. 740-757.

Kalogeropoulos, S. I., 1985, Discriminant analysis for evaluating the use of lithogeochemistry along the Tetsusekiei Horizon as an exploration tool in search for Kuroko type ore deposits: Mineralium Deposita, v. 20, p. 135-142.

Kalogeropoulos, S. I., and Scott, S. D., 1983, Mineralogy and geochemistry of tuffaceous exhalites (tetsusekiei) of the Fukazawa mine, Hokuroku district, Japan: Economic Geology Monograph, v. 5, p. 412-432.

Kalogeropoulos, S. I., and Scott, S. D., 1989, Mineralogy and geochemistry of an Archean tuffaceous exhalite: the Main Contact Tuff, Millenbach mine area, Noranda, Quebec: Canadian Journal of Earth Sciences, v. 26, p. 88-105.

Kamber, B. S., Greig, A., and Collerson, K. D., 2005, A new estimate for the composition of weathered young upper continental crust from alluvial sediments, Queensland, Australia: Geochimica et Cosmochimica Acta, v. 69, p. 1041-1058.

Large, R. R., Maslennikov, V. V., Robert, F., Danyushevsky, L. V., and Chang, Z., 2007, Multistage sedimentary and metamorphic origin of pyrite and gold in the giant Sukhoi Log deposit, Lena Gold Province, Russia: Economic Geology, v. 102, p. 1233-1267.

Lavallière, G., Guha, J., and Daigneault, R., 1994, Cheminées de sulfures massifs atypiques du gisement d'Isle-Dieu, Matagami, Québec; implications pour l'exploration: Exploration and Mining Geology, v. 3, p. 109-129.

Leistel, J. M., Marcoux, E., and Deschamps, Y., 1997, Chert in the Iberian Pyrite Belt: Mineralium Deposita, v. 33, p. 59-81.

Lesher, C. M., Goodwin, A. M., Campbell, I. H., and Gorton, M. P., 1986, Trace-element geochemistry of ore-associated and barren, felsic metavolcanic rocks in the Superior Province, Canada: Canadian Journal of Earth Sciences, v. 23, p. 222-237.

Liaghat, S., and MacLean, W. H., 1992, The Key Tuffite, Matagami mining district; origin of the tuff components and mass changes: Exploration and Mining Geology, v. 1, p. 197-207.

Loftus-Hills, G., and Solomon, M., 1967, Cobalt, nickel and selenium in sulphides as indicators of ore genesis: Mineralium Deposita, v. 2, p. 228-242.

MacLean, W. H., 1988, Rare earth element mobility at constant inter-REE ratios in the alteration zone at the Phelps Dodge massive sulphide deposit, Matagami, Quebec: Mineralium Deposita, v. 23, p. 231-238.

MacLean, W. H., and Kranidiotis, P., 1987, Immobile elements as monitors of mass transfer in hydrothermal alteration; Phelps Dodge massive sulfide deposit, Matagami, Quebec: Economic Geology, v. 82, p. 951-962.

Maier, W. D., Barnes, S.-J., and Pellet, T., 1996, The economic significance of the Bell River Complex, Abitibi subprovince, Quebec: Canadian Journal of Earth Sciences, v. 33, p. 967-980.

Maslennikov, V. V., Maslennikova, S. P., Large, R. R., and Danyushevsky, L. V., 2009, Study of trace element zonation in vent chimneys from the Silurian Yaman-Kasy volcanic-hosted massive sulfide deposit (Southern Urals, Russia) using laser ablation-inductively coupled plasma mass spectrometry (LA-ICPMS): Economic Geology, v. 104, p. 1111-1141.

Mercier-Langevin, P., Gibson, H. L., Hannington, M. D., Goutier, J., Monecke, T., Dubé, B., and Houlé, M. G., 2014, A special issue on Archean magmatism, volcanism, and ore deposits: Part 2. Volcanogenic massive sulfide deposits preface: Economic Geology, v. 109, p. 1-9.

Mercier-Langevin, P., Goutier, J., Ross, P.-S., McNicoll, V. J., Monecke, T., Dion, C., Dubé, B., Thurston, P., Bécu, V., Gibson, H. L., Hannington, M. D., and Galley, A. G., 2011, The Blake River Group of the Abitibi greenstone belt and its unique VMS and gold-rich VMS endowment: GAC-MAC-SEG-SGA Joint Annual Meeting 2011, Ottawa, Field Trip 02B guidebook; Geological Survey of Canada, Open File report 6869, 2011, p. 61.

Michard, A., and Albarède, F., 1986, The REE content of some hydrothermal fluids: Chemical Geology, v. 55, p. 51-60.

Miller, R. J. M., 1960, Geology of Mattagami Lake Mines: Canadian Inst Mining Metall Bull, v. 53, p. 194.

Mortensen, J. K., 1993, U–Pb geochronology of the eastern Abitibi Subprovince. Part 1: Chibougamau–Matagami–Joutel region: Canadian Journal of Earth Sciences, v. 30, p. 11-28.

Mueller, W. U., Daigneault, R., Mortensen, J. K., and Chown, E. H., 1996, Archean terrane docking: upper crust collision tectonics, Abitibi greenstone belt, Quebec, Canada: Tectonophysics, v. 265, p. 127-150.

Mueller, W. U., Stix, J., Corcoran, P. L., and Daigneault, R., 2009, Subaqueous calderas in the Archean Abitibi greenstone belt: An overview and new ideas: Ore Geology Reviews, v. 35, p. 4-46.

Ohmoto, H., 1996, Formation of volcanogenic massive sulfide deposits: The Kuroko perspective: Ore Geology Reviews, v. 10, p. 135-177.

Pearson, V., and Daigneault, R., 2009, An Archean megacaldera complex: The Blake River Group, Abitibi greenstone belt: Precambrian Research, v. 168, p. 66-82.

Peter, J. M., and Goodfellow, W. D., 1996, Mineralogy, bulk and rare earth element geochemistry of massive sulphide-associated hydrothermal sediments of the Brunswick Horizon, Bathurst Mining Camp, New Brunswick: Canadian Journal of Earth Sciences, v. 33, p. 252-283.

Peter, J. M., and Goodfellow, W. D., 2003, Hydrothermal sedimentary rocks of the Heath Steele belt, Bathurst mining camp, New Brunswick: Part 3. Application of mineralogy and mineral and bulk compositions to massive sulfide exploration: Economic Geology Monograph, v. 11, p. 417-433.

Peter, J. M., Goodfellow, W. D., and Doherty, W., 2003a, Hydrothermal sedimentary rocks of the Heath Steele Belt, Bathurst mining camp, New Brunswick: Part 2. Bulk and rare earth element geochemistry and implications for origin: Economic Geology Monograph, v. 11, p. 391-415.

Peter, J. M., Kjarsgaard, I. M., and Goodfellow, W. D., 2003b, Hydrothermal sedimentary rocks of the Heath Steele belt, Bathurst mining camp, New

Brunswick: Part 1. Mineralogy and mineral chemistry: Economic Geology Monograph, v. 11, p. 361-390.

Piché, M., Guha, J., Daigneault, R., Sullivan, J. R., and Bouchard, G., 1990, Les gisements volcanogènes du camp minier de Matagami: Structure, stratigraphie et implications métallogéniques: Canadian Institute of Mining and Metallurgy, v. Special Volume 43, p. 327-336.

Pinti, D. L., Hashizume, K., Sugihara, A., Massault, M., and Philippot, P., 2009, Isotopic fractionation of nitrogen and carbon in Paleoarchean cherts from Pilbara craton, Western Australia: Origin of 15N-depleted nitrogen: Geochimica et Cosmochimica Acta, v. 73, p. 3819-3848.

Ridler, R. H., 1971, Analysis of Archean volcanic basins in the Canadian shield using the exhalite concept [abs.]: Bull. Can. Inst. Mining Met, v. 64, p. 20.

Roberts, R. G., 1975, The geological setting of the Mattagami Lake Mine, Quebec; a volcanogenic massive sulfide deposit: Economic Geology, v. 70, p. 115-129.

Rock, N. M. S., 1988, The need for standardization of normalized multi-element diagrams in geochemistry: A comment: Geochemical Journal, v. 21, p. 75-84.

Rona, P. A., 1984, Hydrothermal mineralization at seafloor spreading centers: Earth Science Reviews, v. 20, p. 1-104.

Sharpe, J. I., 1968, Géologie et gisements de sulfures de la région de Matagami, Comté d'Abitibi-Est, Québec., Ministère des Richesses Naturelles du Québec. Rapport géologique 137, p. 122.

Sun, S.-S., and McDonough, W. F., 1989, Chemical and isotopic systematics of oceanic basalts: implications for mantle composition and processes: Geological Society, London, Special Publications, v. 42, p. 313-345.

Sverjensky, D. A., 1984, Europium redox equilibria in aqueous solution: Earth and Planetary Science Letters, v. 67, p. 70-78.

van den Boorn, S. H. J. M., van Bergen, M. J., Nijman, W., and Vroon, P. Z., 2007, Dual role of seawater and hydrothermal fluids in Early Archean chert formation: Evidence from silicon isotopes: Geology, v. 35, p. 939-942.

CHAPITRE 2

2. THE KEY TUFFITE, MATAGAMI CAMP, ABITIBI GREENSTONE BELT, CANADA: PETROGENESIS AND IMPLICATIONS FOR VMS FORMATION AND EXPLORATION

Dominique Genna, Damien Gaboury, Gilles Roy

Mineralium Deposita, 2014, Vol 49, pp 489-512

2.1. RÉSUMÉ

La Tuffite Clé est un marqueur stratigraphique pour la majorité des gisements de sulfures massifs volcanogènes du camp de Matagami dans la ceinture de roches vertes de l'Abitibi. Cette unité de 2 à 6 mètres d'épaisseur était précédemment interprétée comme résultant du mélange entre des dépôts de cendres (de composition andésitique et rhyolitique) et de précipité chimique (composante exhalative). Les tentatives pour établir des outils géochimiques, basées sur le contenu métallique de la Tuffite Clé, non jamais identifiées de variations cohérentes vers les zones minéralisées, en partie du à la nature complexe de l'unité et la compréhension limitée de sa composition, de son origine et de sa relation avec le système hydrothermal minéralisateur. Les travaux de cartographie détaillée et lithogéochimie approfondie de la Tuffite Clé autour des dépôts de Persévérance et Bracemac-McLeod indiquent que la Tuffite Clé est un tuf andésitique calco-alcalin homogène qui s'est déposé avant la formation des gisements SMV. Cette unité est dépourvue de composante exhalative, mais est fortement altérée à proximité des lentilles minéralisées. L'altération se matérialise par une forte chloritisation proximale et une séricitisation distale qui disparait progressivement avec l'éloignement des gisements. Pour les deux gisements étudiés, ni la Tuffite Clé, ni la minéralisation ont été formé par des processus exhalatif sur le plancher océanique. Ceci explique probablement le manque d'efficacité des modèles d'exploration basés sur la teneur en métaux de la Tuffite

Clé et suggère qu'une ré-évaluation du modèle exhalatif pour expliquer la genèse des gisements du district de Matagami est nécessaire. Cependant, cette étude montre que l'altération hydrothermale dans la Tuffite Clé peut-être utilisée comme vecteur vers les minéralisations.

2.2. ABSTRACT

The Key Tuffite is a stratigraphic marker unit for most of the zinc-rich volcanogenic massive sulfide deposits of the Matagami camp in the Abitibi greenstone belt. This 2 to 6 meter-thick unit was previously interpreted as a mixture between ash fall (andesitic to rhyolitic tuffaceous components) and VMS-related chemical seafloor precipitate (exhalative component). Previous attempts to develop geochemical exploration vectoring tools using metal content within the Key Tuffite were mostly inconclusive due to the complex nature of the Key Tuffite unit and a poor understanding of its composition, origin and relationship with the VMS-forming hydrothermal systems. Detailed mapping and thorough lithogeochemistry of the Key Tuffite in the vicinity of the Perseverance and Bracemac-McLeod deposits indicate that the Key Tuffite is a homogeneous calc-alkaline, andesitic tuff that was deposited before the VMS deposits were formed. The unit is mostly devoid of exhalative component, but it is strongly hydrothermally altered close to orebodies. This is characterized by a strong proximal chloritization and a distal sericitization, which grades laterally into the unaltered Key Tuffite. Neither the Key

Tuffite nor the ore were formed by seafloor exhalative processes for the two studied deposits. This probably explains why previously proposed exploration models based on metal scavenging proved unsuccessful and suggests that a re-evaluation of the exhalative model should be done at the scale of the mining camp. However, as shown in this study, hydrothermal alteration can be used to vector towards ore along the Key Tuffite.

2.3. INTRODUCTION

Since the discovery of the Matagami mining camp (Quebec, Canada) in the Archean Abitibi greenstone belt at the end of the 1950's, there has been a debate over the origin of the zinc-rich volcanogenic massive sulfide (VMS) deposits. Two schools of thought exist. Originally, most of the early workers regarded the ore deposits as epigenetic bodies formed by replacement processes (Miller, 1960; Jenney, 1961; Hallam, 1964; Tully, 1964; Sharpe, 1968). Latulippe (1959) was however the first to propose that most of the features were compatible with a syngenetic exhalative origin, with the main argument based on the association of all the mined deposits with a regional stratigraphic marker known as the Key Tuffite (Miller, 1960). The Key Tuffite is a laterally extensive (~ 17 km), continuous and thinly layered tuffaceous to cherty unit that is 2 to 6 meters-thick on average (Fig. 2.1). This unit has been used as a first order vector for exploration in the camp for the last 50 years. The discovery of the sulfide chimney and mound

deposits on the modern seafloor (e.g., Corliss et al., 1979) at the end of the 1970's gave credence to the exhalative model. Since, this model has been generally accepted for the Matagami mining camp (Roberts, 1975; Roberts and Reardon, 1978; MacGeehan and MacLean, 1980; Costa et al., 1983; Ioannou et al., 2007). As such, Matagami is often quoted as a classical example of exhalative-style mineralization. However, the atypical geometry of the last 2 VMS discoveries at Matagami, the Perseverance (Arnold, 2006) and Bracemac-McLeod (Adair, 2009) deposits, challenges the accepted ore-forming exhalative model. The Perseverance mine consists of three sub-vertical orebodies overlain by a sub-horizontal, barren, but strongly silicified, Key Tuffite. In contrast, the Bracemac-McLeod mine consists of: 1) two main sheet-like massive sulfide deposits (Bracemac and McLeod) occurring at the Key Tuffite stratigraphic interval which exhibit both stratabound and crosscutting relationships, and 2) in the Bracemac deposit, two sheet-like massive sulfide lenses located 180 and 270 metres stratigraphically above the Key Tuffite, respectively. In this contribution, the geological setting of the Perseverance and Bracemac-McLeod deposits is described with an emphasis on the nature and origin of the Key Tuffite and its relationship with the ore-forming hydrothermal systems. Previous studies concluded that the Key Tuffite was the result of the mixing of at least 2 components in varying proportions: 1) tuffaceous (ash) and 2) exhalative (Davidson, 1977). However, proposed geochemical vectoring tools based on

these considerations were mostly inconclusive at Matagami (MacLean and Davidson, 1977), contrary to other VMS districts where exploration vectors based on exhalative units proved to be successful, such as in the Bathurst camp, Canada: (Peter and Goodfellow, 2003) and the Hokuroku District, Japan: (Kalogeropoulos and Scott, 1983). Moreover, most ancient VMS deposits have undergone post-ore, late-stage episodes of hydrothermal alteration and/or seafloor and regional metamorphism, which can alter primary features of tuffaceous exhalites (Franklin et al., 1981; Large, 1992). Therefore, a third component must be taken into consideration when characterizing tuffaceous exhalites and trying to develop geochemical exploration vectors: epigenetic hydrothermal alteration. Although the term epigenetic generally refers to much later events, it is used here to describe all the hydrothermal processes that might have modified the composition of the Key Tuffite after its deposition, which comprises the alteration and mineralization still synvolcanic in origin. The three components of the Key Tuffite (tuffaceous, exhalative and hydrothermal) were independently characterized using field observations, geometric relationships and geochemical data. Our study indicates that the Key Tuffite, although representing a major break in effusive volcanic activity, is not an exhalite unit sensus stricto.

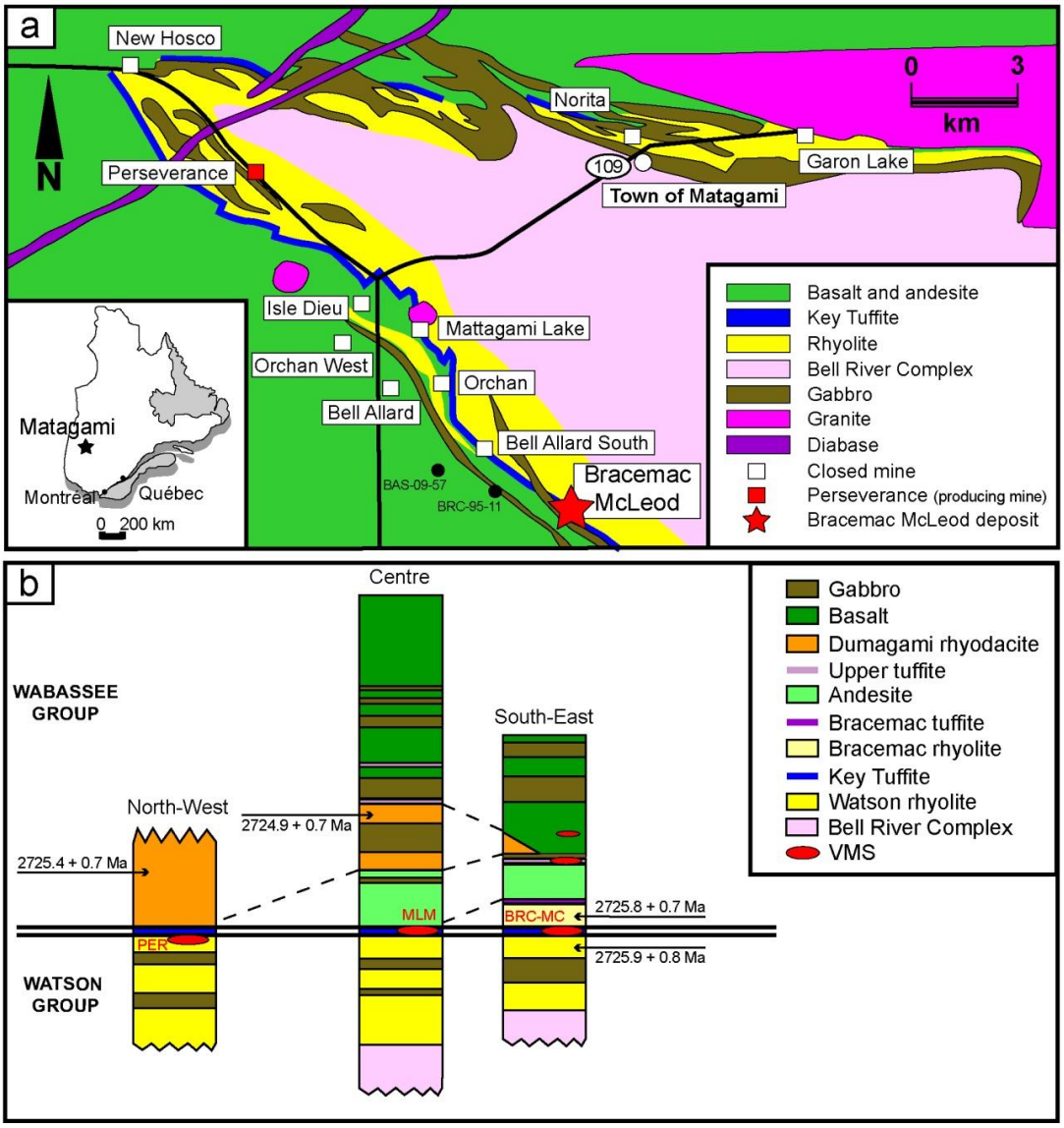

Figure 2.1 Geological setting of the Matagami mining camp. a Simplified regional map (modified from Glencore). The west camp is not presented here. b Stratigraphic columns along the South Flank. Age from Ross et al. (2014). PER=Perseverance, MLM=Mattagami Lake Mine; BRC-MC=Bracemac-McLeod.

The Key Tuffite is now interpreted as a homogeneous calc-alkaline andesitic tuff mostly devoid of exhalative component that is however strongly hydrothermally altered proximal to VMS hydrothermal systems. These features combined with geometric relationships between the Key Tuffite and the orebody shapes imply that the mineralization was mostly formed by sub-seafloor replacement, in agreement with mine-scale observations. Neither the tuffite nor the mineralization was dominantly formed by seafloor exhalative processes, explaining why exploration tools proposed in the past based on metal scavenging were not efficient. However, our study of the Perseverance and Bracemac-McLeod deposits indicates that hydrothermal alteration along the Key Tuffite has a real potential to be used as an exploration tool.

2.4. REGIONAL GEOLOGY

The Archean Abitibi greenstone belt in Canada is the largest (300 x 700 km) and also one of the richest greenstone belts in the world with approximately 90 VMS deposits (Card, 1990; Allen and Weihed, 2002; Mercier-Langevin et al., 2011). The Abitibi greenstone belt is an east-trending volcano-sedimentary sequence intruded by plutonic suites that display evidence of arc evolution, arc–arc collision, and arc fragmentation dating from 2735 to 2670 Ma (Mueller et al., 1996; Daigneault et al., 2004; 2009). The 2.7 Ga (Mortensen, 1993; Ross et al., 2014) Matagami mining camp (Fig. 2.1) is located in the northern part of the Abitibi belt

close to the boundary with the Opatica subprovince to the north. The camp constitutes an important zinc district with more than 60 Mt of zinc-rich ore (19 deposits and prospects, including 13 past and current producers: Mercier-Langevin et al., 2014; Ross et al., 2014). All of the known VMS deposits of the camp are spatially associated with extensive felsic bands that are divided into the North Flank, the South Flank and the West Camp (Fig. 2.1). The intensity of deformation is higher on the North Flank compared to the other felsic bands (Piché et al., 1993), because of its proximity to the Opatica sub-province boundary (Pilote et al., 2011). Regional metamorphism generally reached greenschist facies but locally amphibolite facies on the North Flank (Jolly, 1978). Despite numerous studies (e.g., Jenney, 1961; Sharpe, 1968; Roberts, 1975; Beaudry and Gaucher, 1986; Piché et al., 1990), the understanding of the camp remains limited in part because of the scarcity of outcrops. The general volcanic stratigraphy of the camp, as proposed by Sharpe (1968) and validated by Piché et al. (1990), is divided into the Watson Lake Group at the base and the Wabassee Group at the top (Fig. 2.1b). The Key Tuffite and all the major deposits are located at the interface of these groups. The Watson Lake Group is composed of two felsic units: 1) a poorly exposed lower dacite (500 m thick minimum; Piché et al. 1993) and 2) an upper rhyolite (1500 m thick), termed the Watson rhyolite (2725.9 ± 0.8 Ma: Ross et al., 2014). Both show good evidence of submarine volcanic textures (Piché et al., 1993; Debreil and Ross, 2009). According to the

geochemical classification of rhyolites associated with VMS mineralization (Lesher et al., 1986; Hart et al., 2004), the Watson rhyolite (FIIIb type) is considered particularly fertile (Gaboury and Pearson, 2008). The Wabassee Group (3000 m thick) mostly comprises massive or pillowed mafic lavas of basaltic and andesitic composition. However, two felsic units are present in the Wabassee Group along the South Flank (Fig. 2.1b). At the Perseverance mine, the hanging-wall is the Dumagami rhyolite (up to 400 m thick), whereas the Bracemac rhyolite (up to 70 m thick) is the hanging-wall of the Bracemac-McLeod deposits. The ages of these two rhyolites are 2725.4 ± 0.7 Ma and 2725.8 ± 0.7 Ma, respectively (Ross et al., 2014). Both the Watson Lake and the Wabassee Groups are locally crosscut by late phases of the underlying Bell River Complex, a large synvolcanic tholeiitic gabbro-anorthosite layered intrusion dated at 2724.6 +/- 2.5 Ma (Mortensen, 1993). This intrusion is interpreted as the source for the overlying volcanic units and as the thermal source for the formation of the VMS deposits (Piché et al., 1990; Maier et al., 1996; Ioannou and Spooner, 2007; Carr et al., 2008).

2.5. THE KEY TUFFITE

The Key Tuffite lies at the interface between the Watson and the Wabassee groups. It is a continuous unit which is 0.1 to 10 m thick and extends for over ~ 17 km on strike in a north-west – south-east direction. Recent work on the West

Camp suggests that the Key Tuffite could also be present west of the South Flank (Masson, 2000; Bussières and Théberge, 2006), increasing significantly the lateral extension of the Key Tuffite (>20 km). Observations by many authors on the Key Tuffite in the vicinity of VMS deposits along the South Flank lead to the following characteristics, which over time have been assumed to be representative of the Key Tuffite at the camp scale:

- The Key Tuffite is mostly delicately layered (e.g., Davidson, 1977; Costa et al., 1983; Liaghat and MacLean, 1992) and divided in 3 major zones: an upper fragmental zone, a central well bedded cherty zone, and a lower tuff zone with some larger fragments resembling the Watson rhyolite. One or even two of these zones can be missing in some sections (Davidson, 1977).
- The Key Tuffite is composed of volcanic ash altered to chlorite and sericite and mixed with chemical sediments, including chert, sulfides and carbonates (Davidson, 1977; Liaghat and MacLean, 1992).
- The average metallic content is high (1.4% Zn, 0.1% Cu and anomalous values of Pb, Co, Ni and Cr) as reported in the vicinity of the Bell Allard South deposit by Davidson (1977).

However, these observations on the Key Tuffite are not necessarily valid away from mineralization and alteration. Figure 2.2 presents two sections of Key Tuffite both located at >1 km away from any known deposit. Their position in the mining

camp is illustrated on Figure 2.1. Four main textural features are identified regarding layering: well or poorly developed layering, no bedding (massive), and brecciated (Fig. 2.2). The 2 drill holes are separated by a horizontal distance of ~500m. Lateral layer correlation appears very difficult based solely on the bedding. The thinly laminated layering, dominant in the Key Tuffite close to mineralization, appears to be a minor feature away from the mineralization. The bedding is not always well developed and previously unrecognized massive zones are dominant (Figs. 2.2b and e). The vertical variations proposed by Davidson (1977), based on the observations at Bell Allard South deposit, are not observed in these sections. From a mineralogical point of view, chert, considered to be by far the dominant component (up to 50%) in the Key Tuffite (Davidson, 1977; Liaghat and MacLean, 1992), is present only locally.

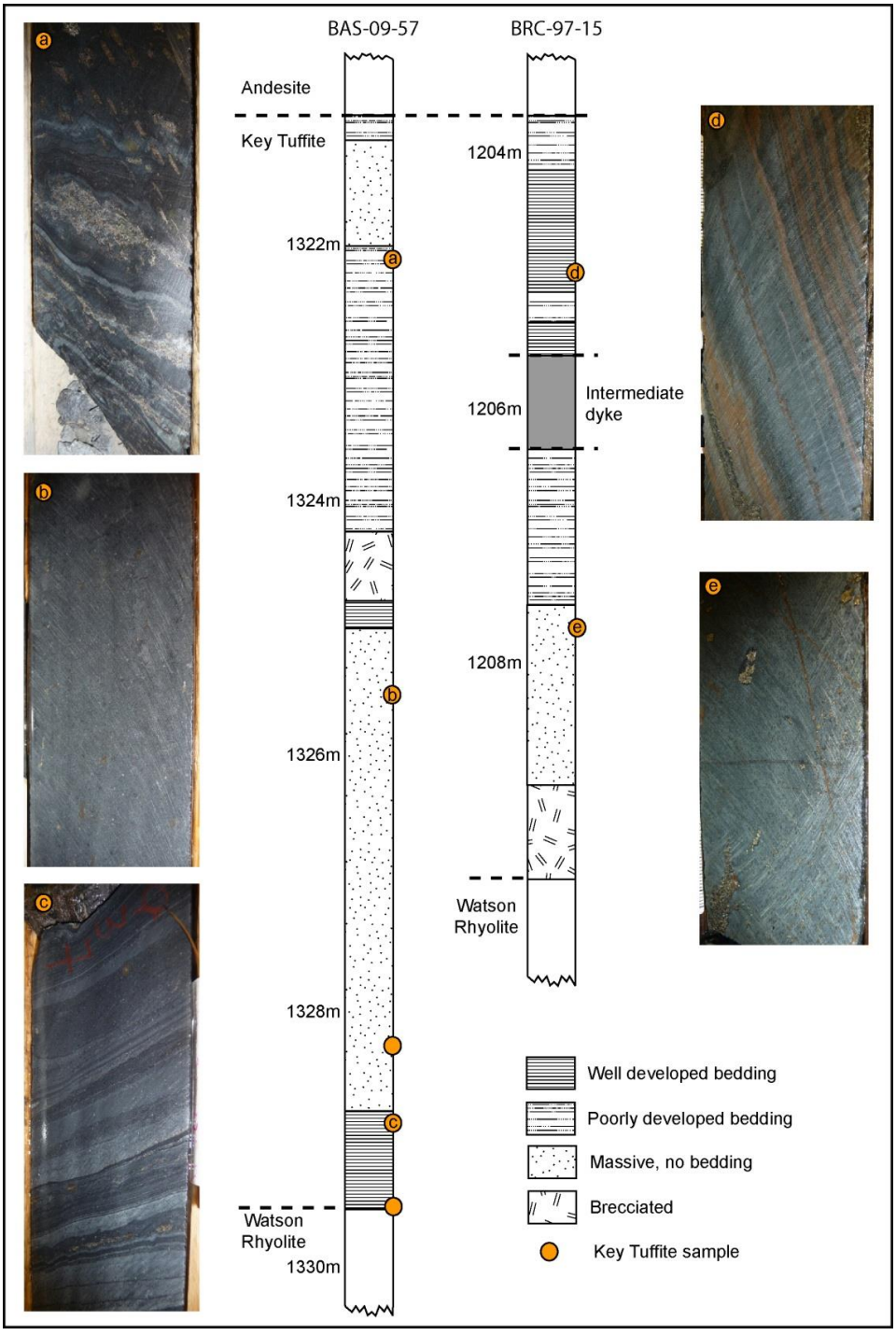

Figure 2.2 Detailed section of the Key Tuffite in two drill holes (BAS-09-57 and BRC-97-15) away from any known mineralization (>1km). The location of the drill holes, projected to the surface, is shown on Figure 2.1.

However, chlorite and sericite represent the dominant assemblage of the Key Tuffite. Finally, the base metal sulfides such as sphalerite and chalcopyrite are absent. These observations challenge the original perception of the Key Tuffite. Specifically, the well-developed layering, considered as the best evidence of component mixing (i.e., tuffaceous, hydrothermal: exhalative/alteration), disappears away from the mineralized lenses, questioning the origin and the source of the different components.

2.6. GEOLOGY OF THE PERSEVERANCE AND BRACEMAC-MCLEOD DEPOSITS

2.6.1. VOLCANIC STRATIGRAPHY

The Perseverance and Bracemac-McLeod deposits are located at the most northern and southern ends of the South Flank, respectively (Fig. 2.1a). The volcanic sequence of the South Flank trends north-west with a variable dip towards the south-west. In the northern part (Perseverance area), the volcanic sequence is sub-horizontal with a shallow dip of 10° towards the south-west. The dip progressively increases going south-east to reach a maximum of 65° in the Bracemac-McLeod area. The general stratigraphic sequence is shown in Figure 2.1b, whereas the detailed geology of both deposits is illustrated in the cross sections of Figures 2.3 and 2.4.

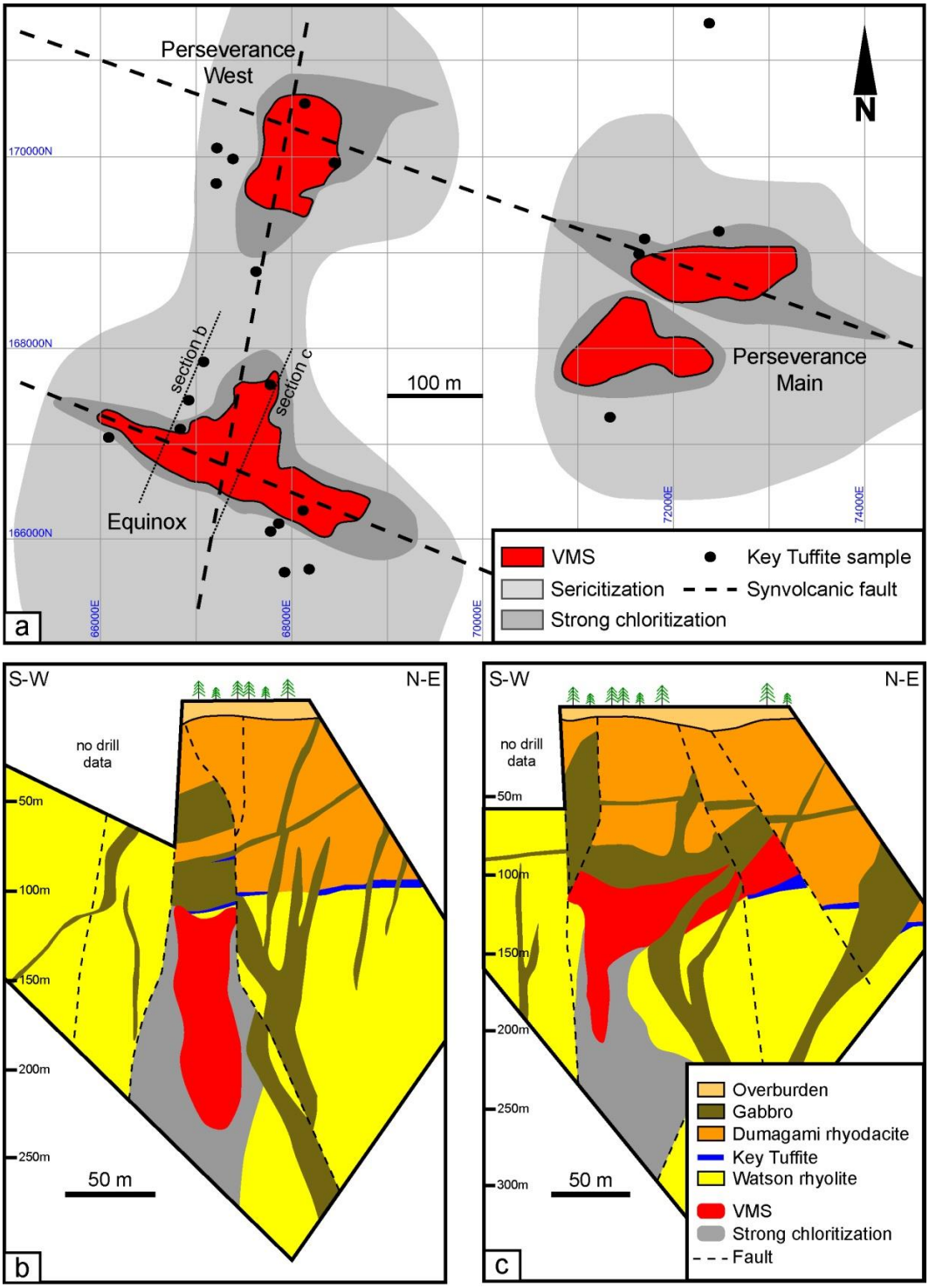

Figure 2.3 Geology of the Perseverance deposit (modified from Glencore). a Plan view. b-c Cross-section of the Equinox orebody.

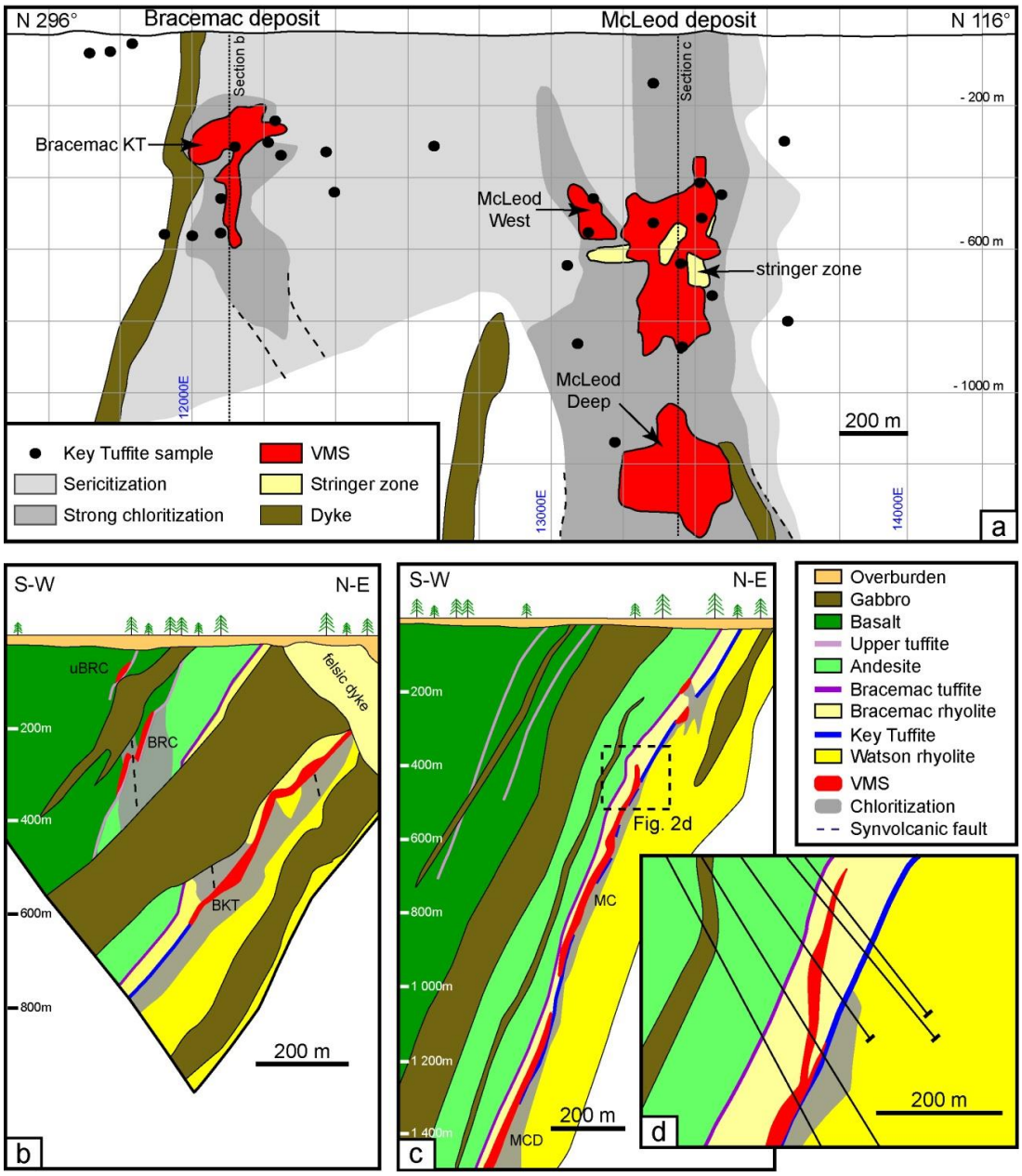

Figure 2.4 Geology of Bracemac-McLeod deposits (modified from Donner Metals). a Composite longitudinal view. b Cross section of the Bracemac area. c Cross section of the McLeod area. uBRC=Upper Bracemac; BRC=Bracemac; BKT=Bracemac KT.

	Mineralization	Lithology		Short description	Thick. (m)	Alteration features	Zr/Y	La/Yb	Affinity
Wabassee Group	uBRC	Basalt	V3B	Dark green, aphanitic to glomeroporphyric Massive, pillowed and hyaloclastites	> 400	Moderate chl and py of pillow margins	2.00	2.31	TH
	BRC	Upper Tuffite	UT	Thinly layered, mafic	0.1 to 2	Chloritisation and pyritization	-	-	-
		Andesite	V2J	Light green, fine grained lavas Massive, pillowed and hyaloclastites	~120	Moderate chl and py of pillow margins	4.00	2.80	TR
Watson Group		Bracemac Tuffite	BT	Thinly layered chert, pyrite and mafic ash	0.2 to 0.3	Silicification and pyritisation	-	-	-
		Bracemac Rhyolite	BRV1B	Grey to dark grey fine-grained lavas 1 to 5% of 1-3mm quartz phenocrysts Mostly massive	25 to 60	Proximal: Strong pervasive sil Local sericitization	2.77	1.96	TH
	BKT, MC, MCW, MCD	Key Tuffite	KT	Thinly layered mafic ash	0.1 to 10	Silicification, chloritization, sericitization, pyritization. Highly variable	10.39	10.44	CA
Watson Group	SZ	Watson Rhyolite	WV1B	Grey to dark grey fine-grained lavas 1 to 5% of 1-3mm quartz phenocrysts Massive, lobes but rare breccias Upper part often hyaloclastite	~200	Proximal: Strong black chl and talc Distal: moderate chl and ser Local silicification	4.10	2.14	TH
		Bell River Complex	BC	Gabbro-anorthosite layered intrusion	~5000		-	0.96	TH

Bracemac-McLeod

Table 2.1 Lithology description and magmatic affinity (Barrett and MacLean 1999) at Bracemac-McLeod and Perseverance. uBRC = Upper Bracemac; BRC = Bracemac; BKT = Bracemac KT; MC = McLeod; MCW = McLeod West; MCD = McLeod Deep; SZ = Stringer Zone; EQ = Equinox; PER = Perseverance Main; PW = Perseverance West.

	Mineralization	Lithology		Short description	Thick. (m)	Alteration features	Zr/Y	La/Yb	Affinity
Wabassee Group		Dumagami Rhyodacite	DV1B	Grey to dark grey fine-grained lavas Up to 90% spherulites (1-5mm) Massive, rare volcanic textures	> 400	Proximal: Strong black chl and talc Distal: moderate chl and ser Local silicification	3.55	-	TH
	EQ	Key Tuffite	KT	Thinly layered mafic ash	0.1 to 10	Strong silicification, moderate chloritisation, barren of sulfides	10.39	10.44	CA
Watson Group	PER, PW	Watson Rhyolite	WV1B	Grey to dark grey fine-grained lavas 1 to 5% of 1-3mm quartz phenocrysts Massive, lobes but rare breccias Upper part often hyaloclastite	~200	Proximal: Strong black chl and talc Distal: moderate chl and ser Local silicification	4.1	2.14	TH

Perseverance

Table 2.1 Lithology description and magmatic affinity (Barrett and MacLean 1999) at Bracemac-McLeod and Perseverance. uBRC = Upper Bracemac; BRC = Bracemac; BKT = Bracemac KT; MC = McLeod; MCW = McLeod West; MCD = McLeod Deep; SZ = Stringer Zone; EQ = Equinox; PER = Perseverance Main; PW = Perseverance West.

The lithological descriptions and main chemical characteristics of each unit are summarised in Table 2.1. The Key Tuffite is well developed in the Perseverance and Bracemac-McLeod areas. Its thickness ranges between 0.1 to 10 m and in some places it is absent. Such variations can occur over short distances and make correlation of specific beds impossible. In addition, there is no systematic increase in the thickness of the Key Tuffite towards the deposits as previously documented around the Bell Allard South deposit (Davidson, 1977), 2.2 km north-west of Bracemac-McLeod (Fig. 2.1).

At Perseverance, the Key Tuffite has a simple homogeneous facies, devoid of sulfides, which is dominated by alternating layers of silica and chlorite. Numerous soft-sediment features, such as convoluted laminations, load and slump structures (Fig. 2.5f), are abundant in the Key Tuffite, which suggest important submarine tuffaceous sedimentation. In contrast the Key Tuffite in the Bracemac-McLeod area contains a larger variety of facies composed of different amounts of quartz, chlorite, sericite, sulfides (mostly pyrite) and carbonate (Figs. 2.5a-e; 2.6). In the chert-rich facies, delicate lamination features are well preserved whereas the bedding appears coarser in chlorite-rich facies. In the vicinity of the Perseverance and Bracemac-McLeod deposits, the Key Tuffite is overlain by felsic rather than mafic units. At Perseverance, the felsic unit is the Dumagami rhyolite, which in fact has a rhyodacitic composition (Table 2.1). At Bracemac-McLeod, the felsic unit is the Bracemac rhyolite.

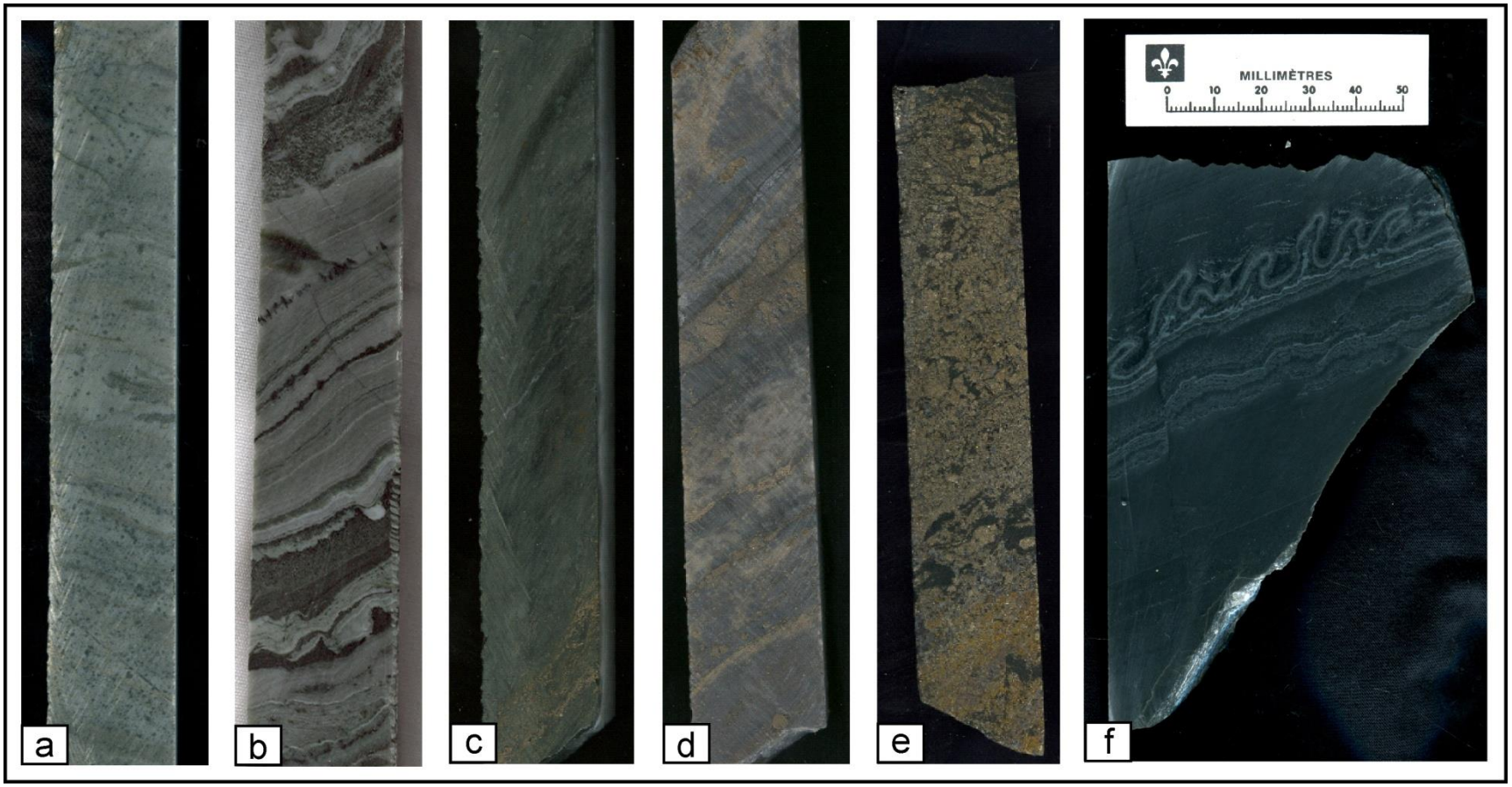

Figure 2.5 Representative mineral assemblages of selected Key Tuffite samples around Bracemac-McLeod (a-e; core width = 2.4 cm) and Perseverance (f) to illustrate the variation in facies. a Silica-sericite (sample 972209 in drillhole BRA-09-06, 85m depth); b Silica-chlorite (716472 in BRC-08-76, 692m); c Chlorite-pyrite (972162 in MC-08-62, 585m); d Silica-sericite-pyrite (972116 in MC-08-55, 513m); e Pyrite-chlorite (972153 in MC-07-23, 519m); f Chlorite-Silica (969357, level 105-PS26, underground).

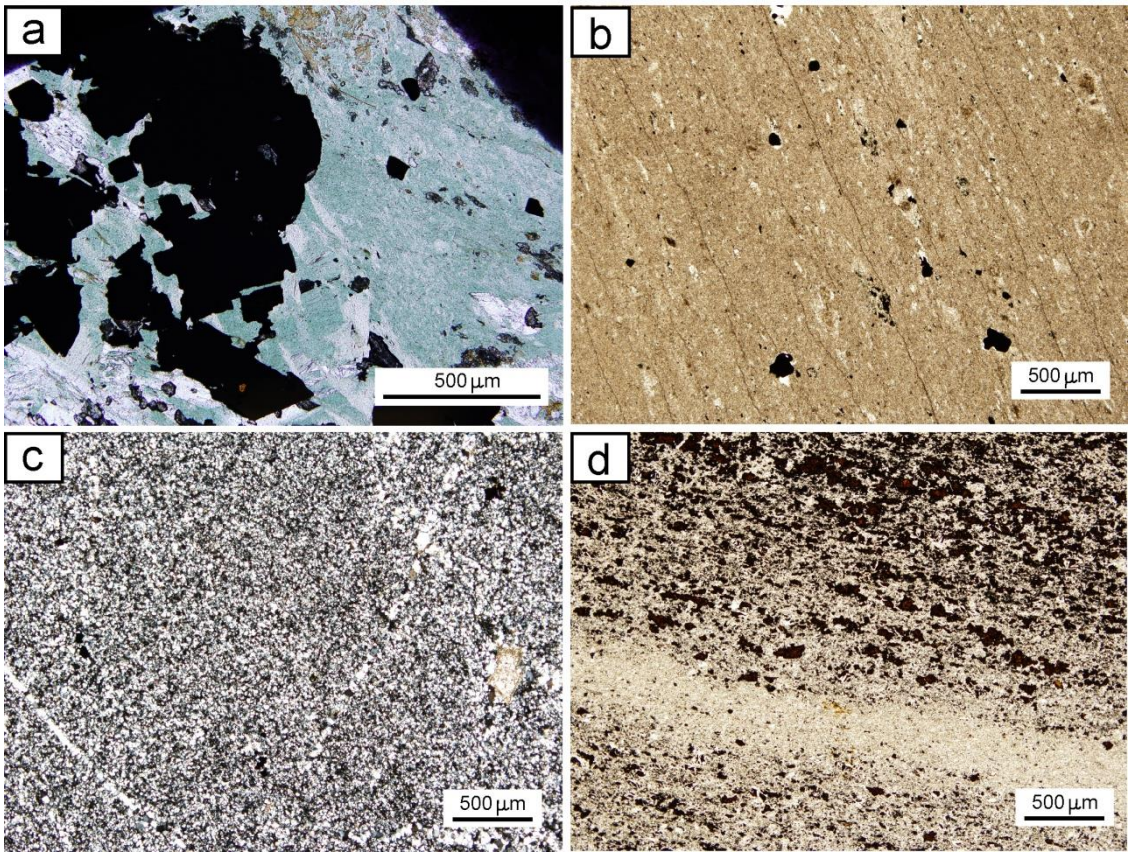

Figure 2.6 Photomicrographs of the Key Tuffite. Dominant assemblages: a Chlorite and pyrite (plane-polarized light=ppl) around McLeod (972110 in MC-07-24, 686m); b Sericite (ppl) around McLeod (716474 in MC-05-19, 821m); c Quartz (cross-polarized light) around McLeod (716489 in MC-05-18, 928m); d Disseminated sphalerite in a chlorite/sericite-rich Key Tuffite (ppl) around Bracemac (972134 in BRC-95-11, 968m).

A narrow (5 to 10 m thick) and sub-vertical intense chloritization (+/- talc) surrounds the mineralization (Figs. 2.3b-c). The sub-horizontal Key Tuffite, devoid of sulfides, systematically covers the mineralization (Figs. 2.3b-c). This unit is very similar (in geochemical composition and in age) to the Watson rhyolite (Table 2.1). In turn, the Bracemac rhyolite is overlain by a thin exhalative unit: the Bracemac Tuffite which marks the transition into the andesitic rocks of the Wabassee Group. Most of the volcanic units in the lower part of the South Flank (mine sequence) are tholeiitic except for the lower andesitic unit of the Wabassee Group which is transitional (Table 2.1).

At Perseverance, a large set of sub-vertical dykes of different orientations and compositions crosscuts the sub-horizontal volcanic strata, hence complicating the reconstruction of the succession (Figs. 2.3b-c). The orientation of the intrusions is different at Bracemac-McLeod where the entire stratigraphic succession has been intruded by gabbroic sills that inflate the volcanic pile (Fig. 2.4b-c).

2.6.2. ALTERATION, MINERALIZATION AND THEIR LINK WITH THE KEY TUFFITE

The Perseverance and Bracemac-McLeod deposits are both surrounded by large (~1.6 km in diameter) alteration halos developed in the footwall Watson rhyolite (Figs. 2.3 and 2.4), which are characterized by a well-developed proximal chloritization (± talc), moderate intermediate chloritization and distal sericitization

(Fig. 2.7). An alteration halo is also present in the overlying Bracemac rhyolite and Dumagami rhyodacite, although less extensive than in the footwall. In both deposits, the hanging-wall alteration is dominated by pervasive and patchy silicification and diffuse chloritization (Figs. 2.7a-b). Such alteration haloes are typical of Archean VMS systems (e.g., Galley, 1993) and represent the main exploration tool (Large et al., 2001a). Despite similar alteration assemblages, the geometry of the alteration haloes and of the orebodies is markedly different at Bracemac-McLeod versus Perseverance (Figs. 2.3 and 2.4). Moreover, both are different to the classic mound-shaped lenses of exhalative VMS systems (e.g., Lydon, 1984; Ohmoto, 1996) as previously described in the Matagami camp for the Mattagami Lake (Costa et al., 1983) and the Isle Dieu mines (Lavallière et al., 1994).

2.6.3. PERSEVERANCE DEPOSIT

The Perseverance deposit consists of 3 main sub-vertical lenses: Perseverance Main, Perseverance West and Equinox (Fig. 2.3a), which are thought to be spatially controlled by synvolcanic structures. Together they contain 5.12 million tonnes with grades of 15.8 % Zn, 1.2 % Cu, 29 g/t Ag and 0.4 g/t Au (Arnold, 2006). The 3 orebodies are preserved in a graben-like structure bounded by two north-west-trending faults (Arnold, 2006; Bloom and Beaudry, 2009).

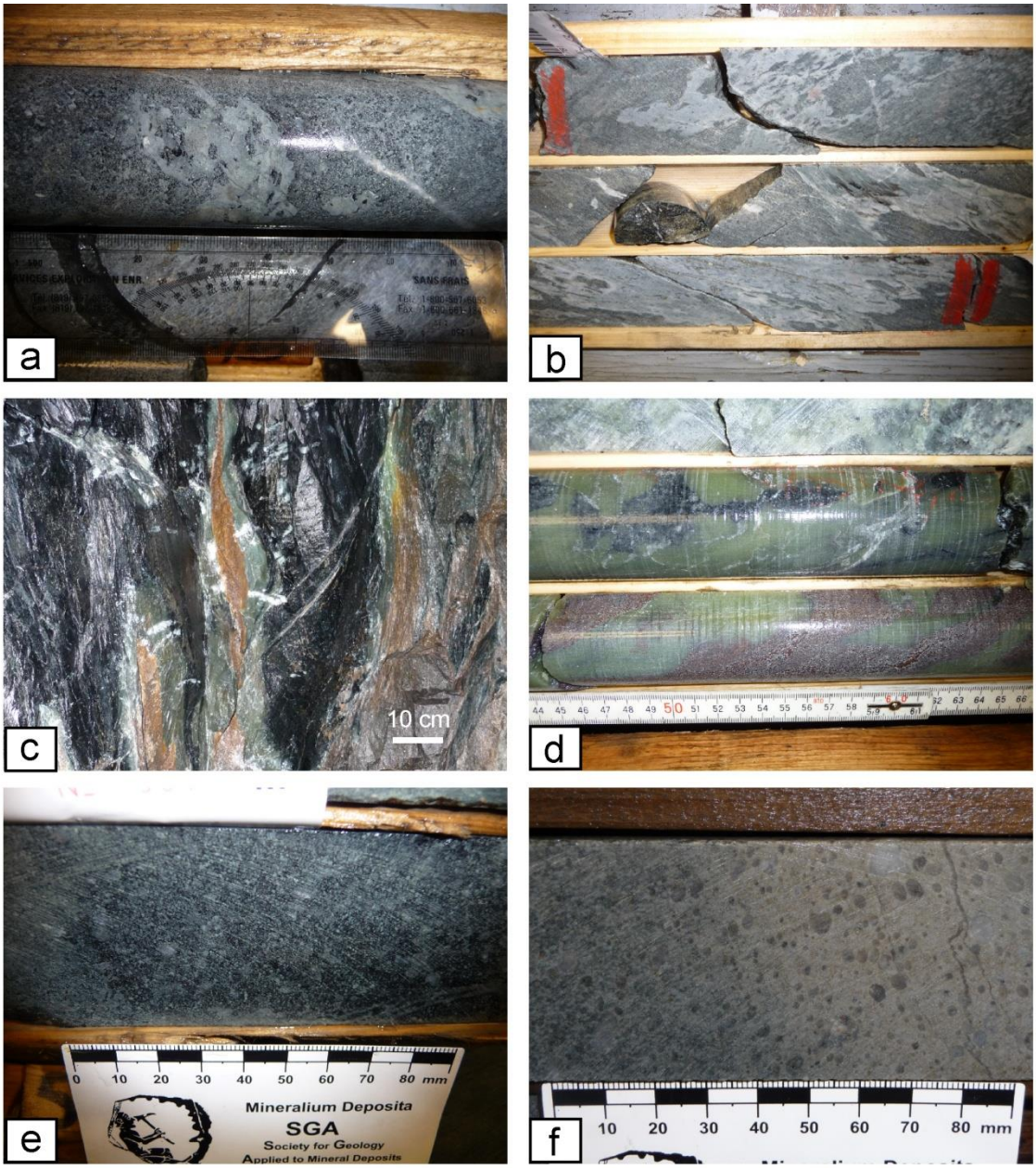

Figure 2.7 Variability in the alteration assemblages at Perseverance and Bracemac-McLeod deposits. a Patchy silicification in the Dumagami rhyodacite at Perseverance (PER-00-54, 74m); b Patchy and pervasive silicification in the Bracemac rhyolite at McLeod (MC-10-92A, 466m); c Talc and sphalerite stringers in the Watson rhyolite at Perseverance (underground); d Strong proximal talc ± chlorite alteration in the Watson rhyolite at Bracemac (BRC-09-152, 546m); e Black chloritization of the Watson rhyolite at McLeod (MC-04-04, 530m); f Distal sericitization of the Watson rhyolite at Bracemac (BRC-07-45, 480m).

Most of the mineralization is present as sub-vertical massive sulfides composed predominately of banded pyrite and sphalerite, with lesser amounts of chalcopyrite, pyrrhotite and magnetite hosted within the Watson rhyolite. The only exception is at Equinox where sulfides are located above the Key Tuffite and appear to replace the Dumagami rhyodacite hanging-wall (Fig. 2.3c). Underground observations (Figs. 2.8a-b and 2.9a) show that silicification and chloritization are also the dominant alteration styles in the Key Tuffite. Hydrothermal fluids have used the primary porosity of the hyaloclastic upper portion of the Watson rhyolite (Fig. 2.8a), or the structural porosity of synvolcanic fractures (Fig. 2.9a) to replace, in some cases totally, the primary textures. This silicification extends into the Dumagami rhyodacite hanging-wall (Fig. 2.8b). The lack of mineralization in the Key Tuffite and the sub-vertical geometry of the orebodies, in a sub-horizontal stratigraphic pile, are unique in the Matagami mining camp. It is apparent from the cross sections (Figs. 2.3b-c) that the orebodies formed by replacement of the Watson rhyolite within synvolcanic structures, below the Archean seafloor. Moreover, both the alteration and mineralization are locally crosscutting the Dumagami rhyodacite hanging-wall indicating that mineralization is mostly epigenetic in origin.

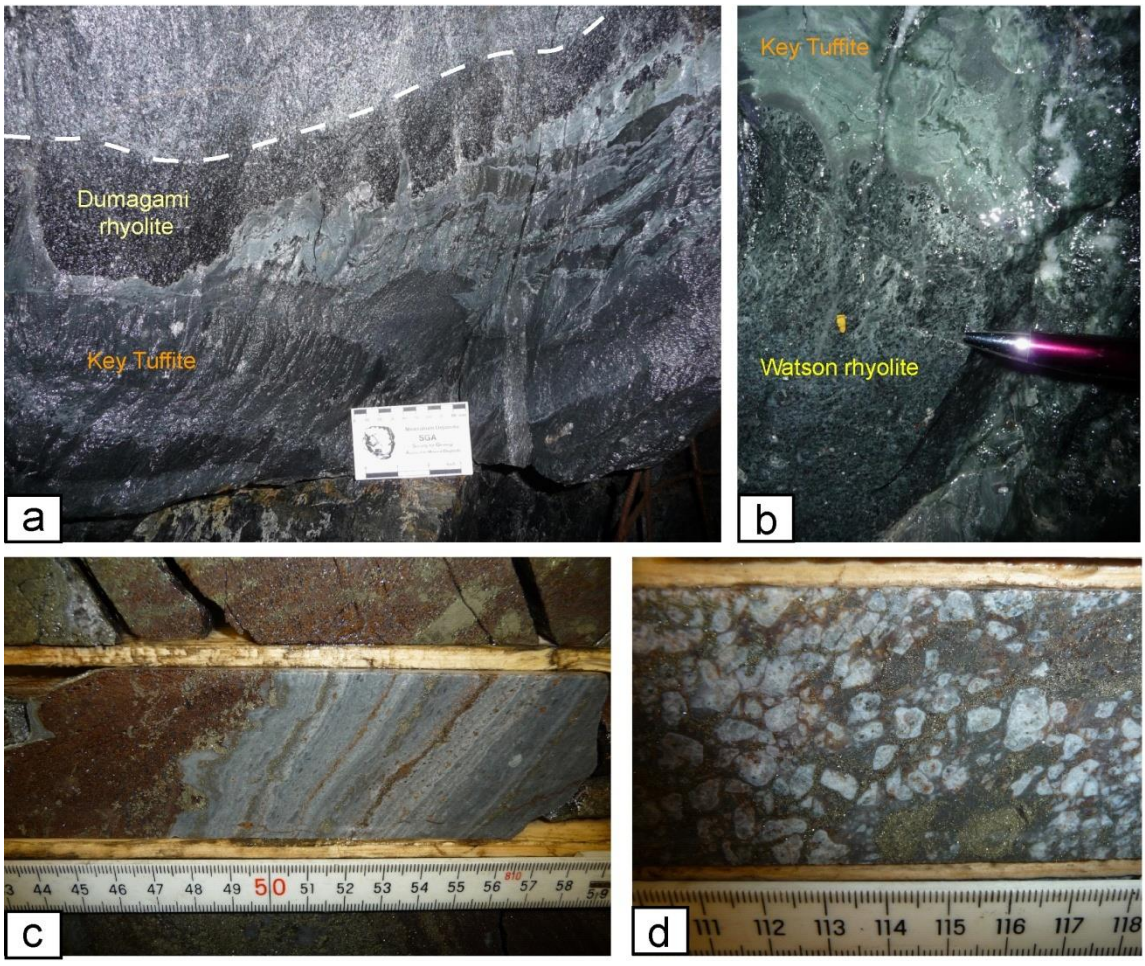

Figure 2.8 Drill-core and underground photographs illustrating the link between Key Tuffite, alteration and mineralization at Perseverance (a-b) and Bracemac-McLeod (c-d). a Silica-rich Key Tuffite and silicification and chloritization of the lower part of the Dumagami rhyodacite (Equinox, underground, level 105-PS26); b Silicification of the hyaloclastic summit of the Watson rhyolite (Equinox, underground, level 105-PS26); c Silicified Key Tuffite enclaved in the massive sulfide zone of Bracemac KT (BRC-09-124, 318m); d Progressive replacement by sphalerite and pyrite of the hyaloclastic summit of the Watson rhyolite at Bracemac (BRC-09-124, 320m).

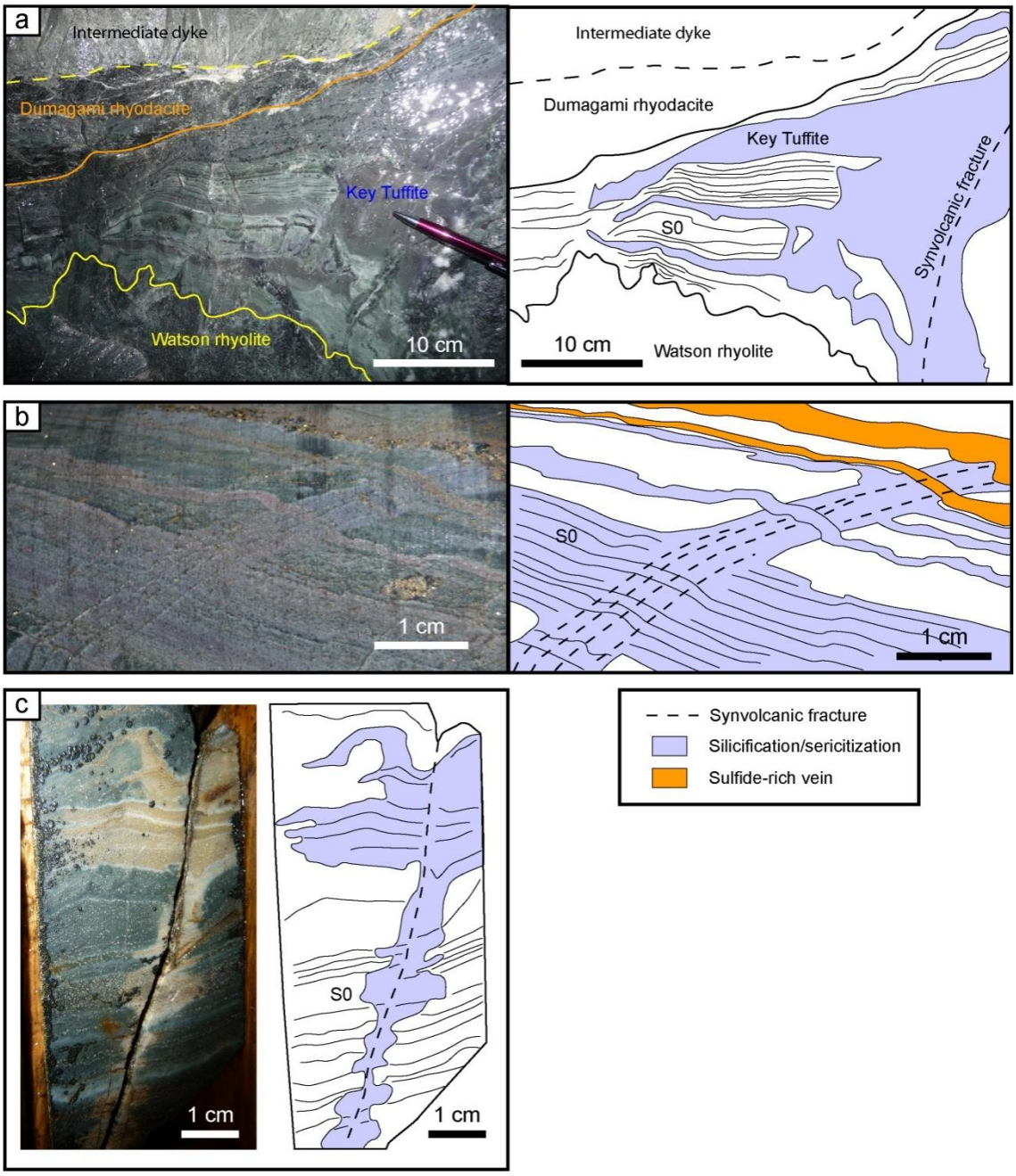

Figure 2.9 Alteration and replacement of specific layers in the Key Tuffite. a Strong silicification of the Key Tuffite at Perseverance (Equinox, underground, level 105-PS26). b Selective silicification at Bracemac (BRC-97-15, 1207m). c Selective silicification/sericitization at Orchan (IM-87-85, 869m).

2.6.4. BRACEMAC-MCLEOD DEPOSITS

The Bracemac-McLeod mine consist of two deposits (Bracemac and McLeod) spatially controlled by synvolcanic faults and separated by a horizontal distance of 1200 m (Fig. 2.4a). In contrast to the sub-vertical conduits of Perseverance, the Bracemac-McLeod orebodies are sheet-like and sub-parallel to the volcanic stratigraphy that dips 55-65° to the south-west. The Bracemac deposit (Fig. 2.4b) comprises 3 distinct lenses, Bracemac KT, Bracemac Main and Upper Bracemac. They form a stacked sequence connected by a chlorite/sulfide alteration structure, which could be interpreted as resulting from the reactivation of a hydrothermal system along a synvolcanic structure after the deposition of the Wabassee Group (Adair, 2009). It is one of the first occurrences of stacked mineralization found in the Matagami Camp. The McLeod deposit is composed of 4 lenses: McLeod Zone, Stringer Zone, McLeod West and the newly discovered McLeod Deep. Apart from the Stringer Zone, which is hosted in the Watson rhyolite, they all occur at the Key Tuffite level. Altogether the Bracemac-McLeod deposits contain measured and indicated mineral resources of 3.6 million tonnes grading 10.6 % Zn and 1.5 % Cu, 32 g/t Ag and 0.5 g/t Au (Côté and Lavigne, 2010). Additional inferred mineral resources of 2.6 million tonnes grading 8.8 % Zn, 1.3 % Cu, 38.8 g/t Ag and 1.1 g/t Au are present in and around the McLeod Zone, including the McLeod Deep lens discovered in 2010 (Roy 2010 in Côté and Lavigne 2010). Geometrically, the extensive and thin stratiform mineralization (~1.6 km and still

open at depth by ~250 m, <20 m thick) of the McLeod deposit along the Key Tuffite unit (Fig. 2.4c) is also divergent from the classic mound-shaped lens model of the Matagami mining camp. The mineralogy of both deposits is dominated by pyrite and sphalerite with lesser amounts of chalcopyrite and pyrrhotite (± magnetite and minor galena). The strong chlorite alteration halo is limited to 50 m stratigraphically below the mineralization, but widespread over 1.6 km along dip (Fig. 2.4). Drill core observations of the Bracemac-McLeod deposits clearly demonstrate that a significant portion of the mineralization crosscuts and locally replaces the following units: 1) the Key Tuffite unit (Figs. 2.8c and 2.9b), 2) the hyaloclastic deposits in the uppermost portion of the footwall Watson rhyolite (Fig. 2.8d), and 3) the Bracemac rhyolite hanging-wall (Fig. 2.4c). In the uppermost portion of the McLeod zone, the majority of the massive sulfide lens is hosted in the Bracemac rhyolite hanging-wall (Fig. 2.4d) whereas at depth it is associated with, or immediately below, the Key Tuffite unit. Genetically, these relationships are not easily reconcilable with an exhalative origin of mineralization on the seafloor; although it can still be argued that the mineralizing event continued after the seafloor covering by the Bracemac rhyolite, as demonstrated by the stacking at Bracemac and McLeod. However, within the Key Tuffite unit both the relative position and textures of the mineralization are highly variable. The silicification and the mineralization commonly crosscuts and replaces the Key Tuffite bedding (Figs. 2.8c and 2.9b) and can occur at any stratigraphic level within the Key

Tuffite, from the upper to the lower contact. These features are not expected for exhalative systems, but are more consistent with a replacement origin (Doyle and Allen, 2003). Based on all the crosscutting, replacement and geometric relationships, it is considered that the epigenetic component of the VMS system was the dominant process in forming the mineralization at Bracemac-McLeod.

2.7. CHEMICAL CHARACTERIZATION OF THE KEY TUFFITE

2.7.1. SAMPLING AND METHODOLOGY

A total of 67 samples of the Key Tuffite, from 48 drill holes, were collected from the surrounding area of Perseverance and Bracemac-McLeod. The position of the samples is illustrated on Figures 2.3a and 2.4a. For comparison, an additional 6 drill-holes (9 samples), located away from all known mineralization (>450 m), were also selected at the scale of the mining camp. Whole-rock geochemistry was carried out on 76 samples of Key Tuffite (20 cm in length) for major, trace and rare earth elements (REE) at the INRS laboratory in Quebec City, Canada. A metaborate fusion was carried out on all samples, prior to Inductively Coupled Plasma-Atomic Emission Spectrometry (ICP-AES) and Mass Spectrometry (ICP-MS) analyses, for a total dissolution of resistant minerals. Standards were used to monitor the accuracy (within 10% relative difference) and reproducibility (< 10% relative standard deviation) of the analyses (electronic supplementary material). Supplementary Key Tuffite data (n = 25) from Perseverance, analysed by

Glencore at ALS Chemex laboratory (Canada), were integrated into our database. Results for major, trace and rare earth elements for all samples are given in the Appendix 2. Table 2.2 presents average concentrations and standard deviation for selected major, trace elements and REE in the Key Tuffite samples from the Perseverance, Bracemac-McLeod deposits and from samples located away from known mineralization.

The composition of individual millimetric layers was analysed by Laser Ablation (LA) ICP-MS at the University of Quebec at Chicoutimi (UQAC), Canada, in order to investigate the origin of the layering of the Key Tuffite. The methodology follows the one described by Baldwin et al. (2011) developed for in situ analyses of chert microbands in iron formations. The results, standards and details on the method are also presented in the electronic supplementary material.

2.7.2. TUFFACEOUS COMPONENT

The characterization of the tuffaceous component is critical to understand the petrogenesis of the Key Tuffite. Furthermore, this component has the potential to dilute the hydrothermal component (i.e., exhalative and/or alteration). The identification of the tuffaceous source/s can only be approached by the use of immobile elements. In VMS systems, most of the major and many of the trace elements are mobile during hydrothermal alteration (Barrett and MacLean, 1999). Only TiO_2 and Zr are considered immobile even during extreme alteration (Finlow-

Bates and Stumpfl, 1981). Thus, the ratio of these two elements is commonly used to discriminate altered rocks in volcanic terranes (e.g., MacLean and Kranidiotis, 1987; Barrett et al., 2005). Figure 2.10a represents a plot of immobile elements for all the volcanic rocks around the Bracemac-McLeod and Perseverance area. Although the absolute TiO_2 and Zr values are highly variable, the ratios remain constant for each lithology and plot along different alteration lines through the origin. The $Zr/(TiO_2 \times 10000)$ ratios of the Bracemac and Watson rhyolites (0.2) are an order of magnitude higher than those of the Wabassee andesite (0.01) and Key Tuffite (0.03) (Table 2.1). The Key Tuffite was interpreted by Liaghat and MacLean (1992) to be a mixture of andesitic calc-alkaline (Wabassee Group) and rhyolitic tholeiitic material (Watson Lake Group). However, the Key Tuffite is clearly different in composition from the underlying Watson rhyolite and overlying Bracemac rhyolite (Fig. 2.10a) suggesting a negligible input of rhyolitic ash. In addition, the samples plot along a line passing through the origin with correlative values for Pearson product of 0.90 and R^2 of 0.81 for these immobile elements (Fig. 2.10). Such a sample distribution clearly indicates that the composition of the tuffaceous component was a homogeneous ash prior to mass gain and loss induced by hydrothermal alteration. If different sources were involved in the formation of the Key Tuffite, a much wider dispersion and/or different slopes of the alteration lines would be expected on the immobile element plots. The similarity of the alteration lines between the Key Tuffite and

the andesitic unit of the hanging-wall Wabassee Group (Fig. 2.10a) and a plot of Nb/Y versus Zr/TiO_2 (Fig. 2.10b) indicate an andesitic composition of the Key Tuffite. The dispersion of samples along the Nb/Y axis indicates that Y was not entirely immobile, as already demonstrated by Finlow-Bates and Stumpfl (1981) in VMS environments.

In order to establish the tuffaceous component composition prior to hydrothermal alteration, the unaltered precursor was calculated using an average of 9 samples from 5 drill holes located more than 450 m away from any known deposit. Two of these 9 selected Key Tuffite sections are presented in Figure 2.2.

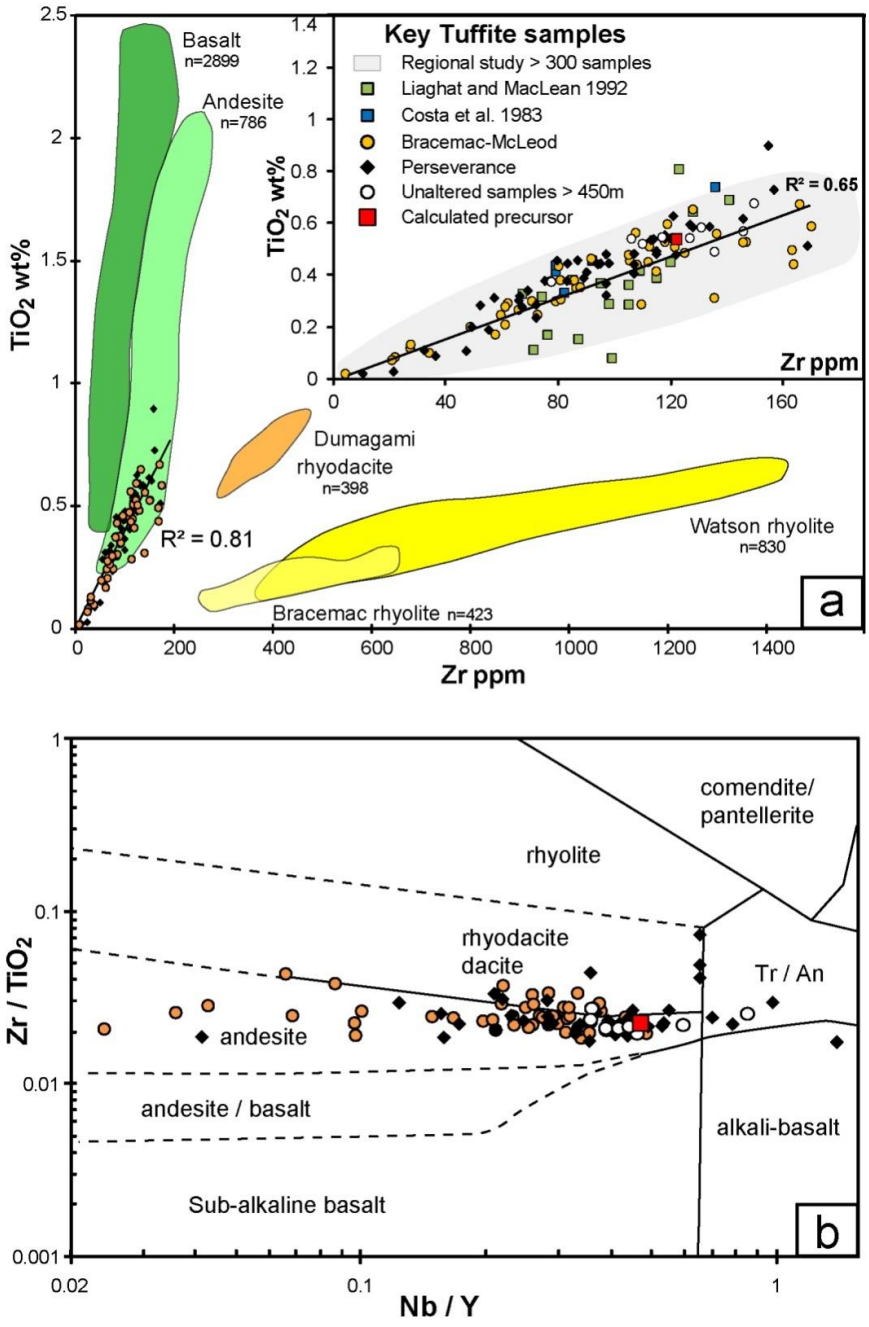

Figure 2.10 Whole-rock geochemistry of the volcanic rocks of Matagami. a. In Zr versus TiO2, fields represent the different lithologies and are based on the Glencore geochemical database. Inset: Key Tuffite data compilation from Genna (unpublished). b. Zr/Ti versus Nb/Y diagram of Winchester and Floyd (1977).

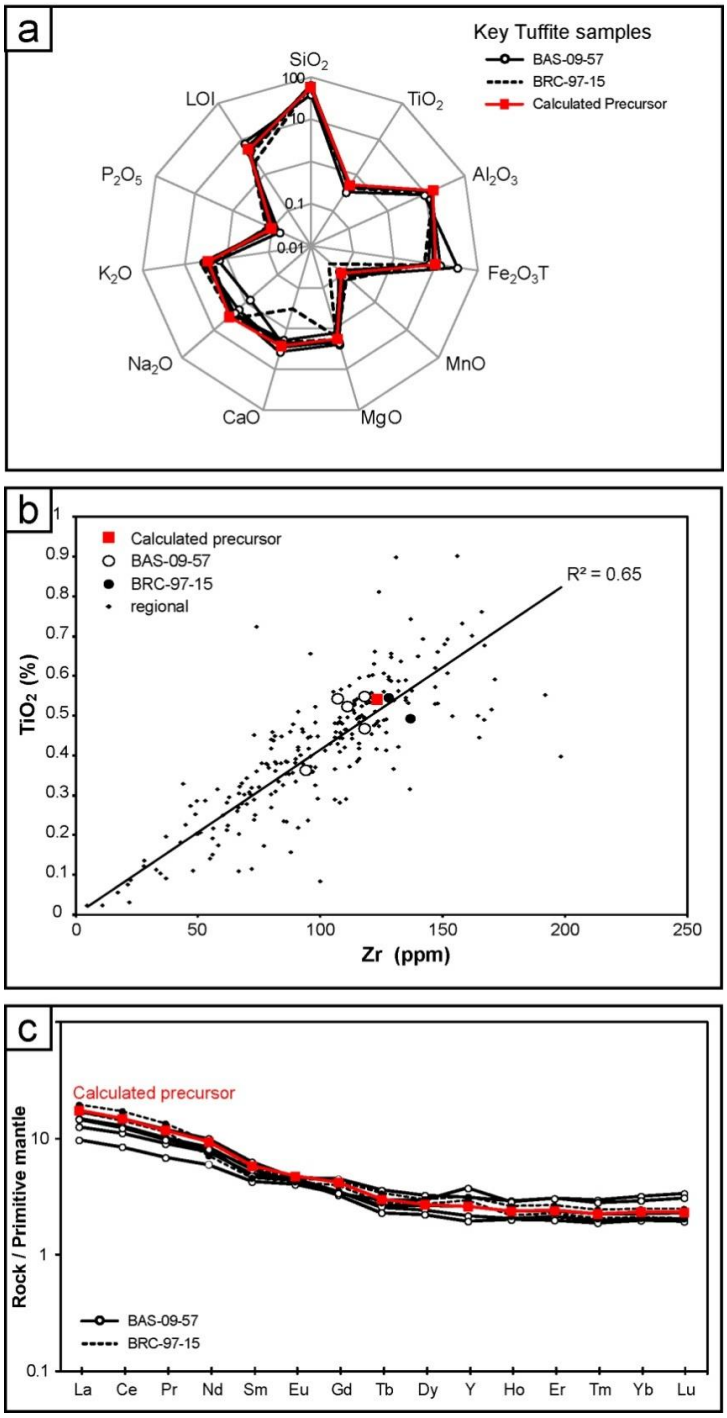

Figure 2.11 Detailed geochemistry of the Key Tuffite away from the mineralization (>1km) from the 2 drill hole (BAS-09-57 and BRC-97-15; Figures 1 and 2). a Spidergram for the major elements. b Zr vs. TiO_2. c REE-Y multi-element variation diagrams normalized to Primitive Mantle values from Sun and McDonough (1989).

Geochemical data confirm the homogeneous composition for the major (Fig. 2.11a), trace (Fig. 2.11b) and rare earth elements (Fig. 2.11c) highlighting the absence of vertical geochemical variation despite the textural diversity. The alteration box plot (Large et al., 2001b), used as an external validation, confirms the minimal chemical change undergone by the 9 samples selected for the precursor calculation (Fig. 2.12). As expected, the selected samples plot within the field of unaltered andesite established by Gemmell and Fulton (2001). All the other samples from around the Perseverance and Bracemac-McLeod deposits, except one, are extremely altered and plot toward the chlorite pole. The arithmetic average of the composition of these 9 samples is considered to represent the initial precursor and thus the tuffaceous component composition (Table 2.2).

The REE are also generally considered as immobile and consequently are widely used for establishing volcanic stratigraphic successions (MacLean, 1988; Barrett et al., 2005) and source determination for sedimentary rocks (Bierlein, 1995). As shown in Figure 2.13a, the Key Tuffite has a different REE-Y pattern to the Bracemac and Watson rhyolites and is closer in composition to the Wabassee mafic units.

	Chlorite Zone Bracemac-McLeod		Chlorite Zone Perseverance		Sericite Zone Bracemac-McLeod		Calculated precursor >450m	
	n=37		n=47		n=8		n=9	
%	Average	σ	Average	σ	Average	σ	Average	σ
Loi	5.80	3.22	5.10	2.01	4.47	1.12	5.26	2.52
Al2O3	9.21	4.59	10.51	4.18	12.75	2.76	15.22	1.60
CaO	0.86	1.43	0.47	1.32	1.41	1.18	2.75	2.06
Fe2O3T	15.64	9.38	7.21	3.12	9.02	2.33	9.47	3.22
K2O	1.59	1.64	0.20	0.35	3.22	1.85	2.77	0.95
MgO	2.66	1.40	9.45	3.61	2.05	1.57	1.85	0.67
MnO	0.11	0.12	0.05	0.03	0.06	0.02	0.09	0.05
Na2O	0.13	0.40	0.32	0.72	0.70	0.81	3.40	1.58
P2O5	0.07	0.04	0.07	0.08	0.09	0.03	0.10	0.03
SiO2	60.92	12.92	65.80	10.57	63.72	4.88	56.12	7.29
TiO2	0.33	0.16	0.39	0.17	0.46	0.09	0.51	0.07
ppm								
Zr	86.75	41.10	93.10	35.66	123.65	34.49	123.21	22.53
Nb	3.44	1.64	3.79	1.79	4.99	1.28	5.59	2.78
La	10.22	7.20	8.30	4.97	16.75	8.07	12.03	3.88
Ce	22.63	16.26	18.01	10.58	37.86	17.25	26.56	8.44
Pr	2.91	2.14	2.22	1.24	4.84	2.27	3.28	1.15
Nd	11.60	9.67	9.27	5.00	20.94	9.62	12.76	4.69
Sm	2.87	2.58	2.18	0.93	5.08	2.73	2.59	0.95
Eu	0.99	0.58	0.62	0.25	1.01	0.33	0.80	0.28
Gd	2.86	2.39	2.00	0.79	4.91	2.75	2.51	1.10
Tb	0.42	0.38	0.28	0.12	0.73	0.40	0.33	0.14
Dy	2.56	2.49	1.72	0.72	4.31	2.22	2.01	0.67
Y	18.40	19.36	11.18	8.11	26.66	14.01	11.94	4.33
Ho	0.54	0.58	0.35	0.14	0.87	0.45	0.39	0.13
Er	1.54	1.55	1.02	0.39	2.40	1.12	1.16	0.33
Tm	0.22	0.22	0.15	0.05	0.35	0.15	0.17	0.05
Yb	1.40	1.29	1.03	0.34	2.18	0.85	1.17	0.32
Lu	0.21	0.19	0.15	0.05	0.33	0.12	0.17	0.05
ΣREE	60.97	44.17	47.30	23.81	102.56	47.07	65.93	21.84

Table 2.2 Median compositions of the Key Tuffite around the Perseverance and Bracemac-McLeod deposits and calculated precursor.

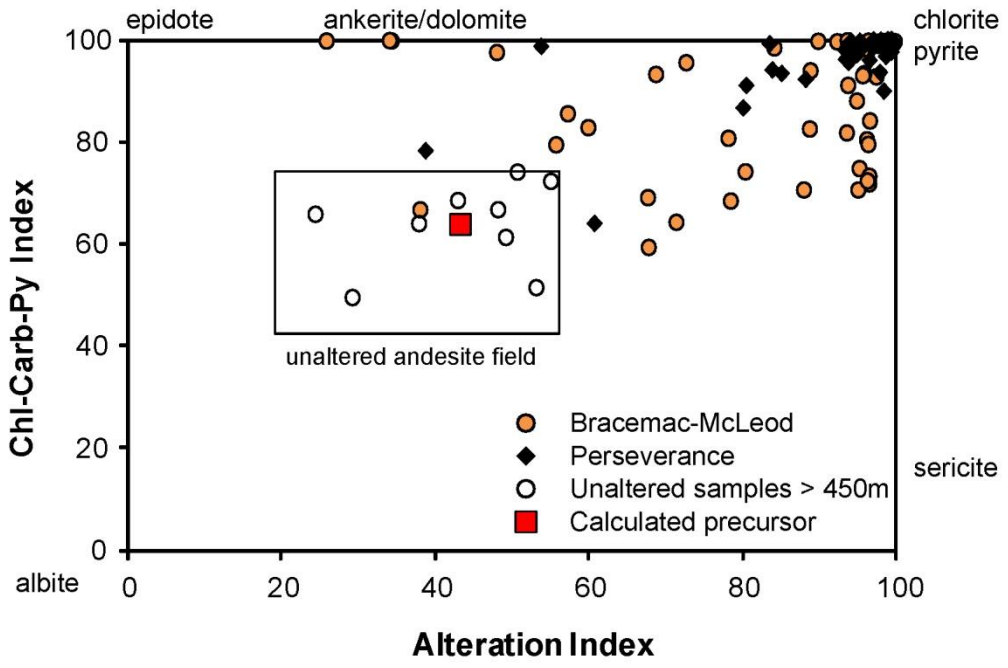

Figure 2.12 Alteration Box Plot for the Key Tuffite samples (modified from Large et al. (2001b). AI = Ishikawa alteration index; CCPI = chlorite-carbonate-pyrite index.

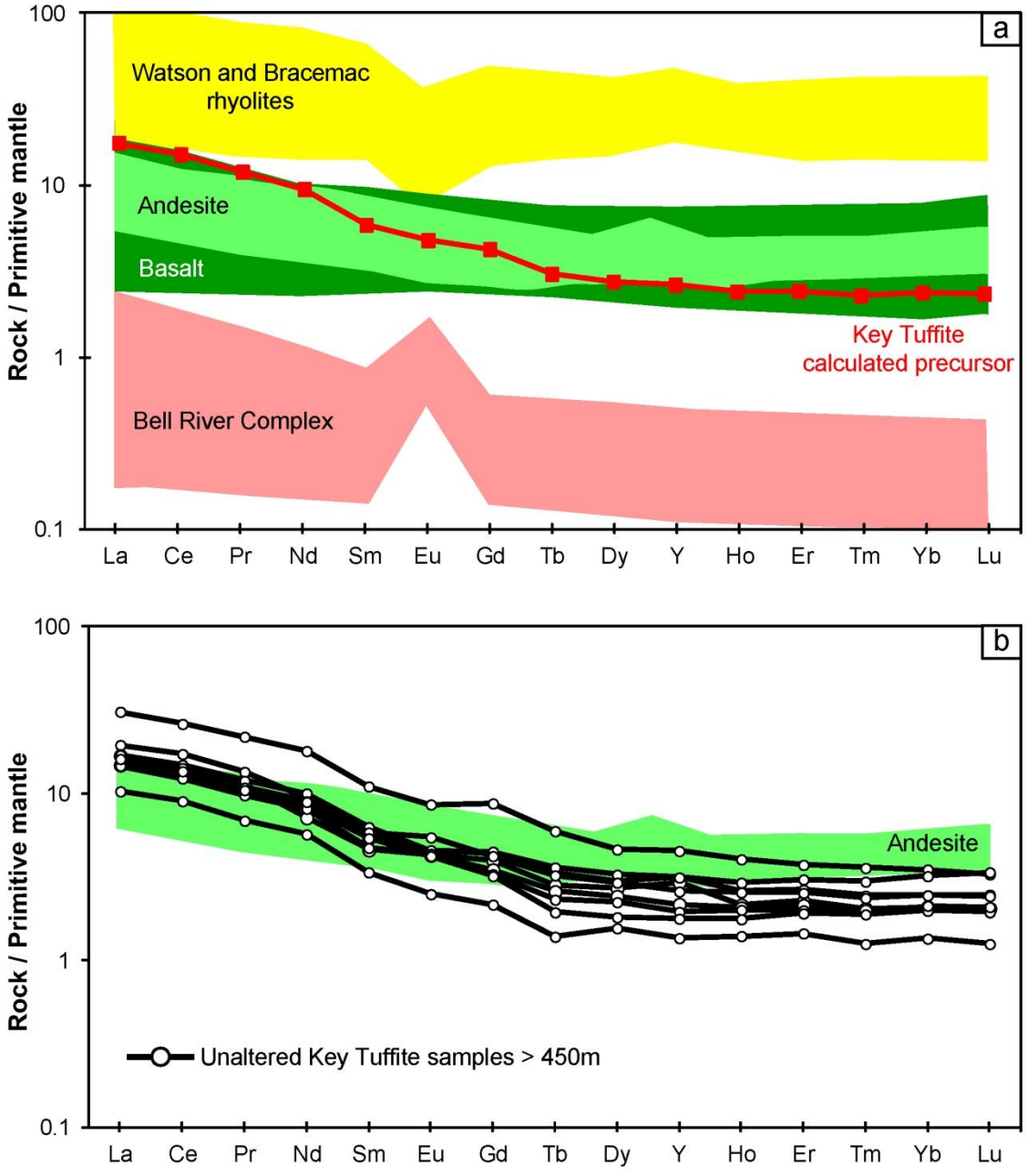

Figure 2.13 REE-Y multi-element variation diagrams normalized to Primitive Mantle values from Sun and McDonough (1989). a Volcanic rocks of Matagami. Fields are from Gaboury and Pearson (2008), Piché (1991), Munoz Taborda (2011), Maier et al. (1996) and Debreil (pers. comm.). b Comparison between unaltered Key Tuffite samples and the lower andesitic unit of the Wabassee. Field from Debreil (pers. comm.).

Taking into account the REE-Y content and the La/Yb and Zr/Y ratios (Table 2.1), the best candidate matching the Key Tuffite composition is the lower andesitic unit of the Wabassee. This unit directly overlies the Key Tuffite along most of the South Flank, but not at Bracemac-McLeod and Perseverance (Figs. 2.3 and 2.4). Figure 2.13b compares the REE-Y content of the unaltered Key Tuffite samples with the Wabassee andesite. Despite the similarity in the REE-Y values, unaltered Key Tuffite samples have a slightly more fractionated pattern compared to the andesite.

2.7.3. HYDROTHERMAL COMPONENT

In order to calculate the hydrothermal effect on the tuffaceous precursor, a mass change calculation was used, based on the MacLean and Kranidiotis (1987) single precursor approach. The gain or loss of an element was calculated by subtracting the reconstituted value of the mobile element in the altered sample from that in the precursor. The general equation, using SiO_2 as an example and TiO_2 as the immobile monitor, is as follows:

$$\Delta\ SiO_2 = (TiO_2\ \text{precursor} / TiO_2\ \text{sample} * SiO_2\ \text{sample}) - SiO_2\ \text{precursor}$$

The results are expressed in terms of mass change in weight percent (Δ). Figure 2.14 represents the results of the mass change calculation for the major elements as a function of the distance toward the Bracemac-McLeod and Perseverance

deposits. The composition far from the deposit is homogeneous with minimal alteration until 230 m from the mineralization. From this point toward the deposits, the composition systematically increases for most elements (except K_2O and Na_2O). In particular, ΔFe_2O_3 and ΔMgO represent a strong chloritization halo about 230 m around Perseverance and Bracemac-McLeod. Despite the similar general increase of these 2 elements towards the mineralization, the behaviour of Fe_2O_3 and MgO in the vicinity of the 2 deposits (last 100 m) is different. At Perseverance, ΔFe_2O_3 is significantly lower than that at Bracemac-McLeod (median of -0.9 % compared to 16.5 %, respectively). This is explained by the lack of sulfides (pyrite) in the Key Tuffite overlying the mineralization at Perseverance. In contrast, ΔMgO is higher at Perseverance than at Bracemac-McLeod (median of 12.1 % against 2.2 %) due to a greater abundance of talc in the alteration halo at Perseverance. Based on petrographic examination (Fig. 2.6b), sericite appears to be the only K-bearing hydrothermal mineral phase; therefore, the ΔK_2O is interpreted to reflect the distribution of sericite alteration. Mass gain of K_2O (up to 3.2 %) occurs between 400 and 230 m and represents a strong sericite alteration. The uniform depletion of Na_2O closer than 400m (median of -3.5 %) illustrates the breakdown of plagioclase during sericitization (e.g. Eastoe et al., 1987).

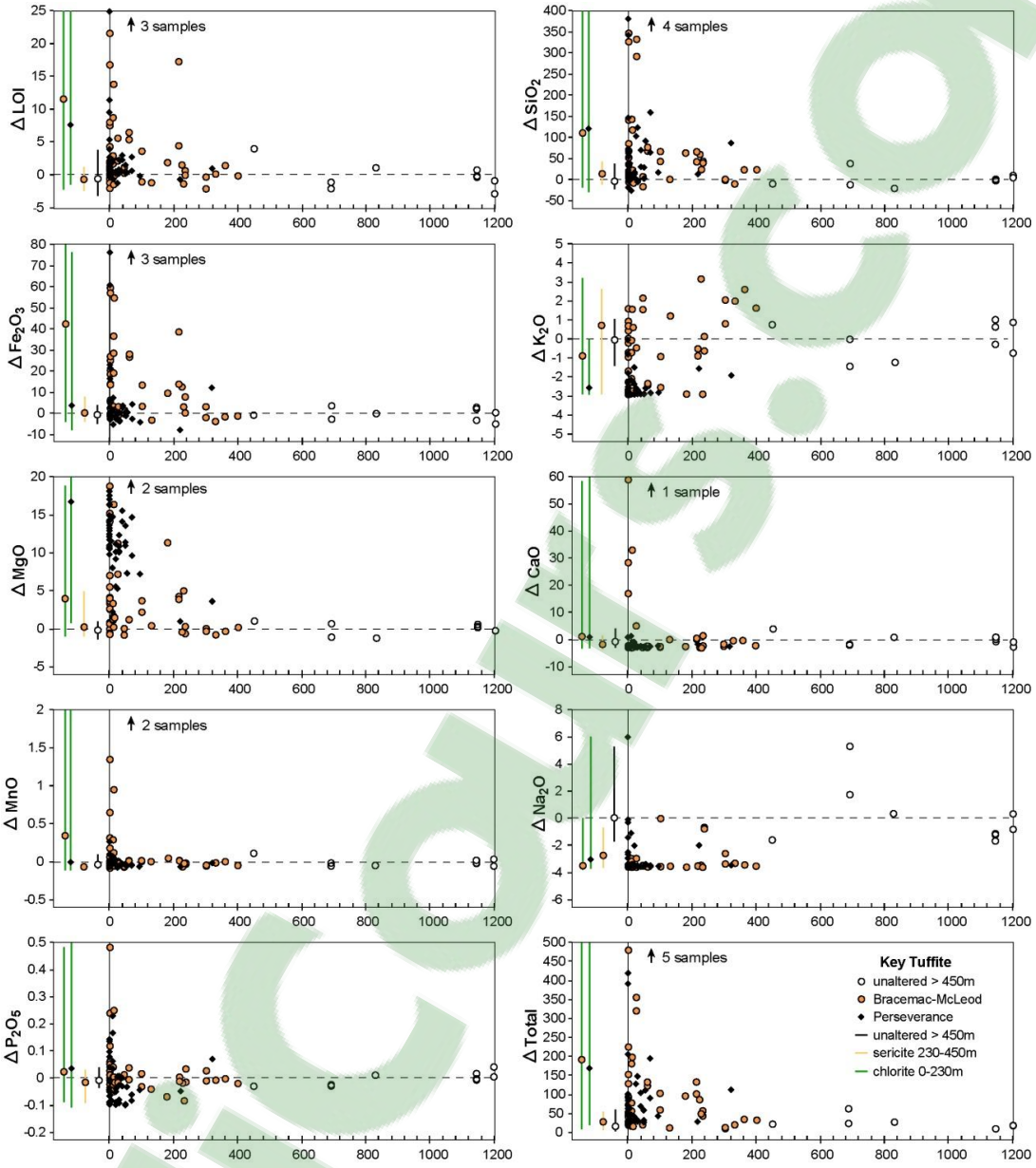

Figure 2.14 Mass balance calculation for the major elements versus distance towards Bracemac-McLeod and Perseverance deposits. The bar graph on the left-hand side of each diagram give the minimum, maximum, and median values for both Perseverance and Bracemac-McLeod deposits and for each alteration facies.

Then mass loss of K_2O (up to -2.9 %) is dominant between 230 and 20 m, apart from one anomalous sample, and illustrates the classic VMS alteration transition by breakdown of sericite to form chlorite (e.g. Sangster, 1972; Lydon, 1984; Large, 1992; Large et al., 2001b). Finally both mass gain and loss in K_2O are recorded in the Key Tuffite in the last 20 m around the mineralized lenses. The more restricted sampling around the Perseverance deposit (only 2 samples between 200 and 400 m) does not allow the observation of the same pattern.

2.7.4. SIGNIFICANCE OF LAYERING

The finely developed layering in the Key Tuffite was previously presented as evidence for component mixing of variable tuffaceous sources (Liaghat and MacLean, 1992) and exhalative chemical precipitates (Davidson, 1977). The layering is particularly well developed in the Key Tuffite at Perseverance (Figs. 2.5f and 2.15) and together with the absence of sulfide implies that it was preserved from later modification by epigenetic mineralization. This portion is thus considered as the best candidate for testing 1) mixing of ash and 2) a possible low temperature chemical silica precipitate. A total of 8 lines from 3 zones (Fig. 2.14 and electronic supplementary material) were ablated by LA-ICP-MS: 6 represent different silica-rich layers and 2 are perpendicular to layering (i.e., including chlorite and silica-rich layers). Results show that REE-Y patterns are very similar to each other, regardless of their silicic or chloritic composition, and

are very similar to the composition of the corresponding whole-rock analysis (Fig. 2.11a). A distinctive felsic ash contribution accounting for the silicic layers can be discarded, as REE patterns are not similar to whole-rock pattern of rhyolites. Furthermore, the similarity of REE patterns from silicic to chloritic layers is more compatible with a silicification overprint of a homogeneous andesitic layered tuffaceous rock rather than that of ash and exhalative chemical precipitate mixing. Therefore, the in-situ LA-ICP-MS results confirm the homogeneous andesitic composition of the Key Tuffite.

2.8. DISCUSSION

2.8.1. ORIGIN OF THE KEY TUFFITE

2.8.1.1. TUFFACEOUS COMPONENT

Liaghat and MacLean (1992) investigated the parental tuffaceous component. They proposed, with a limited number of samples (Fig. 2.10a inset), that the tuffaceous component resulted from mixing calc-alkaline andesite and tholeiitic rhyolite ashes in various proportions. The distinction of these 2 end-member sources was based on wide variation of the LREE-Y values and variable slopes of alteration lines (Figs. 7a-b of Liaghat and MacLean 1992). Instead, our larger database indicates that the Key Tuffite unit, on the South Flank of the Matagami district, is andesitic in composition (Fig. 2.10) with a calc-alkaline affinity (Table 2.1).

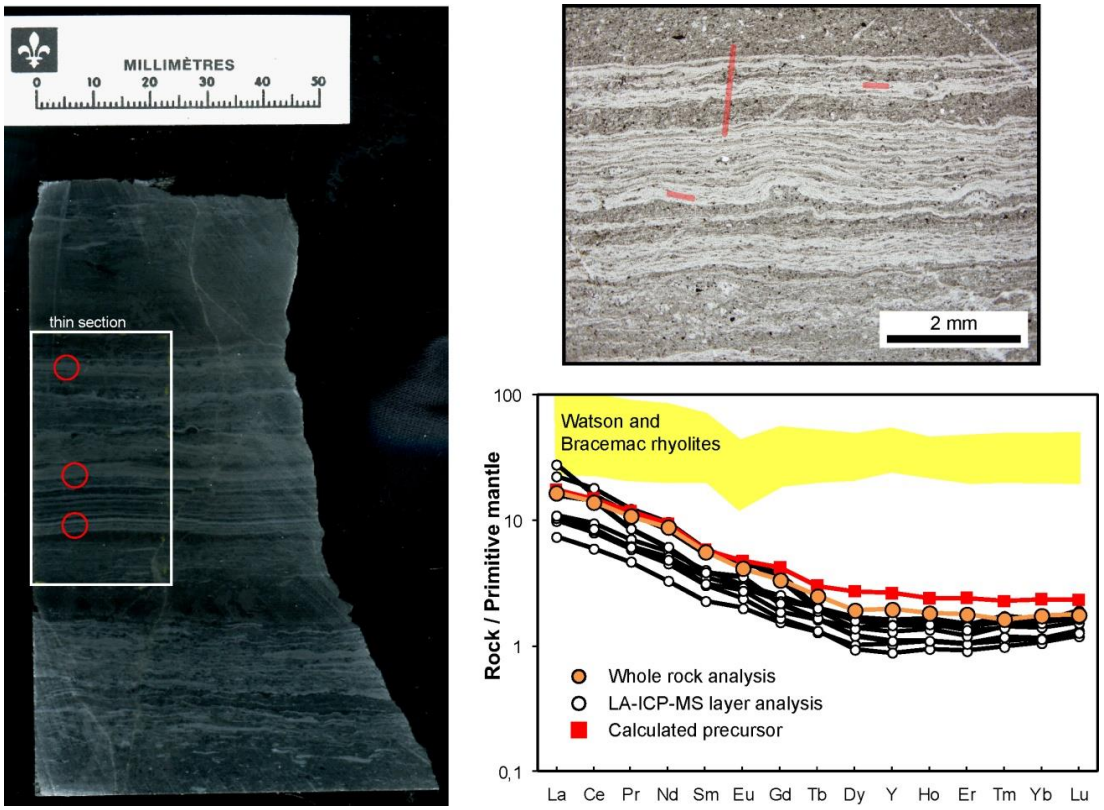

Figure 2.15 In situ LA-ICP-MS analyses in a Key Tuffite sample from Perseverance mine (969352, Equinox, underground, level 105-PS26). Red lines on the microphotograph are laser ablation lines.

The composition prior to hydrothermal alteration was homogeneous as shown by a Pearson product of 0.90 with a R^2 of 0.81 for the immobile elements (Zr-TiO_2, Fig. 2.10a). Furthermore, data from Liaghat and MacLean (1992) also yield a Pearson product of 0.82 with a R^2 of 0.67 indicating, in combination with data from previous studies (Fig. 2.10a inset), that the Key Tuffite unit is not the result of volcanic ash mixing. This is confirmed not only by our regional study (Genna, unpublished) on more than 300 whole rock analyses from the whole mining camp (Fig. 2.10a inset) but also by the LA-ICP-MS analyses at the scale of the thin section (Fig. 2.15). The lower andesitic unit of the Wabassee Group directly overlies the Key Tuffite over most of the South Flank, except in the Perseverance and Bracemac-McLeod areas (Fig. 2.1). The stratigraphic position and the similarity in composition (Fig. 2.10a) of the Key Tuffite with this andesite suggest a genetic link.

The andesite represents the logical effusive equivalent of the Key Tuffite and is the best candidate for the source of the tuffaceous component of the Key Tuffite. The only other alternative would be a hypothetical unknown source from outside the Matagami volcanic succession. However, despite the similarity in the REE-Y values (Fig. 2.13b), unaltered Key Tuffite samples have a slightly more fractionated pattern than the andesite. These differences and any variation within the Key Tuffite itself, such as REE fractionation, could be attributed to 1) physical processes, such as sorting (Fralick and Kronberg, 1997), fragmentation during a

volcanic explosion (Wolff, 1985; Horwell et al., 2001) and/or 2) chemical processes during explosion (Moune et al., 2006) or prolonged interaction between seawater and suspended ash particles (Sholkovitz et al., 1994). The Key Tuffite is only composed of fine ash resulting from an efficient process of subaqueous fragmentation. Thus the Key Tuffite could have been highly susceptible to both the physical and chemical effects. Ultimately, hydrothermal alteration can also mobilize the LREE and Y (Finlow-Bates and Stumpfl, 1981), which has been documented at Matagami in the Watson rhyolite footwall of several deposits (MacGeehan and MacLean, 1980; MacLean, 1988).

Our interpretation is that the Key Tuffite represents the explosive equivalent of the lower andesitic lava of the Wabassee and thus marks the initiation of the mafic volcanism. The volume of ash (up to10 m thick by >17 km in length north-south and by >1km wide east-west) can be explained by a catastrophic explosive event or by a multitude of mafic eruption centers, as proposed by Sharpe (1968) based on the abundance of coarse breccias, and the lateral facies variations within the Wabassee. The lack of lateral variation in grain size, the well-developed planar beds and the uniform thickness of the Key Tuffite draping the topography of the Watson rhyolite indicate that the Key Tuffite formed as a waterlain tuff which saturated the water column (Gibson et al., 1999). The thin laminations preserved in the Key Tuffite suggest quiet depositional conditions in a relatively deep basin. The record of the progressive settling of the fine andesitic ash in suspension

represents an important volcanic hiatus which was previously linked to the mineralization event (Liaghat and MacLean, 1992; Maier et al., 1996). The intercalation of the Key Tuffite within the Watson rhyolite and the Dumagami rhyodacite or Bracemac rhyolite implies a synchronism/overlap between the beginning of the mafic lavas and the end of the felsic volcanic activity.

2.8.1.2. EXHALATIVE COMPONENT

Drill-core observations at Bracemac-McLeod and underground observations at Perseverance (Figs. 2.8 and 2.9) provide evidence that the mineralization formed mainly by replacement processes. As a consequence, the exhalative component should be negligible in the Bracemac-McLeod and Perseverance vicinity, and presumably elsewhere in the camp. This is commonly tested by a Fe/Ti vs. Al/(Al+Mn+Fe) plot which is used to estimate the proportion of tuffaceous and exhalative components in ancient (Barrett, 1981; Wonder et al., 1988; Peter et al., 2003) and modern (Boström, 1973; Slack et al., 2009) deep-sea sediments. The Fe and Mn supposedly represent the exhalative contribution, whereas the Al and Ti represent the tuffaceous component. Liaghat and MacLean (1992) applied this plot for the Key Tuffite and the least altered volcanic rocks from Matagami. The entire set of Key Tuffite samples plot along a curve joining the clusters of fresh mafic and felsic rocks and the metalliferous sediments of the East Pacific Rise (Fig. 2.16a). Therefore, some samples were interpreted to be composed of more

than 80% of metalliferous sediments (Fig. 11 in Liaghat and MacLean 1992). However, altered Watson rhyolite and Wabassee andesite follow the same trend as the Key Tuffite (Fig. 2.16a) indicating that this trend does not only represent an exhalative contribution but can also illustrate the alteration by an increase in sulfides (Fe) and chlorite (Fe+Mn) abundance. These results underline the limitations of this plot for deciphering the contribution of hydrothermal (exhalative or epigenetic) and tuffaceous component in an ancient and altered volcanic sequence.

Figure 2.16b represents a plot of Y/Ho versus Eu/Eu* (modified from Pinti et al., 2009) which has been proposed to discriminate chemical precipitation of chert versus replacement processes based on three end-members: 1) high temperature fluid (Douville et al., 1999); 2) Archean seawater, represented by Strelley Pool stromatolites (Van Kranendonk et al., 2003); and 3) andesite of the Wabassee Group, representing the tuffaceous component of the Key Tuffite. Silica precipitated from Archean seawater (Van Kranendonk et al., 2003) should have high Y/Ho ratios (~ 70) and moderately high europium anomalies (Eu/Eu* ≈ 1). Exhalative chert should be a mixture of seawater and hydrothermal fluids (Pinti et al. 2009), the latter characterized by a positive europium anomaly (Eu/Eu*>>1).

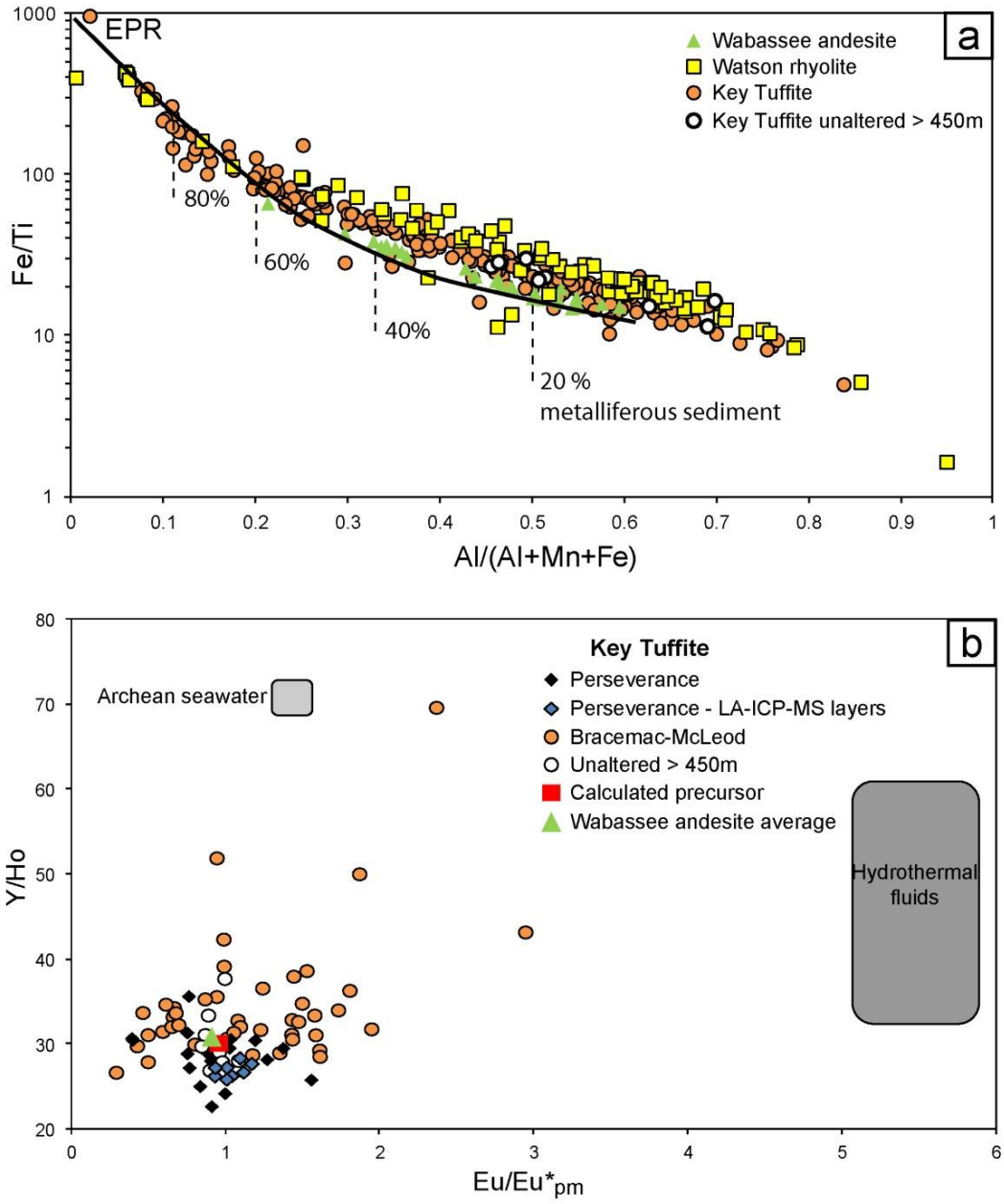

Figure 2.16 Geochemical plots to determine any exhalative component in the Key Tuffite. a Fe/Ti vs. Al/Al+Mn+Fe plot, modified from Boström (1973). Rhyolite and andesite data from Matagami (Glencore) for comparison. EPR=East Pacific Rise metalliferous sediments. b Y/Ho vs. Eu/Eu*pm plot, modified from Pinti et al. (2009). pm=primitive mantle normalization from Sun and McDonough (1989).

The replacement of tuff or volcanoclastic debris by silica from hydrothermal fluids would result in limited dispersion around the original composition of the precursor, which has low europium and Y anomalies. This graph shows that data from individual silicic layers analyzed at Perseverance (Fig. 2.15) plot close to the Wabassee andesite and the Key Tuffite calculated precursor, indicating, in agreement with whole-rock Key Tuffite analyses, that replacement processes are dominant and that an exhalative component from high temperature fluids mixing with seawater is negligible around the Perseverance and Bracemac-McLeod deposits.

2.8.1.3. EPIGENETIC HYDROTHERMAL ALTERATION COMPONENT

Based on new high-precision U-Pb age of the Watson, Dumagami rhyodacite and Bracemac rhyolite, Ross et al. (2014) proposed that the Key Tuffite and mineralization were deposited on the seafloor between 2725.9 Ma and 2725.4 Ma. However field relationships between the mineralization and the Key Tuffite at Perseverance and Bracemac-McLeod (Fig. 2.8) and geochemistry of the Key Tuffite (Fig. 2.16) show that the mineralization was, for a major part, not coeval with the deposition of the Key Tuffite, but younger. Longuépée (2009) documented that an alteration halo is present in the hanging-wall of most of the deposits located along the South Flank of Matagami. Although less extensive than

that of the footwall, the alteration is similar in chemistry and persistent up to 40 m above the mineralization. This pattern, in agreement with our observations of mineralization within the Dumagami and Bracemac rhyolites, indicates that the main stage of mineralization occurred either during the deposition of the hanging-wall rhyolites or that the VMS were mostly formed by sub-seafloor replacement. Consequently, the epigenetic alteration constitutes a significant component in the Key Tuffite, a feature confirmed by the mineral assemblage. The fine-grained mosaic of quartz, sericite, chlorite and carbonates is the typical hydrothermal alteration assemblage observed in the host rocks surrounding the mineralization at Matagami (Figs. 2.3, 2.4 and 2.7). The hydrothermally altered Key Tuffite laterally grades into unaltered equivalent rocks (Fig. 2.2). The lateral alteration of the Key Tuffite was geochemically tested using a mass gain and loss calculation versus the distance towards the deposits. The results (Fig. 2.14) show a coherent alteration pattern around the Bracemac-McLeod deposits: a proximal intense chloritization (<230 m) within a larger sericitization halo (230 to 400 m). Alteration halos present within the Watson rhyolite footwall are identical in chemistry and similar in dimension to the alteration halo in the Key Tuffite. It represents the first documentation of a coherent geochemical variation in the Key Tuffite toward a deposit in the Matagami mining camp, and thus a useful vector for exploration.

2.8.1.4. SILICIFICATION AND LAYERING

Based on geochemistry, it is shown that the layering is not the product of mixing of 2 different source of volcanic ash (Fig. 2.10). The exhalative component is also negligible (Fig. 2.16), even in the finely layered chert zones (Fig. 2.15), confirming that layering is not the result of hydrothermal precipitation on the seafloor. Furthermore, layered and massive samples taken away from VMS deposits have a very similar composition indicating that the composition of the Key Tuffite is homogeneous at all scales (Figs. 2.11 and 2.15). As such the thin planar layering is not the result of mixing multiple components, but instead the result of a progressive deposition of variable grain sizes of one type of ash in the water column (McPhie et al., 1993).

The apparent interbedding of silica, sulfide and chlorite in the Key Tuffite (Fig. 2.5) most likely resulted from selective replacement of more permeable ash layers whereas the finer-grained, and less permeable, layers remained less altered (Bodon and Valenta, 1995; Galley et al., 1995; Doyle and Allen, 2003). Layering is well developed only in the chert-rich sections of the Key Tuffite (Figs. 2.5b and f) suggesting that layering has been preserved and even highlighted by silicification. This process is well exposed at Perseverance where the silicification completely replaced the Key Tuffite in the vicinity of a synvolcanic fracture (Fig. 2.9a). This silicification overprints and destroys the primary bedding in the first 10-

15 cm, on either side of the synvolcanic fracture, but is focussed laterally, for 30cm or more, along 3 specific beds. Around it, the Key Tuffite is highly silicified, but the finer scale layering is preserved. A similar process of selective replacement of the primary layering is present in the Key Tuffite around Bracemac (Fig. 2.9b). The alteration halo around the synvolcanic fractures, which crosscuts the bedding at 45°, is very similar to the silica-rich layers. This indicates that hydrothermal fluids were laterally dispersed from the fractures when the porosity allowed it. However, some sub-parallel sulfide-rich veins crosscut the synvolcanic fractures, indicating that the mineralization of these specific layers occurred after the deposition of the Key Tuffite and after the silicification event. This is further evidence that the sulfide mineralization is not exhalative and overprints the complex hydrothermal history recorded by the Key Tuffite. Finally, another example from Orchan deposit area (Figs. 2.1 and 2.9c) confirms the selective alteration and replacement behaviour of the fluids along the most porous layers of the Key Tuffite. As for the Key Tuffite at Perseverance (Fig. 2.9a), the width of alteration halo surrounding the synvolcanic fracture is variable, probably as a function of the porosity of the layers infiltrated by the fluids.

2.8.1.5. COMPARISON WITH OTHER MISTAKEN EXHALITES

The term exhalite was introduced by Ridler (1971) and refers to the association of interbedded volcaniclastic (ash or sediments) and chemical precipitates (chert

and sulfides) spatially related with VMS deposits. Such markers are useful indicators of the stratigraphic level of hydrothermal seafloor activity (Spry et al., 2000). In Archean VMS environments, these rocks are commonly interpreted as Algoma-type iron formations (Gross, 1980; Spry et al., 2000). The classification of James (1954) distinguishes 4 predominant facies: sulfide, carbonate, oxide and silica. In various VMS contexts, strongly altered tuffaceous deposits comprising any one of these 4 facies have been mistaken for exhalites in the past. For example, the carbonate facies iron-formation in the Hunter Mine Group (Superior Province, Québec) is in fact the result of in situ low temperature replacement of chert and tuff beds (Chown et al., 2000). This hydrothermal activity is interpreted to be the result of late-stage volcanic activity and seawater infiltration. Similar processes have been documented in the Iberian Pyrite Belt (Leistel et al., 1997) where Fe-Mn carbonates and cherts were formed below the seafloor by replacement. The Helen Formation (Superior Province, Ontario) and the chlorite-tremolite-carbonate rocks associated with the Thalanga VMS (North Queensland, Australia), long considered as exhalative, also formed in a similar manner (Morton and Nebel, 1984; Herrmann and Hill, 2001). The omnipresence of silicification in VMS environments can also lead to erroneous interpretation of exhalite. For example, the ore-equivalent horizon of the Currawong Zn-Cu-Pb(-Au) massive sulfide deposit, (Victoria, Australia) had been described as an exhalative unit until the selective replacement of sedimentary layers and the progressive gradation

into fresh equivalent rocks was documented (Allen, 1992; Bodon and Valenta, 1995). Moreover, it was demonstrated that the inter-layering of sulfides within sedimentary rocks was the result of selective replacement of coarser layers. Our results imply that the Key Tuffite is another mistaken exhalite.

2.8.2. A REPLACEMENT MODEL FOR THE FORMATION OF VMS AT MATAGAMI

The origin of the zinc-rich VMS deposits of the Matagami mining camp has long been debated. Previous studies showed evidence that the mineralization was in part epigenetic/replacement in several deposits along the South Flank (e.g., Hallam, 1964; Sharpe, 1968; Clark, 1983). Results of this study also imply that replacement is the dominant process over seafloor accumulation to form the Perseverance and Bracemac-McLeod deposits. The fluids are, however, synvolcanic in origin as demonstrated by the fluid inclusions (Ioannou et al., 2007). Thus, the link with the Key Tuffite is more spatial than genetic. The primary porous, water saturated and glassy nature of the Key Tuffite makes it a favorable host for replacement-type mineralization or silicification as is common for unconsolidated volcanic debris layers (Doyle and Allen, 2003).

Perseverance and Bracemac-McLeod not only represent the 2 extremities of the South Flank but also the 2 end-members considering the geometry of the mineralized lenses: discordant sub-vertical pods versus stratabound sheet-like.

The general geometry of theses lenses is accepted to be mostly primary since the intensity of deformation along the South Flank is weak (Piché et al., 1990; Lavallière et al., 1994) and incompatible with significant remobilization of ore. Despite their geometric differences, the formation of these 2 deposits is best explained by replacement processes. In both cases, ascending hydrothermal fluids were probably focused at depth by synvolcanic faults (Figs. 2.3 and 2.4). However, for Perseverance, the mineralization and hydrothermal alteration reflect the geometry of the sub-vertical structures themselves, indicating focused flow of hydrothermal fluids with minimal lateral dispersion into the volcanic succession. The overlying Key Tuffite is strongly altered (Fig. 2.11) but devoid of sulfides (Figs. 2.5f and 2.8b). The pervasive silicification in the Key Tuffite (Fig. 2.9a) and throughout the Dumagami rhyodacite hanging-wall (Figs. 2.7a, 2.8a-b) could have occurred early in the life of the hydrothermal system by low temperature fluids precipitating silica in pore spaces and fracture fillings. In this scenario, the Key Tuffite represents a cap rock sealing the roof of the system, being impermeable and refractory to mineralization. This process is common and important in replacive VMS processes (Jones et al., 2006; Schardt and Large, 2009) as the mineralization is focalized beneath the impermeable alteration horizon (e.g. Gibson and Kerr, 1993; Galley et al., 1995; Doucet et al., 1998; Sharpe and Gemmell, 2001) and promotes thermal zone refining (Franklin, 1995; Hannington

et al., 1998). Similar geometry has been recognized in several VMS in Australia, where Mount Morgan and Reward (Large, 1992) are good examples.

In contrast, at Bracemac-McLeod, the ascending fluids in synvolcanic structures were dispersed when they reached the porous Key Tuffite to produce widespread stratabound alteration (Fig. 2.14). The sheet-style massive sulfide orebodies of Bracemac-McLeod suggest a progressive replacement induced by fluid percolation focused along the Key Tuffite but also replacing the hyaloclastic upper part of the Watson Group (Fig. 2.8d). This last process was documented for the Mattagami Lake Mine where the top of the Watson rhyolite is described as thick vitroclastic mineralized tuff (Roberts, 1975; Roberts and Reardon, 1978), hence highlighting the importance of the volcanic permeability for replacement. Similar sheet-like and low aspect ratio deposits have been described in Australia and are commonly considered to be formed by synvolcanic sub-seafloor replacement. The best examples are Rosebery, Thalanga and Scuddles (Large, 1992; Allen, 1994).

Replacement processes have probably been underestimated in previous studies of the VMS deposits in the Matagami mining camp due to the obvious link with the Key Tuffite. Indeed, the exhalative model is not the most efficient mineralization process since it has been estimated that 99% of the metals from hydrothermal vents are dispersed in the ocean (Rona, 1984). The replacement model better accounts for the very high zinc grade of the Matagami VMS deposits.

For exploration, the Key Tuffite represents a major volcanic hiatus and the transition from felsic to mafic dominated volcanism. The hydrothermal activity probably started during the deposition of the Key Tuffite and could have contributed to form some VMS deposits as suggested previously (e.g., Lavallière et al., 1994). However, Perseverance and Bracemac-McLeod highlight the fact that the hydrothermal activity continued after the deposition of a part of the Wabassee Group (after 2725.8 Ma, Ross et al., 2014). The mineralization was controlled by the porosity of the overlying volcanic facies (Key Tuffite and hyaloclastic top of the Watson rhyolite) and synvolcanic structures suggesting that economic mineralization could be found at other stratigraphic levels if the permeability allowed mineralizing fluid-flow. However, the Key Tuffite is important because in most cases it was the first thick porous unit that the mineralizing fluids encountered during their migration towards the seafloor.

2.9. CONCLUSIONS

The Key Tuffite is spatially linked with all the exploited zinc-rich VMS deposits in the Matagami mining camp. Previously thought to be exhalative in origin, new field observations and geochemical data at the Perseverance and Bracemac-McLeod deposits demonstrate that the exhalative component is negligible or absent. The unit is only composed of andesitic ash, which probably represents the explosive equivalent of the first mafic units of the overlying Wabassee Group. The

mineralization event was dominantly epigenetic and occurred most likely as sub-seafloor replacement. Mineralizing fluids used synvolcanic structures and replaced units such as the Key Tuffite or the hyaloclastic top of the Watson rhyolite. A coherent geochemical alteration pattern in the Key Tuffite can be used as a vector towards VMS mineralization in the Matagami camp. The VMS mineralization is not limited to the Key Tuffite level and is partly controlled by the permeability of the volcanic facies.

2.10. ACKNOWLEDGEMENTS

This Ph.D. project is a part of a larger research program on the Matagami mining camp, including a volcanology Ph.D. (INRS-Quebec) and a geophysical Ph.D. (École Polytechnique-Montreal). Financial support for this study was provided by NSERC, CONSOREM, DIVEX, Geological Survey of Canada, Glencore (Previously Xstrata Zinc), Donner Metals, SOQUEM, and Nyrstar (previously Breakwater Resources). We thank the companies for the authorization to diffuse these results. J-A Debreil and R. Daigneault are thanked for useful discussions. R. Adair (Donner Metals) is additionally thanked for his informal review of a preliminary version of the document. N. Yapi is thanked for collecting samples in 2008. A. Paulin-Bissonnette is also thanked for his contribution as undergraduate field assistant during the summer 2010. We are grateful to S.A.S. Dare, Research Associate at UQAC, for proof reading the English. Finally, the manuscript greatly

benefited from comments and suggestions by D. Lentz and P. Mercier-Langevin.

Thanks are given to T. Bissig and G. Beaudoin for their editorial handling.

2.11. REFERENCES

Adair, R., 2009, Technical report on the resource calculation for the Bracemac-McLeod discoveries, Matagami Project, Québec: Vancouver, Canada, Donner Metals Ltd., National Instrument 43-101 Report, filled on April 3, 2009, at http://www.sedar.com, p. 194.

Allen, R. L., 1992, Reconstruction of the tectonic, volcanic, and sedimentary setting of strongly deformed Zn-Cu massive sulfide deposits at Benambra, Victoria: Economic Geology, v. 87, p. 825-854.

Allen, R. L., 1994, Syn-volcanic, subseafloor replacement model for Rosebery and other massive sulfide ores [abs.]: Contentious Issues in Tasmanian Geology Symposium, 1994, p. 89-91.

Allen, R. L., and Weihed, P., 2002, Global comparisons of volcanic-associated massive sulphide districts: Geological Society, London, Special Publications, v. 204, p. 13-37.

Arnold, G., 2006, Perseverance Deposit geology: Falconbridge Limited (now Glencore). Internal report, p. 101.

Baldwin, G. J., Thurston, P. C., and Kamber, B. S., 2011, High-precision rare earth element, nickel, and chromium chemistry of chert microbands pre-screened with in-situ analysis: Chemical Geology, v. 285, p. 133-143.

Barrett, T. J., 1981, Chemistry and mineralogy of Jurassic bedded chert overlying ophiolites in the North Apennines, Italy: Chemical Geology, v. 34, p. 289-317.

Barrett, T. J., and MacLean, W. H., 1999, Volcanic sequences, lithogeochemistry, and hydrothermal alteration in some bimodal volcanic-associated massive sulfide systems, *in* Barrie, C. T., and Hannington, M. D., eds., Reviews in Economic Geology 8, 8, p. 101-131.

Barrett, T. J., MacLean, W. H., and Årebäck, H., 2005, The Palaeoproterozoic Kristineberg VMS deposit, Skellefte district, northern Sweden. Part II: chemostratigraphy and alteration: Mineralium Deposita, v. 40, p. 368-395.

Beaudry, C., and Gaucher, E., 1986, Cartographie géologique dans la région de Matagami: Québec., Ministère de l'énergie et des Ressources, Rapport MB 86-32, p. 147.

Bierlein, F. P., 1995, Rare-earth element geochemistry of clastic and chemical metasedimentary rocks associated with hydrothermal sulphide mineralisation in the Olary Block, South Australia: Chemical Geology, v. 122, p. 77-98.

Bloom, L., and Beaudry, C., 2009, Evidence of 25-m of vertical Metal migration over the high-grade Perseverance zinc ore body, Matagami, Quebec.: Proceedings of the 24th IAGS, Fredericton, 2009, p. 357-359.

Bodon, S. B., and Valenta, R. K., 1995, Primary and tectonic features of the Currawong Zn-Cu-Pb(-Au) massive sulfide deposit, Benambra, Victoria; implications for ore genesis: Economic Geology, v. 90, p. 1694-1721.

Boström, K., 1973, The origin of ferromanganoan active ridge sediments: Stockholm Contributions in Geology, v. 27, p. 149-243.

Bussières, Y., and Théberge, D., 2006, Rapport technique NI 43-101, concernant la propriété Caber– Du Dôme, Secteur de Matagami, Nord-ouest du Québec, région de l'Abitibi, p. 125.

Card, K. D., 1990, A review of the Superior Province of the Canadian Shield, a product of Archean accretion: Precambrian Research, v. 48, p. 99-156.

Carr, P. M., Cathles, L. M., and Barrie, C. T., 2008, On the size and spacing of volcanogenic massive sulfide deposits within a district with application to the Matagami district, Quebec: Economic Geology, v. 103, p. 1395-1409.

Chown, E. H., N'dah, E., and Mueller, W. U., 2000, The relation between iron-formation and low temperature hydrothermal alteration in an Archean volcanic environment: Precambrian Research, v. 101, p. 263-275.

Clark, J. R., 1983, The geology and trace element distributions of the sulfide bodies at Orchan mine, Matagami, Quebec, Colorado School of Mines.

Corliss, J. B., Dymond, J., Gordon, L. I., Edmond, J. M., von Herzen, R. P., Ballard, R. D., Green, K., Williams, D., Bainbridge, A., and Crane, K., 1979, Submarine thermal springs on the Galapagos Rift: Science, v. 203, p. 1073-1083.

Costa, U. R., Barnett, R. L., and Kerrich, R., 1983, The Mattagami Lake Mine Archean Zn-Cu sulfide deposit, Quebec; hydrothermal coprecipitation of talc and sulfides in a sea-floor brine pool; evidence from geochemistry, 18 O/ 16 O, and mineral chemistry: Economic Geology, v. 78, p. 1144-1203.

Côté, A., and Lavigne, M., 2010, Report and Feasibility Study for the Bracemac-McLeod Project Matagami Area Quebec, (Xstrata Zinc and Genivar Limited Partnership), p. 315.

Daigneault, R., Mueller, W. U., and Chown, E. H., 2004, Abitibi greenstone belt plate tectonics: the diachronous history of arc development, accretion and collision, *in* Eriksson, P. G., Altermann, W., Nelson, D. R., Mueller, W. U., Catuneau, O., and Strand, K., eds., Developments in Precambrian Geology/Tempos of events in Precambrian time, 12: Amsterdam, Elsevier, p. 88-103.

Davidson, A. J., 1977, Petrography and chemistry of the Key Tuffite at Bell Allard, Matagami, Quebec, McGill University, 131 p.

Debreil, J.-A., and Ross, P.-S., 2009, Volcanic Architecture of the Matagami Mining Camp: Implications for Mineral Exploration.: AGU Spring Meeting Abstracts #V31B-17, 2009, p. 17.

Doucet, P., Mueller, W., and Chartrand, F., 1998, Alteration and ore mineral characteristics of the Archean Coniagas massive sulfide deposit, Abitibi belt, Quebec: Canadian Journal of Earth Sciences, v. 35, p. 620-636.

Douville, E., Bienvenu, P., Charlou, J. L., Donval, J. P., Fouquet, Y., Appriou, P., and Gamo, T., 1999, Yttrium and rare earth elements in fluids from various deep-sea hydrothermal systems: Geochimica et Cosmochimica Acta, v. 63, p. 627-643.

Doyle, M. G., and Allen, R. L., 2003, Subsea-floor replacement in volcanic-hosted massive sulfide deposits: Ore Geology Reviews, v. 23, p. 183-222.

Eastoe, C. J., Solomon, M., and Walshe, J. L., 1987, District-scale alteration associated with massive sulfide deposits in the Mount Read Volcanics, western Tasmania: Economic Geology, v. 82, p. 1239-1258.

Finlow-Bates, T., and Stumpfl, E. F., 1981, The behaviour of so-called immobile elements in hydrothermally altered rocks associated with volcanogenic submarine-exhalative ore deposits: Mineralium Deposita, v. 16, p. 319-328.

Fralick, P. W., and Kronberg, B. I., 1997, Geochemical discrimination of clastic sedimentary rock sources: Sedimentary Geology, v. 113, p. 111-124.

Franklin, J. M., 1995, Volcanic-associated massive sulphide base metals: Geological Survey of Canada, Geology of Canada, v. 8, p. 158-183.

Franklin, J. M., Sangster, D. F., and Lydon, J. W., 1981, Volcanic-associated massive sulfide deposits: Economic Geology 75th Anniversary Volume, p. 485-627.

Gaboury, D., and Pearson, V., 2008, Rhyolite geochemical signatures and association with volcanogenic massive sulfide deposits: Examples from the Abitibi Belt, Canada: Economic Geology, v. 103, p. 1531-1562.

Galley, A. G., 1993, Characteristics of semi-conformable alteration zones associated with volcanogenic massive sulphide districts: Journal of Geochemical Exploration, v. 48, p. 175-200.

Galley, A. G., Watkinson, D. H., Jonasson, I. R., and Riverin, G., 1995, The subsea-floor formation of volcanic-hosted massive sulfide; evidence from the Ansil Deposit, Rouyn-Noranda, Canada: Economic Geology, v. 90, p. 2006-2017.

Gemmell, J. B., and Fulton, R., 2001, Geology, genesis, and exploration implications of the footwall and hanging-wall alteration associated with the Hellyer volcanic-hosted massive sulfide deposit, Tasmania, Australia: Economic Geology, v. 96, p. 1003-1035.

Gibson, H. L., and Kerr, D. J., 1993, Giant volcanic-associated massive sulphide deposits: with emphasis on Archean examples: Economic Geology Special Publication 2, p. 319-348.

Gibson, H. L., Morton, R. L., and Hudak, G. J., 1999, Submarine volcanic processes, deposits and environments favorable for the location of volcanic-associated massive sulfide deposits: Reviews in Economic Geology, v. 8, p. 13-51.

Gross, G. A., 1980, A classification of iron formations based on depositional environments: Canadian Mineralogist, v. 18, p. 215-222.

Hallam, R., 1964, Matagami Lake Mines Ltd., some aspects of the geology and ore control: Monthly bulletin of the Canadian Institute of Mining and Metallurgy, v. 57, p. 389-396.

Hannington, M. D., Galley, A. G., Herzig, P. M., and Petersen, S., 1998, Comparison of the TAG mound and stockwork complex with Cyprus-type massive sulfide deposits.: Proceedings of the Ocean Drilling Program, Scientific results, v. 158, p. 389-415.

Hart, T. R., Gibson, H. L., and Lesher, C. M., 2004, Trace element geochemistry and petrogenesis of felsic volcanic rocks associated with volcanic massive Cu-Zn-Pb sulfide deposits: Economic Geology, v. 99, p. 1003-1013.

Herrmann, W., and Hill, A. P., 2001, The origin of chlorite-tremolite-carbonate rocks associated with the Thalanga volcanic-hosted massive sulfide deposit, North Queensland, Australia: Economic Geology, v. 96, p. 1149-1173.

Horwell, C. J., Braña, L. P., Sparks, R. S. J., Murphy, M. D., and Hards, V. L., 2001, A geochemical investigation of fragmentation and physical fractionation in pyroclastic flows from the Soufrière Hills volcano, Montserrat: Journal of Volcanology and Geothermal Research, v. 109, p. 247-262.

Ioannou, S. E., and Spooner, E. T. C., 2007, Fracture analysis of a volcanogenic massive sulfide-related hydrothermal cracking zone, Upper Bell River Complex, Matagami, Quebec: application of permeability tensor theory: Economic Geology, v. 102, p. 667-690.

Ioannou, S. E., Spooner, E. T. C., and Barrie, C. T., 2007, Fluid temperature and salinity characteristics of the Matagami volcanogenic massive sulfide district, Quebec: Economic Geology, v. 102, p. 691-715.

James, H. L., 1954, Sedimentary facies of iron-formation: Economic Geology, v. 49, p. 235-293.

Jenney, C. P., 1961, Geology and ore deposits of the Mattagami area, Quebec: Economic Geology, v. 56, p. 740-757.

Jolly, W. T., 1978, Metamorphic history of the Archean Abitibi belt., *in* Fraser, J. A., and Heywood, W. W., eds., Metamorphism in the Canadian Shield, Geological Survey of Canada, Paper 78-10, p. 63-78.

Jones, S., Gemmell, J. B., and Davidson, G. J., 2006, Petrographic, geochemical, and fluid inclusion evidence for the origin of siliceous cap rocks above volcanic-hosted massive sulfide deposits at Myra Falls, Vancouver Island, British Columbia, Canada: Economic Geology, v. 101, p. 555-584.

Kalogeropoulos, S. I., and Scott, S. D., 1983, Mineralogy and geochemistry of tuffaceous exhalites (tetsusekiei) of the Fukazawa mine, Hokuroku district, Japan: Economic Geology Monograph, v. 5, p. 412-432.

Large, R. R., 1992, Australian volcanic-hosted massive sulfide deposits; features, styles, and genetic models: Economic Geology, v. 87, p. 471-510.

Large, R. R., Allen, R. L., Blake, M. D., and Herrmann, W., 2001a, Hydrothermal alteration and volatile element halos for the Rosebery K lens volcanic-hosted massive sulfide deposit, Western Tasmania: Economic Geology, v. 96, p. 1055-1072.

Large, R. R., Gemmell, J. B., Paulick, H., and Huston, D. L., 2001b, The alteration box plot: a simple approach to understanding the relationship between alteration mineralogy and lithogeochemistry associated with volcanic-hosted massive sulfide deposits: Economic Geology, v. 96, p. 957-971.

Latulippe, M., 1959, Mattagami area of northwestern Quebec: Geol Assoc Canada Proc, v. 2, p. 45-54.

Lavallière, G., Guha, J., and Daigneault, R., 1994, Cheminées de sulfures massifs atypiques du gisement d'Isle-Dieu, Matagami, Québec; implications pour l'exploration: Exploration and Mining Geology, v. 3, p. 109-129.

Leistel, J. M., Marcoux, E., and Deschamps, Y., 1997, Chert in the Iberian Pyrite Belt: Mineralium Deposita, v. 33, p. 59-81.

Lesher, C. M., Goodwin, A. M., Campbell, I. H., and Gorton, M. P., 1986, Trace-element geochemistry of ore-associated and barren, felsic metavolcanic rocks in the Superior Province, Canada: Canadian Journal of Earth Sciences, v. 23, p. 222-237.

Liaghat, S., and MacLean, W. H., 1992, The Key Tuffite, Matagami mining district; origin of the tuff components and mass changes: Exploration and Mining Geology, v. 1, p. 197-207.

Longuépée, H., 2009, Empreinte hydrothermale au toit de sulfures massifs volcanogènes., Rapport du projet CONSOREM 2007-05, p. 33.

Lydon, J. W., 1984, Volcanogenic Massive Sulphide Deposits Part 1: A Descriptive Model: Geoscience Canada, v. 11, p. 195-202.

MacGeehan, P. J., and MacLean, W. H., 1980, An Archaean sub-seafloor geothermal system, 'calc-alkali' trends, and massive sulphide genesis: Nature, v. 286, p. 767-771.

MacLean, W. H., 1988, Rare earth element mobility at constant inter-REE ratios in the alteration zone at the Phelps Dodge massive sulphide deposit, Matagami, Quebec: Mineralium Deposita, v. 23, p. 231-238.

MacLean, W. H., and Davidson, A. J., 1977, Case history of the Bell-Allard Mine, Matagami, Quebec., Mineral Exploration Researh Institute, Paper 77-3, p. 55.

MacLean, W. H., and Kranidiotis, P., 1987, Immobile elements as monitors of mass transfer in hydrothermal alteration; Phelps Dodge massive sulfide deposit, Matagami, Quebec: Economic Geology, v. 82, p. 951-962.

Maier, W. D., Barnes, S.-J., and Pellet, T., 1996, The economic significance of the Bell River Complex, Abitibi subprovince, Quebec: Canadian Journal of Earth Sciences, v. 33, p. 967-980.

Masson, M., 2000, Option Caber, rapport de sondages 1998-1999. Noranda Inc, Travaux statutaires déposés au Ministère des Ressources naturelles (Québec),, GM 58074, p. 36.

McPhie, J., Doyle, M., and Allen, R., 1993, Volcanic textures: a guide to the interpretation of textures in volcanic rocks: Hobart, CODES Key Centre, University of Tasmania, p. 196.

Mercier-Langevin, P., Gibson, H. L., Hannington, M. D., Goutier, J., Monecke, T., Dubé, B., and Houlé, M. G., 2014, A special issue on Archean magmatism, volcanism, and ore deposits: Part 2. Volcanogenic massive sulfide deposits preface: Economic Geology, v. 109, p. 1-9.

Mercier-Langevin, P., Goutier, J., Ross, P.-S., McNicoll, V. J., Monecke, T., Dion, C., Dubé, B., Thurston, P., Bécu, V., Gibson, H. L., Hannington, M. D., and Galley, A. G., 2011, The Blake River Group of the Abitibi greenstone belt and its unique VMS and gold-rich VMS endowment: GAC-MAC-SEG-SGA Joint Annual Meeting 2011, Ottawa, Field Trip 02B guidebook; Geological Survey of Canada, Open File report 6869, 2011, p. 61.

Miller, R. J. M., 1960, Geology of Mattagami Lake Mines: Canadian Inst Mining Metall Bull, v. 53, p. 194.

Mortensen, J. K., 1993, U–Pb geochronology of the eastern Abitibi Subprovince. Part 1: Chibougamau–Matagami–Joutel region: Canadian Journal of Earth Sciences, v. 30, p. 11-28.

Morton, R. L., and Nebel, M. L., 1984, Hydrothermal alteration of felsic volcanic rocks at the Helen siderite deposit, Wawa, Ontario: Economic Geology, v. 79, p. 1319-1333.

Moune, S., Gauthier, P.-J., Gislason, S. R., and Sigmarsson, O., 2006, Trace element degassing and enrichment in the eruptive plume of the 2000 eruption of Hekla volcano, Iceland: Geochimica et Cosmochimica Acta, v. 70, p. 461-479.

Mueller, W. U., Daigneault, R., Mortensen, J. K., and Chown, E. H., 1996, Archean terrane docking: upper crust collision tectonics, Abitibi greenstone belt, Quebec, Canada: Tectonophysics, v. 265, p. 127-150.

Mueller, W. U., Stix, J., Corcoran, P. L., and Daigneault, R., 2009, Subaqueous calderas in the Archean Abitibi greenstone belt: An overview and new ideas: Ore Geology Reviews, v. 35, p. 4-46.

Munoz Taborda, C. M., 2011, Distribution of Platinum-Group Elements in the Ebay claim, central part of the Bell River Complex, Matagami, Quebec: Unpub. M.Sc. thesis, Université du Québec à Chicoutimi, 206 p.

Ohmoto, H., 1996, Formation of volcanogenic massive sulfide deposits: The Kuroko perspective: Ore Geology Reviews, v. 10, p. 135-177.

Peter, J. M., and Goodfellow, W. D., 2003, Hydrothermal sedimentary rocks of the Heath Steele belt, Bathurst mining camp, New Brunswick: Part 3. Application of mineralogy and mineral and bulk compositions to massive sulfide exploration: Economic Geology Monograph, v. 11, p. 417-433.

Peter, J. M., Goodfellow, W. D., and Doherty, W., 2003, Hydrothermal sedimentary rocks of the Heath Steele Belt, Bathurst mining camp, New Brunswick: Part 2. Bulk and rare earth element geochemistry and implications for origin: Economic Geology Monograph, v. 11, p. 391-415.

Piché, M., Guha, J., and Daigneault, R., 1993, Stratigraphic and structural aspects of the volcanic rocks of the Matagami mining camp, Quebec; implications for the Norita ore deposit: Economic Geology, v. 88, p. 1542-1558.

Piché, M., Guha, J., Daigneault, R., Sullivan, J. R., and Bouchard, G., 1990, Les gisements volcanogènes du camp minier de Matagami: Structure, stratigraphie et implications métallogéniques: Canadian Institute of Mining and Metallurgy, v. Special Volume 43, p. 327-336.

Pilote, P., Debreil, J.-A., Williamson, K., Rabeau, O., and Lacoste, P., 2011, Révision géologique de la région de Matagami., Québec Exploration - Poster 276: Québec.

Pinti, D. L., Hashizume, K., Sugihara, A., Massault, M., and Philippot, P., 2009, Isotopic fractionation of nitrogen and carbon in Paleoarchean cherts from Pilbara craton, Western Australia: Origin of 15N-depleted nitrogen: Geochimica et Cosmochimica Acta, v. 73, p. 3819-3848.

Ridler, R. H., 1971, Analysis of Archean volcanic basins in the Canadian shield using the exhalite concept [abs.]: Bull. Can. Inst. Mining Met, v. 64, p. 20.

Roberts, R. G., 1975, The geological setting of the Mattagami Lake Mine, Quebec; a volcanogenic massive sulfide deposit: Economic Geology, v. 70, p. 115-129.

Roberts, R. G., and Reardon, E. J., 1978, Alteration and ore-forming processes at Mattagami Lake Mine, Quebec: Canadian Journal of Earth Sciences, v. 15, p. 1-21.

Rona, P. A., 1984, Hydrothermal mineralization at seafloor spreading centers: Earth Science Reviews, v. 20, p. 1-104.

Ross, P.-S., McNicoll, V. J., Debreil, J.-A., and Carr, P., 2014, Precise U-Pb geochronology of the Matagami Mining Camp, Abitibi Greenstone Belt, Quebec: stratigraphic constraints and implications for volcanogenic massive sulfide exploration: Economic Geology, v. 109, p. 89-101.

Sangster, D., 1972, Precambrian volcanogenic massive sulphide deposits in Canada: a review, Gological Survey of Canada Paper 72-22, p. 44.

Schardt, C., and Large, R. R., 2009, New insights into the genesis of volcanic-hosted massive sulfide deposits on the seafloor from numerical modeling studies: Ore Geology Reviews, v. 35, p. 333-351.

Sharpe, J. I., 1968, Géologie et gisements de sulfures de la région de Matagami, Comté d'Abitibi-Est, Québec., Ministère des Richesses Naturelles du Québec. Rapport géologique 137, p. 122.

Sharpe, R., and Gemmell, J. B., 2001, Alteration characteristics of the Archean Golden Grove Formation at the Gossan Hill deposit, Western Australia: induration as a focusing mechanism for mineralizing hydrothermal fluids: Economic Geology, v. 96, p. 1239-1262.

Sholkovitz, E. R., Landing, W. M., and Lewis, B. L., 1994, Ocean particle chemistry: The fractionation of rare earth elements between suspended particles and seawater: Geochimica et Cosmochimica Acta, v. 58, p. 1567-1579.

Slack, J. F., Grenne, T., and Bekker, A., 2009, Seafloor-hydrothermal Si-Fe-Mn exhalites in the Pecos greenstone belt, New Mexico, and the redox state of ca. 1720 Ma deep seawater: Geosphere, v. 5, p. 302-314.

Spry, P. G., Peter, J. M., and Slack, J. F., 2000, Meta-exhalites as exploration guides to ore: Reviews in Economic Geology, v. 11, p. 163-201.

Sun, S.-S., and McDonough, W. F., 1989, Chemical and isotopic systematics of oceanic basalts: implications for mantle composition and processes: Geological Society, London, Special Publications, v. 42, p. 313-345.

Tully, D. W., 1964, Notes on the geology of the No. 1 orebody, Mattagami Lake Mines Ltd: Canadian Institute of Mining and Metallurgy, v. Field Excursion Guide Book, p. 7-19.

Van Kranendonk, M. J., Webb, G. E., and Kamber, B. S., 2003, Geological and trace element evidence for a marine sedimentary environment of deposition and biogenicity of 3.45 Ga stromatolitic carbonates in the Pilbara Craton, and support for a reducing Archaean ocean: Geobiology, v. 1, p. 91-108.

Winchester, J. A., and Floyd, P. A., 1977, Geochemical discrimination of different magma series and their differentiation products using immobile elements: Chemical Geology, v. 20, p. 325-343.

Wolff, J. A., 1985, The effect of explosive eruption processes on geochemical patterns within pyroclastic deposits: Journal of Volcanology and Geothermal Research, v. 26, p. 189-201.

Wonder, J. D., Spry, P. G., and Windom, K. E., 1988, Geochemistry and origin of manganese-rich rocks related to iron-formation and sulfide deposits, western Georgia: Economic Geology, v. 83, p. 1070-1081.

CHAPITRE 3

3. EVOLUTION OF A VOLCANOGENIC HYDROTHERMAL SYSTEM RECORDED BY THE BEHAVIOR OF LREE AND EU: CASE STUDY OF THE KEY TUFFITE AT BRACEMAC-MCLEOD DEPOSITS, MATAGAMI, CANADA.

Dominique Genna, Damien Gaboury, Gilles Roy

Ore Geology Reviews, 2014, Vol 63, pp 160-177

3.1. RÉSUMÉ

La distribution des éléments des terres rares (ETR) dans les zones d'altération associées aux sulfures massifs volcanogènes (SMV) anciens ou modernes et souvent caractérisée par des gains et des pertes de terres rares légères (TRL : La à Sm) et d'Europium. L'évolution du système hydrothermal est enregistrée par des assemblages de minéraux et par leur composition chimique. Pour comprendre le comportement des ETR dans un tel contexte, le gisement SMV archéen de Bracemac-McLeod, dans le camp minier de Matagami, a été étudié. Les minéralisations sont le résultat de processus de remplacement, sous le plancher océanique, le long d'une unité marqueur (Tuffite Clé) de composition andésitique homogène. L'étude de la Tuffite Clé est ainsi simplifiée grâce à un protolithe unique pour étudier les variations chimiques et minérales causées par les processus d'altération. Cette étude combine analyses en roche totale et analyses de minéraux contenant des ETR dans les halos d'altération en séricite (distal), et chlorite (proximal) qui entourent les minéralisations. Un modèle intégrant : observations texturales, données géochimiques et compréhension actuelle de la stabilité des minéraux, est proposé pour expliquer la redistribution des ETR durant l'évolution du système hydrothermal de type SMV. Les zones distale séricitisées représentent le meilleur équivalent de l'amorce du système hydrothermal (basse température). Cette zone est caractérisée par la destruction de verre volcanique et de plagioclases. Géochimiquement, cela ce traduit par une

anomalie négative en Eu et une perte des TRL. La zone chloritisée, proximale au gisement, est le produit de l'augmentation en température des fluides minéralisateurs. Cette zone est généralement caractérisée par des gains en TRL et Eu. Les observations pétrographiques indiquent que la co-précipitation d'allanite avec la chlorite explique le gain en TRL. Cependant, un calcul de bilan de masse démonte que c'est la précipitation d'apatite (± carbonates) qui contrôle l'anomalie positive en Eu. La silicification locale, survenant sous forme de pulses pendant le système hydrothermal, est aussi d'intérêt puisqu'elle peut avoir préservé un état d'altération intermédiaire et ainsi fournir des informations additionnelles sur l'évolution du système hydrothermal. La mobilité des ETR est indicatrice de conditions d'hydrothermalisme spécifique, qui peut refléter l'efficacité du système minéralisateur. À Matagami, la mobilité des TRL et de l'Eu peut être utilisée en exploration. En particulier l'Eu qui a un comportement anormal qui s'étend bien plus loin que les zones minéralisées, dans les zones d'altération en séricite de basse température (jusqu'à 400 m des minéralisations).

3.2. ABSTRACT

The distribution of rare earth elements (REE) in the alteration zones surrounding modern and ancient volcanogenic massive sulfide (VMS) deposits is often characterized by a wide range of variations comprising both gains and losses of light REE (LREE: La to Sm) and europium. The evolution of the hydrothermal

system is recorded by mineral assemblages and their chemical composition. To address the behavior of the REE in such a context, the Bracemac-McLeod Archean VMS deposits of the Matagami district are used. There, mineralization was formed mainly by subsea-floor replacement along a tuffaceous marker unit (Key Tuffite) of homogenous andesitic composition, hence providing a single protolith to account for mineral and chemical variations in relation to ore position. We combine whole-rock and mineral REE data in both distal sericite and proximal chlorite alteration surrounding the mineralization. A model, integrating observed textural relationships, geochemical data and current understanding of mineral stabilities, is proposed to explain the redistribution of the REE during the evolution of the VMS hydrothermal system. The distal sericite zone represents the early, low temperature alteration. It is characterized by the destruction of volcanic glass and plagioclase leading to a negative Eu anomaly in the whole-rock analyses and the depletion of LREE. The proximal chlorite zone was formed during the thermal evolution of a fertile VMS hydrothermal system. It is generally characterized by gains of LREE and Eu, although some chloritized samples are depleted in LREE. Petrographic observations suggest that the coprecipitation of allanite with chlorite explains the increase of LREE, whereas a mass balance calculation indicates that the precipitation of apatite (± carbonates) essentially controls the Eu. Local silicification, occurring as pulses during the hydrothermal system life, is also of interest because it could preserve an intermediate alteration state and thus

provide additional information on the evolution of the hydrothermal system. The mobility of REE is indicative of specific hydrothermal conditions, which may reflect the efficiency of a mineralizing hydrothermal system. At Matagami, the mobility of LREE and Eu could be used for vectoring in exploration, especially Eu which has an anomalous behavior that extends far beyond the limit of the sulfide zone, into the distal sericitic low-temperature alteration (up to 400 m from the ore zones).

3.3. INTRODUCTION

Mobility of the rare earth elements (REE) and yttrium in hydrothermal fluids has been documented in a variety of modern volcanogenic massive sulfide (VMS) environments (e.g., Michard and Albarède, 1986; Michard, 1989; Mills and Elderfield, 1995; Douville et al., 1999; Craddock et al., 2010; Schmidt et al., 2010) and validated by experimental studies (Gammons et al., 2002; Migdisov et al., 2009). Studying the composition of modern fluids had greatly enhanced our knowledge of the source and mobility of REE in aqueous systems. These studies also provided a good understanding of the behavior of the REE at the precipitation site (i.e. where the hydrothermal fluids encounter the seawater) over a relatively short period of the lifetime of the hydrothermal system. Normalized REE patterns of fluids from hydrothermal vents on the seafloor are in general relatively uniform and characterized by a substantial enrichment in LREE and Eu compared to seawater (e.g. Mitra et al., 1994; Douville et al., 1999). However, recent studies

showed that the distribution of REE in fluids could have a much wider range of composition than previously thought (Craddock et al., 2010; Schmidt et al., 2010). Therefore, deciphering the behavior of REE during the evolution of a hydrothermal event related to VMS formation remains a challenge, especially in ancient systems where both gains and losses of light REE (LREE: La to Sm) and Eu have been documented in altered rocks surrounding economic mineralization (e.g. Graf, 1977; Campbell et al., 1984; MacLean, 1988; Whitford et al., 1988). This is of importance as some REE ratios have been proposed as geochemical indexes for the exploration of VMS deposits (Gale and Fedikow, 1999; Shikazono et al., 2008).

This study focuses on the VMS deposits of the Bracemac-McLeod mine, in the Matagami district of the Archean Abitibi greenstone belt (Quebec, Canada), and specifically on the Key Tuffite, a stratigraphic marker horizon intimately associated with the mineralization. Previous work has been done in the district to investigate the behavior of the REE, from a whole-rock approach (MacGeehan and MacLean, 1980; MacLean, 1988) and at the mineral scale (Pan et al., 1994), providing evidence that the hydrothermal conditions were favorable for the mobility of REE during formation of the VMS deposits. In order to better understand the behavior of REE during the evolution of a volcanogenic hydrothermal system, this contribution proposes an approach combining both whole-rock and mineral REE data. To date, only a limited number of studies have identified the host minerals

of REE in VMS alteration zones (e.g. Matagami - Pan et al. (1994); Kidd Creek, Canada - Schandl and Gorton (1991)). In ancient systems, where it is not possible to sample hydrothermal fluids, REE-bearing hydrothermal minerals provide critical information on REE redistribution during the lifetime of the hydrothermal system. Thus the analysis of REE-bearing minerals should provide important information on the composition of the hydrothermal fluids from which they precipitated.

Our recent characterization of the Key Tuffite at Bracemac-McLeod (Genna et al., 2014) demonstrated that this unit was a tuffaceous accumulation on the seafloor, of homogeneous andesitic composition, at the district-scale. As the mineralisation at Bracemac-McLeod was formed mainly by replacement processes along the Key Tuffite and other permeable volcanic units (Genna et al., 2014), the Key Tuffite recorded the classic hydrothermal alteration assemblages of Lydon (1984, 1988) with a proximal chlorite alteration and a distal sericitization. This allows us to study the effect of REE mobility related to hydrothermal alteration of a single homogeneous protolith, the Key Tuffite, in areas proximal to distal relative to VMS ores. A high density of samples was taken at various locations around the VMS lenses to better constrain in two dimensions the REE compositional variations.

It is demonstrated that LREE and Eu were leached at an early stage, whereas Eu and LREE were later enriched in the higher temperature chlorite-rich alteration zones. However Eu and LREE can have a decoupled behavior because of their

incorporation in different hydrothermal minerals. Our results provide a comprehensible model of mineral reactions to account for REE behavior that maybe applicable to other VMS systems and be useful for geochemical exploration.

3.4. PREVIOUS WORK ON THE MOBILITY OF REE AT MATAGAMI

MacGeehan and MacLean (1980) were the first to highlight the mobility of REE at Matagami. They proposed that the tholeiitic magmatic affinity of the volcanic rocks hosting the Garon Lake deposit (Fig. 3.1) was converted to an apparent calc-alkaline affinity by the transport of LREE. Later, MacLean (1988) quantified the mobility of the REE (from La to Ho) in rocks near the Phelps Dodge deposit (20 km W of the area shown in Fig. 3.1), where La concentration increased by six times and the $[La/Yb]_N$ ratio steepened from 1.9 to 13. Both gains and losses of LREE were observed in the intensively chloritized zones surrounding the mineralization at Phelps Dodge. More recently, Pan et al. (1994) investigated the rare earth element mineralogy and geochemistry of rocks near the Mattagami Lake deposit (Fig. 3.1).

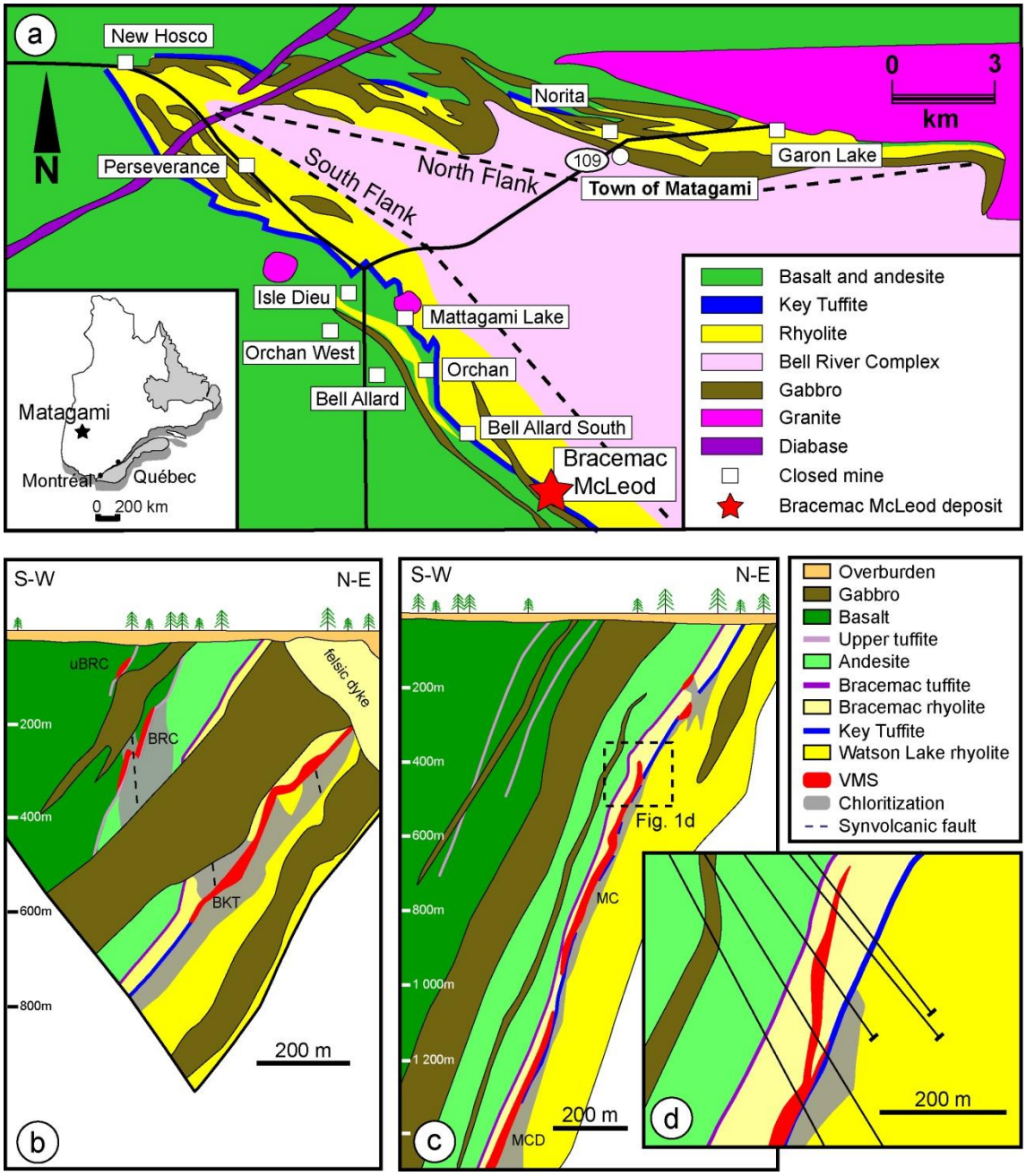

Figure 3.1 Geological setting of the Matagami district. a) Simplified regional map. The West Camp is not presented. b) Cross-section of the Bracemac deposits. c) Cross-section of the McLeod deposits. Ore zones: uBRC Upper Bracemac, BRC Bracemac Main, BKT Bracemac KT (modified from Donner Metals and Genna et al., 2014).

Their results revealed that a large proportion of the REE is hosted in allanite (LREE) and zircon (heavy rare earth elements - HREE). The stability of these minerals under hydrothermal conditions controls the behavior of the REE. Specifically, the mobility of LREE is controlled by the preferential dissolution and recrystallization of allanite by hydrothermal fluids. However, the minerals hosting Eu have not yet been identified in the Matagami district, and are only speculated upon in other VMS deposits.

3.5. GEOLOGICAL SETTING: BRACEMAC-MCLEOD GEOLOGY

The 2.7 Ga (Mortensen, 1993; Ross et al., 2014) Matagami mining district (Fig. 3.1) is located in the northern part of the Abitibi greenstone belt. The district has produced more than 60 Mt of zinc-rich ore (19 deposits and prospects, including 13 past and current producers; Mercier-Langevin et al., 2014). All of the known VMS deposits are spatially related with extensive felsic bands which are divided into the North Flank, the South Flank (Fig. 3.1) and the West Camp. Regional metamorphism reached greenschist facies and locally amphibolite facies on the North Flank (Jolly, 1978). Details of the geology of the Matagami area are available from Sharpe (1968), Beaudry and Gaucher (1986), Piché (1991), Pilote et al. (2011) and (Genna et al., 2014).

The present study is focused on the new Bracemac-McLeod mine, comprising two VMS deposits (Bracemac and McLeod) spatially controlled by synvolcanic

faults and separated by a horizontal distance of 1200 m. Together, they represent the second largest of the 19 VMS deposits in the district with 3.6 million tonnes of measured and indicated mineral resources grading 10.62% Zn, 1.45% Cu, 32.3 g/t Ag, and 0.48 g/t Au (Côté and Lavigne, 2010) and inferred mineral resources of 2.6 million tonnes grading 8.79% Zn, 1.31% Cu, 38.84 g/t Ag and 1.06 g/t Au (Côté and Lavigne, 2010).

The general stratigraphic sequence is shown in Figure 3.1b whereas the detailed description of each unit is compiled in Genna et al. (2014). The main part of the mineralization occurs at the Key Tuffite level, between two rhyolites of similar composition: the Watson Lake rhyolite in the footwall and the Bracemac rhyolite in the hanging-wall. In turn the Bracemac rhyolite is overlain by a thin tuff layer, the Bracemac Tuffite, which marks the transition into the mafic to intermediate volcanic rocks of the Wabassee Group. The volcanic rocks are locally crosscut by late phases of the underlying Bell River Complex, a large synvolcanic tholeiitic gabbro-anorthosite layered intrusion interpreted as the source for the overlying volcanic units and as the thermal source for the formation of the VMS deposits (Piché et al., 1990; Maier et al., 1996; Ioannou and Spooner, 2007; Carr et al., 2008).

The Bracemac-McLeod deposits are surrounded by a large (~1.6 km in diameter) alteration halo in the Watson Lake rhyolite footwall which is manifested by strong

proximal chloritization (± talc), moderate intermediate chloritization and distal sericitization. An alteration halo is also present in the overlying Bracemac rhyolite, although less extensive than in the footwall. The hangingwall alteration is dominated by pervasive and patchy silicification and diffuse chloritization. Such alteration haloes are typical of VMS systems (e.g. Galley, 1993) and are commonly used as the main exploration guide (Large et al., 2001a).

The mineralization at Bracemac-McLeod was originally thought to be exhalative in origin (i.e. precipitated on the sea floor). However, based on detailed core logging and more than 300 Key Tuffite geochemical analyses at the district scale, it has been recently proposed by Genna et al. (2014) that the mineralization at Bracemac-McLeod was mostly formed by sub-sea floor replacement of the Key Tuffite and surrounding porous units, such as the hyaloclastic top of the Watson Lake rhyolite. Volcanological work on the Watson Lake rhyolite and the Bracemac rhyolite is compatible with this interpretation (Debreil, 2014).

The Key Tuffite is well developed in the Bracemac-McLeod area, with a thickness ranging from 0.1 to 10 m.

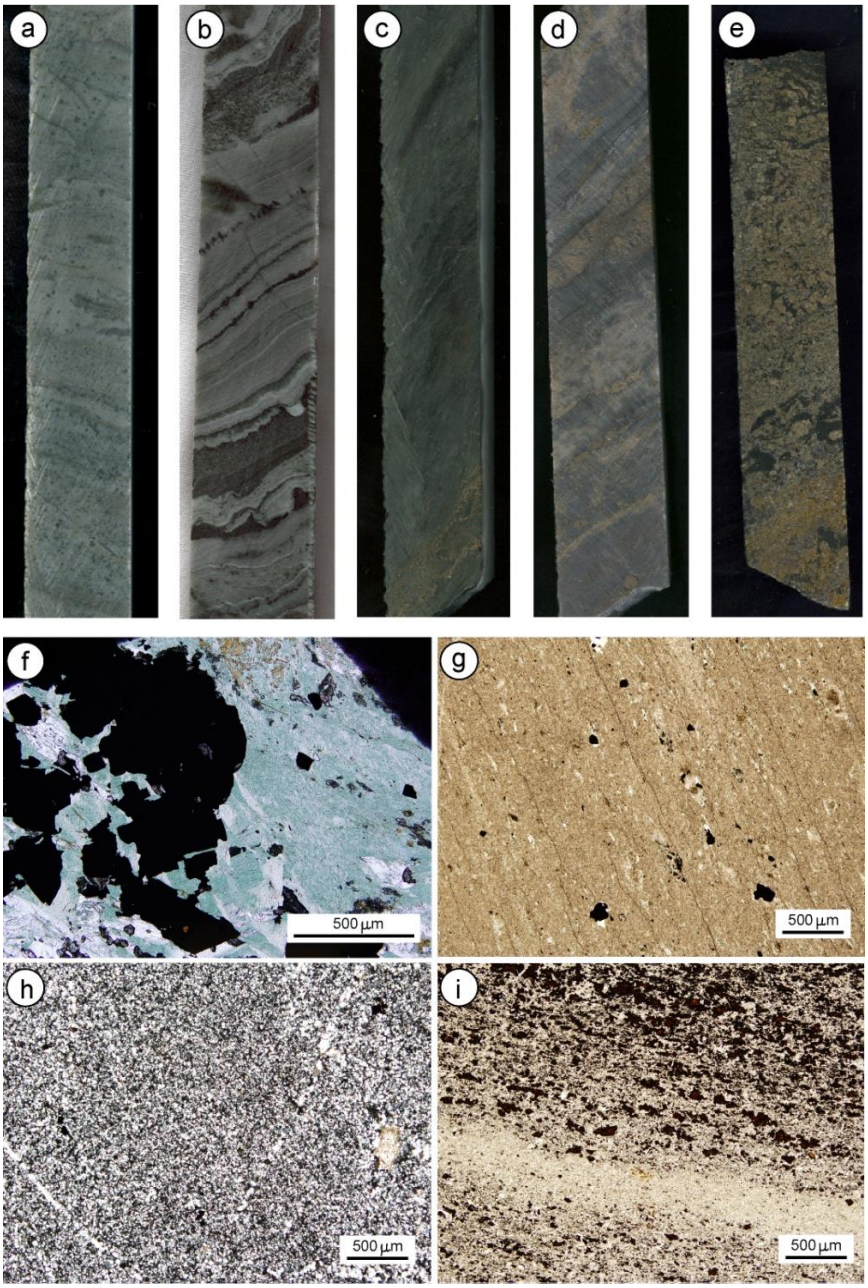

Figure 3.2 Representative mineral assemblages of selected Key Tuffite samples around Bracemac (BRA or BRC)-McLeod (MC) in core (a-e; core width = 2.4 cm) and thin section (f-i). a) Silica-sericite (sample 972209 in drillhole BRA-09-06, 85 m depth); b) Silica-chlorite (716472 in BRC-08-76, 692 m); c) Chlorite-pyrite (972162 in MC-08-62, 585 m); d) Silica-sericite-pyrite (972116 in MC-08-55, 513 m); e) Pyrite-chlorite (972153 in MC-07-23, 519 m). f-i) Photomicrographs of the dominant assemblages in the Key Tuffite. f) Chlorite and pyrite (plane-polarised light = ppl; 972110 in MC-07-24, 686 m). g) Sericite (ppl; 716474 in MC-05-19, 821 m). h) Quartz (cross-polarized light; 716489 in MC-05-18, 928 m). i) Disseminated sphalerite in a chlorite/sericite rich Key Tuffite (ppl; 972134 in BRC-95-11, 968 m). Modified from Genna et al. (2014).

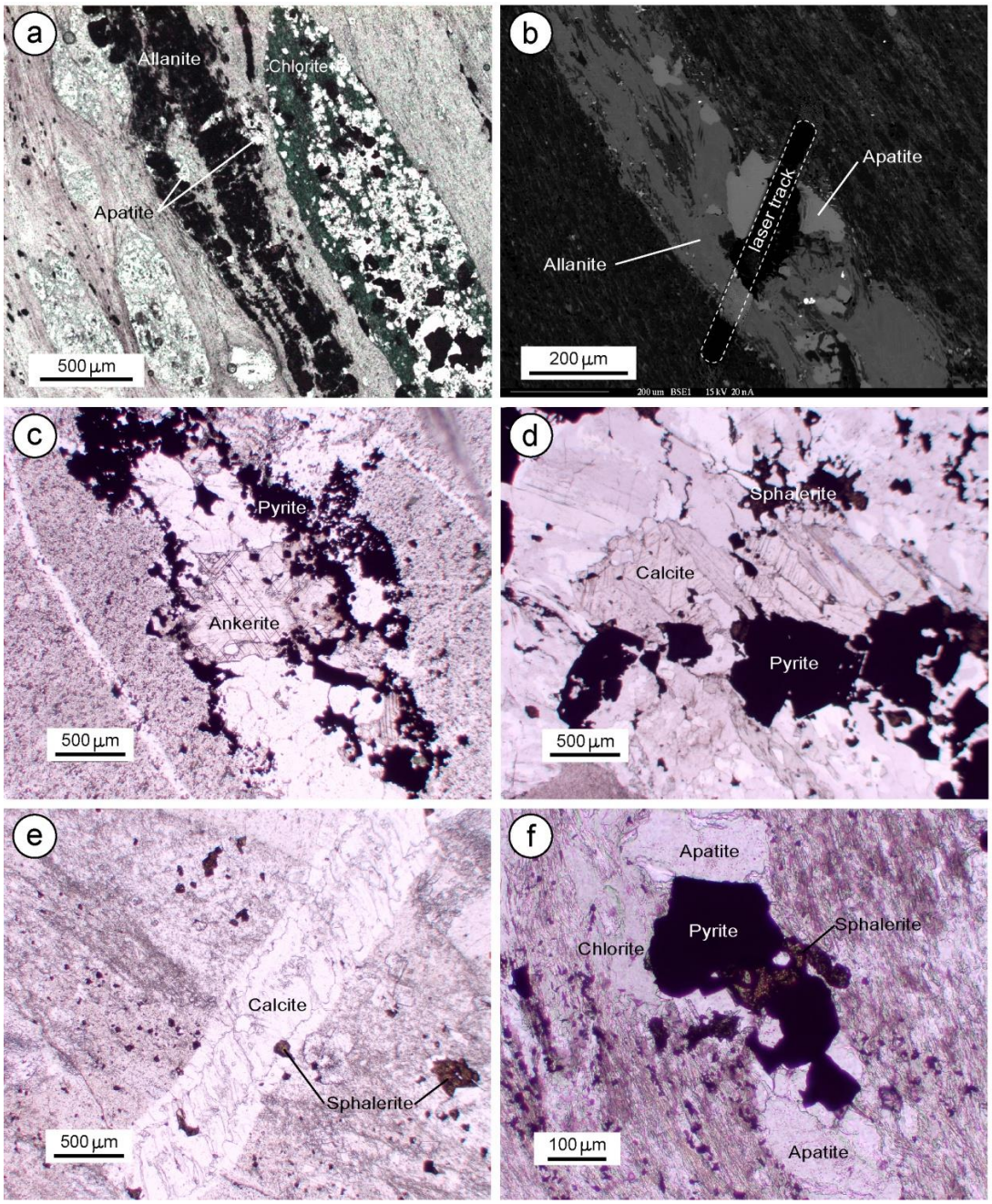

Figure 3.3 Photomicrographs of accessory minerals in the Key Tuffite. a) Allanite-rich bands in a chlorite-rich matrix. Disseminated apatite is associated with allanite (sample 716495, in drill hole MC-07-28, 556 m depth). b) Back-scattered image of the same sample. Track of laser ablation-ICP-MS shown. c) Ankerite associated with pyrite and quartz (716489 in MC-05-18, 928 m). d) Calcite associated with sphalerite and pyrite (972117 in MC-08-55, 517 m). e) Late calcite vein crosscutting a sericite-rich matrix (972116 in MC-08-55, 513 m). f) Apatite associated with pyrite and allanite in a chlorite-rich matrix (716495 in MC-07-28, 556 m).

Prior to hydrothermal alteration, the Key Tuffite was a thinly layered andesitic tuff unit (Genna et al., 2014) and thus dominantly composed of volcanic glass, plagioclase (microliths and phenocrysts) with pyroxene and/or hornblende. During the mineralizing event, the Key Tuffite was progressively replaced by sulfides and alteration minerals. Today, the Key Tuffite is composed of a fine grained mosaic of quartz, sulfides, chlorite, sericite and carbonates (Fig. 3.2), with minor amounts of albite, allanite, rutile and apatite (Fig. 3.3). The two dominant alteration assemblages observed in the Key Tuffite are similar to those present in the Watson Lake rhyolite footwall: 1) sericite in the outer part of the hydrothermal system, and 2) chlorite close to the massive sulfide mineralization.

3.6. WHOLE-ROCK GEOCHEMISTRY

3.6.1. SAMPLING AND ANALYTICAL METHODS

A total of 54 whole-rock analyses of Key Tuffite samples from Genna et al. (2014) were used in this study. These samples (20 cm of drill core) are distributed along 33 drill holes from the Bracemac-McLeod area and provide good spatial coverage of all the different alteration zones. For comparison, an additional six drill-holes (nine samples), located away from all known mineralization (>450 m), were also selected at the district scale to establish the composition of the unaltered precursor for the Key Tuffite (Genna et al., 2014).

Whole-rock analysis was carried out for major and trace elements including REE at the Institut National de la Recherche Scientifique (INRS) laboratory in Quebec City, Canada. A metaborate fusion was carried out on all samples, prior to Inductively Coupled Plasma-Mass Spectrometry (ICP-MS) analyses, for a total dissolution of resistant minerals. Reference materials were used in order to assure the accuracy (within 10% relative difference) and reproducibility (<10% relative standard deviation) of the analyses. REE results for all samples, including reference materials, are given in an electronic supplement.

3.6.2. RARE EARTH ELEMENT GEOCHEMISTRY

Abundances of the REE and Y analyzed in the Key Tuffite are listed in Appendix 3.1, along with the calculated $[La/Yb]_{PM}$ ratio and the Eu anomaly. The $[La/Yb]_{PM}$ ratio represents the slope of the normalized REE pattern and is often used to discriminate the magmatic affinity of volcanic rocks (Barrett and MacLean, 1999). The REE and Y are normalized to primitive mantle values (subscript PM, Sun and McDonough, 1989). The behavior of europium is quantified as the Eu anomaly (Eu/Eu*), where Eu is the measured concentration and Eu* is the predicted concentration calculated by straight-line interpolation between Sm and Gd (Rollinson, 1993). In this study, the europium anomaly has been calculated as follows: $(Eu/Eu^*)_{PM} = 2 \times Eu_{PM} / (Sm_{PM} + Gd_{PM})$.

Figure 3.4a shows a compilation of the REE patterns of some fresh volcanic and intrusive rocks in the South Flank of the Matagami district. The magmatic affinity of these rocks is reported to be mostly tholeiitic (Maier et al., 1996) apart from the Key Tuffite and the overlying Lower Andesite in the Wabassee Group, which are transitional to calc-alkaline (Genna et al., 2014). However, a large variability in the concentration of LREE exists for the altered Key Tuffite samples (Fig. 3.4b). Based on the $[La/Yb]_{PM}$ ratio, the Key Tuffite can be divided into four groups (Group I – IV), with values ranging from 1.4 to 23.9. The different degree of fractionation of the REE-Y pattern is clearly related to hydrothermal alteration since the $[La/Yb]_{PM}$ ratio is homogeneous away from the deposit ($[La/Yb]_{PM}$ ratio of the Key Tuffite precursor = 7.4) and only starts to vary within the alteration halos (Fig. 3.5a). Mass changes induced by alteration, such as leaching, silicification or mineralization for example, can significantly modify the REE-Y values.

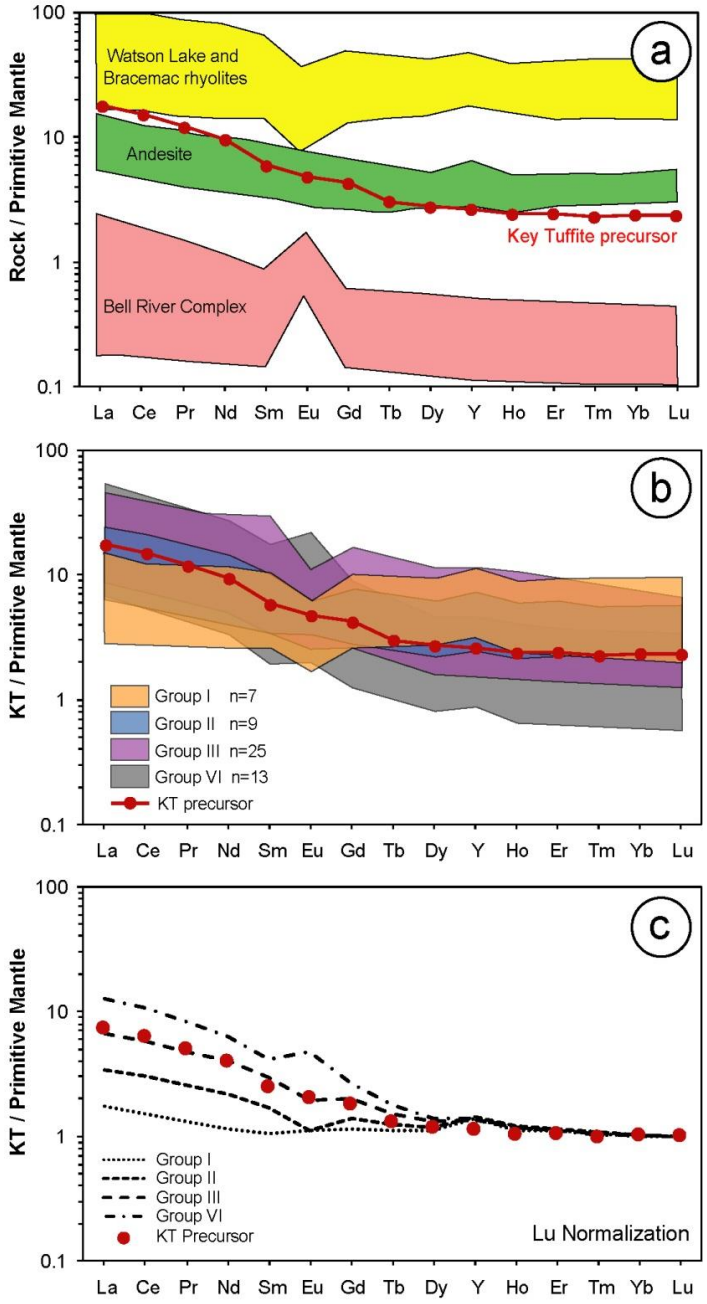

Figure 3.4 REE-Y multi-element variation diagrams normalized to primitive mantle (Sun and McDonough, 1989). a) Selected volcanic rocks of the South Flank including the precursor of the Key Tuffite. Fields are from Gaboury and Pearson (2008), Piché (1991), Munoz Taborda (2011), Maier et al. (1996) and Debreil (personal communication). Modified from Genna et al. (2014). b) Altered Key Tuffite samples surrounding the Bracemac-McLeod deposits. Groups I to IV are based on an increase of the La/Yb ratio. c) Normalization of the median of the groups I to IV by Lu. Refer to text for more details.

Following the approach of Ludden and Thompson (1979) and MacLean (1988), these effects of concentration or dilution of the REE-Y were removed by normalizing the REE and Y to Lu, the most immobile REE. Comparing the pattern of these groups with the pattern of the Key Tuffite precursor (Fig. 3.4c), it appears that the mobility of the REE is mostly limited to the LREE (La to Sm). The HREE (Dy to Lu) were relatively immobile during the hydrothermal alteration around the Bracemac-McLeod deposits, as previously recognized by MacLean and Kranidiotis (1987) and MacLean (1988) for the Phelps Dodge deposit. Group III is similar to the precursor (Fig. 3.4c). Compared to the precursor, both depletion (Groups I and II) and enrichment (Group IV) of LREE are observed. It is noteworthy that Eu is also widely mobile and both negative (Group II) or positive (Group IV) anomalies are recorded in the altered Key Tuffite samples.Figure 3.5a illustrates the variation of $[La/Yb]_{PM}$ versus the distance to the massive sulfide zones, where zero is adjacent to ore and 1200 m is the furthest away. Variation of the $[La/Yb]_{PM}$ ratio is significant. Gains of LREE ($[La/Yb]_{PM} > 7.4$) are restricted to the proximal chloritization zone (0-200 m), whereas losses ($[La/Yb]_{PM} < 7.4$) start in the distal sericitization zone (200 to 400 m) but are also present in the chloritization zone (0 to 200 m). A very similar behavior exists for the Eu anomaly (Figs. 3.5b and 3.6). Eu/Eu* values vary between 0.3 and 3.0.

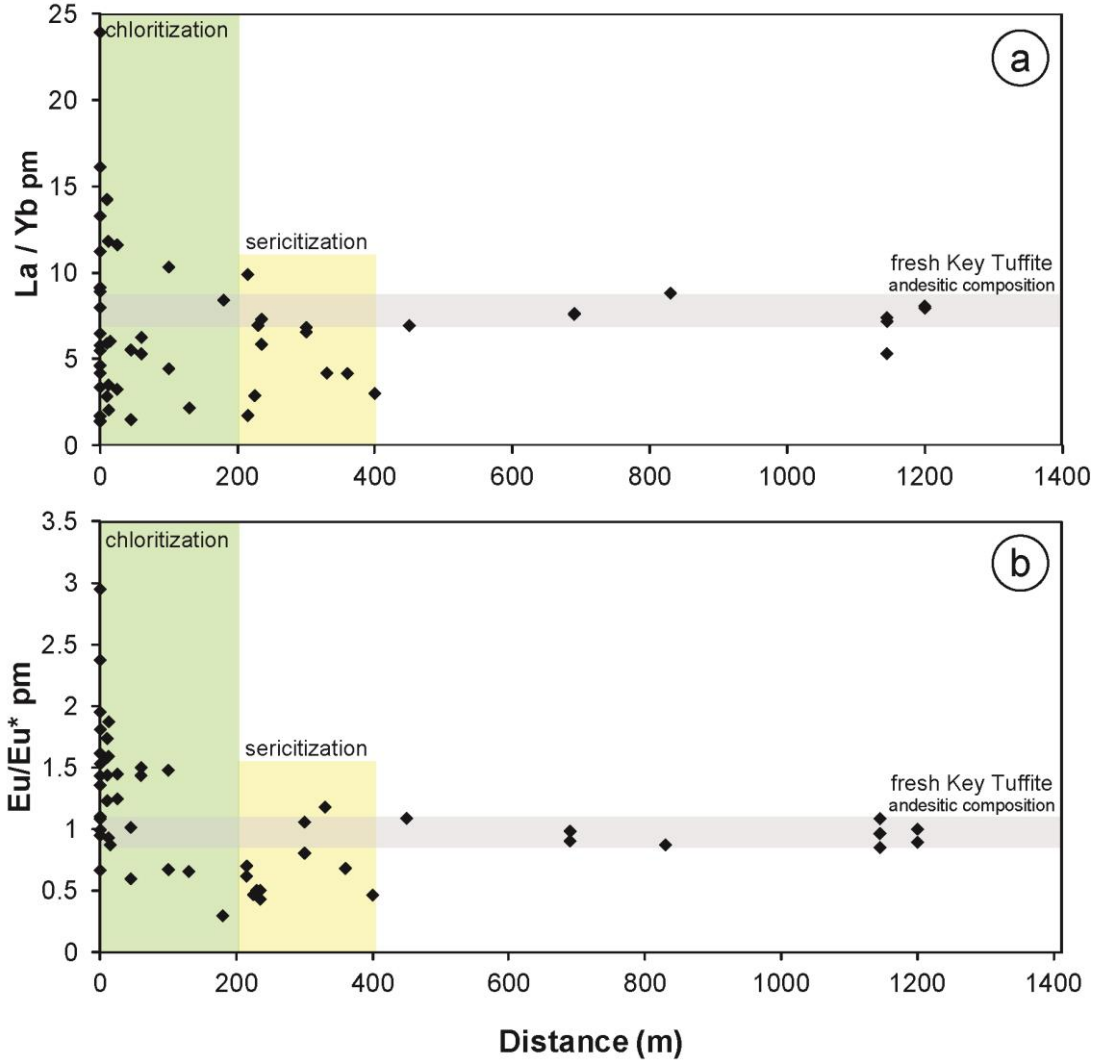

Figure 3.5 Variation of a) [La/Yb]PM and b) Eu/Eu* versus distance from the Bracemac-McLeod deposits, where 0 m is immediately adjacent to the deposit. Alteration zones of sericitization (0 – 200 m) and chloritization (200 – 400 m) are based on gains of K2O and MgO respectively, as determined by Genna et al. (2014).

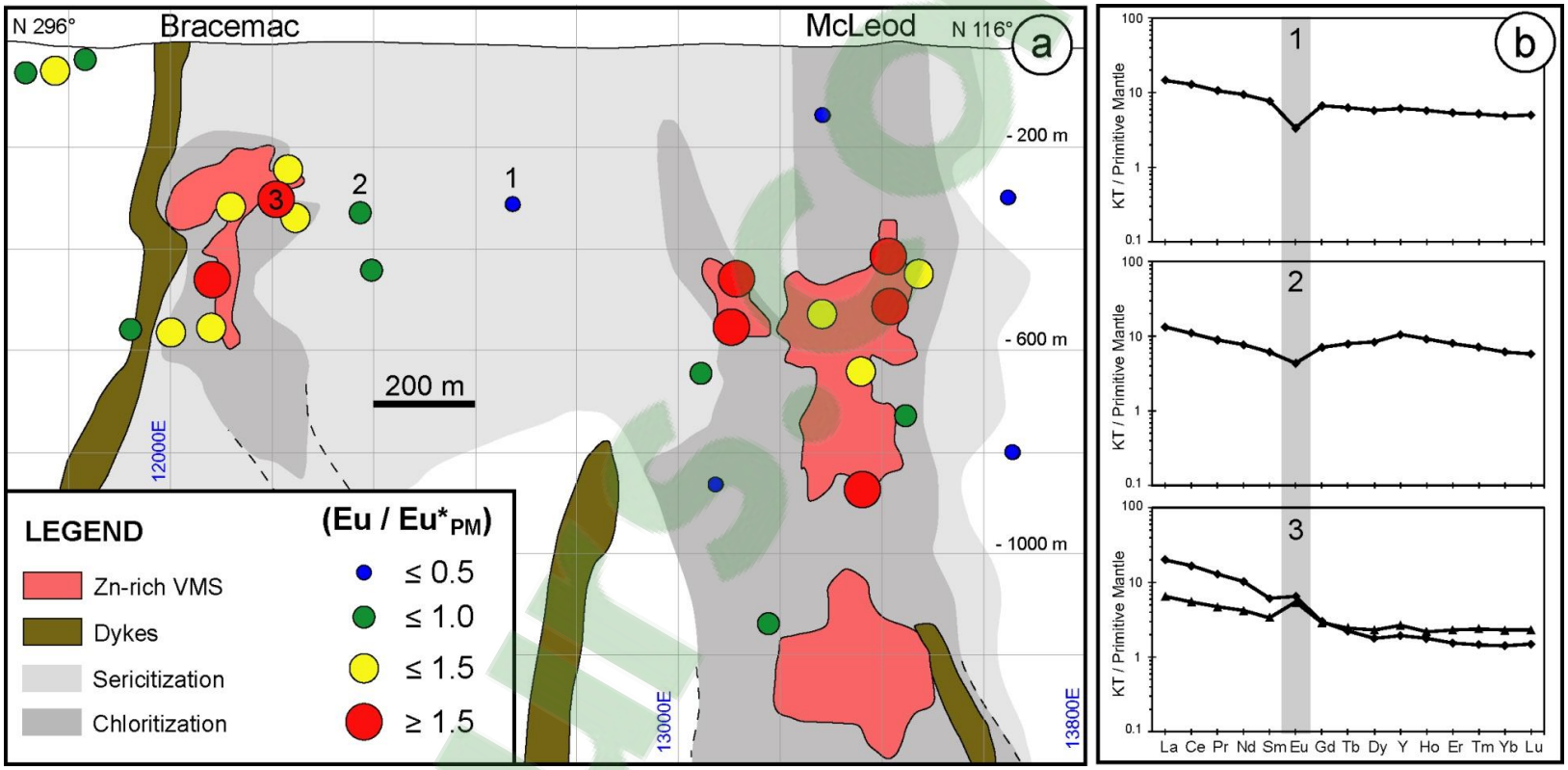

Figure 3.6 a) Spatial distribution of Eu anomaly (Eu/Eu*) along a composite longitudinal view of the Bracemac-McLeod deposits. The Eu anomaly progressively increases towards mineralization and can be used as an exploration tool. b) REE-Y multi-element variation diagrams, normalized to primitive mantle (Sun and McDonough, 1989), of three Key Tuffite samples (1-3) distributed around the Bracemac lens (labelled on a).

Away from the deposit, the anomaly is absent (Eu/Eu* = 1, similar to a fresh andesite). The anomaly becomes negative (<1) in the sericite zone (Figs. 3.5b and 3.6). Progressively towards the deposit, the anomaly becomes mostly positive (>1) and reaches a maximum value of 3.0 in the Key Tuffite samples close to the mineralized lenses (Figs. 3.5b and 3.6b). This positive Eu anomaly is persistent up to 100 m from the deposit, but the negative anomaly extends out to 400 m.

3.7. MINERAL CHEMISTRY

The volcanic glass and magmatic plagioclase crystals might have been important host of REE in the Key Tuffite. However, the high reactivity of the volcanic glass interacting with aqueous fluids (i.e. seawater or hydrothermal fluids) probably lead to the complete replacement by secondary phases. The Key Tuffite is now mainly composed of variable amount of quartz, sulfides, sericite, chlorite and carbonates (Fig. 3.2). Sulfides and quartz are known to have very low REE content (e.g. Mills and Elderfield, 1995; Monecke et al., 2002; Rimskaya-Korsakova et al., 2003) and will not be discussed further. Rare earth elements are commonly concentrated in certain calcium-rich minerals by their substitution of Ca^{2+} (Möller et al., 1984; Kontak and Jackson, 1995; Davies et al., 1998). Carbonates, apatite and allanite are the calcium-rich minerals present in the Key Tuffite according to petrography,

micro-XRF and electron microprobe works and were thus analyzed to investigate the distribution of the REE and Y.

Calcite and Fe-carbonate occur in proximity to some VMS deposits (e.g. Noranda, Canada - Hannington et al., 2003), and have also been documented in the Key Tuffite (Liaghat and MacLean, 1992). However, the genetic relationship between carbonate alteration and VMS deposit formation is uncertain (Gibson and Galley, 2007). Nevertheless, it was important to characterize the potential of REE incorporation into carbonates in order to estimate the contribution of these minerals to the corresponding whole-rock analysis.

Apatite [$Ca_5(PO_4)_3(F,OH,Cl)$] formed in various environments (magmatic and hydrothermal) can contain a significant amount of REE, generally ranging from 0.1 to 1.7 wt.% (Belousova et al., 2002), substituting for Ca^{2+} (Roeder et al., 1987; Rønsbo, 1989; Pan and Fleet, 2002). Apatite was not previously reported in the Key Tuffite and is rarely analyzed from VMS environments.

Allanite is a monoclinic epidote with general formula $CaREEAl_2Fe^{2+}Si_3O_{11}O(OH)$. Together with monazite, allanite is the main host of LREE in the continental crust (Gromet and Silver, 1983; Hermann, 2002). This mineral should be unstable when exposed to low temperature hydrothermal fluids (Wood and Ricketts, 2000; Harlavan and Erel, 2002). However, some studies from granite (Wood and Ricketts, 2000; Poitrasson, 2002) demonstrated that the breakdown of allanite

only has a negligible effect on the global REE composition of the host granite, because LREE were mobilized only at the micrometer scale and trapped in secondary phases such as monazite. Nevertheless, at higher temperature and salinity, the LREE hosted in allanite may have the potential to be mobilized and could be a significant source for redistribution at the deposit scale. Allanite has been previously observed in the alteration zone of the Mattagami Lake deposit (Pan et al., 1994).

Sericite and chlorite are not Ca-bearing phases and hence not-typical REE-hosting minerals. Nevertheless, they too were analyzed because they may be important to the global REE contribution due to their high abundance in both proximal and distal alteration. Other accessory phases, such as monazite [(REE)PO_4] and xenotime (YPO_4) are more resistant to hydrothermal alteration (Cetiner et al., 2005). They were reported from the Mattagami Lake mine (Pan et al., 1994) but are very scarce in the Key Tuffite, and thus were not considered further in this study.

3.7.1. ANALYTICAL METHODS

Eleven representative Key Tuffite samples, representing the two main hydrothermal alteration assemblages (i.e. sericite and chlorite), were chosen for analysis of allanite, carbonates and apatite.

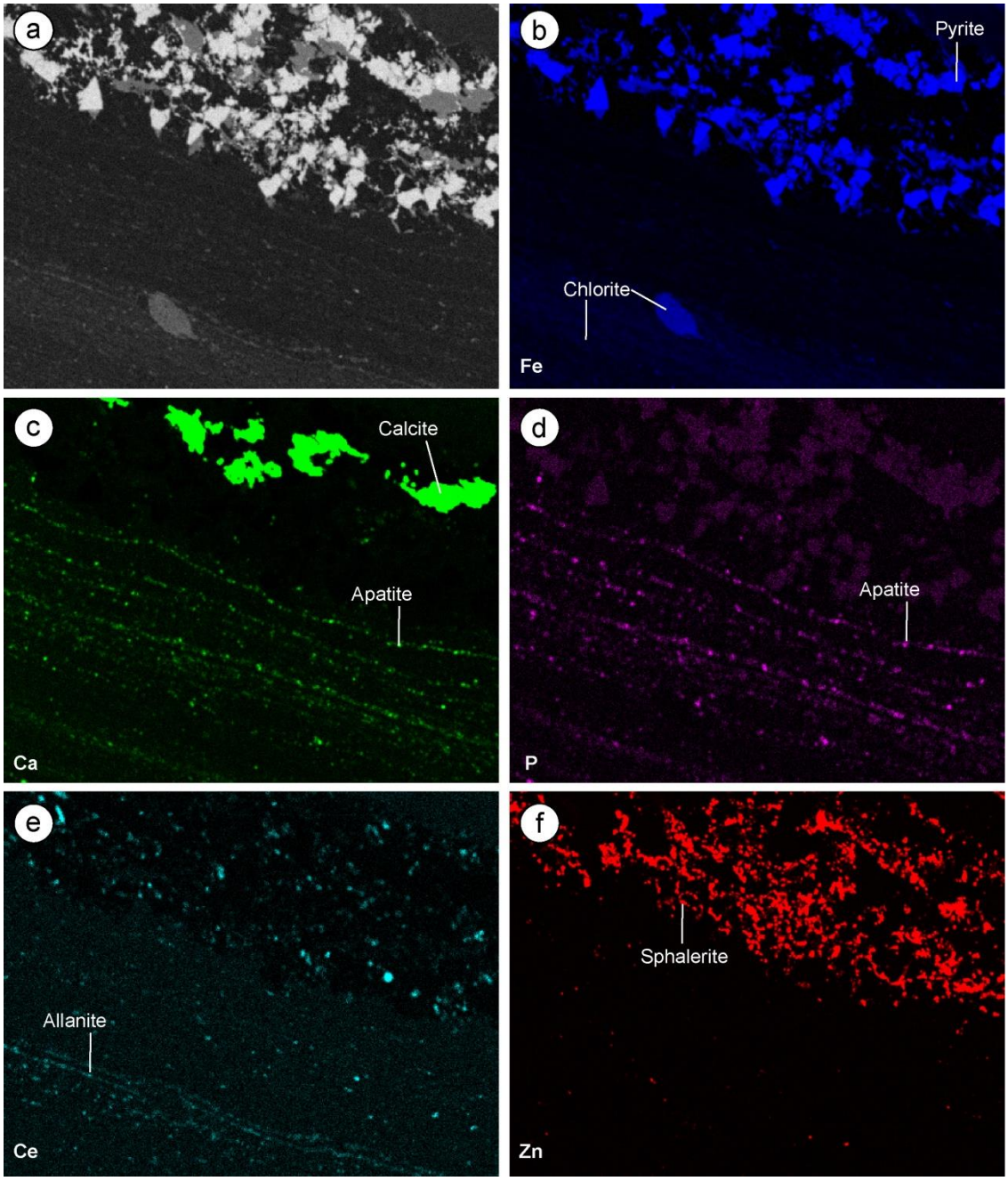

Figure 3.7 Elemental micro-XRF maps (1.7 x 1.3 cm) from a Key Tuffite thin section (sample 972117 in drill hole MC-08-55, 517 m depth). Fe, Ca, P, Ce, and Zn are presented allowing the observation of pyrite, chlorite, calcite, apatite, allanite and sphalerite.

Micro-XRF mapping of 1.7 x 1.3 cm of the fine-grained Key Tuffite was conducted on thin sections following the method and parameters of Genna et al. (2011). This approach was used to quickly locate calcium-bearing phases, which are potential REE-bearing minerals (Fig. 3.7). These selected calcium-bearing minerals were analyzed for major elements using a CAMECA SX-1000 electron microprobe at Université Laval, Quebec, Canada. For the trace and rare earth elements, LA-ICP-MS (Resonetics 193nm Laser Ablation System coupled with an Agilent ICP-MS) analyses were carried out at Université du Québec à Chicoutimi, Canada. Following 30 s of background analyses, minerals were analyzed along lines in an ultrahigh purity He-Ar atmosphere. Samples were analyzed with a beam size of 15 to 75 µm, at speed of 5 µm/second and laser energy of 5 mJ. Details of the analytical method are presented in the electronic supplementary material together with the results of reference materials, used to monitor the calibration, and the samples. Figure 3.8 illustrates the element distribution (in counts per second) in a single crystal of apatite in sericite-rich (Fig. 3.8a) and chlorite-rich (Fig. 3.8b) matrices as a function of time.

3.7.2. SERICITE AND CHLORITE

Sericite and chlorite are the main alteration minerals in the Key Tuffite. They typically form a very fine-grained mosaic with quartz (Fig. 3.2).

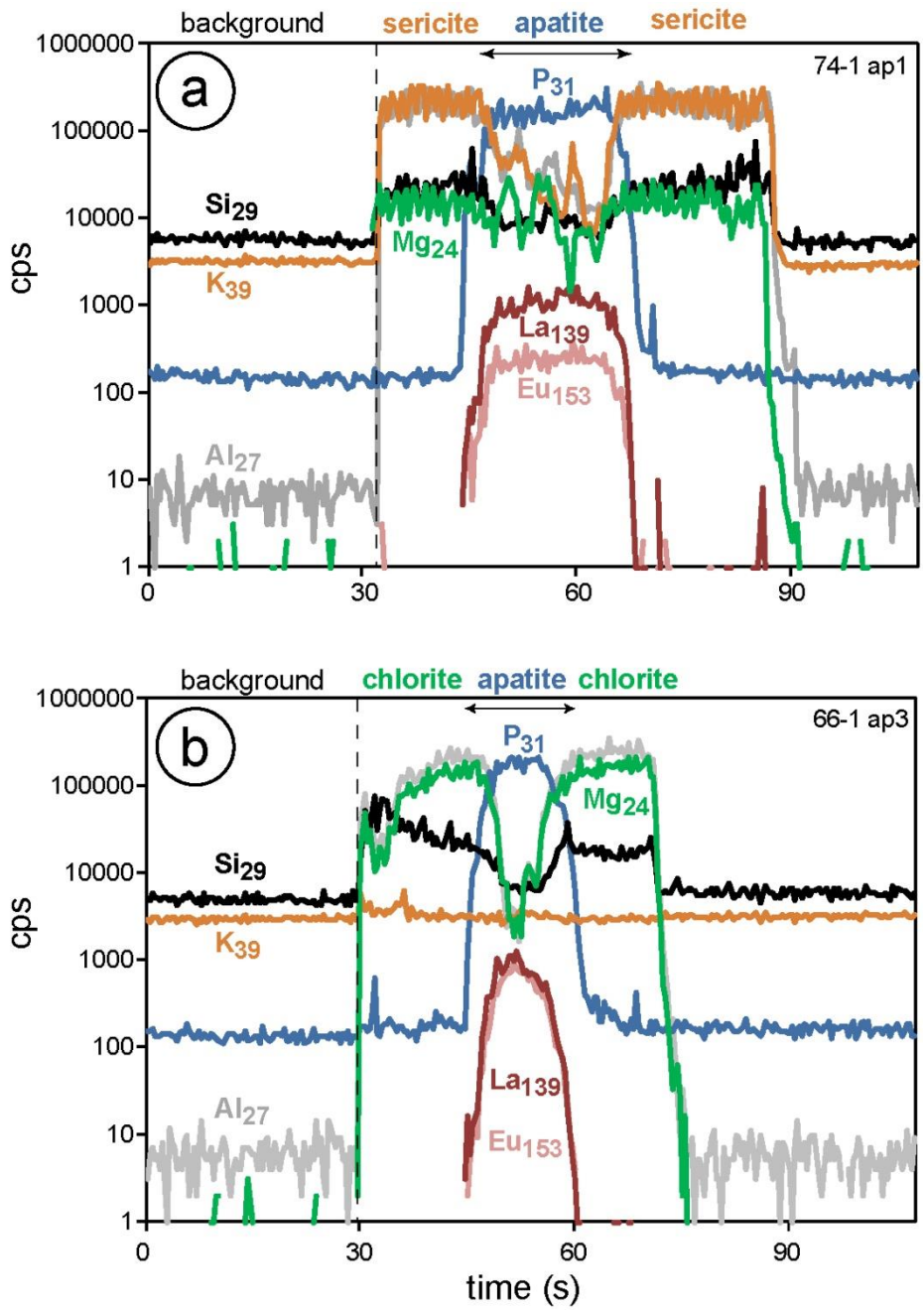

Figure 3.8 a. Time (in seconds) versus counts per second spectra for laser ablation ICP-MS analyses of apatite grains in a) sericite-rich matrix (74-1 ap1, sample 716474 in drill hole MC-05-19, 821 m depth) and b) chlorite-rich matrix (66-1 ap1, sample 972166 in MC-07-25, 702 m). No REE were detected in either sericite or chlorite. Lines were preferred to spot analyses because there is a better control of the mineral phase analyzed and no loss of signal with depth.

Despite the very low detection limits (Electronic Supplementary Material) of the LA-ICP-MS analyses, no REE or Y was detected in the sericite and chlorite-rich matrices of the Key Tuffite (Figs. 3.8a and b). Quantitatively, it means that the amount of REE and Y hosted in sericite and chlorite is negligible, i.e. below the detection limit, with the sum of the LREE (ΣLREE = La to Sm) < 0.4 ppm, and Eu < 0.05 ppm.

3.7.3. ALLANITE

Allanite is observed as an accessory mineral of variable size (20-200 µm) in numerous Key Tuffite samples. Generally present as isolated grains within patchy chlorite alteration, as previously documented by Pan et al. (1994) for the Mattagami Lake mine, it can also form larger aggregates parallel to bedding (Figs. 3.2a and b) and not necessarily associated with chlorite. Due to its small size, only two grains have been analyzed by microprobe and LA-ICP-MS to confirm the values documented by Pan et al. (1994).

Microprobe data indicate that allanite (Fig. 3.9) can host up to 21 wt. % rare earth-oxides (REO), mostly Ce_2O_3 (up to 9 wt. %). LA-ICP-MS analysis reveals a highly fractionated REE (Fig. 3.9) pattern expressed by a $[La/Yb]_{PM}$ ratio of 237, on average, and a weak negative Eu anomaly (but still containing 500 ppm Eu). These data are similar to those obtained by Pan et al. (1994) by microprobe analyses.

3.7.4. CARBONATES

Based on major element mineral chemistry of 38 grains, two main carbonate phases have been identified in the Key Tuffite at Bracemac-McLeod: calcite and ankerite (Fig. 3.10). Calcite (Figs. 3.3d-e and 3.7b) occurs mainly as disseminated subhedral crystals (100 μm to 1 mm). In some cases they can represent up to 25 wt. % of the sample. Coarse-grained calcite (generally >1.5 mm) is also observed in late brittle veins associated with quartz (Fig. 3.3e) and thus interpreted to have precipitated from late metamorphic fluids. Ankerite is less abundant and has been identified in only two samples. Ankerite appears as isolated grains (100 μm to 1 mm), associated with sulfides (Fig. 3.3c) suggesting a link with the synvolcanic mineralization. Microprobe data (electronic supplementary material) indicate that calcite is close to the ideal end-member calcite composition and similar to those analyzed by Costa et al. (1983) in the alteration zone of the Mattagami Lake Mine (Fig. 3.10a). However, our ankerites are less Fe-rich than those of the ore zone of the Mattagami Lake Mine (Fig. 3.10a). A total of 45 grains have been analyzed (31 calcites and 14 ankerites) by LA-ICP-MS (electronic supplementary material). Based on textures and REE-Y patterns, two groups of calcites have been identified (Fig. 3.10c-d). Group I comprises the disseminated calcite grains which have a relatively flat REE-Y pattern ($[La/Yb]_{PM}$ = 2.8) and a weak positive Eu anomaly (Eu/Eu* = 2.1).

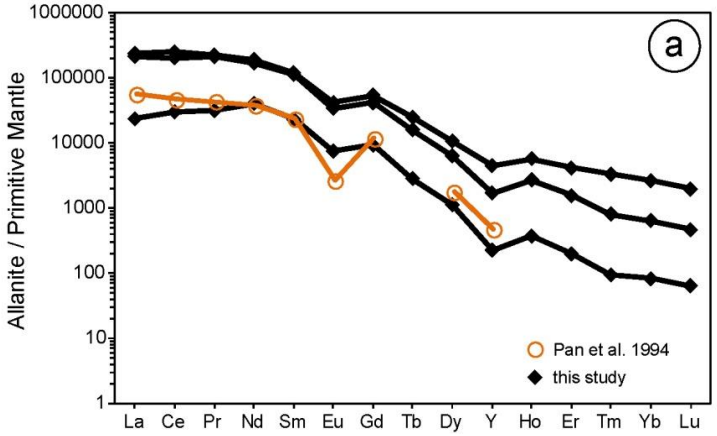

b	#1	#2
	742_5	742_6
SiO_2	31.54	31.12
Al_2O_3	16.99	16.43
FeO	17.06	14.08
MgO	1.60	0.07
CaO	7.45	11.26
Na_2O	0.04	0.03
ThO_2	0.08	0.02
La_2O_3	3.15	3.83
Ce_2O_3	9.07	9.47
Pr_2O_3	1.34	1.40
Nd_2O_3	4.82	5.83
SmO	0.83	0.93
REO	**19.21**	**21.46**

Figure 3.9 Composition of allanite. a) REE-Y multi-element variation diagram of allanite normalized to primitive mantle (Sun and McDonough, 1989) from this study (LA-ICP-MS) compared to that of Pan et al. (1994) from the Mattagami Lake mine. b) Microprobe data of allanite (74 2_5 and 74 2_6). REO represents the sum of La_2O_3 to SmO.

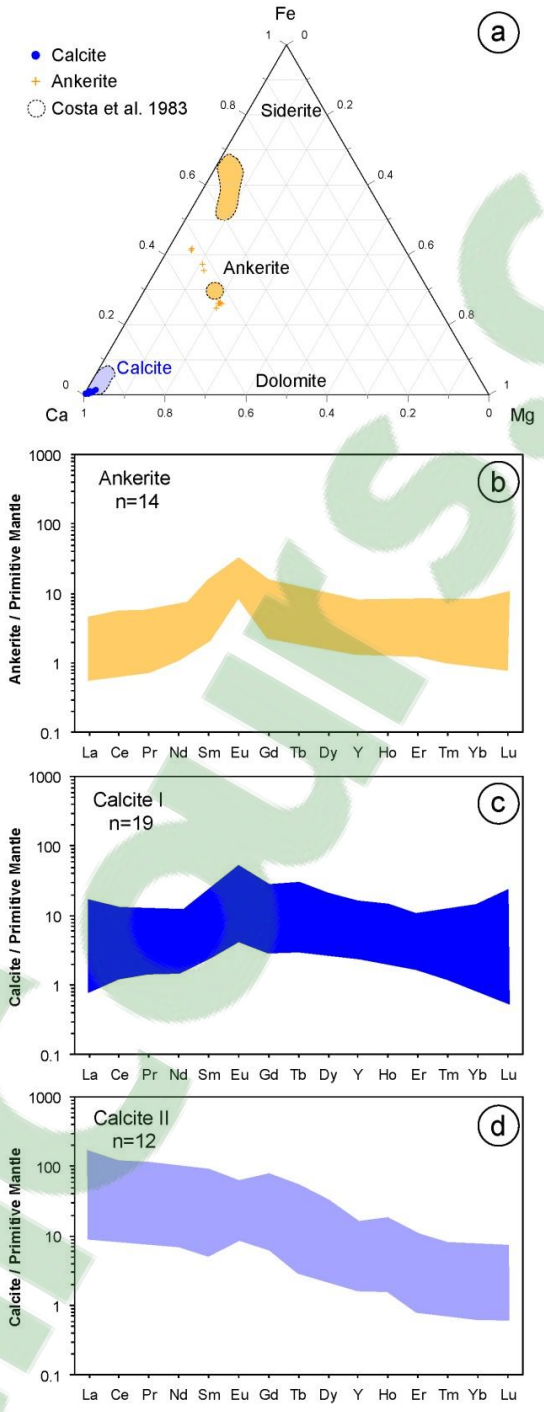

Figure 3.10 Composition of carbonates. a) Ca-Fe-Mg ternary diagram using microprobe data. b-d) REE-Y multi-element variation diagrams, normalized to primitive mantle (Sun and McDonough, 1989), of ankerite (b), calcite I (synvolcanic -c) and calcite II (late veins-d) analyzed by LA-ICP-MS.

Group II is the calcite from the quartz-carbonate veins and has a more fractionated REE-Y pattern, with a ratio of $[La/Yb]_{PM}$ of 33.5 on average with variable positive or negative Eu anomalies. Ankerite has a REE pattern very similar to Group I disseminated calcite (Fig. 3.10b), with a relatively flat pattern ($[La/Yb]_{PM}$ = 2.9) and a positive Eu anomaly (Eu/Eu*=3.8). Compared to allanite, the REE-Y budget of the carbonates is low but varies with the type of carbonate. Ankerite has the lowest sum of REE-Y (ΣREE and Y = 46.1 ppm), Group I disseminated calcite has very low ΣREE-Y (78.3 ppm) content, and Group II calcite from the late veins has a low content (350.5 ppm). However, as more than 20 wt. % of carbonates is present in some samples, carbonates could have an important contribution to the total REE-Y budget.

3.7.5. APATITE

Apatite typically forms subhedral disseminated crystals of relatively small size (25-200 μm), with crystals commonly aligned along some preferential beds of the Key Tuffite (Fig. 3.3 and 3.7c-d). Some grains show good evidence of co-precipitation with sulfides (Fig. 3.3f). Microprobe analyses were conducted on 56 apatite grains (electronic supplementary material). The composition of apatite analyzed in the Key Tuffite is mostly between fluoroapatite and hydroxylapatite (Fig. 3.11a), with the F-rich end member clearly the dominant pole, and Cl is absent. The OH

component of apatite has been calculated following the method described in the appendix of Piccoli and Candela (2002).

LA-ICP-MS analyses of apatite (47 grains) are presented in the electronic supplementary material. Apatite is clearly an important REE-Y host mineral with ΣREE-Y of 2445 ppm on average but varying from 486 to 5273 ppm. Their REE-Y pattern (Fig. 3.11b-c) exhibits a fractionated pattern with $[La/Yb]_{PM}$ between 0.4 and 111.1, but 29.9 on average. Two main groups are identified: one with a negative Eu anomaly and one with a positive one (Fig. 3.11b-c). Europium values range from 6.6 to 580 ppm. Both groups are characterized by a wide variation of the LREE. Figure 3.11d illustrates this variation and highlights two sub-groups based on the ratio $[La/Yb]_{PM}$ vs. $[La/Nd]_{PM}$, irrespective of the Eu anomaly. This suggests that the behavior of LREE is decoupled from the behavior of Eu (Fig. 3.11d).

Crystallographic considerations can give some insights to explain these results. Two Ca sites are present in the apatite structure: nine-coordinated Ca1 and seven-coordinated Ca2 (Hughes et al., 1989). The ionic radius of Ca^{2+} is different for both sites (1.18Å and 1.06Å for Ca1 and Ca2, respectively). This is of importance because both sites will incorporate REE-Y differently thus triggering sector zoning (Rakovan and Reeder, 1994, 1996). This behavior is well documented for hydrothermal vein-filling apatite from Llallgua, Bolivia (Rakovan

et al., 1997; 2001). Quantitative determination of the REE concentration by Synchrotron X-Ray fluorescence (SXRFMA) between non-equivalent subsectors (i.e. crystallographically distinct surfaces) indicated that all the REE and in particular the LREE, except Eu, are intra-sectorally zoned (Rakovan et al., 2001). The different behavior of europium is explained by its heterovalent state, as both Eu^{2+} and Eu^{3+} can fit in the Ca1 and Ca2 sites. Roughly, equal and opposite partitioning in the sites would yield the generally observed lack of intra-sectoral zoning of total Eu (Rakovan et al., 2001). However, our data suggest that Eu is also affected by the sectoral zoning (Fig. 3.11d), implying that the relative amount of Eu^{2+} and Eu^{3+} is variable (i.e. one ion is dominant).

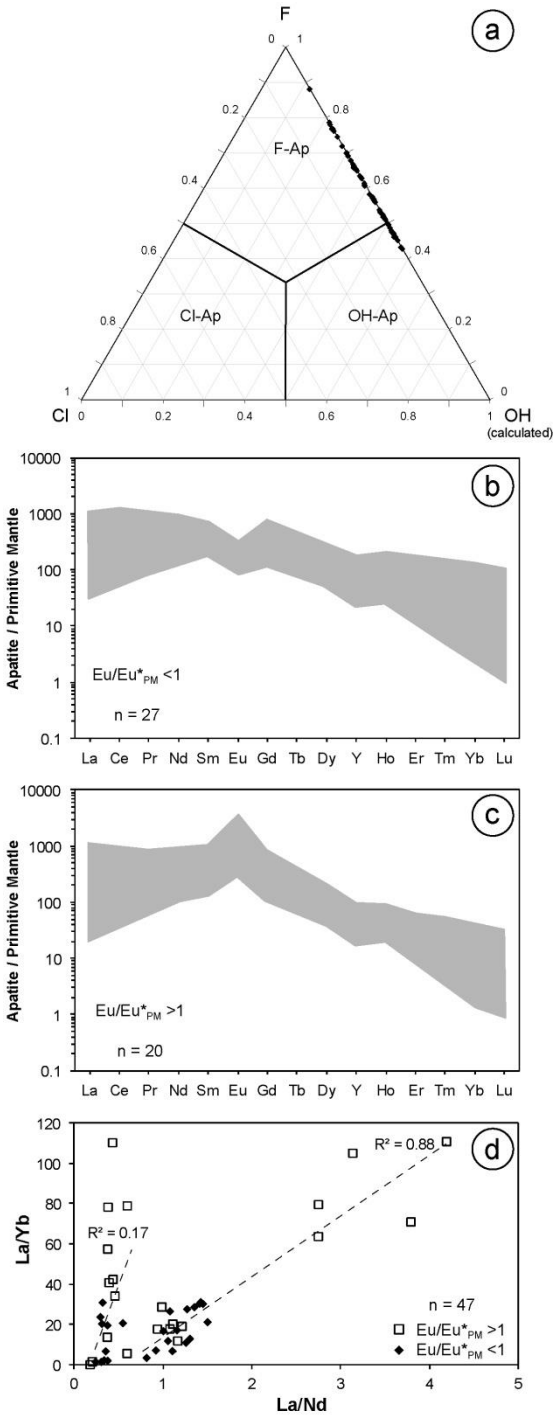

Figure 3.11 Composition of apatite. a) Cl-F-OH ternary diagram using microprobe data. b-c) REE-Y multi-element variation diagrams normalized to primitive mantle (Sun and McDonough, 1989) for apatite analyzed by LA-ICP-MS showing both positive (b) and negative (c) Eu/Eu*. d) $[La/Yb]_{PM}$ versus $[La/Nd]_{PM}$ ratios in apatite, as a function of the Eu/Eu*.

3.8. MINERALOGICAL MASS BALANCE

3.8.1. METHOD

In order to quantify the proportion (wt. %) of the REE hosted by the main Ca-minerals analyzed (apatite and carbonates) in each alteration zone of the Key Tuffite a mineralogical mass balance was carried out (e.g. Dare et al., 2010). This calculation requires: 1) the concentration of the REE, Ca and P from the whole rock, 2) the proportion (wt. %) of apatite and carbonates calculated from the whole-rock analyses (see below), and 3) the concentration of REE in apatite and carbonates (electronic supplementary material). The proportion of apatite, calcite and ankerite was calculated as wt. % using whole-rock P and Ca and the micro-XRF and microprobe data. Based on petrographic observations, it was assumed that apatite is the main P-bearing mineral. Thus, all the P in the whole rock was assigned to apatite. After subtracting the amount of Ca necessary to form apatite, the remaining Ca was attributed to calcite or ankerite according to the micro-XRF and microprobe identification of the carbonates. Ankerite was never found with calcite in the same sample, simplifying the calculations. The mass balance was calculated for the each sample with available mineral data. The proportion of allanite could not be determined based on either visual (small size and scarcity) or geochemical estimation (REE mineral). Thus, allanite was not included in this calculation.

3.8.2. RESULTS

Figure 3.12 present the results of the mineralogical mass balance calculation. From the 11 Key Tuffite samples studied in details, four representative examples are given: one for the sericite-rich zone and three for the chlorite-rich zone. Figures 3.12a-d show the REE and Y multi-element variation diagrams of both whole-rock and analyzed Ca-rich minerals. The REE and Y patterns of carbonates and apatite reflect in most cases the REE and Y pattern of their respective whole-rock analysis, including the negative (sericite zone) or positive Eu anomalies (chlorite zone). The difference between the apatite and whole-rock analyses in Fig 3.12.b can be explained by sector zoning in the apatite (see Section 5.5). Figures 3.12e-h show the results of the mineralogical mass balance calculation for apatite and carbonates (calcite or ankerite). In general, less than 20% of the REE in the whole rock are hosted by these Ca-rich minerals, except Eu which can vary from 15% to 100%. In the chlorite zone, accessory amounts of apatite control most (56, 83 and 96%: Fig. 3.12e) of the Eu in some cases. In two cases where carbonate is abundant (>15 wt. %) in the chlorite zone, it is ankerite rather than apatite which controls most (67%) of the Eu anomaly (Fig. 3.12f) in spite of the low concentration of Eu (~10 ppm) in carbonate. However, in samples from the sericite zone, and the remaining three samples from the chlorite zone, both apatite and carbonates host less than 20% of Eu (Fig. 3.12f-g).

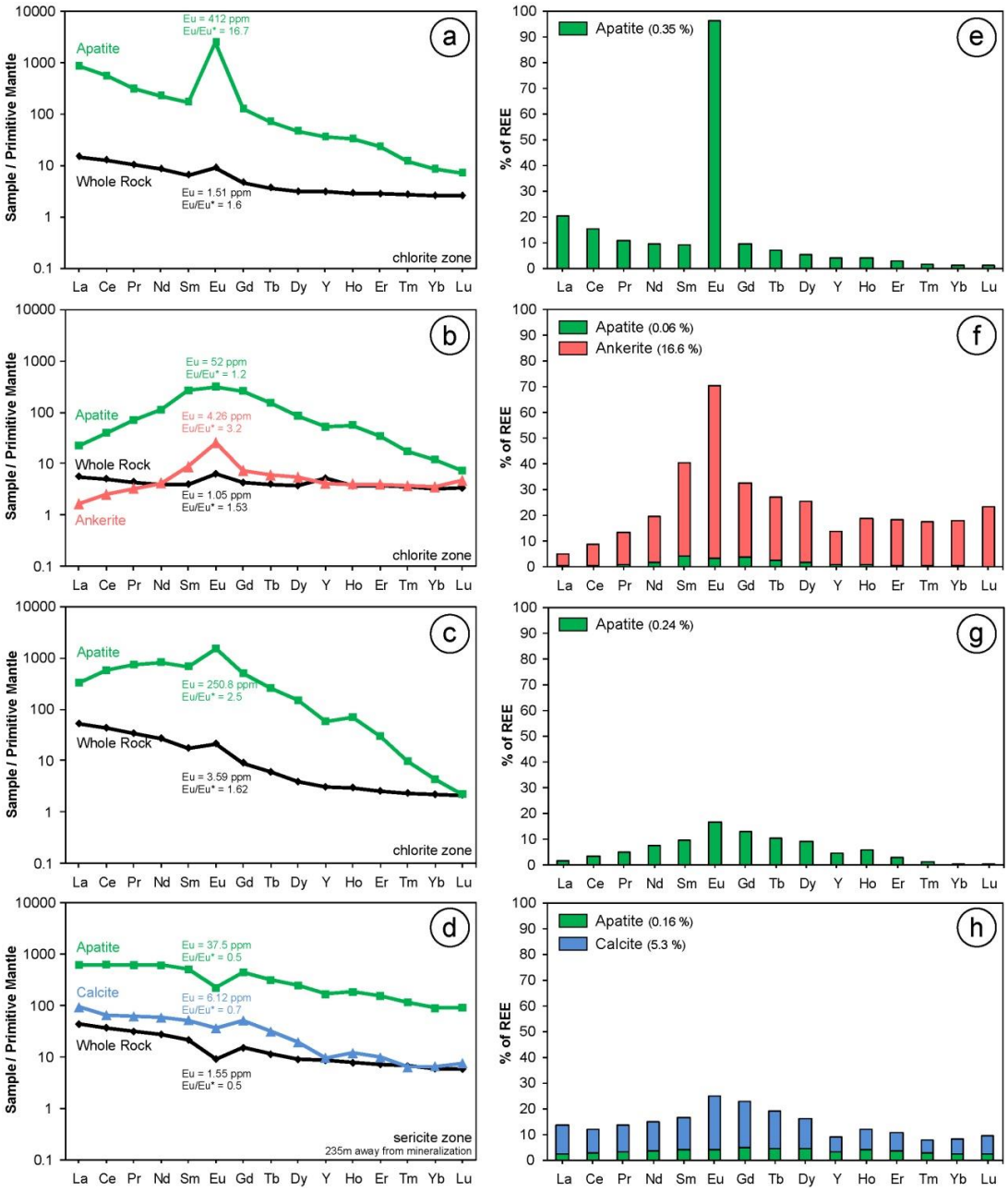

Figure 3.12 REE-Y multi-element variation diagrams (a-d), normalized to primitive mantle (Sun and McDonough, 1989), of whole-rock Key Tuffite samples and analyzed carbonates or apatite used in the mineralogical mass balance calculations (e-h) to determine the amount (%) of REE-Y hosted by these Ca-rich minerals. a and e) sample 716595, in drill hole MC-07-28, 556 m depth; b and f) 716489, in MC-05-18, 928 m; c and g) 716477, in MC-04-04, 523 m; d and h) 716479, in MC-05-15, 324m.Abundance (in weight %) of each Ca-rich mineral is given in brackets in e-h.

The rather low concentration of Ca in the whole rock (<3 wt.% CaO) indicates that Eu should be hosted in either Ca-poor or Ca-absent accessory phases (e.g., monazite, xenotime) which have not been analyzed in this study.

A detailed study coupling counting grains of allanite with mineralogical mass balance calculations by Pan et al. (1994) revealed that allanite hosts a large proportion of the LREE (91% of La; 73% of Ce; 66% of Nd; and 55% of Sm) in the chloritized Watson Lake rhyolite footwall of the Mattagami Lake mine (Fig. 3.1a). Although our study did not reach the same level of detail, the proportion of allanite and the amount of LREE contained in this mineral is assumed to be similar in the case of the Bracemac-McLeod deposits (Fig. 3.9). Allanite can also host up to 500 ppm of Eu in spite of its negative Eu anomaly (Fig. 3.9). Only 0.25% of allanite in the sample is required to contribute several ppm of Eu in the whole-rock analysis, which could account for the missing Eu and LREE in the mass balance.

3.9. DISCUSSION

The REE behave as a coherent group of elements, because of similar charge (+3) and ionic radius, and are rarely decoupled in geochemical processes. However, under specific hydrothermal conditions, REE may react differently. The most direct evidence comes from modern hydrothermal vents, where the fluids sampled show enrichment in LREE and Eu compared to HREE (e.g. Michard, 1989; Mitra et al., 1994; Douville et al., 1999). Experiments at relatively high temperature (up

to 300°C) from Migdisov et al. (2009) show that LREE and Eu form more stable complexes, with chloride and fluoride, than HREE, facilitating the mobility of LREE in hydrothermal fluids. Moreover, the mobility of Eu is amplified by the heterovalent character of this element. Unlike the other REE which have only a +3 valence, Eu has two valences (+2 and +3) of which only the +2 species can be transported by hot and reducing Cl-rich fluids (Sverjensky, 1984). The LREE and Eu have been documented as mobile in a variety of ancient VMS settings (Graf, 1977; Campbell et al., 1984) including the Matagami district (MacGeehan and MacLean, 1980; MacLean, 1988). The major source of REE in submarine hydrothermal systems is the leaching of host rocks via the partitioning of REE between alteration minerals and the fluids (Schmidt et al., 2010). At Matagami, LREE and Eu are generally depleted in the strongly leached zone at depth and redeposited in the overlying chloritized Watson Lake rhyolite, just below the mineralization (MacLean, 1988). This process is illustrated on Figure 3.13, where selected altered samples from the Watson Lake rhyolite from the footwall of the Bell Allard South and Mattagami Lake mines are characterized by a strong depletion of LREE compared to the unaltered equivalent.

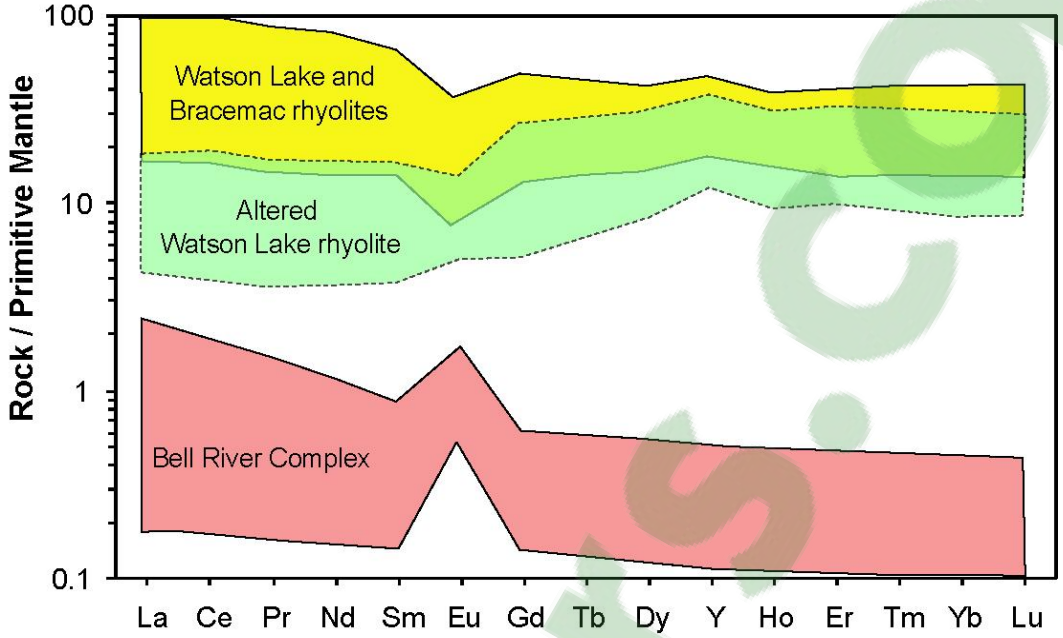

Figure 3.13 REE-Y multi-element variation diagram normalized to primitive mantle (Sun and McDonough, 1989) of the Bell River Complex and fresh and altered Watson Lake rhyolite footwall. Fields compiled from Costa et al. (1983); Piché (1991); Maier et al. (1996); Gaboury and Pearson (2008); Munoz Taborda (2011).

However, this study highlights that, at the stratigraphic level of the mineralization, such as along the Key Tuffite, the behavior of the LREE and Eu is relatively complex and varies not only as a function of the distance to the mineralization, but also as a function of the two main alteration assemblages in the Key Tuffite: distal sericite-rich and proximal chlorite-rich (Fig. 3.5). Prior to sericitization and chloritization, the breakdown of volcanic glass present in the tuffaceous Key Tuffite might have played an important role in the redistribution of the REE. Silicate glass is very unstable when reacting with aqueous solutions (i.e. seawater or hydrothermal fluids) because of its thermodynamic instability and high reactivity (Utzmann et al., 2002). The dissolution of volcanic glass is faster than that of minerals (Wolff-Boenisch et al., 2006) and follows a complex sequence of reactions (Gifkins et al., 2005 and references therein). Staudigel and Hart (1983) showed that during the alteration of a basaltic glass more than 60% of the REE are removed. However, most of the trace elements are only locally redistributed, with the REE retained by the fine-grained clay minerals and secondary accessory phosphate minerals that replace the former volcanic glass (Utzmann et al., 2002; Valle et al., 2010). Therefore, it is considered that in the Key Tuffite no significant loss of REE occurred during the breakdown of the volcanic glass at the seafloor. Magmatic plagioclase phenocrysts (and microliths) undergo only minor dissolution during the breakdown of volcanic glass during interaction with

seawater (Gifkins et al., 2005). Therefore, during later hydrothermal alteration (sericitization and chloritization), major redistribution of REE occurred as follows.

Sericitization is a low temperature (<250°C) VMS alteration (e.g. Eastoe et al., 1987; Large et al., 2001b) generally formed during either the early stage or at the outer margins of a hydrothermal system. This process is characterized by the breakdown of plagioclase to sericite (fine-grained white mica). It can be illustrated by the following reaction:

$$3NaAlSi_3O_8 + K^+ + 2H^+ = KAl_3Si_3O_{10}(OH,F)_2 + 6SiO_2 + 3Na^+ \quad \text{(eq. 1)}$$
albite sericite quartz

Chloritization generally follows sericitization during intense alteration when the temperature of the hydrothermal system reaches 300°C (e.g. Sangster, 1972; Schardt et al., 2001) and fluids carry Fe^{2+} and Mg^{2+}. This process is characterized by the progressive transformation of sericite into chlorite in the inner part of the hydrothermal system, proximal to the sulfide mineralization. It can be illustrated as follows:

$$2KAl_3Si_3O_{10}(OH,F)_2 + 3H_4SiO_4 + 9Fe^{2+} + 6Mg^{2+} + 18H_2O =$$
Sericite

$$3Mg_2Fe_3Al_2Si_3O_{10}(OH)_8 + 2K^+ + 28H^+ \quad \text{(eq. 2)}$$
Chlorite

Petrographic evidence of this reaction is ubiquitous in the Key Tuffite (Fig. 3.2) and in the Watson Lake rhyolite footwall.

The mobility of the REE is controlled by the degree of resistance to hydrothermal leaching of specific minerals hosting a significant amount of REE. These minerals are rarely identified (Pan et al., 1994) and knowledge of the REE redistribution processes is very limited. The results of the mineralogical mass balance calculations are used below together with mineral chemistry to highlight the contribution of specific minerals on LREE and Eu behavior.

3.9.1. BEHAVIOR OF LREE

Figure 3.14 illustrates the behavior of the LREE as a function of the alteration zones. Four parameters of alteration are presented: ΔK_2O, ΔMgO, $[La/Yb]_{PM}$ and ΔSiO_2, where Δ represents the gain or loss of the element. The petrographic study confirmed that sericite, chlorite and quartz are the main K_2O, MgO and SiO_2 bearing minerals, respectively. Gain or loss (Δ) of these elements, compared to the unaltered precursor, is thus assumed to directly represent an increase or decrease of the corresponding mineral in the sample. These values are considered more reliable than a modal estimation because of the very fine-grained texture of the Key Tuffite. Based on Figures 3.5 and 3.14, three groups are identified and are discussed in detail below: 1) loss of LREE in the sericite zone (Group I: $[La/Yb]_{PM} < 7.4$ and $\Delta K_2O > 0$); 2) gain of LREE and silica in the chlorite zone (Group II: $[La/Yb]_{PM} > 7.4$ and $\Delta MgO > 0$); 3) loss of LREE in the

chlorite zone with major gain in silica (Group III: $[La/Yb]_{PM}$ <7.4, ΔMgO >0, ΔSiO_2>0)

3.9.1.1. SERICITE ZONE

Whole-rock analyses of the Key Tuffite revealed that sericitized samples are characterized by a significant loss in LREE (Fig. 3.5a). Loss in LREE in the alteration zone of the Mattagami Lake mine, in the Watson Lake rhyolite footwall (Costa et al., 1983), was interpreted to result from the preferential dissolution of primary metamict allanite (Pan et al., 1994). A similar process can be invoked in the Key Tuffite at Bracemac-McLeod where allanite has been observed in several samples beyond the sericite zone (Fig. 3.3). The high LREE content (Fig. 3.9) and the low resistance of this mineral during hydrothermal alteration (Wood and Ricketts, 2000) could effectively explain the loss of LREE in the sericite zone. However, the negative correlation between the loss of LREE and the gain of K_2O (Group I: R^2=0.23; Pearson product = -0.48; Fig. 3.13a) and the absence of REE in sericite (ΣREE detection limit of LA-ICP-MS = 0.4 ppm, Fig. 3.8) suggests an additional process: the inability of sericite to fix the REE during the breakdown of plagioclase (± altered glass) thus releasing REE into the fluids. Studies of modern hydrothermal fluids (Klinkhammer et al., 1994; Douville et al., 1999) revealed that the REE distribution in fluids is strongly controlled by the content of REE in the plagioclase from the underlying leached rocks. In addition to the leaching of

primary allanite, the release of REE during the transformation of plagioclase to sericite explains the loss of REE in this alteration zone.

3.9.1.2. CHLORITE ZONE

Chloritized samples are characterized by two different mobility behaviors of the LREE (Fig. 3.14b): 1) gain of LREE with gain of MgO and SiO_2 (Group II) and 2) loss of LREE, with gain in MgO and SiO_2 (Group III). The gain of LREE (Group II) is clearly linked with precipitation of hydrothermal allanite (Fig. 3.2a-b) and apatite (Fig. 3.2f) during the mineralization event, as illustrated by the petrographic observations. Allanite has been identified to carry a significant amount of LREE (Fig. 3.9) and is likely to be the main host (55 – 91%) of LREE (Pan et al., 1994). The results of our mineralogical mass balance indicate that apatite is also an important LREE-bearing mineral in proximity of the mineralization, where it hosts up to 20% of the total La (Fig. 3.12d).

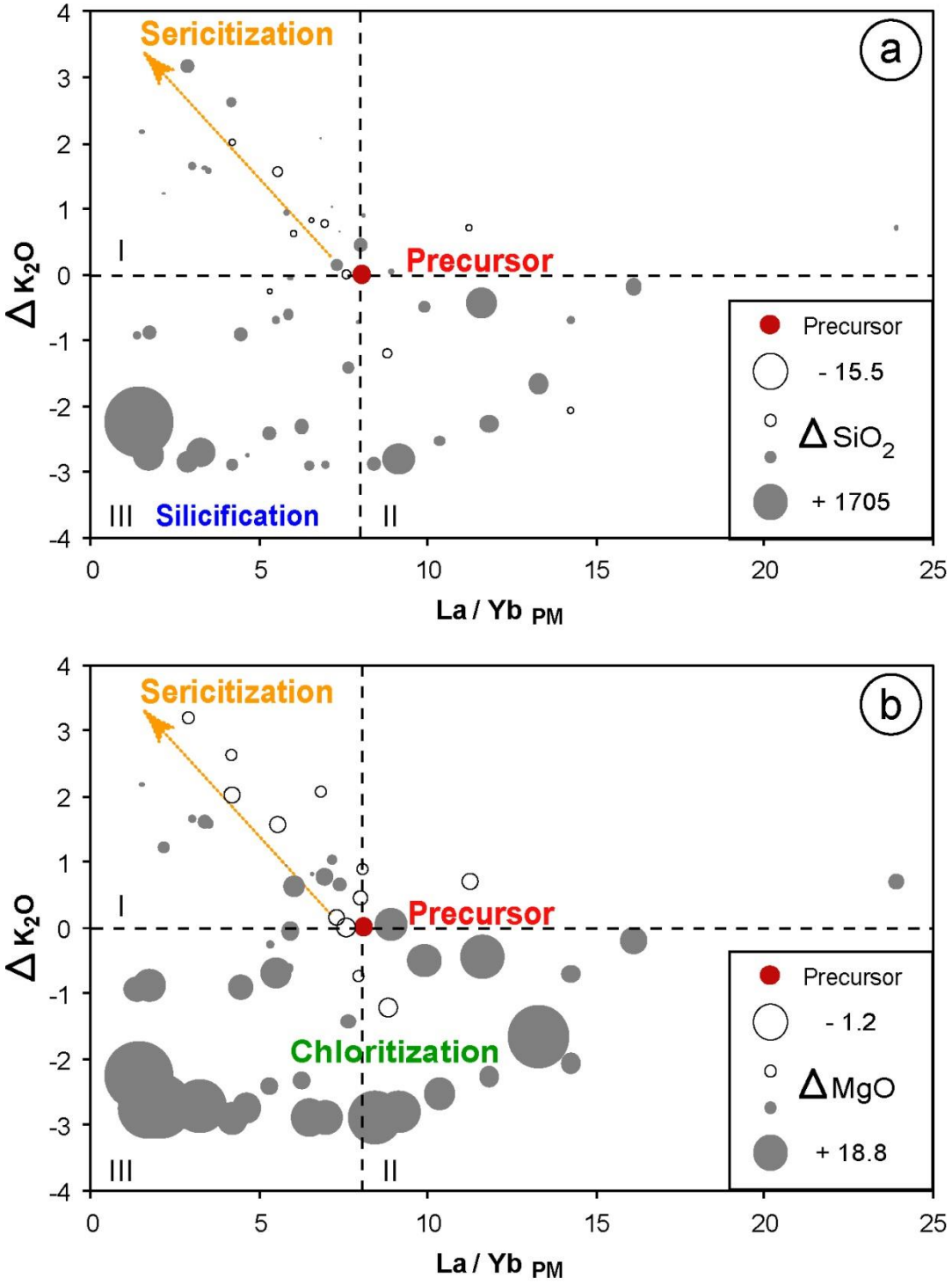

Figure 3.14 Gain or loss (Δ) of K_2O versus $[La/Yb]_{PM}$ as a function of a) Δ SiO_2 and b) Δ MgO. Refer to text for details on groups I, II and III.

The loss of LREE in the chlorite zone (Group III) is more complex to interpret. This group of samples shares a common enrichment in SiO_2 (Fig. 3.14a), characteristic of silicification (Fig. 3.2). Silicification is a low temperature VMS alteration (Jones et al., 2006; Schardt and Large, 2009) that can occur as pulses, several times during the hydrothermal system life. This alteration is characterized by the local precipitation of silica in pore spaces and fracture fillings which may ultimately lead to the sealing of the system. Such silicified rock portions may have been less prone to further alteration. This group of samples (Group III) is interpreted to have undergone silicification which preserved the state of alteration of previously sericitized rock. The sericitization explains the loss of LREE as described above (section 5.1.1). However, the lack of correlation among the samples of this group (Pearson product of 0.11) could be explained by the fact that this process happened early in the life of the hydrothermal system and was overprinted, to variable degrees, by the later chloritization event.

In summary, the gain in LREE in the chlorite zone is a combination of precipitation of allanite and apatite in the vicinity of the ore deposits. The loss of LREE in some samples is inherited from the lower temperature sericitization, preserved by the silicification and overprinted to various degrees by chloritization.

3.9.2. BEHAVIOR OF EU

3.9.2.1. SERICITE ZONE

The loss of Eu during sericitization is well documented (e.g. Alderton et al., 1980). Plagioclase is an important source of Eu because of its substitution with Ca (Budzinski and Tischendorf, 1989). However, only a minor part of Eu can be incorporated in sericite during the breakdown of plagioclase (Alderton et al., 1980). In the sericite zone, the relatively hot (<250°C) and reduced fluids favored the reduction and transport of Eu. The Eu^{2+} is thus preferentially removed from the sericite zone, carried away by the hydrothermal fluids and probably disseminated at the margin of the hydrothermal system. In the Key Tuffite, this process is illustrated by a decrease of the europium anomaly values from 1 in the fresh rock to 0.3 in the sericite zone (Figs. 3.5b and 3.6). Similar Eu depletions were observed in the most intensely altered portions of the footwall of some VMS from the Flin-Flon – Snow Lake area, Manitoba (Gale and Fedikow, 1999). However, to our knowledge, depletion of Eu has never been documented in the pervasive external low-grade alteration halo of VMS deposits (Campbell et al., 1984).

3.9.2.2. CHLORITE ZONE

The behavior of europium in the chlorite zone is simpler than that of the LREE and is characterized by a progressive increase of the europium anomaly, from 0.3

to 3.0, towards the mineralization (Fig. 3.5). This homogeneous behavior may indicate that the addition of Eu occurred late in the hydrothermal system evolution, overprinting the sericitization and the associated loss of LREE. Positive europium anomalies are common in hydrothermal fluids from seafloor vents (e.g. Michard, 1989; Mitra et al., 1994; Douville et al., 1999). They are also well documented in the VMS ore zone (Barrett et al., 1990; Adair, 1992; Lottermoser, 1992) and common in the lateral tuffaceous exhalite (Gale and Fedikow, 1999; Peter et al., 2003). However, the mineral phases hosting the europium in close proximity to any VMS deposits have never been clearly identified.

The LA-ICP-MS study confirms the positive correlation between the Eu anomaly in apatite (R^2=0.62, Pearson product 0.59) and carbonates (R^2=0.44, Pearson product 0.46) with the Eu anomaly in the whole rock (Fig. 3.15a). However, Figure 3.15b highlights the increase in the amount of Eu hosted in apatite toward the mineralization (R^2=0.56, Pearson product 0.71), whereas the amount of Eu in carbonate remains relatively constant (R^2=0.007, Pearson product -0.29). The higher Eu concentration in the vicinity of the mineralization results from accumulation of Eu in several minerals. The mineralogical mass balance calculation shows that the positive Eu anomaly is controlled mainly by apatite and carbonates (Figs. 3.12 and 3.15b) but that accessory phases, such as monazite, xenotime or allanite (Fig. 3.9) must also account for the balance of Eu. The amount of apatite in the Key Tuffite (calculated using whole-rock P_2O_5) only

weakly increases toward the Bracemac-McLeod deposits (Genna et al., 2014). Consequently, the positive Eu anomaly toward the mineralization appears more related to an enrichment of Eu in apatite.

3.9.3. PROPOSED MODEL OF THE BEHAVIOR OF THE REE DURING THE EVOLUTION OF THE HYDROTHERMAL SYSTEM

The study of the hydrothermal minerals hosting REE gives useful information on the evolution of the REE transport and precipitation. The main ligands (Cl^-, F^-, OH^-) derived from seawater and used in the transport of metals and REE are enriched in hydrothermal fluids. Thermodynamic calculations (Haas et al., 1995), experiments (Migdisov et al., 2009) and observations (Craddock et al., 2010) show that in an acidic hydrothermal fluid (pH<3) derived from seawater, the LREE and Eu are strongly complexed by Cl, whereas F, and OH are dominant for more neutral (3<pH<6) and more basic (pH>6) conditions, respectively. Destabilization of REE-complexes controls the concentration and distribution of REE within hydrothermal minerals.

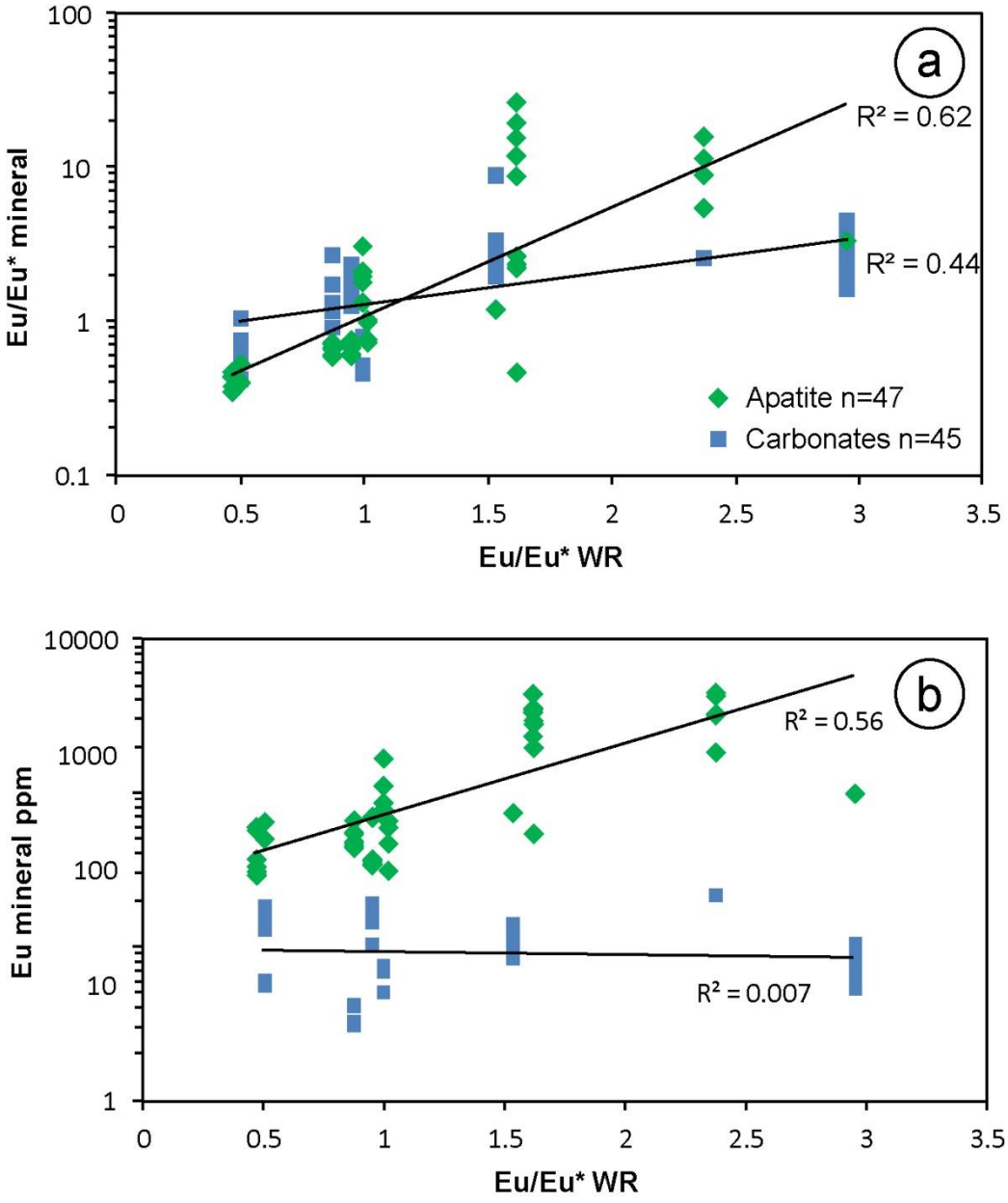

Figure 3.15 a) Eu/Eu* in apatite or carbonates versus Eu/Eu* in the corresponding whole-rock (WR) analyses. b) Eu concentrations in apatite and carbonates versus Eu/Eu* in the corresponding whole-rock analyses.

At Bracemac-McLeod, the hydrothermal fluids were focussed upward along synvolcanic faults up to the stratigraphic level of the Key Tuffite where they dispersed laterally within the primary porosity of this tuffaceous layer and adjacent rhyolites (Genna et al., 2014). In this study, the following evolution model is proposed (Fig. 3.16) to explain the geochemical zoning with respect to the minerals present in the Key Tuffite. The model is consistent with thermodynamic stabilities of minerals, the observed textural relationships and geochemical data accounting for the redistribution of the REE at the scale of the hydrothermal system. Original parameters are presented in Figure 16a before the beginning of the hydrothermal system. The early hydrothermal system started at moderate temperatures (<250°), with the glass-rich Key Tuffite (± plagioclase) progressively replaced by sericite (Fig. 3.16b). During this reaction, fluorine present in seawater was probably fixed in the sericite structure (eq. 1). Fluorine is generally depleted in hydrothermal vent fluids relative to seawater (Von Damm et al., 1985) but enriched in the alteration zone of ancient VMS systems (Lavery, 1985) below the seafloor level. The experiments of Seyfried and Ding (1995) showed that this depletion reflects the precipitation of F-rich minerals, at about 250°C, which also corresponds to the breakdown of plagioclase to sericite. The destruction of plagioclase (+/- primary allanite) and the apparent inability of sericite to fix REE led to the depletion of LREE and Eu in the sericitized alteration halo (Figs. 3.5 and 3.16b).

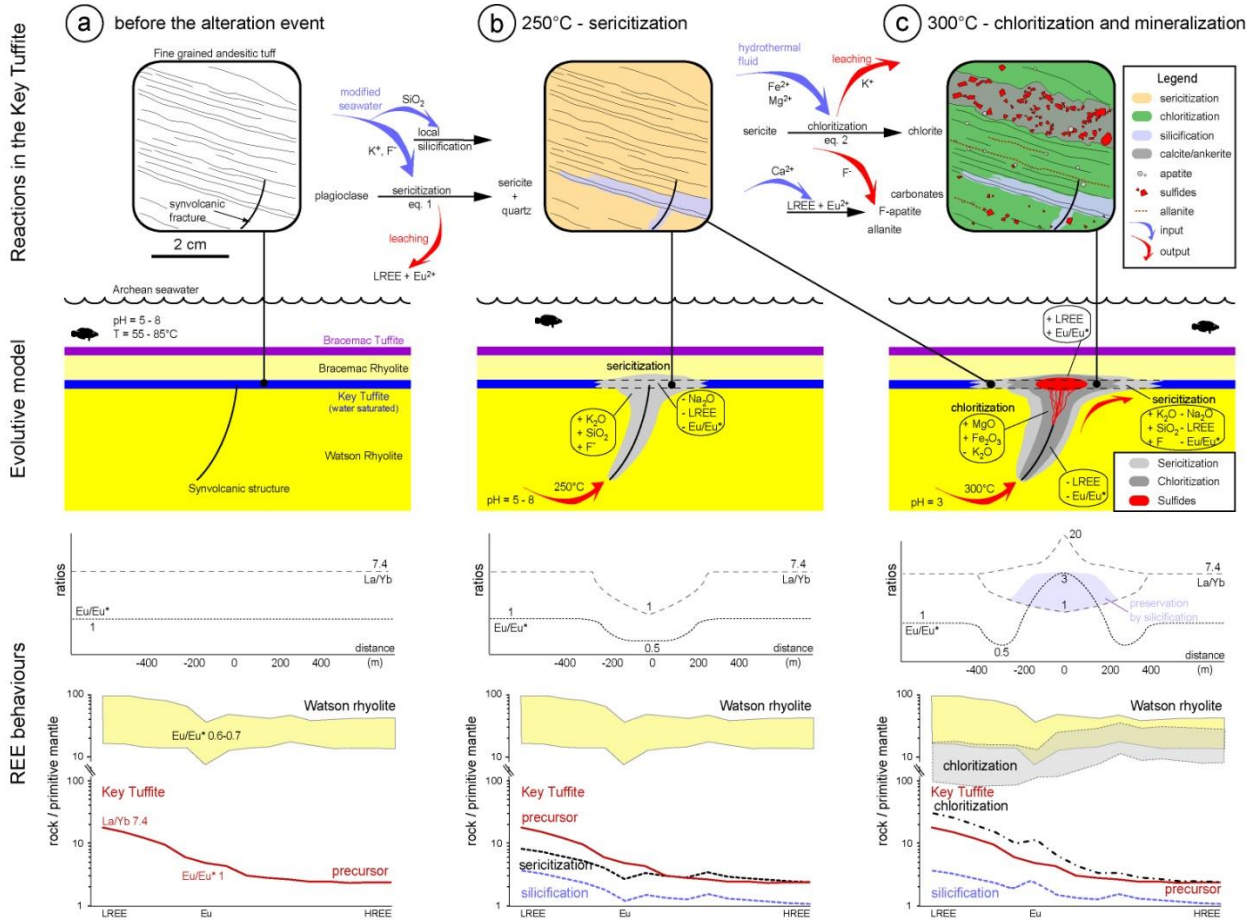

Figure 3.16 Synthesis of the behavior of LREE and Eu during the formation of the Bracemac-McLeod deposits: a) before the alteration event, b) during the sericitization of the Key Tuffite (<250°C) and c) during chloritization of the Key Tuffite and mineralization (300°C). For each stage of the evolution model (not to scale) both geochemical reactions at the mineral scale and whole-rock REE-Y behaviors are presented.

These elements were probably dispersed in the outer margin of the hydrothermal system or flushed away by discharging hydrothermal fluids.

With an increase of temperature (300°C) of the hydrothermal system, the acidic fluid leached Eu and LREE from the underlying Watson Lake rhyolite or Bell River Complex (Figs. 3.16c). This process is illustrated on Figure 3.13, where selected altered samples from the Watson Lake rhyolite from the footwall of the Bell Allard South and Mattagami Lake mines are characterized by a strong depletion of LREE compared to the unaltered equivalent. When the fluids reached the Key Tuffite horizon, sericite was transformed into chlorite by the iron-enriched hydrothermal fluids. However, F is not present in the structure of chlorite (eq. 2) and thus had to be released into the fluid. Present in excess in the fluid, F was probably re-used during the formation of fluorapatite. This hypothesis is supported by the conditions of stability of apatite. The solubility of apatite decreases when the pH increases (Ayers and Watson, 1991). The hot, acid (pH≈3.5), Cl-rich hydrothermal fluids carrying LREE and Eu suddenly encountered dramatically different conditions when mixing with the cooler (55-85°C), alkaline (pH = 5.6 to 8.1) Archean seawater (Grotzinger and Kasting, 1993; Knauth and Lowe, 2003) which saturated the porous Key Tuffite. These conditions are ideal to precipitate apatite, which is mostly controlled by the neutralization of acidic fluids (Ayers and Watson, 1991). However, the synthesis of apatite from modern seawater demonstrates that Mg has an inhibiting effect on the precipitation of apatite (Gulbrandsen et al.,

1984; Cappellen and Berner, 1991). During the transformation of sericite into chlorite, the amount of Mg present in the fluid will drastically decrease and could allow the precipitation of hydrothermal fluorapatite, using the F released by the breakdown of the sericite. Co-precipitating with chlorite, allanite fixed most of the LREE, whereas the remains of the LREE and most of the Eu are hosted in apatite (Figs. 3.15b, 3.16c). Hydrothermal carbonates, if present, might have also contributed to the fixation of Eu (Fig. 3.15a). Progressively, with the formation of the Ca-rich alteration mineral/s, the Eu content decreased in the fluids accounting for the spartial zoned distribution of Eu (Fig. 3.6).

3.9.4. IMPLICATIONS AND LIMITATIONS FOR MINERAL EXPLORATION

Both Eu and LREE are of interest for lithogeochemical VMS exploration and as vectors toward the mineralization (Fig. 3.5). A gain in the concentration of LREE is common in the hydrothermal alteration zone of the Bracemac-McLeod deposit, but shows a relatively complex behavior related to the long evolution of the hydrothermal system (Fig. 3.14). The behavior of Eu is simpler because it is linked to higher temperature fluids and specific conditions of precipitation. The genetic link with the mineralization event makes it more useful for exploration purposes than LREE. Positive Eu anomalies have been recognized but are often of limited extension (Campbell et al., 1984). However, at Matagami the anomalous behavior

of europium can extend far beyond the limit of the sulfide zone: a positive anomaly is recorded up to 100 m from the deposit (Fig. 3.16) whereas a negative Eu anomaly is persistent up to 400 m from the deposit, in the outer margin of the hydrothermal system (sericite zone). This represents a useful tool for exploration at the district scale.

In order to use REE in exploration, it is important to characterize first the geochemistry of the fresh volcanic sequence before the hydrothermal imprint. Both LREE and Eu are influenced by magmatic processes and it is critical to establish the LREE and Eu thresholds of the equivalent unaltered rock. At Matagami, the Watson Lake and Bracemac rhyolites are depleted in Eu and have negative anomalies. However, the mafic units of the Wabassee Group (basalt to andesite) have no Eu anomaly (Fig. 3.4). The identification of the rock prior to hydrothermal alteration (i.e. precursor) is of major importance for using the Eu anomaly as an exploration tool. Moreover, extra care must be taken when carbonates are present. Europium can be hosted in both synvolcanic ankerite/calcite (Fig. 3.10b-c) and late calcite, such as metamorphic quartz-calcite veins (Fig. 3.10d). The latter must be excluded from whole-rock analyses as they can modify the hydrothermal VMS-related Eu/Eu*.

3.10. CONCLUSIONS

This contribution aimed at understanding the behavior of the rare earth elements during the formation of the Bracemac-McLeod Archean VMS deposits in the Matagami district, Abitibi greenstone belt, Canada. More specifically, the focus was on the Key Tuffite, a stratigraphic marker horizon intimately associated with the mineralization. Using an approach combining both whole-rock and mineral data, this study showed that both LREE (La to Sm) and Eu are mobile in the alteration halo of the Bracemac-McLeod deposits, but have different behaviors during the evolution of the hydrothermal system. The distal sericite zone represents the early, low temperature alteration. It is characterized by the destruction of plagioclase (and primary allanite?) leading to negative Eu anomalies and depletion of LREE in whole-rock analyses. The proximal chlorite zone represents the evolution (i.e. thermal increase) of a VMS hydrothermal system. It is generally characterized by gains of LREE and Eu. The co-precipitation of allanite with chlorite and sulfides explains the increase of LREE, whereas the precipitation of apatite (± carbonates) essentially controls the Eu. Not all chloritized samples however show gains in LREE. Silicification is a low temperature VMS alteration that can occur as pulses, several times during the hydrothermal system life. Silicified samples are of interest because they preserve an early alteration state and can provide additional information on the evolution of the hydrothermal system. Both Eu and LREE are of interest for lithogeochemical

VMS exploration and as vectors toward the mineralization. In particular the anomalous behavior of europium can extend far beyond the limit of the sulfide zone, into the distal sericitic low-temperature alteration.

3.11. ACKNOWLEDGEMENTS

The first author's PhD project is a part of a larger research program on the Matagami district, including a volcanology PhD (INRS-Quebec) and a geophysical PhD (École Polytechnique-Montreal). Financial support for this study was provided by NSERC, CONSOREM, DIVEX, the Geological Survey of Canada, Glencore (previously Xstrata Zinc), Donner Metals, SOQUEM and Nyrstar (previously Breakwater Resources). We would like to thank the companies for the authorization to publish these results; N. Yapi for collecting samples in 2008; A. Paulin-Bissonnette for his contribution as undergraduate field assistant during the summer 2010; D. Savard and S. Medhi for their support with LA-ICP-MS analyses; M. Choquette for his support with the microprobe analysis. We are grateful to S.A.S. Dare, Research Associate at UQAC, for proof reading the English text. Finally, the manuscript benefited from comments and suggestions by P-S. Ross.

3.12. REFERENCES

Adair, R. N., 1992, Stratigraphy, structure, and geochemistry of the Halfmile Lake massive-sulfide deposit, New Brunswick: Exploration and Mining Geology, v. 1, p. 151-166.

Alderton, D. H. M., Pearce, J. A., and Potts, P. J., 1980, Rare earth element mobility during granite alteration: Evidence from southwest England: Earth and Planetary Science Letters, v. 49, p. 149-165.

Ayers, J. C., and Watson, E. B., 1991, Solubility of Apatite, Monazite, Zircon, and Rutile in Supercritical Aqueous Fluids with Implications for Subduction Zone Geochemistry: Philosophical Transactions of the Royal Society of London, Series A, v. 335, p. 365-375.

Barrett, T. J., Jarvis, I., and Jarvis, K. E., 1990, Rare earth element geochemistry of massive sulfides-sulfates and gossans on the Southern Explorer Ridge: Geology, v. 18, p. 583-586.

Beaudry, C., and Gaucher, E., 1986, Cartographie géologique dans la région de Matagami: Québec., Ministère de l'énergie et des Ressources, Rapport MB 86-32, p. 147.

Belousova, E. A., Griffin, W. L., O'Reilly, S. Y., and Fisher, N. I., 2002, Apatite as an indicator mineral for mineral exploration: trace-element compositions and their relationship to host rock type: Journal of Geochemical Exploration, v. 76, p. 45-69.

Budzinski, H., and Tischendorf, G., 1989, Distribution of REE among minerals in the Hercynian postkinematic granites of Westerzgebirge-Vogtland, GDR: Zeitschrift für Geologische Wissenschaften, v. 17, p. 1019-1031.

Campbell, I. H., Lesher, C. M., Coad, P., Franklin, J. M., Gorton, M. P., and Thurston, P. C., 1984, Rare-earth element mobility in alteration pipes below massive Cu-Zn-sulfide deposits: Chemical Geology, v. 45, p. 181-202.

Cappellen, P. V., and Berner, R. A., 1991, Fluorapatite crystal growth from modified seawater solutions: Geochimica et Cosmochimica Acta, v. 55, p. 1219-1234.

Carr, P. M., Cathles, L. M., and Barrie, C. T., 2008, On the size and spacing of volcanogenic massive sulfide deposits within a district with application to the Matagami district, Quebec: Economic Geology, v. 103, p. 1395-1409.

Cetiner, Z. S., Wood, S. A., and Gammons, C. H., 2005, The aqueous geochemistry of the rare earth elements. Part XIV. The solubility of rare

earth element phosphates from 23 to 150 °C: Chemical Geology, v. 217, p. 147-169.

Costa, U. R., Barnett, R. L., and Kerrich, R., 1983, The Mattagami Lake Mine Archean Zn-Cu sulfide deposit, Quebec; hydrothermal coprecipitation of talc and sulfides in a sea-floor brine pool; evidence from geochemistry, 18 O/ 16 O, and mineral chemistry: Economic Geology, v. 78, p. 1144-1203.

Côté, A., and Lavigne, M., 2010, Report and Feasibility Study for the Bracemac-McLeod Project Matagami Area Quebec, (Xstrata Zinc and Genivar Limited Partnership), p. 315.

Craddock, P. R., Bach, W., Seewald, J. S., Rouxel, O. J., Reeves, E., and Tivey, M. K., 2010, Rare earth element abundances in hydrothermal fluids from the Manus Basin, Papua New Guinea: Indicators of sub-seafloor hydrothermal processes in back-arc basins: Geochimica et Cosmochimica Acta, v. 74, p. 5494-5513.

Dare, S. A. S., Barnes, S.-J., and Prichard, H. M., 2010, The distribution of platinum group elements (PGE) and other chalcophile elements among sulfides from the Creighton Ni–Cu–PGE sulfide deposit, Sudbury, Canada, and the origin of palladium in pentlandite: Mineralium Deposita, v. 45, p. 765-793.

Davies, J. F., Prevec, S. A., Whitehead, R. E., and Jackson, S. E., 1998, Variations in REE and Sr-isotope chemistry of carbonate gangue, Castellanos Zn–Pb deposit, Cuba: Chemical Geology, v. 144, p. 99-119.

Debreil, J.-A., 2014, Évolution volcanologique et chimico-stratigraphique du district minier de Matagami, sous-province de l'Abitibi, Québec: Unpub. Ph.D. thesis thesis, Université du Québec Institut National de la Recherche Scientifique, 256 p.

Douville, E., Bienvenu, P., Charlou, J. L., Donval, J. P., Fouquet, Y., Appriou, P., and Gamo, T., 1999, Yttrium and rare earth elements in fluids from various deep-sea hydrothermal systems: Geochimica et Cosmochimica Acta, v. 63, p. 627-643.

Eastoe, C. J., Solomon, M., and Walshe, J. L., 1987, District-scale alteration associated with massive sulfide deposits in the Mount Read Volcanics, western Tasmania: Economic Geology, v. 82, p. 1239-1258.

Gaboury, D., and Pearson, V., 2008, Rhyolite geochemical signatures and association with volcanogenic massive sulfide deposits: Examples from the Abitibi Belt, Canada: Economic Geology, v. 103, p. 1531-1562.

Gale, G. H., and Fedikow, M. A. F., 1999, The application of rare earth element analyses in the exploration for volcanogenic massive sulphide type deposits in Manitoba, Report of Activities, Manitoba Industry, Trade and Mines, Geological Services, p. 9-12.

Galley, A. G., 1993, Characteristics of semi-conformable alteration zones associated with volcanogenic massive sulphide districts: Journal of Geochemical Exploration, v. 48, p. 175-200.

Gammons, C. H., Wood, S. A., and Younging, L., 2002, Complexation of the rare earth elements with aqueous chloride at 200°C and 300°C and saturated water vapor pressure, *in* Hellmann, R., and Wood, S. A., eds., Water-rock interaction, Ore deposits and environmental geochemistry: a tribute to David A. Crerar, 7, The Geochemical Society Special Publication, p. 191-207.

Genna, D., Gaboury, D., Moore, L., and Mueller, W. U., 2011, Use of micro-XRF chemical analysis for mapping volcanogenic massive sulfide related hydrothermal alteration: Application to the subaqueous felsic dome-flow complex of the Cap d'Ours section, Glenwood rhyolite, Rouyn-Noranda, Québec, Canada: Journal of Geochemical Exploration, v. 108, p. 131-142.

Genna, D., Gaboury, D., and Roy, G., 2014, The Key Tuffite, Matagami Camp, Abitibi Greenstone Belt, Canada: petrogenesis and implications for VMS formation and exploration: Mineralium Deposita, v. 49, p. 489-512.

Gibson, H. L., and Galley, A. G., 2007, Volcanogenic massive sulphide deposits of the Archean, Noranda District, Quebec, *in* Goodfellow, W. D., ed., Mineral Deposits of Canada: A Synthesis of Major Deposit-types, District Metallogeny, the Evolution of Geological Provinces, and Exploration Methods, Special Publication No. 5, Special Publication No. 5, Mineral Deposits Division, Geological Association of Canada, p. 533-552.

Gifkins, C. C., Herrmann, W., and Large, R. R., 2005, Altered volcanic rocks: A guide to description and interpretation, Centre for Ore Deposit Research, University of Tasmania.

Graf, J. L., 1977, Rare earth elements as hydrothermal tracers during the formation of massive sulfide deposits in volcanic rocks: Economic Geology, v. 72, p. 527-548.

Gromet, P. L., and Silver, L. T., 1983, Rare earth element distributions among minerals in a granodiorite and their petrogenetic implications: Geochimica et Cosmochimica Acta, v. 47, p. 925-939.

Grotzinger, J. P., and Kasting, J. F., 1993, New Constraints on Precambrian Ocean Composition: Journal of Geology, v. 101, p. 235-243.

Gulbrandsen, R. A., Roberson, C. E., and Neil, S. T., 1984, Time and the crystallization of apatite in seawater: Geochimica et Cosmochimica Acta, v. 48, p. 213-218.

Haas, J. R., Shock, E. L., and Sassani, D. C., 1995, Rare earth elements in hydrothermal systems: Estimates of standard partial molal thermodynamic properties of aqueous complexes of the rare earth elements at high pressures and temperatures: Geochimica et Cosmochimica Acta, v. 59, p. 4329-4350.

Hannington, M. D., Santaguida, F., Kjarsgaard, I. M., and Cathles, L. M., 2003, Regional-scale hydrothermal alteration in the Central Blake River Group, western Abitibi subprovince, Canada: implications for VMS prospectivity: Mineralium Deposita, v. 38, p. 393-422.

Harlavan, Y., and Erel, Y., 2002, The release of Pb and REE from granitoids by the dissolution of accessory phases: Geochimica et Cosmochimica Acta, v. 66, p. 837-848.

Hermann, J., 2002, Allanite: thorium and light rare earth element carrier in subducted crust: Chemical Geology, v. 192, p. 289-306.

Hughes, J. M., Cameron, M., and Crowley, K. D., 1989, Structural variations in natural F, OH, and Cl apatites: American Mineralogist, v. 74, p. 870-876.

Ioannou, S. E., and Spooner, E. T. C., 2007, Fracture analysis of a volcanogenic massive sulfide-related hydrothermal cracking zone, Upper Bell River Complex, Matagami, Quebec: application of permeability tensor theory: Economic Geology, v. 102, p. 667-690.

Jolly, W. T., 1978, Metamorphic history of the Archean Abitibi belt., *in* Fraser, J. A., and Heywood, W. W., eds., Metamorphism in the Canadian Shield, Geological Survey of Canada, Paper 78-10, p. 63-78.

Jones, S., Gemmell, J. B., and Davidson, G. J., 2006, Petrographic, geochemical, and fluid inclusion evidence for the origin of siliceous cap rocks above volcanic-hosted massive sulfide deposits at Myra Falls, Vancouver Island, British Columbia, Canada: Economic Geology, v. 101, p. 555-584.

Klinkhammer, G. P., Elderfield, H., Edmond, J. M., and Mitra, A., 1994, Geochemical implications of rare earth element patterns in hydrothermal fluids from mid-ocean ridges: Geochimica et Cosmochimica Acta, v. 58, p. 5105-5113.

Knauth, L. P., and Lowe, D. R., 2003, High Archean climatic temperature inferred from oxygen isotope geochemistry of cherts in the 3.5 Ga Swaziland Supergroup, South Africa: Geological Society of America Bulletin, v. 115, p. 566-580.

Kontak, D. J., and Jackson, S. E., 1995, Laser-ablation ICP-MS micro-analysis of calcite cement from a mississippi valley-type Zn-Pb deposit, Nova Scotia; dramatic variability in REE content on macro- and micro-scales: Canadian Mineralogist, v. 33, p. 445-467.

Large, R. R., Allen, R. L., Blake, M. D., and Herrmann, W., 2001a, Hydrothermal alteration and volatile element halos for the Rosebery K lens volcanic-hosted massive sulfide deposit, Western Tasmania: Economic Geology, v. 96, p. 1055-1072.

Large, R. R., Gemmell, J. B., Paulick, H., and Huston, D. L., 2001b, The alteration box plot: a simple approach to understanding the relationship between alteration mineralogy and lithogeochemistry associated with volcanic-hosted massive sulfide deposits: Economic Geology, v. 96, p. 957-971.

Lavery, N. G., 1985, The use of fluorine as a pathfinder for volcanic-hosted massive sulfide ore deposits: Journal of Geochemical Exploration, v. 23, p. 35-60.

Liaghat, S., and MacLean, W. H., 1992, The Key Tuffite, Matagami mining district; origin of the tuff components and mass changes: Exploration and Mining Geology, v. 1, p. 197-207.

Lottermoser, B. G., 1992, Rare earth elements and hydrothermal ore formation processes: Ore Geology Reviews, v. 7, p. 25-41.

Ludden, J. N., and Thompson, G., 1979, An evaluation of the behavior of the rare earth elements during the weathering of sea-floor basalt: Earth and Planetary Science Letters, v. 43, p. 85-92.

Lydon, J. W., 1984, Volcanogenic Massive Sulphide Deposits Part 1: A Descriptive Model: Geoscience Canada, v. 11, p. 195-202.

Lydon, J. W., 1988, Volcanogenic Massive Sulphide Deposits Part 2: Genetic Models: Geoscience Canada, v. 15, p. 43-65.

MacGeehan, P. J., and MacLean, W. H., 1980, An Archaean sub-seafloor geothermal system, 'calc-alkali' trends, and massive sulphide genesis: Nature, v. 286, p. 767-771.

MacLean, W. H., 1988, Rare earth element mobility at constant inter-REE ratios in the alteration zone at the Phelps Dodge massive sulphide deposit, Matagami, Quebec: Mineralium Deposita, v. 23, p. 231-238.

MacLean, W. H., and Kranidiotis, P., 1987, Immobile elements as monitors of mass transfer in hydrothermal alteration; Phelps Dodge massive sulfide deposit, Matagami, Quebec: Economic Geology, v. 82, p. 951-962.

Maier, W. D., Barnes, S.-J., and Pellet, T., 1996, The economic significance of the Bell River Complex, Abitibi subprovince, Quebec: Canadian Journal of Earth Sciences, v. 33, p. 967-980.

Mercier-Langevin, P., Gibson, H. L., Hannington, M. D., Goutier, J., Monecke, T., Dubé, B., and Houlé, M. G., 2014, A special issue on Archean magmatism, volcanism, and ore deposits: Part 2. Volcanogenic massive sulfide deposits preface: Economic Geology, v. 109, p. 1-9.

Michard, A., 1989, Rare earth element systematics in hydrothermal fluids: Geochimica et Cosmochimica Acta, v. 53, p. 745-750.

Michard, A., and Albarède, F., 1986, The REE content of some hydrothermal fluids: Chemical Geology, v. 55, p. 51-60.

Migdisov, A. A., Williams-Jones, A. E., and Wagner, T., 2009, An experimental study of the solubility and speciation of the Rare Earth Elements (III) in

fluoride- and chloride-bearing aqueous solutions at temperatures up to 300°C: Geochimica et Cosmochimica Acta, v. 73, p. 7087-7109.

Mills, R. A., and Elderfield, H., 1995, Rare earth element geochemistry of hydrothermal deposits from the active TAG Mound, 26°N Mid-Atlantic Ridge: Geochimica et Cosmochimica Acta, v. 59, p. 3511-3524.

Mitra, A., Elderfield, H., and Greaves, M. J., 1994, Rare earth elements in submarine hydrothermal fluids and plumes from the Mid-Atlantic Ridge: Marine Chemistry, v. 46, p. 217-235.

Möller, P., Morteani, G., and Dulski, P., 1984, The origin of the calcites from Pb-Zn veins in the Harz Mountains, Federal Republic of Germany: Chemical Geology, v. 45, p. 91-112.

Monecke, T., Kempe, U., and Götze, J., 2002, Genetic significance of the trace element content in metamorphic and hydrothermal quartz: a reconnaissance study: Earth and Planetary Science Letters, v. 202, p. 709-724.

Mortensen, J. K., 1993, U–Pb geochronology of the eastern Abitibi Subprovince. Part 1: Chibougamau–Matagami–Joutel region: Canadian Journal of Earth Sciences, v. 30, p. 11-28.

Munoz Taborda, C. M., 2011, Distribution of Platinum-Group Elements in the Ebay claim, central part of the Bell River Complex, Matagami, Quebec: Unpub. M.Sc. thesis, Université du Québec à Chicoutimi, 206 p.

Pan, Y., and Fleet, M. E., 2002, Compositions of the Apatite-Group Minerals: Substitution Mechanisms and Controlling Factors: Reviews in Mineralogy and Geochemistry, v. 48, p. 13-49.

Pan, Y., Fleet, M. E., and Barnett, R. L., 1994, Rare-earth mineralogy and geochemistry of the Mattagami Lake volcanogenic massive sulfide deposit, Quebec: Canadian Mineralogist, v. 32, p. 133-147.

Peter, J. M., Goodfellow, W. D., and Doherty, W., 2003, Hydrothermal sedimentary rocks of the Heath Steele Belt, Bathurst mining camp, New Brunswick: Part 2. Bulk and rare earth element geochemistry and implications for origin: Economic Geology Monograph, v. 11, p. 391-415.

Piccoli, P. M., and Candela, P. A., 2002, Apatite in Igneous Systems: Reviews in Mineralogy and Geochemistry, v. 48, p. 255-292.

Piché, M., 1991, Synthèse géologique et métallogénique du camp minier de Matagami, Québec: Unpub. Ph.D. thesis thesis, Université du Québec à Chicoutimi, 269 p.

Piché, M., Guha, J., Daigneault, R., Sullivan, J. R., and Bouchard, G., 1990, Les gisements volcanogènes du camp minier de Matagami: Structure, stratigraphie et implications métallogéniques: Canadian Institute of Mining and Metallurgy, v. Special Volume 43, p. 327-336.

Pilote, P., Debreil, J.-A., Williamson, K., Rabeau, O., and Lacoste, P., 2011, Révision géologique de la région de Matagami., Québec Exploration - Poster 276: Québec.

Poitrasson, F., 2002, In situ investigations of allanite hydrothermal alteration: examples from calc-alkaline and anorogenic granites of Corsica (southeast France): Contributions to Mineralogy and Petrology, v. 142, p. 485-500.

Rakovan, J., McDaniel, D. K., and Reeder, R. J., 1997, Use of surface-controlled REE sectoral zoning in apatite from Llallagua, Bolivia, to determine a single-crystal Sm-Nd age: Earth and Planetary Science Letters, v. 146, p. 329-336.

Rakovan, J., Newville, M., and Sutton, S., 2001, Evidence of heterovalent europium in zoned Llallagua apatite using wavelength dispersive XANES: American Mineralogist, v. 86, p. 697-700.

Rakovan, J., and Reeder, R. J., 1994, Differential incorporation of trace elements and dissymmetrization in apatite: The role of surface structure during growth: American Mineralogist, v. 79, p. 892-903.

Rakovan, J., and Reeder, R. J., 1996, Intracrystalline rare earth element distributions in apatite: Surface structural influences on incorporation during growth: Geochimica et Cosmochimica Acta, v. 60, p. 4435-4445.

Rimskaya-Korsakova, M. N., Dubinin, A. V., and Ivanov, V. M., 2003, Determination of Rare-Earth Elements in Sulfide Minerals by Inductively Coupled Plasma Mass Spectrometry with Ion-Exchange Preconcentration: Journal of Analytical Chemistry, v. 58, p. 870-874.

Roeder, P. L., MacArthur, D., Ma, X.-P., Palmer, G. R., and Mariano, A. N., 1987, Cathodoluminescence and microprobe study of rare-earth elements in apatite: American Mineralogist, v. 72, p. 801-811.

Rollinson, H. R., 1993, Using geochemical data: evaluation, presentation, interpretation: UK, Longman, p. 352.

Rønsbo, J. G., 1989, Coupled substitutions involving REEs and Na and Si in apatites in alkaline rocks from the Ilimaussaq Intrusion, South Greenland, and the petrological implications: American Mineralogist, v. 74, p. 896-901.

Ross, P.-S., McNicoll, V. J., Debreil, J.-A., and Carr, P., 2014, Precise U-Pb geochronology of the Matagami Mining Camp, Abitibi Greenstone Belt, Quebec: stratigraphic constraints and implications for volcanogenic massive sulfide exploration: Economic Geology, v. 109, p. 89-101.

Sangster, D., 1972, Precambrian volcanogenic massive sulphide deposits in Canada: a review, Gological Survey of Canada Paper 72-22, p. 44.

Schandl, E. S., and Gorton, M. P., 1991, Postore mobilization of rare earth elements at Kidd Creek and other Archean massive sulfide deposits: Economic Geology, v. 86, p. 1546-1553.

Schardt, C., Cooke, D. R., Gemmell, J. B., and Large, R. R., 2001, Geochemical modeling of the zoned footwall alteration pipe, Hellyer volcanic-hosted massive sulfide deposit, Western Tasmania, Australia: Economic Geology, v. 96, p. 1037-1054.

Schardt, C., and Large, R. R., 2009, New insights into the genesis of volcanic-hosted massive sulfide deposits on the seafloor from numerical modeling studies: Ore Geology Reviews, v. 35, p. 333-351.

Schmidt, K., Garbe-Schönberg, D., Bau, M., and Koschinsky, A., 2010, Rare earth element distribution in >400°C hot hydrothermal fluids from 5°S, MAR: The role of anhydrite in controlling highly variable distribution patterns: Geochimica et Cosmochimica Acta, v. 74, p. 4058-4077.

Seyfried, W. E., and Ding, K., 1995, The hydrothermal chemistry of fluoride in seawater: Geochimica et Cosmochimica Acta, v. 59, p. 1063-1071.

Sharpe, J. I., 1968, Géologie et gisements de sulfures de la région de Matagami, Comté d'Abitibi-Est, Québec., Ministère des Richesses Naturelles du Québec. Rapport géologique 137, p. 122.

Shikazono, N., Ogawa, Y., Utada, M., Ishiyama, D., Mizuta, T., Ishikawa, N., and Kubota, Y., 2008, Geochemical behavior of rare earth elements in hydrothermally altered rocks of the Kuroko mining area, Japan: Journal of Geochemical Exploration, v. 98, p. 65-79.

Staudigel, H., and Hart, S. R., 1983, Alteration of basaltic glass: Mechanisms and significance for the oceanic crust-seawater budget: Geochimica et Cosmochimica Acta, v. 47, p. 337-350.

Sun, S.-S., and McDonough, W. F., 1989, Chemical and isotopic systematics of oceanic basalts: implications for mantle composition and processes: Geological Society, London, Special Publications, v. 42, p. 313-345.

Sverjensky, D. A., 1984, Europium redox equilibria in aqueous solution: Earth and Planetary Science Letters, v. 67, p. 70-78.

Utzmann, A., Hansteen, T., and Schmincke, H.-U., 2002, Trace element mobility during sub-seafloor alteration of basaltic glass from Ocean Drilling Program site 953 (off Gran Canaria): International Journal of Earth Sciences, v. 91, p. 661-679.

Valle, N., Verney-Carron, A., Sterpenich, J., Libourel, G., Deloule, E., and Jollivet, P., 2010, Elemental and isotopic (29Si and 18O) tracing of glass alteration mechanisms: Geochimica et Cosmochimica Acta, v. 74, p. 3412-3431.

Von Damm, K. L., Edmond, J. M., Measures, C. I., and Grant, B., 1985, Chemistry of submarine hydrothermal solutions at Guaymas Basin, Gulf of California: Geochimica et Cosmochimica Acta, v. 49, p. 2221-2237.

Whitford, D. J., Korsch, M. J., Porritt, P. M., and Craven, S. J., 1988, Rare-earth element mobility around the volcanogenic polymentallic massive sulfide deposit at Que River, Tasmania, Australia: Chemical Geology, v. 68, p. 105-119.

Wolff-Boenisch, D., Gislason, S. R., and Oelkers, E. H., 2006, The effect of crystallinity on dissolution rates and CO2 consumption capacity of silicates: Geochimica et Cosmochimica Acta, v. 70, p. 858-870.

Wood, S. A., and Ricketts, A., 2000, Allanite-(Ce) from the eocene Casto Granite, Idaho: Response to hydrothermal alteration: Canadian Mineralogist, v. 38, p. 81-100.

CHAPITRE 4

4. DECIPHERING THE HYDROTHERMAL EVOLUTION OF A VMS SYSTEM USING TRACE ELEMENTS IN PYRITE BY LASER ABLATION ICP-MS: AN EXAMPLE FROM THE BRACEMAC-MCLEOD DEPOSITS, ABITIBI, CANADA AND IMPLICATIONS FOR EXPLORATION.

Dominique Genna, Damien Gaboury

Economic Geology (soumis décembre 2014)

4.1. RÉSUMÉ

La caractérisation texturale et chimique des sulfures, en particulier la pyrite, a été utilisée pour reconstruire l'évolution hydrothermale du gisement SMV Archéen de Bracemac-McLeod (~6Mt) dans le camp minier de Matagami, Abitibi, Canada. La minéralisation, contenue dans une séquence volcanique bimodale, est divisée en: 1) une zone riche en zinc, concordante à la tuffite clé – un horizon marqueur à l'échelle du camp, 2) une zone riche en cuivre qui recoupe localement la séquence stratigraphique et 3) des zones localement riches en magnétique, en remplacement de sphalérite et pyrite. Une étude pétrographique et LA-ICP-MS des grains complets de pyrite (comprenant inclusions et zonalités) de la Tuffite Clé et des différentes zones minéralisées des gisements ont permis d'étudier non seulement la distribution des éléments traces dans la pyrite associée à un large spectre de sulfures et à des températures différentes, mais aussi d'évaluer le potentiel d'utilisation des éléments traces dans la pyrite comme un outil d'exploration pour les SMV. Cinq types de pyrites ont été mis en évidence. Les pyrites nodulaires (pyrite I) présente dans la Tuffite Clé et les pyrites sub-idiomorphe de relative basse température (250°C) associées aux zones riches en zinc (pyrite II) ont des signatures chimiques similaires indiquant que ces deux types de pyrites se sont formées avec des conditions physico-chimiques et des fluides identiques. Ces pyrites sont caractérisées par la présence d'un large spectre d'éléments (Cu, Zn, Ag, Sn, Sb, Te, Au, Pb, Bi), mais surtout par un

enrichissement significatif en Sb et Tl par rapport aux autres types de pyrites. Les pyrites sub-idiomorphes associées aux zones riches en cuivre ont une signature différente, enrichie seulement en Se ± Co, In, Pb et Bi. Ces pyrites sont souvent en surcroissance aux pyrites I et II et son associées à un fluide de plus haute température (300°C). La présence de magnétite remplacant la pyrite et la sphalérite est généralement indicatrice de fluide très haute température (>350°C). Les pyrites (pyrite IV), préservées du remplacement, sont recristallisées et sont elles aussi caractérisées par des valeurs élevées en Se, mais complètement appauvri de tout autres éléments. Cette signature se retrouve aussi dans les pyrites idiomorphes d'origine métamorphique que l'on observe à l'échelle du camp. Durant la recristallisation à haute température des pyrites IV et V, seulement les éléments en substitution directe dans la structure cristalline de la pyrite (Ni, Co, As et Se) sont préservées. En conséquence, seulement Ni, Co, As, Se, Sb et Tl ont été utiles dans la reconstruction de l'évolution hydrothermale du système SMV de Bracemac-McLeod. Spécifiquement, le ratio Se/Tl permet de différencier les pyrites provenant de zones minéralisées riches en zinc (Se/Tl<10), de celles provenant de zones riches en cuivre (10<Se/Tl<10000), et même celles associées à des zones non-économiques (remplacées par la magnétite ou d'origine métamorphique : Se/Tl>10000). L'approche innovante de cette étude, basée sur l'analyse complète des grains, rends nos résultats directement applicables pour l'exploration. En conséquence, des analyses de concentrées de

pyrite, où As, Tl et Se sont analysés par des méthodes de spectrométrie de masse plus classique, ont le potentiel d'être utilisées en exploration par le biais des diagrammes de discrimination proposés.

4.2. ABSTRACT

Textural and chemical characterization of sulfides, in particular pyrite, was used to reconstruct the hydrothermal evolution of the Bracemac-McLeod Archean volcanogenic massive sulfide (VMS) deposits (~6 Mt) in the Matagami district, Abitibi, Canada. The mineralization, hosted in a bimodal volcanic sequence, is divided into a 1) Zn-rich zone, concordant to the Key Tuffite - a marker horizon at the district-scale, 2) a Cu-rich zone which locally crosscuts the stratigraphic pile above and below the Key Tuffite and 3) some localized magnetite-rich zones replacing sphalerite and pyrite massive sulfides. Detailed petrographic and LA-ICP-MS studies of whole pyrite grains (including inclusions and zonation) from the Key Tuffite and from the different ore zones of the deposits, provided the opportunity to not only investigate the distribution of trace elements in pyrite over a wide range of sulfide assemblages related to temperature, but also to evaluate the potential use of trace elements in pyrite as an exploration tool for VMS exploration. The study has revealed five pyrite types. Nodular pyrites (I) in the Key Tuffite and sub-idiomorphic pyrites from the low temperature (250°C) Zn-rich zone (II) have the same chemical signature suggesting that both precipitated from

similar physicochemical conditions. A wide range of trace elements (Cu, Zn, Ag, Sn, Sb, Te, Au, Pb, Bi) is present in both, but compared to the other types they are significantly enriched in Sb and Tl. Sub-idiomorphic pyrites from the Cu-rich zone (III) have a different signature, enriched only in Se ± Co, In, Pb and Bi. These pyrites commonly overgrow the nodular pyrites and are related to later synvolcanic higher-temperature fluids (300°C). Pyrite preserved during a later magnetite-replacement (>350°C) stage (IV) are also characterized by enrichment in Se, but are depleted in all other elements. A similar signature is found in idiomorphic metamorphic pyrite (V), which occurs at both the deposits and district-scale. During high temperature recrystallization of pyrite IV and V, only the contents of Ni, Co, As and Se are mostly preserved whereas other base metals are expelled from the pyrite structure. Consequently, only Ni, Co, As, Se, Sb and Tl were useful to reconstruct the hydrothermal evolution of the VMS system and used to build a suite of discrimination diagrams. Specifically, the ratio Se/Tl can discriminate pyrites from mineralized Zn-rich zone (Se/Tl<10), from pyrites associated with Cu-rich zone (10<Se/Tl<10000) and pyrites from non-economic parts of the deposit (replaced by magnetite or metamorphogenic; Se/Tl>10000). The innovative approach of this study, based on LA-ICP-MS acquisition of the chemistry of entire pyrite grains, make our results directly applicable for exploration. Consequently, pyrite concentrate samples, analyzed for As, Tl and

Se by more classical mass-spectrometric techniques, have the potential to be used for vectoring to ore by using the proposed discriminating diagrams.

4.3. INTRODUCTION

Pyrite is a major constituent of hydrothermal mineralization in a wide variety of ore systems. Pyrite has an ideal chemistry of FeS_2, however this is never the case in natural samples (Abraitis et al., 2004). Pyrite commonly contains a high level of trace elements either hosted by substitution within the crystal lattice or as nanoparticles or micro-inclusions (Huston et al., 1995; Deditius et al., 2011). Previous studies have shown that, as long as complete recrystallization did not occur, pyrite can record changes in fluid chemistry during the evolution of the hydrothermal system from which it has precipitated (e.g. Large et al., 2007; Agangi et al., 2013; Reich et al., 2013). Differences in composition of fluid and/or conditions of precipitation generally lead to textural and geochemical variations. Detailed studies with in situ analyses (spots, lines or maps) of pyrite can detect these subtle variations and provide critical information about pyrite growth history and physicochemical conditions during and after ore formation. This approach has been successfully applied for several gold (Large et al., 2009; Thomas et al., 2011; Hazarika et al., 2013), porphyry (Reich et al., 2013; Franchini et al., in press), and uranium (Ingham et al., 2014) deposits. However, a comprehensive

study of a whole suite of trace elements at the scale of a volcanogenic hydrothermal system is lacking.

In ancient volcanogenic massive sulfide (VMS) settings, only a few studies have investigated the trace element distribution in pyrite at the scale of a deposit and these studies are often focused on the distribution of semi-precious or precious metals (Larocque et al., 1995; McClenaghan et al., 2009). More recent publications have focused on sulfide chimneys in well-preserved (Maslennikov et al., 2009; Revan et al., 2014) or modern (Kristall et al., 2011) VMS environments. Based on *in situ* analysis of sulfides from rim to core of the chimneys, in both low and high temperature environments, these studies have highlighted important element associations providing significant data for the understanding of the depositional histories of massive sulfides on the seafloor (i.e. exhalative type mineralization). However, they also revealed a high variability in the distribution of trace elements in pyrite at the centimetric to decimetric scale of the sulfide chimney. Such variability, added to the complexity of using LA-ICP-MS (e.g. cost, accessibilities and data reduction time), could be a limiting factor for the use of trace elements in pyrite by exploration companies.

Sub-seafloor replacement processes may provide a more homogeneous distribution of trace elements in pyrite at the scale of a VMS deposit due to the constant zone refining process along a porous mineralized horizon. Unlike exhalative-type mineralization, where a significant portion of the metals is lost by

dispersion on the seafloor during mixing of the hydrothermal fluids with seawater (Rona, 1984), one should expect that sulfides from replacement-type VMS could provide a better capture of the geochemical record of the hydrothermal fluids and its evolution. Furthermore, the well developed alteration halo present in both footwall and hangingwall of this type of VMS deposit offers the best opportunity to evaluate the potential use of trace elements in pyrite as an exploration tool.

In this context, the Bracemac-McLeod mine of the Matagami district, Abitibi, Canada, is an ideal candidate. Recent characterization of the Key Tuffite (Genna et al., 2014b), the marker unit of the Zn-rich mineralization at the district scale, demonstrates that it represents a tuffaceous accumulation on the seafloor. Furthermore, we showed that the mineralization at Bracemac-McLeod formed mainly by sub-seafloor replacement processes along the Key Tuffite and other permeable units. A relatively wide alteration halo (up to 400m), characterized by chlorite-sericite but also by the redistribution of REE in the Key Tuffite (Genna et al., 2014a), imply that the lateral fluid flow along this porous unit was efficient and widespread. The ubiquitous distribution of pyrite in the Key Tuffite confirms this concept of lateral replacement and thus provides the opportunity to test the potential of using trace elements in pyrite as a vectoring tool toward the mineralization. The presence of spatially constrained Zn-rich, Cu-rich and magnetite-rich portions of the orebodies provides the unique opportunity to investigate the distribution of trace elements in pyrite over a wide range of sulfide

assemblages in relation to temperature of formation. In addition, the low grade of metamorphism (greenschist) and low degree of deformation preserved most of the primary pyrite textures and compositions.

This study provides the first comprehensive dataset on pyrite geochemistry from replacement-type VMS deposits. Using pyrite textures, trace element distribution and mineral paragenesis we decipher the geochemical evolution of the fluids involved in the formation of the Bracemac-McLeod VMS deposits. Finally, we demonstrate how pyrite chemistry can be applied in VMS exploration.

4.4. GEOLOGICAL BACKGROUND

The 2.7 Ga (Mortensen, 1993; Ross et al., 2014) Matagami mining camp (Fig. 4.1) is located in the northern part of the Abitibi greenstone belt, Canada. The camp constitutes an important zinc district with more than 60 Mt of Zn-rich ore produced (19 deposits and prospects, including 13 past and current producers; Mercier-Langevin et al., 2014). Three extensive felsic volcanic domains: the North Flank, the South Flank and the West Camp, host all of the known VMS deposits (Fig. 4.1). Regional metamorphism reached greenschist facies thoughout the camp and locally amphibolite facies on the North Flank (Jolly, 1978). Details of the geology of the Matagami area are available from Sharpe (1968); Beaudry and Gaucher (1986); Piché (1991); Pilote et al. (2011) and (Genna et al., 2014b).

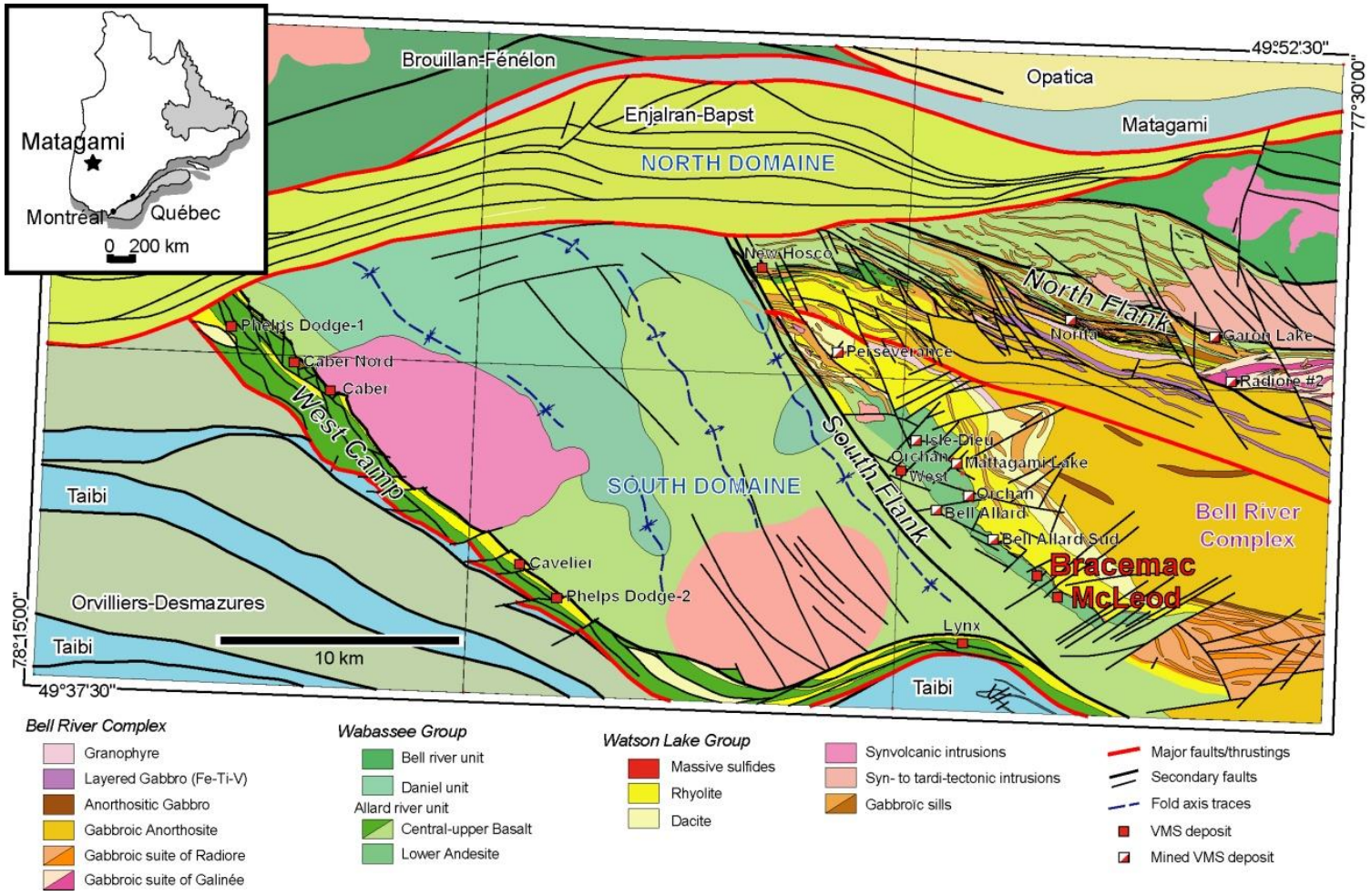

Figure 4.1: Geological map of the Matagami mining district. Modified from Pilote et al. (2011).

The present study is focused on the Bracemac–McLeod mine, comprising two VMS deposits (Bracemac and McLeod) spatially controlled by synvolcanic faults and separated by a horizontal distance of 1200 m (Fig. 4.2A). Together, they represent the second largest of the 19 VMS deposits in the district with 3.6 million tonnes of measured and indicated mineral resources grading 10.62% Zn, 1.45% Cu, 32.3 g/t Ag, and 0.48 g/t Au (Côté and Lavigne, 2010). Additional inferred mineral resources are 2.6 million tonnes with a grade of 8.79% Zn, 1.31% Cu, 38.84 g/t Ag and 1.06 g/t Au (Côté and Lavigne, 2010).

The general stratigraphic sequence is shown in Figure 2B whereas the detailed description of each unit is compiled in (Genna et al., 2014b).

The main part of the mineralization occurs at the Key Tuffite horizon (described below), between two rhyolites of similar composition: the Watson Lake rhyolite in the footwall and the Bracemac rhyolite in the hanging-wall. The Bracemac rhyolite is overlain by a thin tuff layer, the Bracemac Tuffite, which marks the transition into the mafic to intermediate volcanic rocks of the Wabassee Group (Fig. 4.2B and C). The volcanic rocks are locally crosscut by late phases of the underlying Bell River Complex, a large synvolcanic tholeiitic gabbro-anorthosite layered intrusion interpreted as the source for the overlying volcanic units and as the thermal source for the formation of the VMS deposits (Piché et al., 1990; Maier et al., 1996; Ioannou and Spooner, 2007; Carr et al., 2008).

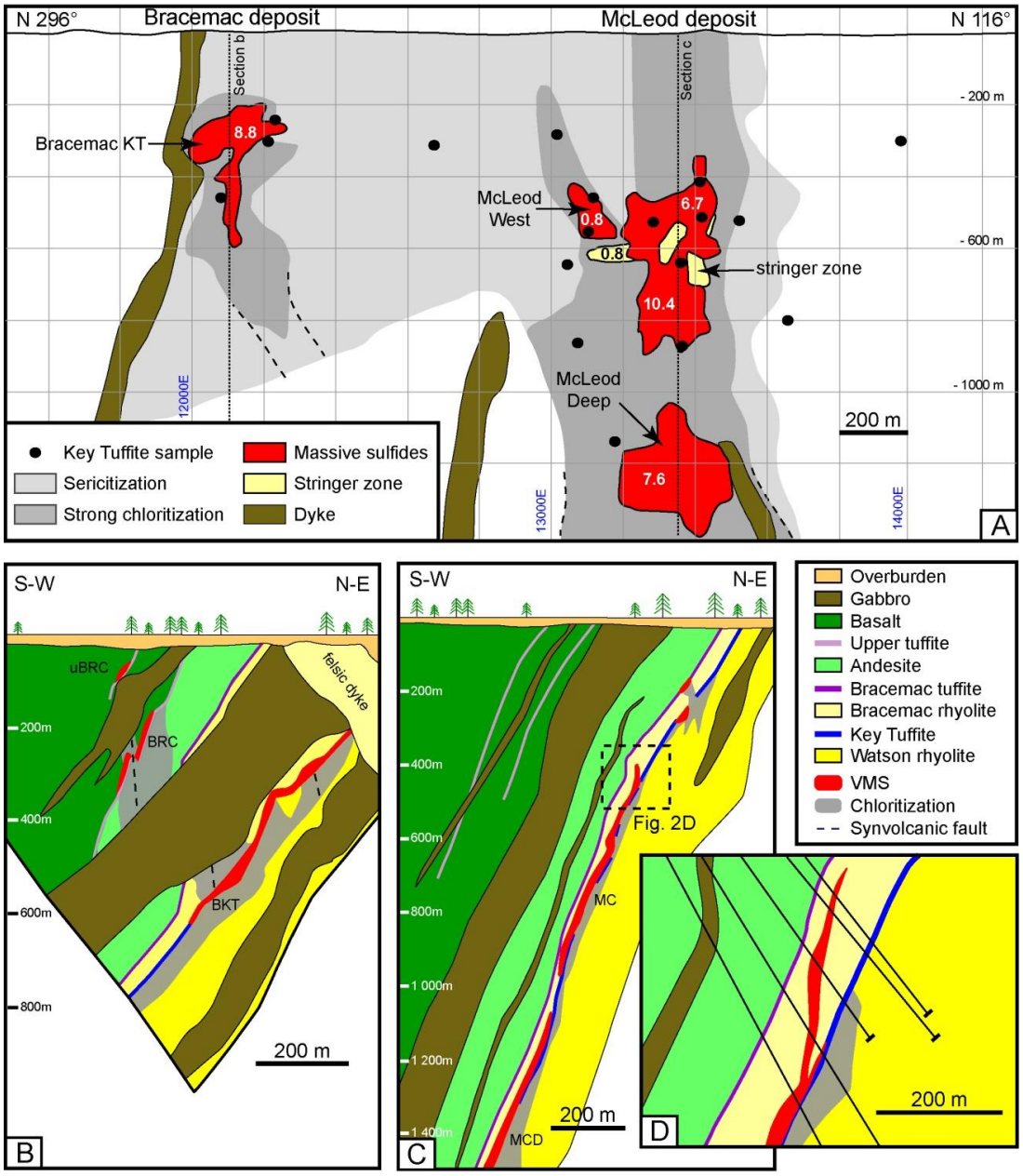

Figure 4.2: Geological setting of the Bracemac-McLeod mine. A. Composite longitudinal view and spatial repartition of pyrite-bearing samples in the vicinity of the mine. Zn/Cu ratio are given for each ore zone. B. Cross section of the Bracemac deposit. C and D. Cross-section of the McLeod deposit. Ore zones: uBRC Upper Bracemac, BRC Bracemac Main, BKT Bracemac KT, MC McLeod, MCD McLeod Deep. Modified from Donner Metals and Genna et al. (2014b).

The Bracemac-McLeod deposits are surrounded by a large (~1.6 km in diameter), classical alteration halo (chlorite, sericite) developed in the Key Tuffite, the footwall Watson Lake rhyolite (Fig. 4.2A) and, although less extensive, in the Bracemac rhyolite and Wabassee andesite. Details on the mineralogy and chemistry of the alteration halo around the Bracemac-McLeod deposits are given in (Genna et al., 2014b, a). Mineralization at Bracemac-McLeod was originally thought to be exhalative (i.e. precipitated on the seafloor by processes described by Franklin et al., (1981) and Lydon (1984)). However, based on detailed core logging, underground observations and more than 300 Key Tuffite lithogeochemical analyses, it has been demonstrated by Genna et al. (2014b) that the mineralization at Bracemac-McLeod was formed mostly by sub-seafloor replacement of the Key Tuffite and the surrounding porous units facies, such as the hyaloclastic top of the Watson Lake rhyolite. A detailed volcanological study of the Watson Lake and Bracemac rhyolites completed by Debreil (2014) is compatible with this interpretation.

4.5. GEOLOGY OF PYRITE-BEARING LITHOLOGIES

Pyrite is a ubiquitous sulfide in the Matagami district. Pyrite occurs along the VMS marker horizon (Key Tuffite) and in the ore zones, as described below.

4.5.1. THE KEY TUFFITE

The Key Tuffite is well developed in the Bracemac-McLeod areas. It consist of an originally seawater saturated thinly layered andesitic tuff unit ranging from 0.1 to 10m in thickness (Genna et al., 2014b). During the mineralizing event, the Key Tuffite was progressively replaced and infilled by sulfides and alteration minerals. As a result, the Key Tuffite comprises a large variety of facies composed of variable amounts of quartz, chlorite, sericite, sulfides (mostly pyrite) and carbonates reflecting various intensities of hydrothermal alteration (Genna et al., 2014b). These consist of the two classic alteration assemblages for VMS systems: 1) sericite in the outer part of the hydrothermal system (200-400 m away from the deposit), and 2) chlorite closer to the massive sulfide mineralization (<200m). Pyrite is an ubiquitous constituent of the Key Tuffite (Liaghat and MacLean, 1992) and is present far beyond the visible alteration halo (>1km), raising the question of its origin (i.e. hydrothermal or diagenetic/metamorphogenic). In the alteration halo, pyrite most commonly occurs as fine grained crystals forming massive layers from 0.2 to 20 mm parallel to bedding and the principal schistosity (Fig. 4.3A). In close vicinity of the Bracemac-McLeod deposit, pyrite also forms ovoid nodules ranging from 0.2 to 30 mm (Fig. 4.3B) which locally crosscut the bedding. Beyond the visible alteration halo, pyrite occurs as disseminated euhedral porphyroblasts (Fig. 4.3C), and in late quartz-carbonate cross-cutting veinlets (Fig. 4.3D).

4.5.2. BRACEMAC-MCLEOD DEPOSITS

The Bracemac-McLeod orebodies are sheet-like and sub-parallel to the volcanic stratigraphy, which dips 55-65° to the south-west. The Bracemac deposit (Fig. 4.2B) comprises 3 distinct lenses: Bracemac KT, Bracemac Main and Upper Bracemac. They form a stacked sequence connected by a chlorite/sulfide alteration corridor, which is interpreted to be a reactivated synvolcanic fault during and after the deposition of the Wabassee Group (Adair, 2009). The McLeod deposit is composed of 4 lenses: McLeod Zone, Stringer Zone, McLeod West and McLeod Deep (Fig. 4.2). Apart from the Stringer Zone, which is hosted in the Watson rhyolite, they all occur at the stratigraphic level of the Key Tuffite.

The mineralogy of both deposits is dominated by sphalerite and pyrite with lesser amounts of chalcopyrite and pyrrhotite (± magnetite and minor galena). As expected for VMS deposits, the distribution of these minerals is not uniform (Hannington et al., 1998). Based on mineralogy and stratigraphic relationships, the massive sulfides lenses can be divided into Zn-rich and Cu-rich facies. The Zn-rich facies consists of metric-size massive sulfide intervals, where coarse grained sphalerite forms centimetric to decimetric bands alternating with coarse-grained pyrite (Fig. 4.3E) and locally overprinted by chalcopyrite veins or veinlets. Pyrrhotite and galena and are also locally present. Galena is very fine-grained and only associated with the Zn-rich portions of the deposit (Fig. 4.3E). The Cu-rich facies is present in the deepest parts of the deposits, such as the lower of

Bracemac KT and the Stringer Zone below McLeod. However, unlike other classic Noranda type VMS deposits, the Cu-rich zones are not limited to those deep zones. Locally, the upper part of the McLeod deposit and McLeod West are also Cu-rich as illustrated by lower Zn/Cu ratios (Fig. 4.2A). Massive chalcopyrite veins (Fig. 4.3F), associated with a variable amount of pyrite and lesser amount of sphalerite stringers, is the most common mineralization type of the Cu-rich zones. Magnetite is also locally present, and sometimes constitutes an important proportion of the ore and the Key Tuffite (Fig. 4.3F-H), in proximity to the deposits. Disseminated or stringers of magnetite are associated with Cu-rich zones, but also locally replace sphalerite and pyrite (Fig. 4.3G). These overprinting relationships suggest that the formation of magnetite may represent the final stage of the hydrothermal system as proposed for the Ansil VMS deposit in the Noranda district, Abitibi (Galley et al., 1995).

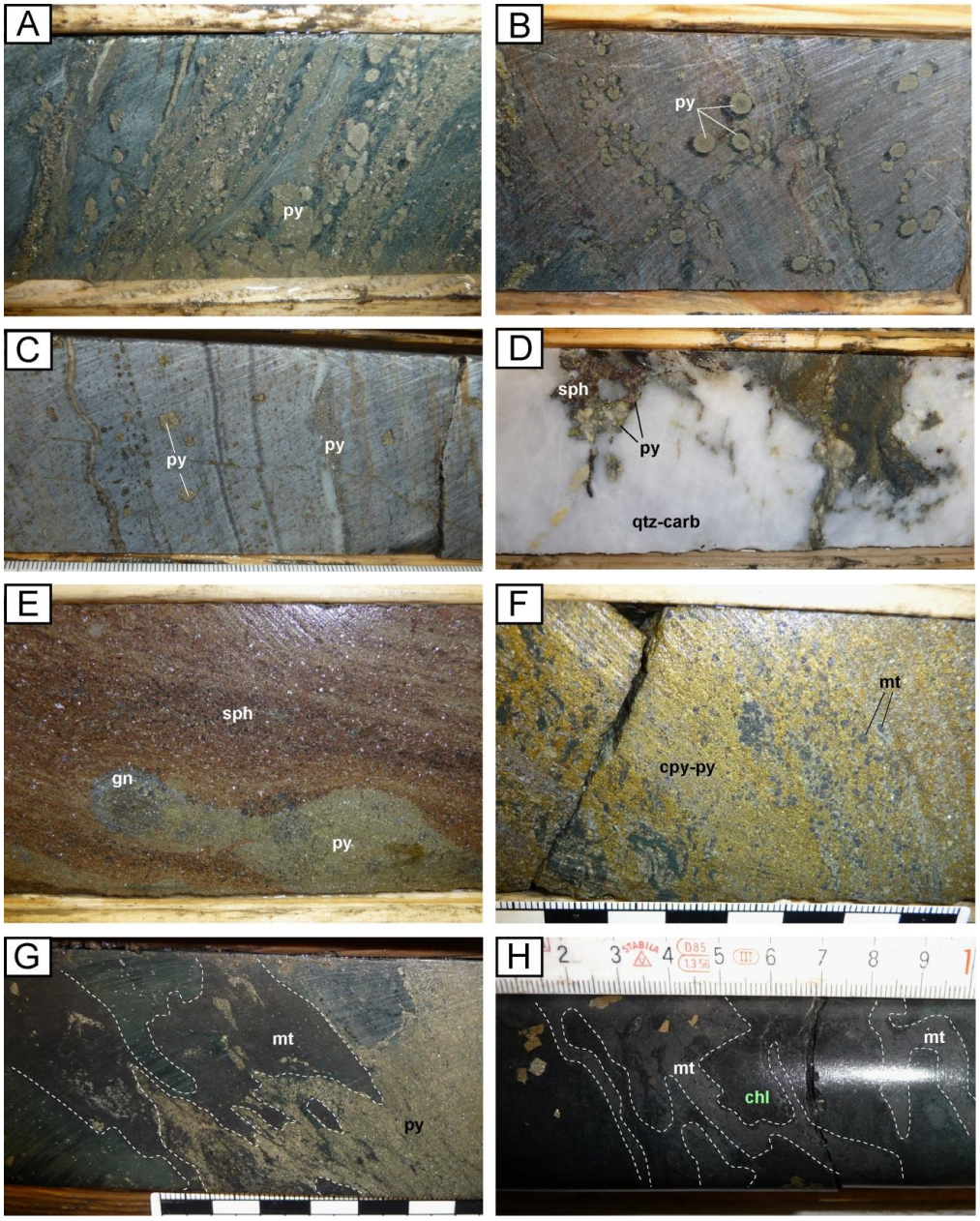

Figure 4.3: Macroscopic drill core observations of the different mineralization facies at Bracemac (BRA or BRC) and McLeod (MC). A. Fine grained pyrite (py) along bedding or as nodules (Drill hole number: MC-10-107A). B. Nodular pyrite disseminated in the Key Tuffite (BRA-09-02). C. Disseminated pyrite in the Key Tuffite (BRA-09-03). D. Quartz-carbonate (qtz-carb) vein with disseminated pyrite and sphalerite (sph: BRA-09-06). E. Massive sphalerite-pyrite with localized galena (gn: MC-07-25). F. Massive, decimetric chalcopyrite (cpy) stringer with disseminated pyrite and magnetite (mt: MC-07-23). G. Pyrite stringer partially replaced by magnetite (MC-07-24). H. Magnetite stringer in the chloritized (chl) Watson Lake rhyolite (BRC-09-108). Note the presence of idiomorphic pyrite crystals.

4.6. METHODOLOGY AND ANALYTICAL TECHNIQUES

4.6.1. SAMPLING STRATEGY

The ubiquitous occurrence of pyrite in the Key Tuffite within and beyond clearly defined the alteration halo (distal sericite, proximal chlorite) surrounding the Bracemac-McLeod deposits provides the opportunity to test the potential use of variations in trace element concentrations in pyrite as a vectoring tool toward the mineralization. A total of 27 pyrite-bearing samples, from 19 drill holes in and around the vicinity of the Bracemac-McLeod deposits, were selected for this LA-ICP-MS pyrite study. Sixteen of these samples (Fig. 4.2A) were collected in the Key Tuffite at regular intervals away from the orebodies, with a close spacing within the alteration halo (<400m), and 4 samples were taken outside and away from any known mineralisation (>1000m). The latter samples are considered barren as the presence of other indicator sulfides (sphalerite and chalcopyrite) is very limited. A smaller suite of pyrite-bearing mineralized samples, representative of the different ore facies (Zn-rich, Cu-rich, presence of magnetite), was selected for analysis to constrain the chemical signature of these end-members and to establish the chemical variations of pyrite formed during the evolution of the hydrothermal system. Finally, an additional 2 pyrite-bearing samples were collected from the highly altered footwall (Watson Lake rhyolite) in vicinity of McLeod deposit. Table 4.1 presents the sample list along with host lithologies, sulfide paragenesis, and the distance toward the deposit. Prior to LA-ICP-MS

analysis, all samples were examined optically under reflected light microscopy to identify the mineralogy and textures of the sulfides and oxides.

4.6.2. IN SITU LA-ICP-MS ANALYSES

Twenty five elements were determined on 252 pyrite grains, using a New Wave 213nm Nd:YAG UV laser connected to a Thermo Elemental X-7 ICP-MS at Labmater, Université du Québec à Chicoutimi, Quebec, Canada. Isotopes measured were ^{28}Si, ^{33}S, ^{34}S, ^{51}V, ^{52}Cr, ^{55}Mn, ^{57}Fe, ^{59}Co, ^{60}Ni, ^{65}Cu, ^{66}Zn, ^{71}Ga, ^{72}Ge, ^{75}As, ^{82}Se, ^{107}Ag, ^{111}Cd, ^{115}In, ^{118}Sn, ^{121}Sb, ^{126}Te, ^{197}Au, ^{205}Tl, ^{208}Pb, ^{209}Bi. The analytical parameters are summarized in Table 4.2. Following a 20 to 30 s of background acquisition of the gas blank, lines were ablated across pyrite (Fig. 4.6) by moving a laser spot size of 80 µm at a speed of 5 or 10 µm/s across the entire grain to determine if any zonation is present. In addition to the line analyses, 5 pyrite grains, representative of each facies, were mapped (Figs. 4.10 to 15) by LA-ICP-MS, using a Excimer 193nm Resonetics Resolution M-50 laser connected to a Agilent 7700x ICP-MS at Labmater. Analytical parameters are also provided in Table 4.2. This was carried out in order to 1) compare with the line analysis, 2) determine trace element spatial distribution, and 3) decipher overprinting or growing events on pyrite in relation to pyrite type. Moreover, insights into element distribution among co-existing sulfides can be gained with the aim of understanding factors controlling trace element incorporation in pyrite. Semi-

quantitative mapping was carried out by ablating a series of lines over the area (~0.5 x 0.5 to 1 x 1mm) of the whole pyrite grain, using a beam size of 15 µm, a laser frequency of 10 Hz, and a stage speed of 5 to 10 µm/s, following the method presented in Dare et al. (2014).

Both line and map analyses of pyrite, were calibrated with MASS-1, a USGS reference material (Fe-Cu-Zn-S pressed pellet), using values published by Wilson et al. (2002). Iron was used as the internal standard using a stoichiometric value. As there was no certified value for Tl in MASS-1, we determined this to be 66 ppm using NIST-610 with Mn as internal standard and this is within range of values given on Georem. Previous studies at UQAC have successfully demonstrated that MASS-1 is a suitable calibration reference material to determine trace elements in base metal sulfides, including pyrite. This has been shown by repeated analysis of a synthesized Fe-sulfide ‘in house’ reference material (JBMSS5) doped with 50 – 80 ppm of Ag, As, Au, Bi, Cu, Pb, Ni, Sb, Se, Te and platinum-group elements (Dare et al., 2011; Djon and Barnes, 2012; Piña et al., 2012, 2013). NIST 610 glass was analysed each run to monitor the reproducibility of the analyses (Table A1). For this, Mn was used as the internal standard because the Fe signal in NIST 610 was not significantly above detection limit.

Host rock / Orebody	Samples	Drill hole	Distance (m)	Sulfide and oxyde mineralogy	Main pyrite textures	Dominant pyrite type
Key Tuffite	972124	BRC-97-15	1500	py	diss, bed	zoned
	972127	BRC-97-15	1500	po, py	diss	zoned
	972130	BRC-95-11	1200	py	vein	Py V
	972122	BRC-04-22	1000	py	diss, bed	zoned
	68	BRC-07-40	400	py	diss	zoned
	74	MC-05-19	225	py	diss	zoned
	972120	MC-08-39	125	py	vein	Py V
	972110	MC-07-24	94	py, mt	sms	Py IV
	972105	MC-04-09	62.5	py ± sph	sms	zoned
	63	MC-05-20	50	py ± cpy, sph	diss	zoned
	92	BRC-08-73	25	py	diss	zoned
	972153	MC-07-23	12.5	py, mt	sms	Py IV
	87	BRC-07-51	12.5	py ± cpy	diss, bed, vein	zoned
	MAT-07-31	BRC-07-57	12.5	py	diss, bed	zoned
	972116	MC-08-55	0	py ± cpy, sph	nod, diss, bed	Py I
	89	MC-05-18	0	py	ss	zoned
	972117	MC-08-55	0	py ± sph	diss, bed	zoned
	96	MC-07-28	0	py	nod, diss, bed	Py I
	972167	MC-07-25	0	py, sph, mt ± cpy	ss	Py IV
	77	MC-04-04	0	py	diss	zoned
McLeod	972165	MC-07-25	0	sph, py ± gn	ms	Py II
Massive	95b	MC-07-28	0	sph, py ± cpy	ms	Py II
sulfide	972160	MC-08-62	0	py, cpy ± sph	ms	Py III
Stringer Zone	972168	MC-07-25	0	py, cpy ± sph	ss	Py III
Waton Lake	972162	MC-08-62	0	py	ss	zoned
rhyolite	972101	MC-07-28	25	py	ss	zoned

py = pyrite; cpy = chalcopyrite; sph = sphalerite; mt = magnetite; gn = galena
nod = nodules; diss = disseminated; bed = bedded; ss = stringer sulfide; sms = semi-massive sulfide; ms = massive sulfide

Table 4.1: Characteristics of pyrite-bearing samples studied from the Bracemac-McLeod area.

	Line analysis	Map analysis
Laser ablation system	Thermo Elemental X-7	Agilent 7700x
ICP-MS	New Wave Research 213nm Nd:YAG UV	Excimer 193nm Resonetics Resolution M-50
Laser frequency	10 Hz	15 Hz
Pulse energy	0.4 mJ	5 mJ
Stage speed	5 or 10 µm/s	5 or 10 µm/s
Beam size	80 µm	15 µm
Dwell time	10 ms/peak	10 ms/peak
Analysis	single line raster	map, series of line rasters with no gap or overlap
	30 s gas blank	10 s gas blank
	60 s of signal	variable
	Fully-quantitative	Semi-quantitative
Internal standard	Fe (stoichiometric values)	Fe (stoichiometric values)
Reference material for calibration	MASS-1	MASS-1
Reference material for monitoring	NIST-610	
Monitor signal for inclusions	Si, Cu, Zn, Pb	Si, Cu, Zn, Pb
Data reduction	Plasmalab	Iolite software (IGOR pro 6.3)

Table 4.2: Analytical details of LA-ICP-MS analysis of pyrite.

4.7. PYRITE TEXTURES AND TRACE ELEMENT CHEMISTRY

The ubiquitous presence of pyrite with varied textures in the Matagami district is challenging for establishing link with specific mineralizing events. Furthermore, pyrite can be of both diagenetic and metamorphic origin. To account for this, pyrite within close vicinity of the Bracemac-McLeod deposits were used to define end-member compositions associated to specific volcanogenic-related sulfide assemblages. However, each pyrite from the selected end-member pyrite may have preserved earlier pyrite types. Five forms of pyrite (Pyrite I to V) were identified on the basis of textural criteria, mineral association (Figs. 4.3-4.5) and trace element chemistry (Figs. 4.7 and 4.8). These are 1) fine-grained aggregates (forming layers or nodules); 2) sub-euhedral pyrites predominantly associated with sphalerite; 3) chalcopyrite; or 4) magnetite; and 5) euhedral overgrowth on pre-existing pyrite or pyrite hosted in late veins. Pyrite from the Key Tuffite and the altered Watson Lake rhyolite footwall are commonly zoned, comprising an earlier inclusion-rich core, and a clear, well crystallized rim (Figs. 4.4C-E) indicating that more than one pyrite precipitation event has been recorded. Median values for each major pyrite type are given in Table 3, along with minimal, maximal and standard deviation values. The complete dataset is presented in the Table 4.A2 and includes 128 analyses from zoned pyrites from the Key Tuffite/Watson Lake rhyolite, 30 of fine-grained pyrite (Pyrite I), 23 from Zn-rich

ore (Pyrite II), 24 from Cu-rich ore (Pyrite III), 30 from magnetite-rich zone (Pyrite IV) and 17 from late overgrowth or veins (Pyrite V).

Figure 4.7 presents the statistical results for each pyrite group. Pyrite-bearing samples from the barren Key Tuffite and from the different zones of the deposits exhibit wide ranges in trace element contents, with some elements varying over several orders of magnitude (Fig. 4.7). The high variance of some elements is a common feature in LA-ICP-MS studies (Winderbaum et al., 2012), mostly caused by elements occurring as micro-inclusions (Fig. 4.6). Trace elements in pyrite can occur as: 1) lattice substitution i.e. as solid solution, 2) nanoparticles, or 3) visible inclusions (Huston et al., 1995; Deditius et al., 2011). It has been considered in this study that inclusions provide additional information on the metal content of the hydrothermal fluids.

These inclusions may have formed during co-precipitation with pyrite or be the result of exsolution during recrystallization due to zone refining or later metamorphism. A careful inspection of the LA-ICP-MS spectra (Fig. 4.6) of each laser line enables an estimation of the host site of each element in zoned pyrite. A relatively homogeneous flat time-resolved analytical signal indicates that the element is either in solid solution or included as nanoparticles within the pyrite structure. Using this approach, only Co, Ni, As, Se, Sb and Tl are homogenously distributed in the analyzed pyrites (either as nanoparticles or within the lattice structure).

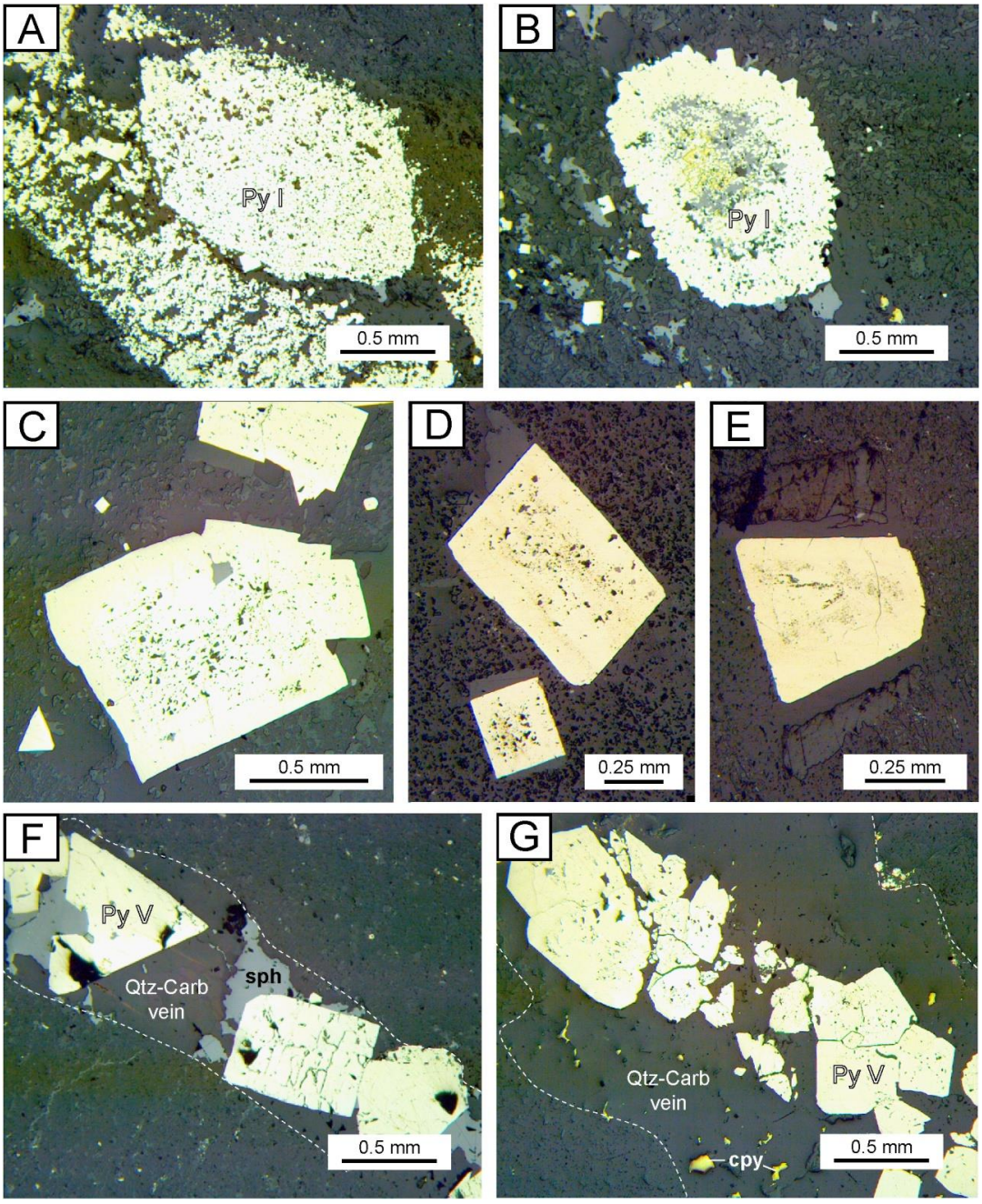

Figure 4.4: Microscopic sulfide observations from pyrite-bearing (py) Key Tuffite samples (reflected light). A. Fine grained aggregates of pyrite (sample number: 972116, drill hole number: MC-08-55). B. Nodular pyrite with sphalerite (sph) and chalcopyrite (cpy) core inclusions (972116, MC-08-55). C. Zoned pyrite (972122, BRC-04-22, 1000 m from the deposit). D. Zoned pyrite (58, MC-05-20, 50m from the deposit). E. Zoned pyrite (MC-04-04, above the mineralisation). F. Late quartz-carbonate (qtz-carb) vein with idiomorphic pyrite and remobilized sphalerite (972130, BRC-95-11). G. Late quartz-carbonate vein with idiomorphic pyrite and remobilized chalcopyrite (972120, MC-08-39).

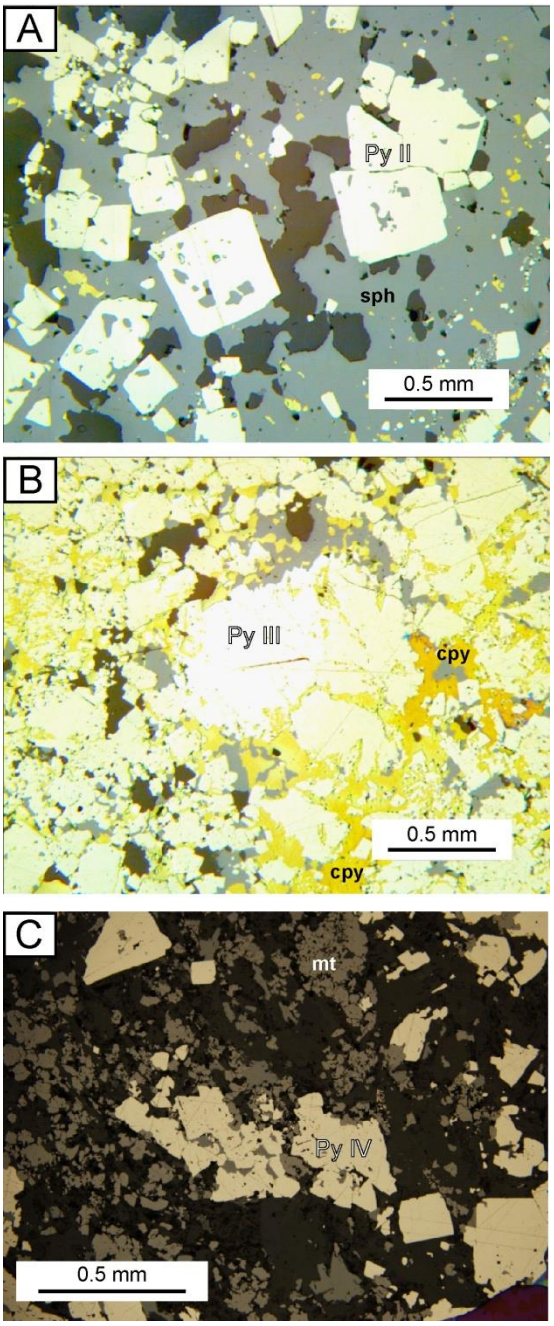

Figure 4.5: Microscopic sulfide observations (reflected light) from the Bracemac-McLeod mine. A. Massive sphalerite (sph) with disseminated subidiomorphic pyrite (py) and trace chalcopyrite (cpy) (sample number: 972160, drill hole number: MC-08-62). B. Subidiomorphic pyrite with xenomorphic chalcopyrite from the Stringer Zone (972165, MC-07-25). C. Disseminated magnetite (mt) replacing pyrite (972110, MC-07-24).

Pyrite Type		Mn	Co	Ni	Cu	Zn	As	Se	Ag	Cd	In	Sn	Sb	Te	Au	Tl	Pb	Bi
Average detection Limit		0.087	0.046	2.262	0.484	0.309	0.200	0.415	0.009	0.065	0.004	0.038	0.012	0.107	0.002	0.003	0.005	0.002
Py I	Median	109	582	329	1427	1591	1333	65	87	6.2	0.8	16	65	143	1.1	52	397	85
n = 29	sd	244	251	153	15095	17513	703	94	172	63	5.1	232	52	146	0.7	49	333	241
	Min	3.9	53.7	176.0	44.5	3.1	0.4	28.2	8.7	0.3	0.1	0.7	3.5	0.9	0.002	1.0	36.7	2.0
	Max	959.7	1082	919	82320	90920	2922	547	660	298	18	1213	244	563	3.0	154	1634	1065
Py II	Median	61	53	196	1491	725	485	3.4	18	1.4	0.03	2	13	6	0.4	62	88	2
n = 23	sd	177	134	64	3370	25276	233	7.0	15	60	0.4	116	38	9	0.2	143	140	26
	Min	4.2	2.4	122.3	36.3	16.3	114.9	1.8	0.7	bdl	bdl	0.2	1.8	1.4	0.05	9.2	2.8	0.1
	Max	784	611	361	12300	122000	1003	29	64	292	1.7	536	161	37	0.9	488	538	101
Py III	Median	11.5	375.3	103.2	771.7	242.5	117.0	76.2	11.1	0.8	1.1	2.8	5.4	1.9	0.2	0.4	110.6	79.2
n = 24	sd	27	309	90	946	4392	336	99	373	14	2.1	16	172	2.8	0.3	11	19292	425
	Min	0.36	112.70	44.37	2.46	2.23	26.66	11.03	0.24	0.04	0.04	0.17	0.08	0.08	0.00	0.00	0.82	0.06
	Max	115	1025	402	3977	17000	1413	344	1766	49	7	72	800	11	1.6	46	91540	2077
Py IV	Median	18	174	169	118	16	24	151	1.1	0.1	0.1	0.5	0.3	2.0	0.02	0.01	33	4.1
n = 30	sd	44	313	65	334	3385	359	203	246	11	1.0	10	0.5	265	1.4	1.2	30	7.4
	Min	0.25	24	62	1.4	0.8	1.5	26	0.0	0.04	bdl	bdl	bdl	0.1	bdl	bdl	0.1	0.01
	Max	203	1390	315	1285	18470	1082	1059	1302	58	5.0	54	1.9	1328	6.2	6.3	138	23
Py V	Median	2.2	3536.0	533.2	52.8	181.5	1216.0	171.6	3.7	0.7	0.1	0.3	0.3	22.5	0.3	0.01	9.3	4.7
n = 17	sd	24.8	4699.0	435.9	754.4	1263.3	3541.0	51.5	197.0	4.9	1.5	24.8	1.6	222.9	10.2	0.02	210.0	26.6
	Min	1.1	211.2	118.9	1.8	0.3	181.6	81.2	0.02	0.02	bdl	0.2	0.03	3.1	bdl	bdl	0.2	0.07
	Max	100	14880	1871	2796	3893	11530	276	780	17	5.0	92	6.8	883	36	0.1	881	103
Zoned pyrite	Median	23	346	315	91	65	518	95	4.2	0.3	0.07	1.3	0.8	16	0.1	0.01	23	6.0
n = 128	sd	305	1825	375	636	2803	1068	88	425	13	1.3	83	3.6	6431	2.5	1.4	5450	373
	Min	0.3	1.6	34.4	0.9	0.4	3.7	19	0.03	bdl	bdl	0.09	0.02	0.51	bdl	bdl	0.32	0.03
	Max	2328	14870	2410	4913	16840	7439	509	4791	89	13	859	36	72770	26	16	61640	4221

Table 4.3: Trace element concentrations (ppm) for each pyrite types from the Bracemac-McLeod area. sd = standard deviation; bdl = below detection limit

Consequently, only this suite of elements was useful to discriminate the different pyrite types (Fig. 4.8). The remaining trace elements typically occur as visible inclusions, identified as peaks in the analytical signal of pyrite (Fig. 4.6C). Although some of these elements also reside in the pyrite structure (e.g. Te and Ag; Fig. 4.6C), they were not used to further discriminate pyrite type. Nevertheless, these inclusions are an intrinsic part of pyrite chemistry and consequently, their importance as trace metal host is addressed below.

4.7.1. INCLUSIONS

Sphalerite, chalcopyrite and galena represent the only visible sulfide inclusions in pyrite. It is thus not surprising that among all the analyzed elements, Zn, Cu and Pb are the most abundant elements in pyrite, with concentrations that are highly variable ranging from ~1 ppm to several weight percent (Fig. 4.7).

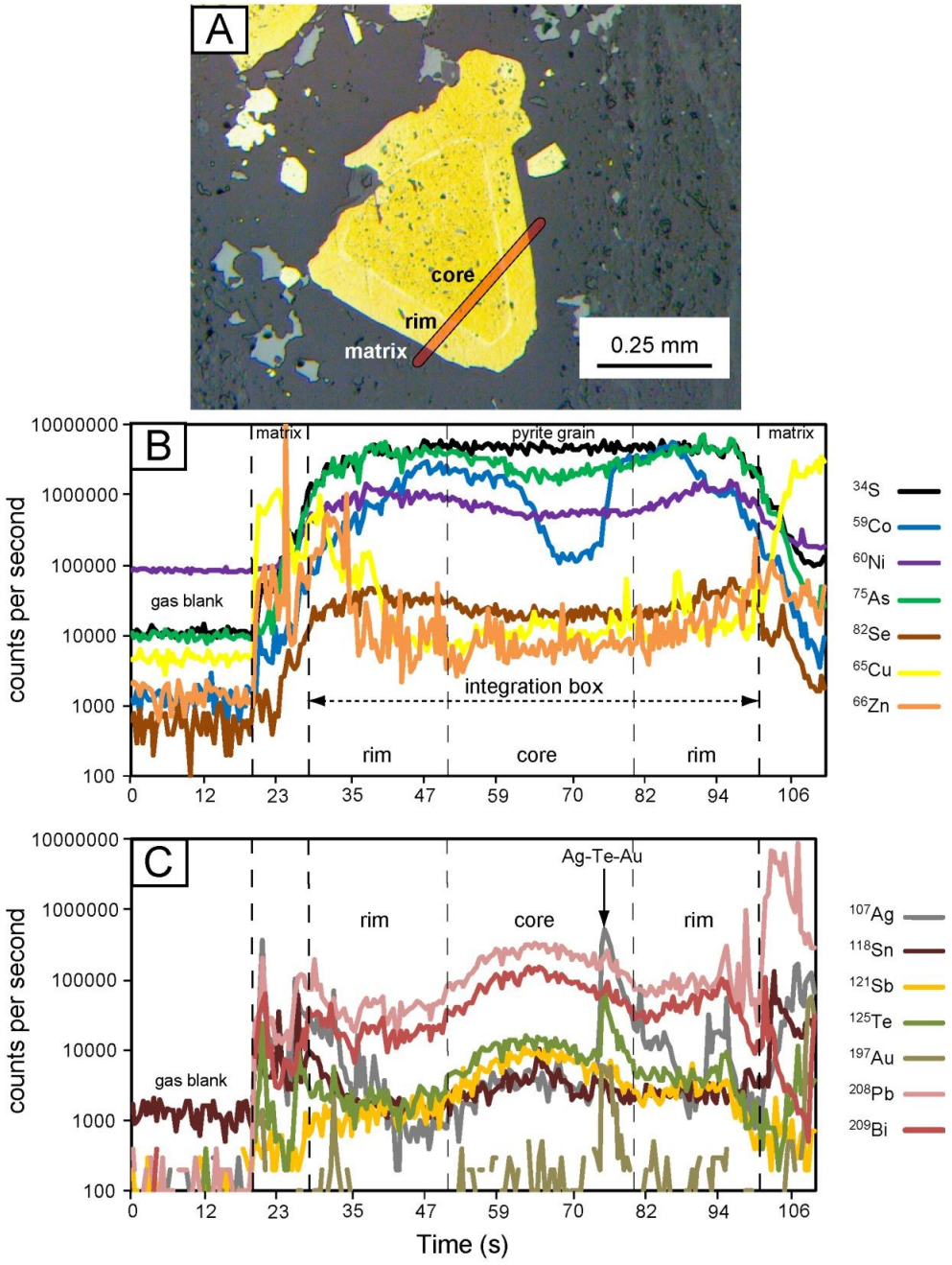

Figure 4.6: A. Example of a zoned pyrite grain analyzed by LA-ICP-MS. Zoning is highlighted by different tint of oxidation on thin section (reflected light). B and C. Time-resolved signal (count per second vs. time) recorded on the mass spectrometer during line analysis (in red in A) across the entire pyrite grain. The laser ablation started after 20 s of gas blank acquisition. Irregular patterns observed for Co, Ag, Sn, Sb, Te, Pb and Bi are associated with the two generations of pyrite analyzed. Peaks of Ag, Te and Au indicate a micro-inclusion.

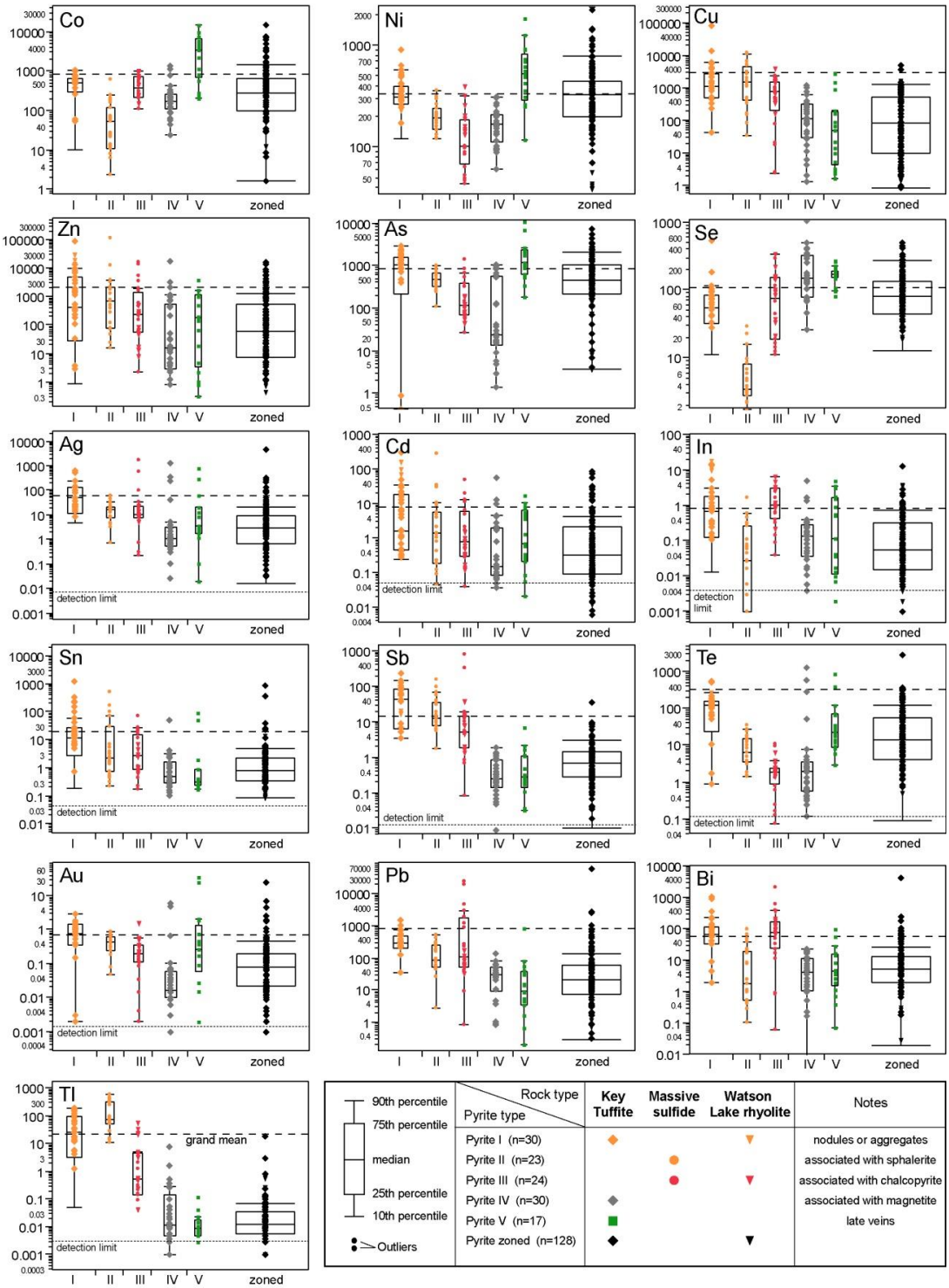

Figure 4.7: Statistical representation of the different types of pyrite analyzed by LA-ICP-MS. Detection limits are shown only when they are close to the concentrations measured in pyrite.

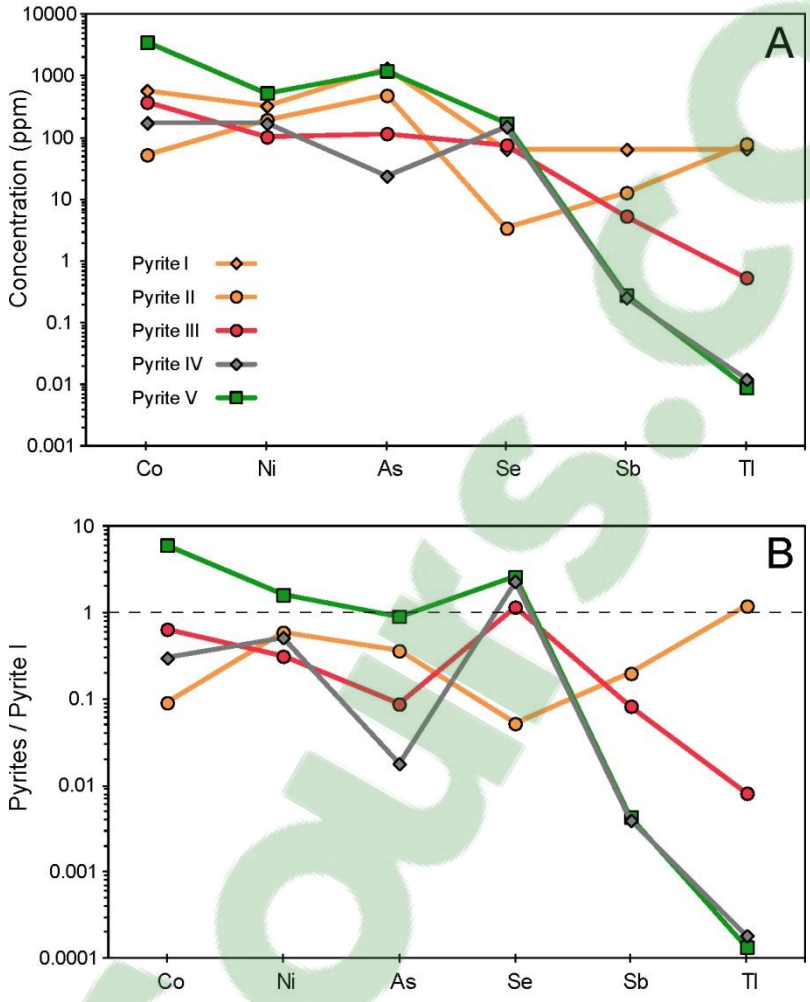

Figure 4.8: Multi-element variation diagrams for key elements in pyrite. A. Comparison of the median values of the different pyrite types identified. B. Normalization of the median of each pyrite type to the median of Pyrite I.

The effect of the inclusions on the total trace element content of pyrite was investigated by looking at positive correlations between Zn, Cu and Pb with other elements. Figure 4.9 illustrates the elements that have the best correlation with the inclusions of sphalerite, chalcopyrite and galena. Correlation tables for each pyrite group are presented in Annexe 4.3. The almost perfect positive correlation between Zn and Cd (Fig. 4.9B) indicates that in all cases, the Cd measured in pyrite is hosted in sphalerite inclusions. The positive correlation of Zn with Co and Se, in not all but several pyrite groups, suggests that under specific conditions these elements can also be incorporated into the lattice structure of sphalerite inclusions. In Figure 4.9B, copper is associated, to different degrees, with Ag, Sn and In, indicating that these elements in pyrite might be influenced by chalcopyrite inclusions. Finally for most pyrite, positive correlations among Pb, Bi and Ag also suggest that Bi and Ag are present in galena inclusions (Fig. 4.9C). For certain pyrite groups, Se is also correlated with Pb and thus interpreted to be incorporated in the structure of galena. All of these positive correlations are also validated by the trace element mapping (Figs. 4.10 to 4.14).

4.7.2. PYRITE I

Pyrite I is composed of fine-grained aggregates of pyrite (<5-40 µm) grouped in layers or nodules, both of which can be centimetric in size (Fig. 4.3A and B).

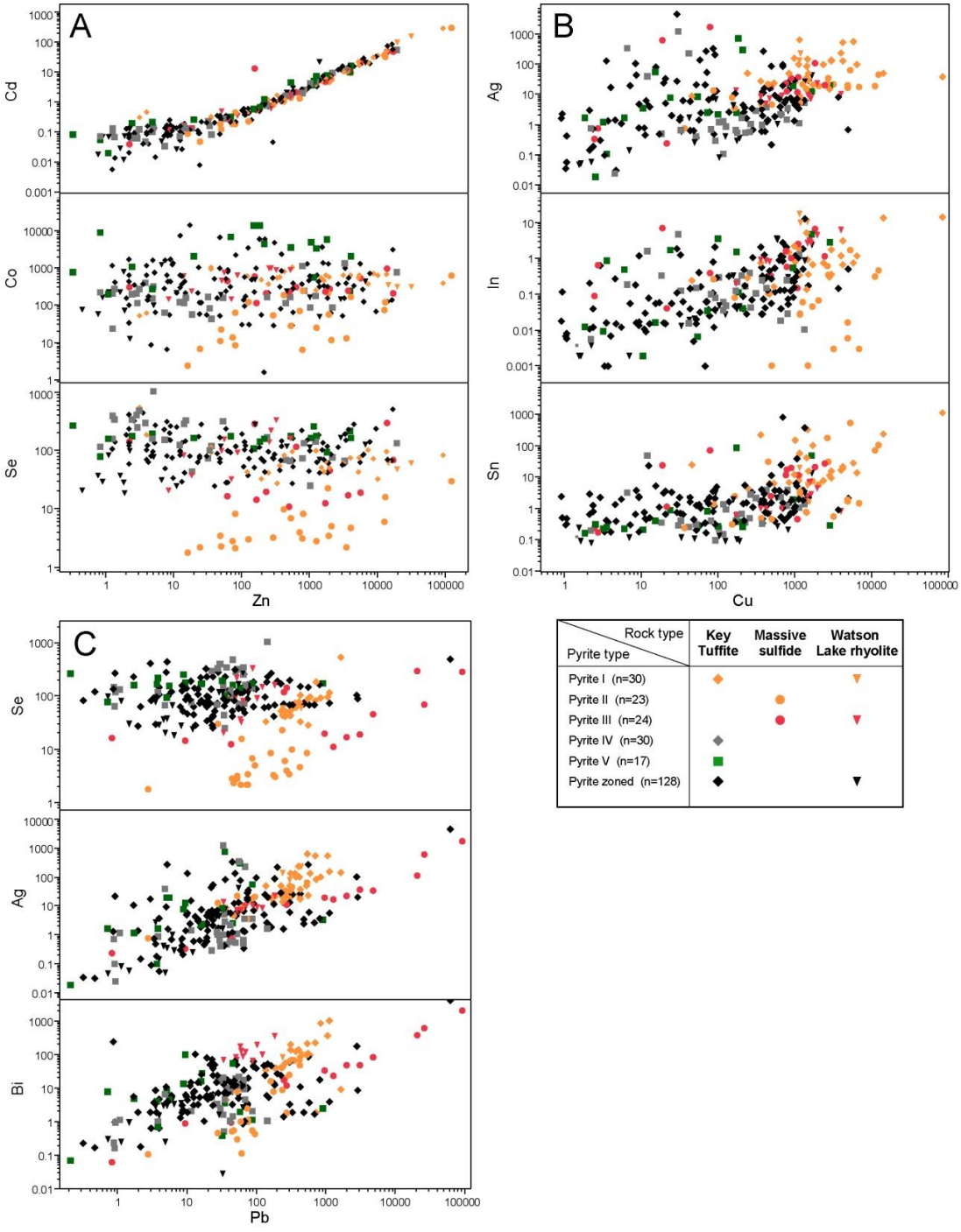

Figure 4.9: Binary diagrams for selected elements in pyrite analyzed from the Bracemac-McLeod mine. A. Zn vs. Cd, Co and Se. B. Cu vs. Ag, In and Sn. C. Pb vs. Se, Ag and Bi.

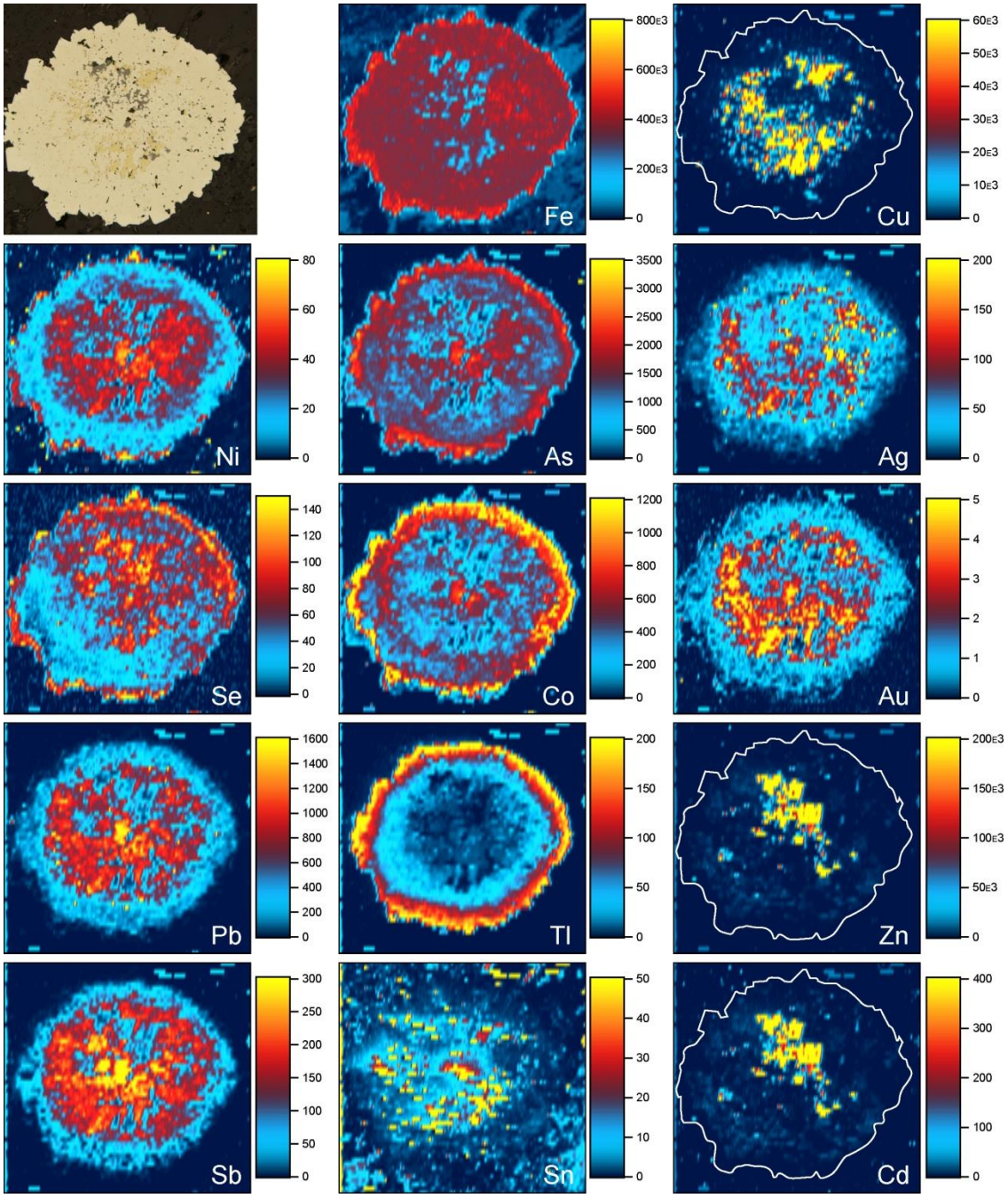

Figure 4.10: LA-ICP-MS elemental map of a pyrite nodule (Pyrite I). Semi-quantitative concentrations are given in ppm.

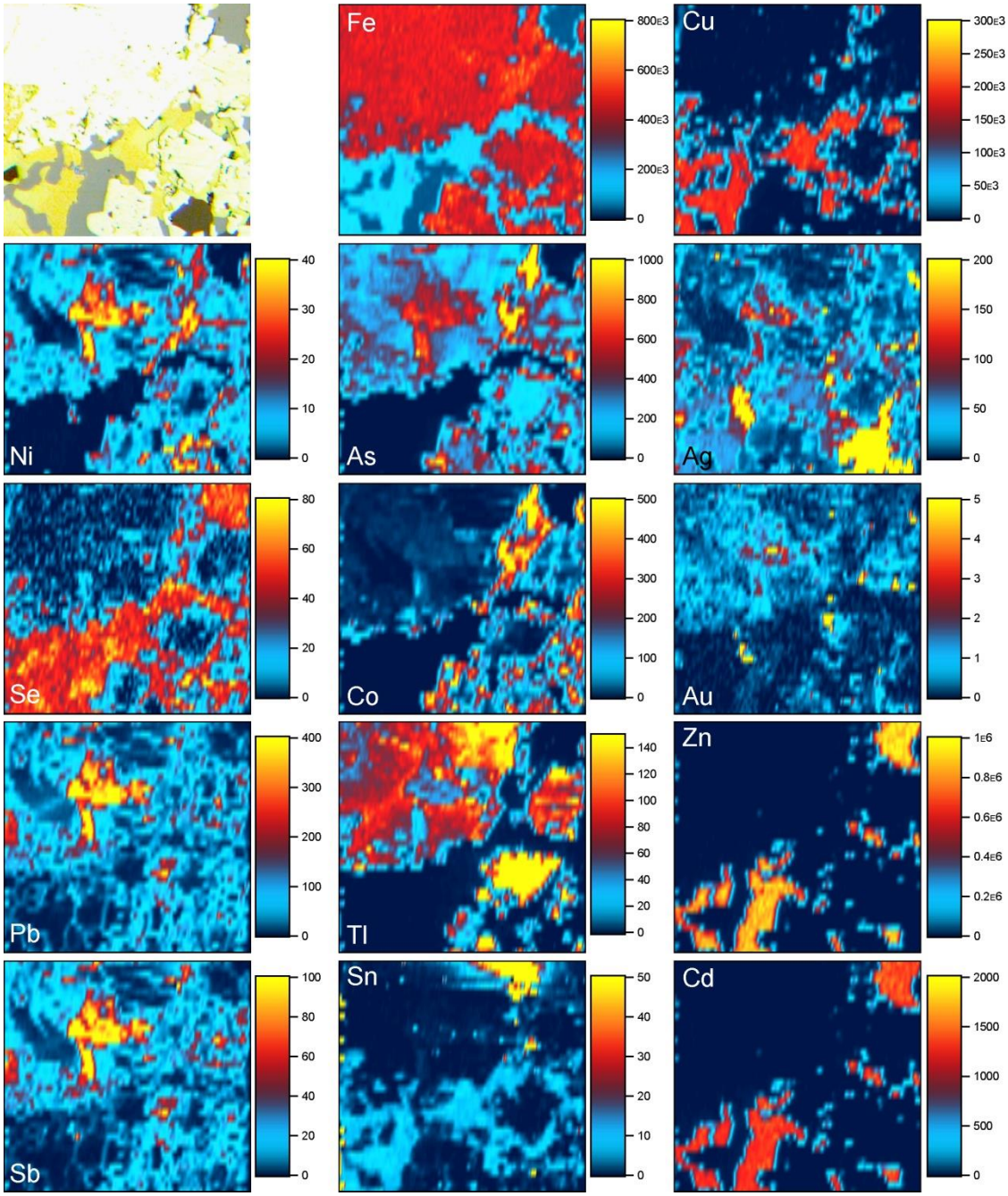

Figure 4.11: LA-ICP-MS elemental map of pyrite crystals from the Zn-rich zone (Pyrite II). Semi-quantitative concentrations are given in ppm.

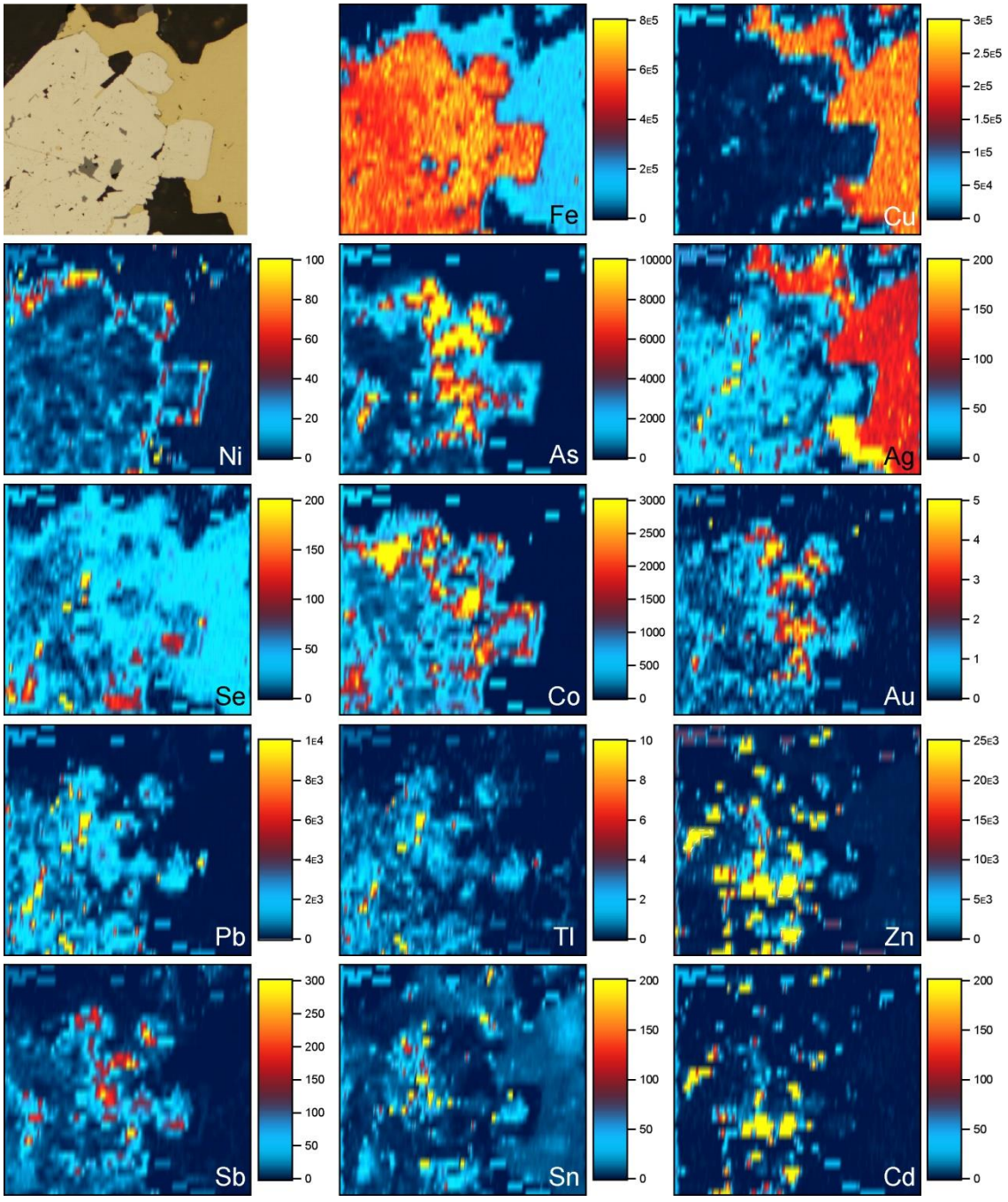

Figure 4.12: LA-ICP-MS elemental map of pyrite crystals from the Cu-rich zone (Pyrite III). Semi-quantitative concentrations are given in ppm.

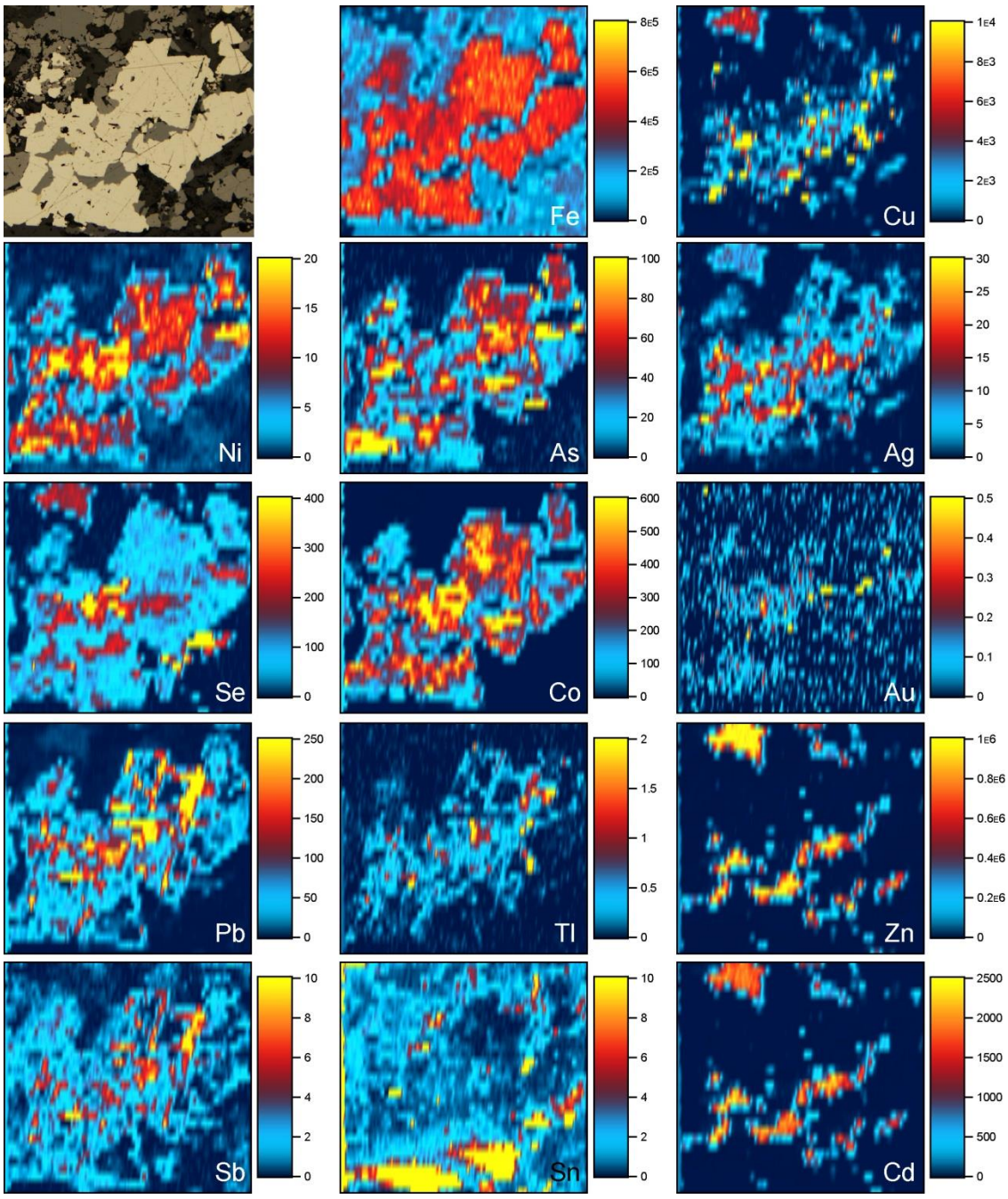

Figure 4.13: LA-ICP-MS elemental map of pyrite crystals from the magnetite-rich zone (Pyrite IV). Semi-quantitative concentrations are given in ppm.

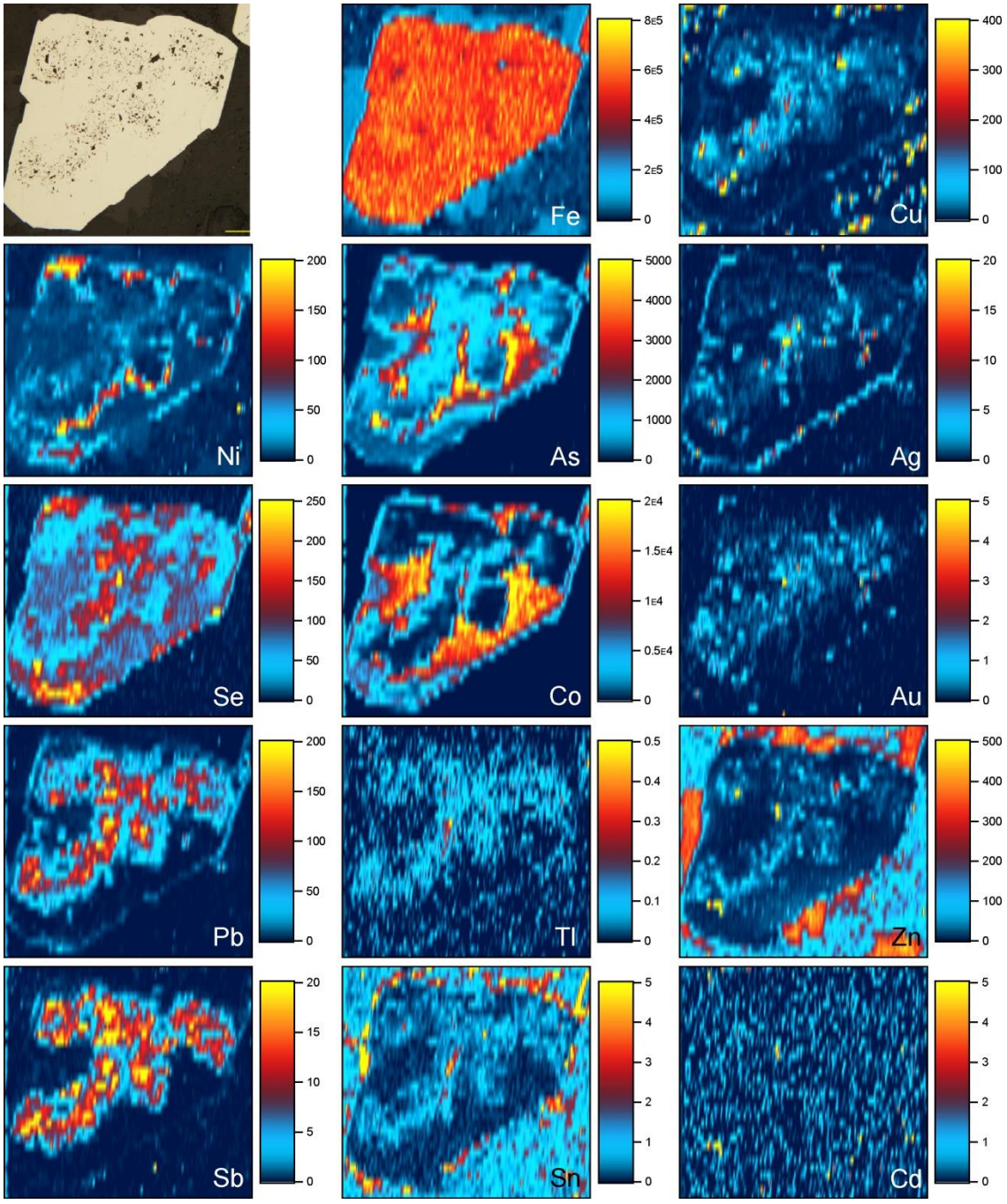

Figure 4.14: LA-ICP-MS elemental map of a zoned pyrite from the Key Tuffite. Semi-quantitative concentrations are given in ppm.

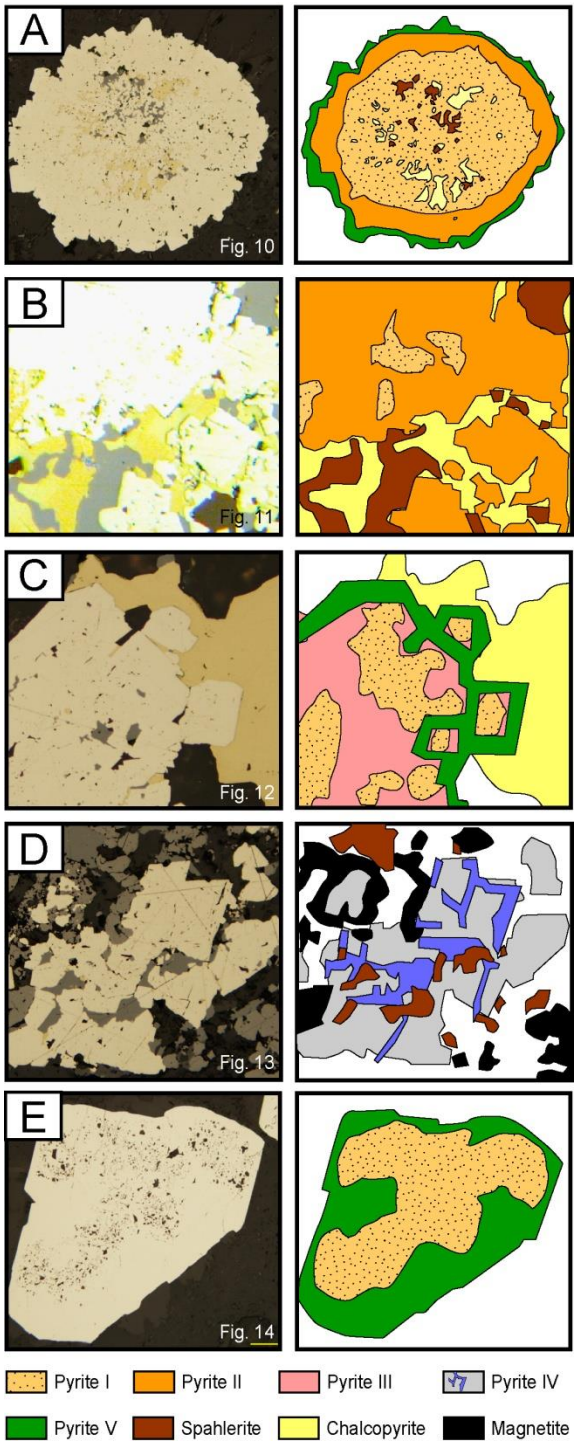

Figure 4.15: Schematic and interpretative representation of the four presented pyrite grains (Fig. 10 to 14) analyzed by LA-ICP-MS trace element mapping technique.

These pyrite layers follow the bedding in the Key Tuffite, whereas pyrite nodules can be disseminated either in the Key Tuffite or in the Watson Lake rhyolite footwall. These nodules have been observed only in the vicinity of the deposits, as far as 75 m away from the ore bodies. Pyrite I is characterized by a high density of silicate and sulfide inclusions (Fig. 4.4A and B). LA-ICP-MS results show that a full range of trace elements (Figs. 4.7 and 4.8) are present in Pyrite I. Specifically, this group contains the highest content of Cu, Zn, Ag, Sn, Sb, Te, Au, Pb, Bi and significant contents of As, Se and Tl (Table 4.3). Detailed mapping of a nodule (Fig. 4.10), from the Key Tuffite above the mineralisation at McLeod, reveals a complex distribution for most elements due to the high density of inclusions. Sphalerite and chalcopyrite are the main sulfide inclusions present in Pyrite I and thus explain the high Zn (± Cd) and Cu (± Sn and In) contents. However, Ag, Au, Te and Sb are not associated with sulfide inclusions and must be present as nanoparticles or micro-inclusions. Thallium content of this pyrite nodule shows a marked increase from core (< 10 ppm) to rim (> 200 ppm). It also revealed the presence of two generations of pyrite overgrowth (Fig. 15A) which are described below (Pyrites II and V).

4.7.3. PYRITE II

Pyrite II corresponds to sub-euhedral pyrite associated with the Zn-rich part of the ore. The grains (0.25 to 1mm, 0.5mm on average) are generally disseminated in

massive sphalerite or are grouped along centimetric bands (Figs. 4.3E and 4.5A). Pyrite II commonly contains an earlier core of Pyrite I (Figs. 4.10, 4.15A and B). Visible inclusions comprise chalcopyrite, sphalerite and galena. Chemically, the suite of elements present in Pyrite II is very similar, but slightly depleted, compared to the chemistry of Pyrite I (Figs. 4.7 and 4.8). Significant differences include lowest values of Co (52 vs. 582 ppm) and Se (3 vs. 65 ppm) for all pyrite groups analyzed. Pyrite II is also characterized by the highest Tl concentrations (up to 488 ppm, 79 ppm in average). These statistics are confirmed by the spatial elemental distribution of elements in Pyrite II overgrowing Pyrite I (Figs. 4.10 and 4.11).

4.7.4. PYRITE III

Pyrite III is associated with the Cu-rich part of the deposits (Fig. 4.3F; Stringer Zone, McWest, upper part of McLeod, lower part of Bracemac KT). Pyrite III occurs as sub-euhedral grains which are coarser (0.2 to 3.5mm, with an average of 1mm) than Pyrite II in the Zn-rich zone (Fig. 4.5B). LA-ICP-MS analysis indicates that Pyrite III contains significantly lower concentrations of most elements (Figs. 6 and 7), including Ni, As, Sb, and Tl, than Pyrites I and II. However, Se is significantly enriched in Pyrite III (76 ppm) compared to Pyrite II (3 ppm) but only slightly enriched compared to Pyrite I (65 ppm). Other differences comprise modest enrichment in Co, In, Pb and Bi in Pyrite III. Trace element

mapping (Fig. 4.12) shows that the distribution of most of these elements is relatively uniform in Pyrite III. However, Pyrite III contains an earlier core of Pyrite I in addition to a late pyrite overgrowth (Pyrite V) rich in Co, Ni and As (Fig. 4.15C).

4.7.5. PYRITE IV

Pyrite IV is defined by its association with magnetite both in and away from the deposit. Numerous macroscopic and petrographic observations show that magnetite locally replaced sphalerite and pyrite (Figs. 4.3G and H and 4.5C). When preserved, pyrite grains are coarser (0.3 to 2.5, average of 1mm) than in any other part of the deposit, probably due to recrystallization. Pyrite IV is depleted in most trace elements compared to Pyrite I, II or III (Figs. 4.6 and 4.7), except Se which shows the highest values (up to 1059 ppm, 151 ppm in average). High Se values contrast with the extremely low As values (24 ppm) compared to the other pyrite types (>100 ppm). Chemical mapping (Fig. 4.13) highlights a complex pattern in the structure of the Pyrite IV (Fig. 4.15D). Apart from Se, which is homogeneously distributed in pyrite, all other elements are concentrated along straight and angular lines.

4.7.6. PYRITE V: EUHEDRAL LATE VEINS

Pyrite V forms almost perfectly euhedral crystals of variable sizes (0.2 to 2mm) and are concentrated in late veins of quartz-carbonate along with remobilized

sphalerite (Fig. 4.4F) or chalcopyrite (Fig. 4.4G), or as overgrowths or recrystallized rims of any other types of pyrite (Figs. 4.4C-E, 4.15). The well crystallized rim appears to be common around disseminated pyrite (Figs. 4.10, 4.14) or stringer pyrite (Fig. 4.13), but is absent in pyrite from the center of the massive sulfide zones (Fig. 4.11). Such a euhedral overgrowth is recognized in pyrite at the scale of the mining camp, even in Key Tuffite sections far from the deposits, and suggests that Pyrite V most likely results from the regional late metamorphic event. Pyrite V is characterized (Figs. 4.7 and 4.8) by high average concentrations of Co (3536 ppm), Ni (533 ppm), As (1216 ppm), Se (172 ppm) but very low concentration (< 5 ppm) of all other elements (except Cu, Zn, Te and Pb with 53, 182, 22 and 9 ppm, respectively, as a result of inclusions).

4.7.7. SUMMARY: KEY DIAGRAMS TO DISCRIMINATE HYDROTHERMAL VS METAMORPHIC PYRITES

Figure 4.16 displays a series of diagrams to discriminate the different pyrite types described above, including hydrothermal and metamorphic pyrites. The elements (Ni, Co, As, Se, Sb and Tl) used are those which are the most representative of the pyrite chemistry.

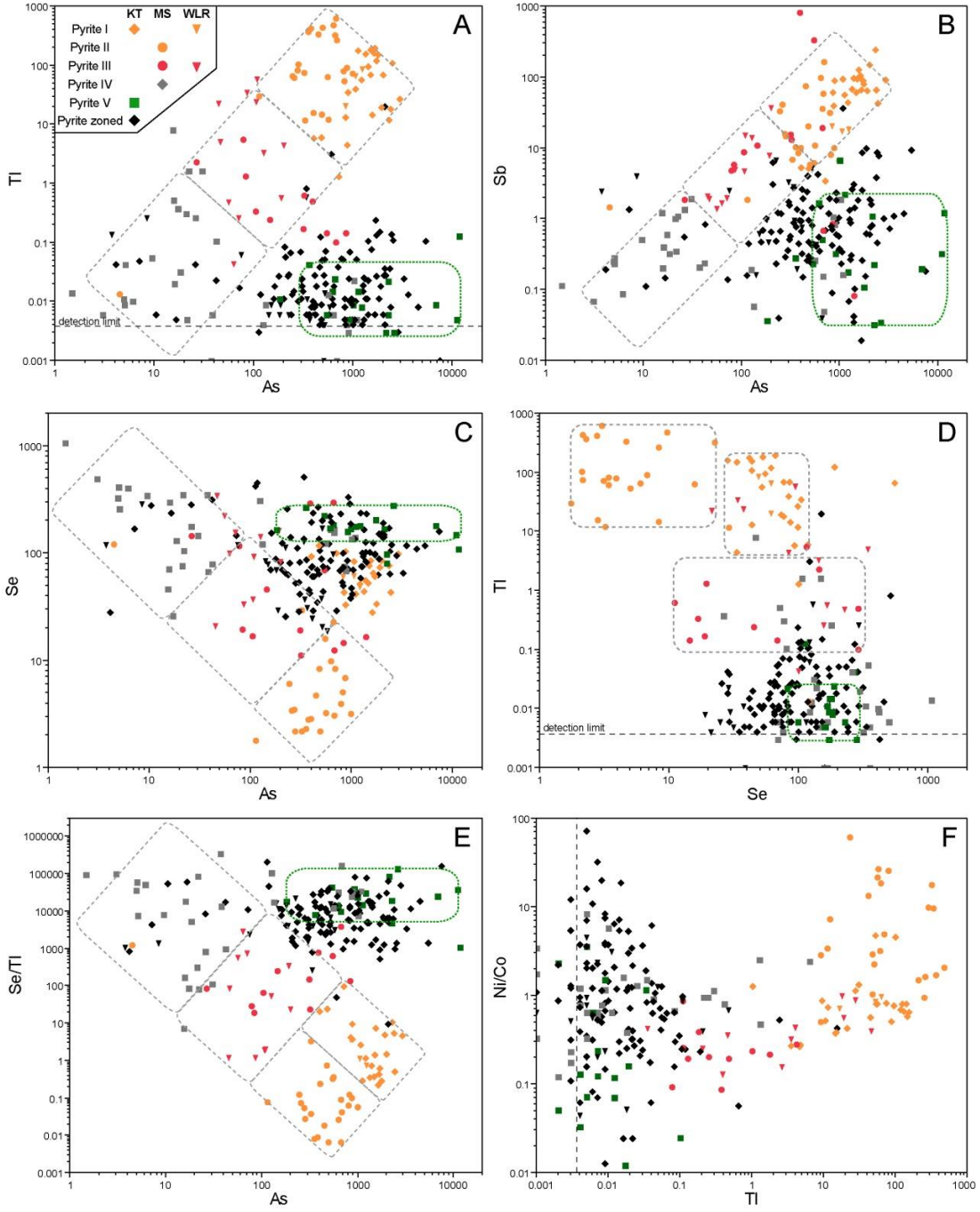

Figure 4.16: Discrimination binary diagrams of the different pyrite types identified in the Bracemac-McLeod mine. A. Tl vs. As. B. Sb vs. As. C. Se vs. As. D. Tl vs. Se. E. Se/Tl vs. As. F. Ni/Co vs. Tl.

Hydrothermal pyrites (Pyrite I to IV) define a positive correlation on Tl-As and Sb-As plots (Fig. 4.16A and B), whereas metamorphic (Pyrite V) and zoned pyrites plot out of the hydrothermal trend to higher As values for low Tl and Sb contents. Within the hydrothermal trends, there is a progressive decrease of Tl-Sb-As contents from Pyrite I-II to Pyrite III to Pyrite IV. Conversely, Se displays a progressive increase from Pyrite I to IV (Fig. 4.16C and D). The plots of Tl versus Se and Se/Tl versus As (Fig. 4.16D and E) allows further discrimination of Pyrite I from Pyrite II due to the low Se values characterizing Pyrite II (Fig. 4.8). Finally Ni/Co ratios were often used in the literature to discriminate pyrite origin (Loftus-Hills and Solomon, 1967; Bralia et al., 1979; de Kersabiec and Roger, 1979). However, Figure 4.16F clearly shows that Ni and Co are not useful for discriminating the 5 pyrite types.

4.7.8. ZONED PYRITE

Zoned pyrite represents the majority of the pyrite analyzed (128 grains). They generally form perfectly euhedral crystals of variable size (0.1 to 3.5mm) disseminated in the Key Tuffite and in the Watson Lake rhyolite footwall.

They have an internal core rich in silicate inclusions (Fig. 4.4C and E), which is interpreted to be an earlier generation of pyrite, possibly Pyrite I, and a euhedral rim resulting from recrystallization or late overgrowth (Pyrite V). Zoned pyrite along the Key Tuffite (Fig. 4.4E) displays similar textures regardless of their

position, from 1000m (Fig. 4.4C) to 50m (Fig. 4.4D) away from the deposit. Chemically, zoned pyrites have highly variable compositions and cover most of the range of values of all pyrite types defined above (Fig. 4.6). On the discrimination diagrams (Fig. 4.16), very few of the zoned pyrites (averaged values for the entire grain) plot on the hydrothermal trends and the majority plot near Pyrite V of metamorphic origin. Trace element mapping confirms that the euhedral rim is chemically similar to Pyrite V (Fig. 4.14) as characterized by enrichments in Co, Ni, and As compared to the core. The core displays the same suite of elements present in Pyrite I (Cu, Sb, Tl, Pb, Bi, Te...) although less abundant. In order to compare with the five pyrite end-members defined above, core and rim of zoned pyrites have been separately quantified using a subset of 38 representative grains from 15 samples. Results, presented on Figure 4.17, confirm that the rim is similar in composition to Pyrite V, and thus metamorphic in origin, whereas the core of some zoned pyrite is Pyrite I (enriched in Tl and Sb). However, the concentration of these two key elements in the core of the zoned pyrite is variable.

4.7.9. TRACE ELEMENTS IN PYRITE AND VARIATION WITH DISTANCE TOWARDS THE ORE

The average content (per sample) of Co, Ni, As, Se, Sn, Sb and Tl in all pyrite types as a function of the distance to the Bracemac-McLeod mine is presented in

Figure 4.18. Using whole grain chemistry, no significant or coherent variation is observed in, or outside the alteration halo. Contents of Co and Ni are highly variable and unpredictable (Fig. 4.18A and B), whereas As, Se, Sb and Tl are relatively uniform away from the deposit (Fig. 18C-F) and only start to vary in the last 50m or less (i.e. within the chlorite zone). Thallium and Sb have low values away from the deposit (0.01 and 1ppm, respectively), but significant gains are present in pyrite from the last 25m from the deposit (Fig. 4.18E and F). In opposite, As and Se display both gains and losses in the vicinity compared to pyrite away from the deposit (Fig. 4.18C and D). These results suggest that the use of trace elements in pyrite, using the chemistry of the whole grain, as a vectoring tool appear to be limited for the exploration of VMS deposits. However, when looking at the chemistry of the core only of the zoned pyrite from the Key Tuffite, a slight enrichment in Sb and Tl towards the deposit is detected about 250m away from the deposit (median values of 0.6 to 5 ppm and 0.02 to 0.12 ppm, respectively).

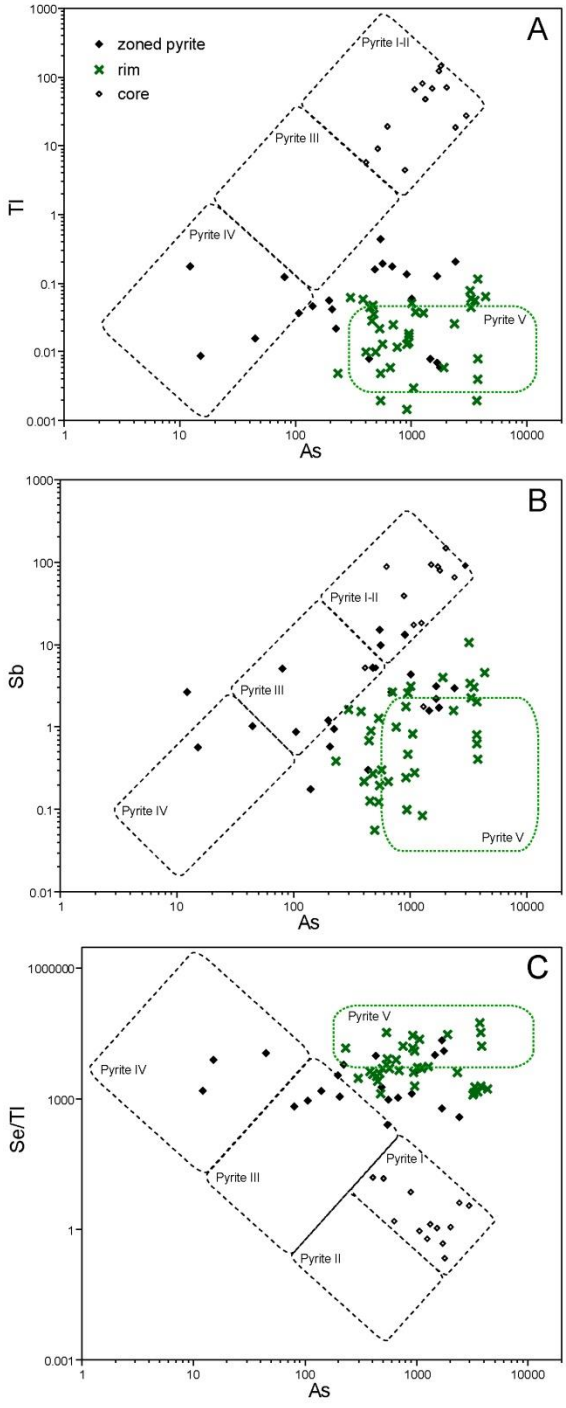

Figure 4.17: Discrimination binary diagrams of zoned pyrites (rim, core and whole grain) from the Bracemac-McLeod mine. A. Tl vs. As. B. Sb vs. As. C. Se/Tl vs. As.

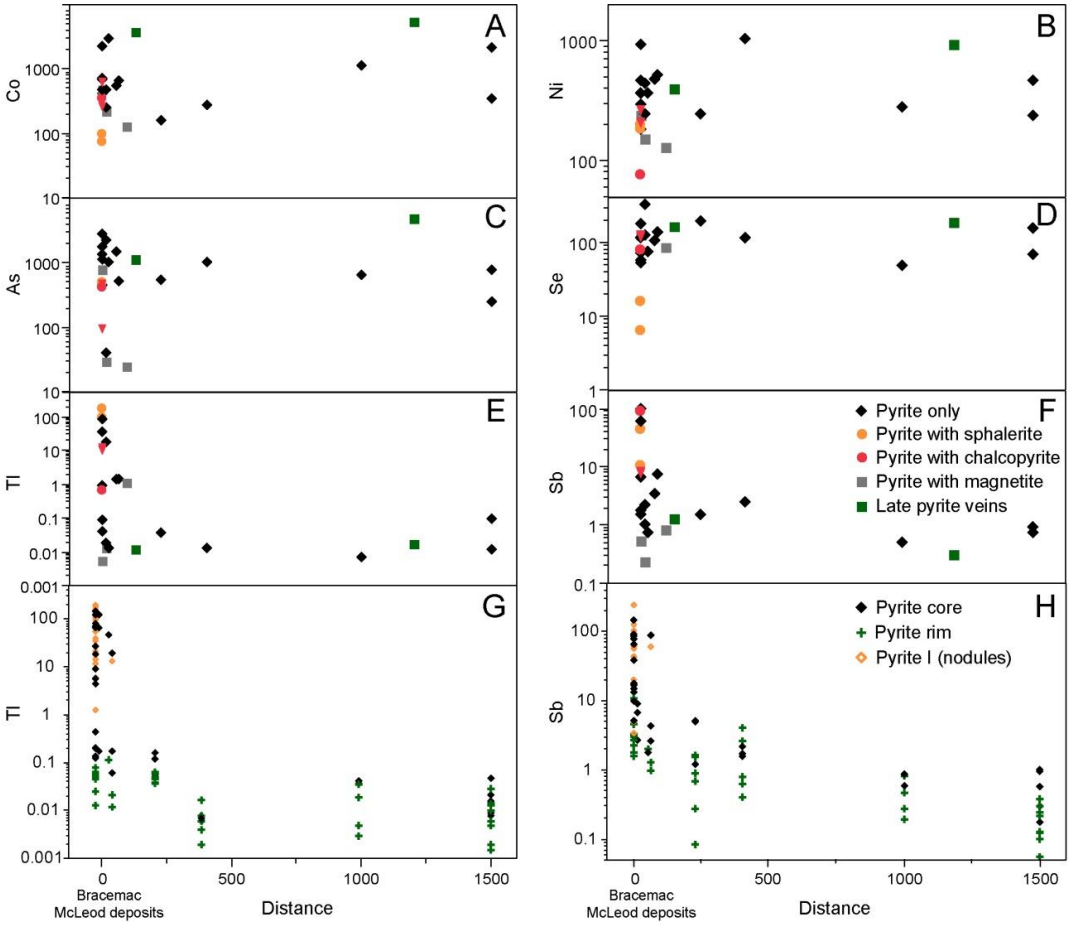

Figure 4.18: A to F. Variation of Co, Ni, As, Se, Sb and Tl content in pyrite versus distance from the Bracemac-McLeod deposits. Each point represents the median of the pyrite grains (~10) analyzed in the sample. G and H. Variation of Tl and Sb in pyrite nodules (Pyrite I), compared to rim and core analyses of zoned pyrites, versus distance from the Bracemac-McLeod deposits.

The core of zoned pyrites from the Key Tuffite directly above or below the mineralization are significantly enriched in Sb and Tl (>10 and >1 ppm, respectively). The enrichment in Sb is also recorded in the recrystallized rim (Fig. 4.17H) and systematically increase from 0.1 to >1 ppm in the close vicinity of the Bracemac-McLeod deposits. In zoned pyrites from samples just above the mineralization, two distinct populations are also present and characterized by concentrations above 10 ppm for Sb and of 1ppm for Tl. All these results could be of interest for ore vectoring.

4.8. DISCUSSION

Temperature is a key factor controlling the distribution of Cu and Zn in VMS deposits. As shown by thermodynamic calculations based on experimental studies (Large, 1977; Bourcier and Barnes, 1987; Metz and Trefry, 2000) and compilation of modern VMS-forming deposits (Hannington et al., 2005), hydrothermal mineralizing fluids preferentially precipitate zinc, as sphalerite, at a temperature equal to or below 250°C whereas copper precipitates as chalcopyrite at higher temperatures (280 to 320°C). Although the timing of magnetite precipitation in VMS is debated, it is interesting to notice that the occurrence of magnetite-rich zones seem to be a distinctive feature of many replacement-type VMS deposits like Currawong, Australia (Bodon and Valenta, 1995), Gossan Hill, Australia (Sharpe and Gemmell, 2002) and Ansil, Canada (Galley et al., 1995). A

variety of models have been proposed for the formation of magnetite, but for nearly all cases, magnetite is interpreted to have formed during a late hydrothermal stage, as replacement of earlier sulfides. In VMS systems, magnetite is proposed to precipitate from high-temperature (>350°C), relatively low-fO_2, reducing fluids (Galley et al., 1995; Sharpe and Gemmell, 2002). The diversity of sulfide assemblages at the Bracemac-McLeod deposits (from sphalerite, to chalcopyrite, to magnetite-rich) thus reflects the evolution of the conditions of precipitation of a mature hydrothermal system (Annexe 4.4). In-situ LA-ICP-MS analysis of pyrite from each of these zones provides a near complete record of the evolution of the hydrothermal system.

Most elements present in pyrite reside in nanoparticles or micro-inclusions, except Ni, Co and As, Se which substitute to Fe or S, respectively (e.g. Vaughan and Rosso, 2006). Coupled with textural observations, these four elements, in addition to Sb and Tl were used to identify 5 pyrite types and propose an evolutive model of the hydrothermal mineralizing system for a replacement-type VMS deposit (Fig. 19).

4.8.1. EVOLUTION OF HYDROTHERMAL FLUIDS FORMING A REPLACEMENT-TYPE VMS

During the early period of the hydrothermal system (<250°C), ascending hydrothermal fluids, focused at depth by synvolcanic faults (Fig. 4.2 and 4.19A),

mixed with cold seawater that saturated the porous Key Tuffite. This mixing created intense contrasts of temperature and pH and caused the precipitation of Pyrite I. The fine-grained nature and the abundance of inclusions (sphalerite, chalcopyrite and silicates) present in Pyrite I (Fig. 4.4A and B) are characteristic of a rapid nucleation of the mineral at relatively low temperature from a supersaturated solution (Butler and Rickard, 2000). Pyrite I contains the highest contents of most trace elements (Figs. 4.7 and 4.8). Rapid nucleation of pyrite crystals and the large surface to volume ratio facilitates the incorporation of impurities as inclusions or sorption processes (Scott et al., 2009), as expressed by the wide enrichment of a large number of trace elements (Cu, Zn, Ag, Sn, Sb, Te, Au, Pb, Bi, ± As, Se, Tl). This significant enrichment of trace elements can be explained by the fact that no other mineral phases, susceptible to incorporate trace elements from the fluids, co-precipitated with pyrite.

As the hydrothermal system gained in maturity and temperature increased (up to 250°C), the most economic part of the deposit was formed: the Zn-rich part (Fig. 4.19B) comprising sphalerite and Pyrite II (± galena).

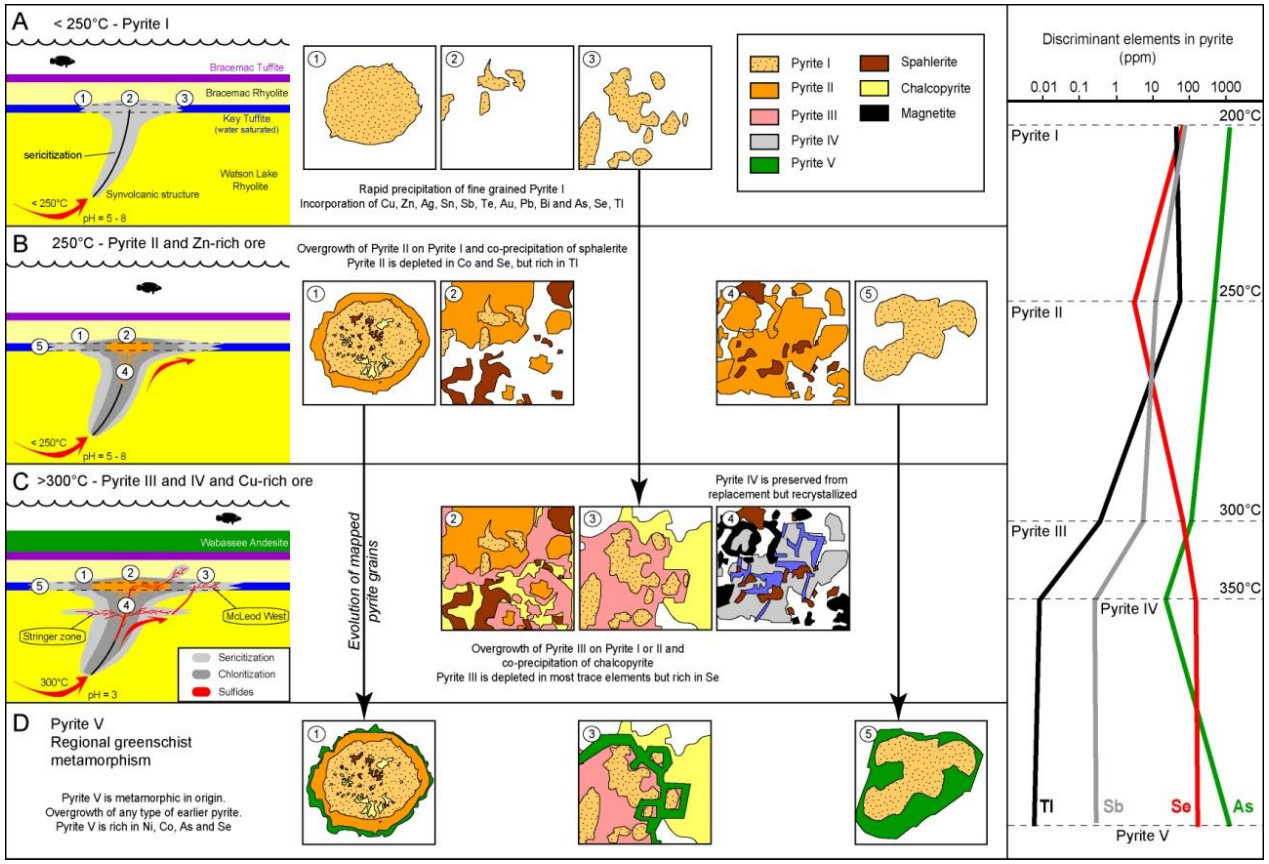

Figure 4.19: Synthesis of the trace element compositions of pyrite during the evolution of the hydrothermal system at Bracemac-McLeod deposits: A. During the early stage, at low temperature (<250°C), B. During the main mineralization event leading to the formation of the Zn-rich ore (250°C), C. During the high temperature formation of the Cu-rich ore (300°C) and magnetite replacement (350°C) and D. During late regional greenschist metamorphism. For each stage of the evolutive model (not to scale), the interpretation of the elemental LA-ICP-MS maps are used to illustrate the evolution of the trace element compositions, mineral assemblages and textures.

The similarity of the trace element signature between Pyrite I and Pyrite II (Fig. 4.6 and 4.7) suggests that both types are genetically related with similar compositions of fluid and conditions of precipitation. Slight variations in the condition of precipitation of Pyrite I in the Key Tuffite (e.g. temperature contrast, seawater/hydrothermal fluid ratio) could account for both textural and slight chemical differences. However, it cannot explain the significant depletion of Co and Se in Pyrite II compared to Pyrite I. Elements such as Cd, Co and Ni, which have ionic radii and charges similar to Zn, and Se, with a similar ionic radius to S, can substitute into sphalerite (e.g. Vaughan and Rosso, 2006) but they are also common in pyrite. It is thus expected that sulfides co-precipitating from the same trace metal-bearing hydrothermal fluid will compete for metal incorporation in their respective structure. Our results suggest that, under the condition of sphalerite precipitation at Bracemac-McLeod, Co and Se were preferentially incorporated into sphalerite rather than pyrite thus leading to significant depletion of these two elements in Pyrite II. This hypothesis is supported by the elemental distribution of Co and Se in sphalerite provided by the LA-ICP-MS mapping (Fig. 4.11) and by the positive correlation between Zn and Co and Zn and Se (Pearson product >0.74). Pyrite II is also characterized by the highest Tl values present in this study (up to 488 ppm, 79 ppm in average). Zhou et al. (2005) demonstrated that pyrite can incorporate significant amount of Tl (5 800 to 35 000 ppm) in the Xiangquan thallium deposit, China. Thallium can be enriched in a variety of hydrothermal ore

deposits (e.g. Ikramuddin et al., 1983; Ikramuddin et al., 1986; Graham et al., 2009; Baker et al., 2010), but only few studies (Murao and Itoh, 1992; Large et al., 2001) have presented an empirical association between Tl and Zn in ancient VMS settings. Thermodynamic calculations (Xiong, 2007) showed that the most favorable conditions for leaching, transport and deposition of Tl (specifically neutralization of the acidic fluids during the mixing with seawater) are very similar to those for Zn. Thus it is not unexpected to document Tl enrichment in pyrite which co-precipitated with sphalerite.

With the continued increase of the hydrothermal fluid temperature (300°C), chalcopyrite precipitated not only in the deepest parts of the hydrothermal system but also in the upper parts of McLeod and McLeod West (Fig. 4.2, 4.19C). Such a feature is uncommon, even in replacement-type VMS deposits. This can be related to the burial of the hydrothermal system due to the progressive volcanic effusion above (Wabassee Group) and the consequent displacement of the hydrothermal convection system upwards in the stratigraphic pile, as manifested by ore stacking (Fig. 4.2B). Pyrite III, which co-precipitated with chalcopyrite, is characterized by higher concentrations of Se ± Co, In, Pb, Bi compared to Pyrite I and II. Similar enrichments in Se have been reported, from whole rock and in situ sulfide analyses, in massive sulfides associated with chalcopyrite from modern and ancient VMS (Auclair et al., 1987; Hannington et al., 1991;

Hannington et al., 1999; Layton-Matthews et al., 2008; Sharman et al., 2014) and are indicative of sulfides forming at high temperatures.

Pyrite III is also characterized by lower As content compare to Pyrites I and II. The negative correlation between As and Se (Fig. 4.16C) present in hydrothermal pyrites (I to IV) suggests that As and Se are competing to substitute into the same S site (Cook and Chryssoulis, 1990; Dare et al., 2011). However, Pyrite III is also characterized by lower abundance of all other trace elements. Three hypotheses are proposed to explain the lower trace elements content of Pyrite III: 1) trace elements where depleted in the evolved hydrothermal fluids, 2) trace elements were expelled from the structure of earlier-forming pyrite (I or II) during hydrothermal recrystallization and formation of pyrite III, or 3) trace elements were present in the fluid but incorporated into other minerals (such as chalcopyrite) or formed accessory phases (e.g. such as Au-tellurides, As-bearing minerals).

Magnetite is present, although as a minor constituent, in all the deposits of the Matagami district. The Caber Nord deposit, on the West Camp (Fig. 4.1), is an exception in the district with sections up to 40 m thick and 500 m strike length of semi-massive to massive magnetite (Salmon et al., 2007). At Bracemac-McLeod, magnetite is limited to the lower part of Bracemac KT and the central part of the McLeod deposit (Fig. 4.2) and it is interpreted to be associated with the highest temperatures reached by the hydrothermal system (350-400°C; Galley et al.,

1995; Galley et al., 2000). Such temperatures might have been reached due of the burial of the still active hydrothermal system under a portion of the overlying volcanic rocks of the Wabassee Group (Fig. 4.19D). Magnetite replaced sphalerite and pyrite (Figs. 4.3G and 4.5C). We interpret Pyrite IV, associated with magnetite, to be the result of the recrystallization of earlier pyrite (I to III) at these elevated temperatures before their replacement. Trace elements were expelled from the pyrite crystal structure during the recrystallization (Huston et al., 1995) leading to very low trace element content in pyrite (Figs. 4.7 and 4.8). Only Se, which substituted for S, was preserved in pyrite and even enriched. Large et al. (2007) and Thomas et al. (2011) shown that Se remains in pyrite even after significant recrystallization. The LA-ICP-MS mapping confirm that most trace elements (including Se) are not incorporated into magnetite (Fig. 4.13). Boucher (2011) showed similar results at the Ansil West deposit (Noranda, Quebec) where the magnetite replacing earlier sulfides is almost barren of trace elements. The highest values of Se in the preserved Pyrite IV (up to 1059 ppm, 151 ppm in average) could be explained by the progressive incorporation of Se from the surrounding Se-bearing minerals already replaced by magnetite (pyrite and sphalerite), or simply by incorporation from the fluid. Low concentration of all other trace elements (except Se) in Pyrite IV suggests that most elements have been redistributed at the grain scale forming a complex geometric pattern during recrystallization (Figs. 4.13 and 4.19E)

Regional greenschist metamorphism commonly leads to various degrees of recrystallization of pyrite (Craig and Vokes, 1993) and expulsion of most trace elements present in inclusions (Huston et al., 1995; Wagner et al., 2007). However, it could also result in enrichment in trace elements that remain in solid solution (Craig et al., 1998; Large et al., 2007; Thomas et al., 2011). Thus, elements present in pyrite by direct substitution (particularly As, Se, Ni, Co) are preserved and even enriched during metamorphism (Figs. 4.7 and 4.19F). The effect of the expulsion of trace elements is illustrated by enrichment of many elements on the outside margin of pyrite grains disseminated in the Key Tuffite (e.g. Ag and Pb, Fig. 4.14). However, the recrystallized rim of pyrite is not always present and seems better developed in pyrite in form of dissemination or stringers rather than massive. Despite the generally low content in other trace elements, significant positive correlation between the elements present in substitution (As, Se, Ni, Co) and Ag, Te and Au (Pearson product >0.7) suggest the incorporation of these elements from the metamorphic fluids.

4.8.2. IMPLICATIONS FOR EXPLORATION

The potential of using trace elements in pyrite for exploration purposes has been recognized since the end of the 1960's. Many of the first studies focused on discriminating ore types (Roberts, 1982), mainly using Co/Ni ratio in pyrite (e.g. Loftus-Hills and Solomon, 1967; Bralia et al., 1979; de Kersabiec and Roger,

1979). However, in the last decade, significant advances have been made on the understanding of the incorporation of trace elements into pyrite. LA-ICP-MS analysis of pyrite is a powerful tool to investigate the evolution of a hydrothermal system (e.g. Large et al., 2007; Agangi et al., 2013), as it has been shown here. However, the use of trace elements in pyrite as an exploration tool vectoring towards mineralization has to be assessed. Preliminary tests on the lateral variation of pyrite chemistry in the alteration halo of the McArthur River sediment-hosted Pb-Zn deposit (Maier and McGoldrick, 2005) revealed that the spatial distribution patterns of trace elements are erratic. These authors suggested that it might reflect variation in the conditions of precipitation. Our results are in agreement. Using the chemistry of whole pyrite grains (i.e. including rim and core), no coherent pattern of variation in the trace elements present in pyrite has been found in and outside the alteration halo surrounding the Bracemac-McLeod deposit (Fig. 4.18). These results are probably best explained by the mixed signal given by the metamorphic rim and hydrothermal core from zoned pyrite, the dominant pyrite form in the Key Tuffite outside the deposit (Fig. 4.14). However, when looking at the composition of the hydrothermal core of the zoned pyrite as a function of the distance (Fig. 4.18E and F) a discrete increase in the composition of Tl and Sb is recorded around 250m and 400m, respectively, and could be useful in VMS exploration. The enrichment in Sb is even preserved in the euhedral rim suggesting that Sb has not been completely expelled from the crystal structure

during the metamorphic recrystallization. However, in practise the use of LA-ICP-MS analysis of pyrite in an exploration program would be difficult: sample size is limited, analysis costs are high (relative to whole rock analysis), and time of treatment are long, especially for zoned pyrites.

The main contribution of this paper resides in a series of discrimation diagrams of hydrothermal versus metamorphic pyrites (Fig. 4.17). The plot Se/Tl versus As (Fig. 4.17E) best summarizes our results. Arsenic and Se are well correlated in hydrothermal pyrites (Pyrite I to IV) due to their competition for the S site. Arsenic incorporation in pyrite is favored at low temperature (Pyrite I and II; Ballantyne and Moore, 1988), whereas Se progressively increases in pyrites formed at higher temperature (Pyrite III to V). Se/Tl ratio was first used by Maslennikov et al. (2009) to separate, based on the temperature of precipitation, pyrites from vent chimneys from the Silurian Yaman-Kasy VMS deposit, S. Urals, Russia. They proposed that the contents of Tl and Se in pyrite are respectively the best proxy for inferring low and high temperature of precipitation. The results of our study are in agreement. Pyrite I and II, associated with the start of the hydrothermal system and the Zn-rich zones (i.e. low temperature) have the lowest Se/Tl (<10). This ratio is significantly higher for Pyrite III (10<Se/Tl<10 000), associated with the Cu-rich zone. Finally pyrites associated with higher temperature of formation, but often non-economic part of the deposit (i.e. metamorphic or zones replaced by

magnetite) display a Se/Tl ratio >10 000. Thus, this discrimination diagram could be used to differentiate pyrites from mineralized versus non-economic samples.

The innovative approach of this study, based on LA-ICP-MS acquisition of the chemistry of entire pyrite grains, including inclusions and zonation, make our results directly applicable for exploration. Consequently, pyrite concentrate samples, analyzed for As, Tl and Se by more classical mass-spectrometric techniques, have the potential to be used for vectoring to ore by using the proposed discriminating diagrams.

4.9. CONCLUSIONS

The first comprehensive LA-ICP-MS study of the chemistry of pyrite within and outside a replacement-type VMS deposit reveals that it is possible to decipher the evolution of the hydrothermal system using textures, mineral paragenesis and trace element compositions. Based on this approach, five pyrite types were identified. LA-ICP-MS lines and elemental mapping revealed that only few elements (Ni, Co, As, Se, Sb and Tl) are homogeneously distributed in pyrite, and least affected by inclusion, and thus useful for discrimination purposes. Among those elements, Tl and Sb are associated with the formation of the Zn-rich zones of the deposits, whereas Se is associated with the higher temperature Cu-rich and magnetite-rich zones. These results point toward a decoupled behaviour of Sb-Tl and Se with variable temperatures. Diagrams based on Se/Tl and As are a

powerful tool to discriminate between pyrites related to specific ore zones from the VMS systems and later pyrite formed during regional metamorphism. These diagrams have the potential to be used for VMS exploration, using bulk pyrite analyses, for discriminating between fertile VMS-related and metamorphogenic pyrites.

4.10. ACKNOWLEDGMENTS

The first author's PhD project is a part of a larger research program on the Matagami district, including a volcanology PhD (INRS-Quebec) and a geophysical PhD (École Polytechnique-Montreal). Financial support for this study was provided by NSERC (CRDPJ 371131-08), CONSOREM, DIVEX (SC-30), the Geological Survey of Canada, Glencore (previously Xstrata Zinc), Donner Metals, SOQUEM and Nyrstar (previously Breakwater Resources). We would like to thank the companies for the authorization to publish these results; G. Roy for his informal review of a preliminary version of the document; N. Yapi for collecting samples in 2008; A. Paulin-Bissonnette for his contribution as undergraduate field assistant during the summer 2010; D. Savard, S. Medhi and J. Béland for their support with LA-ICP-MS analysis. We are grateful to S.A.S. Genna, for proof reading the English text.

4.11. REFERENCES

Abraitis, P. K., Pattrick, R. A. D., and Vaughan, D. J., 2004, Variations in the compositional, textural and electrical properties of natural pyrite: a review: International Journal of Mineral Processing, v. 74, p. 41-59.

Adair, R., 2009, Technical report on the resource calculation for the Bracemac-McLeod discoveries, Matagami Project, Québec: Vancouver, Canada, Donner Metals Ltd., National Instrument 43-101 Report, filled on April 3, 2009, at http://www.sedar.com, p. 194.

Agangi, A., Hofmann, A., and Wohlgemuth-Ueberwasser, C. C., 2013, Pyrite zoning as a record of mineralization in the Ventersdorp Contact Reef, Witwatersrand Basin, South Africa: Economic Geology, v. 108, p. 1243-1272.

Auclair, G., Fouquet, Y., and Bohn, M., 1987, Distribution of selenium in high-temperature hydrothermal sulfide deposits at 13 degrees North, East Pacific Rise: The Canadian Mineralogist, v. 25, p. 577-587.

Baker, R. G. A., Rehkämper, M., Ihlenfeld, C., Oates, C. J., and Coggon, R., 2010, Thallium isotope variations in an ore-bearing continental igneous setting: Collahuasi Formation, northern Chile: Geochimica et Cosmochimica Acta, v. 74, p. 4405-4416.

Ballantyne, J. M., and Moore, J. N., 1988, Arsenic geochemistry in geothermal systems: Geochimica et Cosmochimica Acta, v. 52, p. 475-483.

Beaudry, C., and Gaucher, E., 1986, Cartographie géologique dans la région de Matagami: Québec., Ministère de l'énergie et des Ressources, Rapport MB 86-32, p. 147.

Bodon, S. B., and Valenta, R. K., 1995, Primary and tectonic features of the Currawong Zn-Cu-Pb(-Au) massive sulfide deposit, Benambra, Victoria; implications for ore genesis: Economic Geology, v. 90, p. 1694-1721.

Boucher, S. M., 2011, Ore petrology and alteration of the West Ansil volcanic-hosted Massive sulphide deposit of the Noranda mining camp, Rouyn-Noranda, Quebec: Unpub. M.Sc. thesis, University of Ottawa, 193 p.

Bourcier, W. L., and Barnes, H. L., 1987, Ore solution chemistry; VII, Stabilities of chloride and bisulfide complexes of zinc to 350 degrees C: Economic Geology, v. 82, p. 1839-1863.

Bralia, A., Sabatini, G., and Troja, F., 1979, A revaluation of the Co/Ni ratio in pyrite as geochemical tool in ore genesis problems: Mineralium Deposita, v. 14, p. 353-374.

Butler, I. B., and Rickard, D., 2000, Framboidal pyrite formation via the oxidation of iron (II) monosulfide by hydrogen sulphide: Geochimica et Cosmochimica Acta, v. 64, p. 2665-2672.

Carr, P. M., Cathles, L. M., and Barrie, C. T., 2008, On the size and spacing of volcanogenic massive sulfide deposits within a district with application to the Matagami district, Quebec: Economic Geology, v. 103, p. 1395-1409.

Cook, N. J., and Chryssoulis, S. L., 1990, Concentrations of invisible gold in the common sulfides: The Canadian Mineralogist, v. 28, p. 1-16.

Côté, A., and Lavigne, M., 2010, Report and Feasibility Study for the Bracemac-McLeod Project Matagami Area Quebec, (Xstrata Zinc and Genivar Limited Partnership), p. 315.

Craig, J. R., and Vokes, F. M., 1993, The metamorphism of pyrite and pyritic ores: an overview: Mineralogical Magazine, v. 57, p. 3-18.

Craig, J. R., Vokes, F. M., and Solberg, T. N., 1998, Pyrite: physical and chemical textures: Mineralium Deposita, v. 34, p. 82-101.

Dare, S. A. S., Barnes, S.-J., Beaudoin, G., Méric, J., Boutroy, E., and Potvin-Doucet, C., 2014, Trace elements in magnetite as petrogenetic indicators: Mineralium Deposita, v. 49, p. 785-796.

Dare, S. A. S., Barnes, S.-J., Prichard, H. M., and Fisher, P. C., 2011, Chalcophile and platinum-group element (PGE) concentrations in the sulfide minerals from the McCreedy East deposit, Sudbury, Canada, and the origin of PGE in pyrite: Mineralium Deposita, v. 46, p. 381-407.

de Kersabiec, A. M., and Roger, G., 1979, Eléments en traces dans les pyrites de la province de Huelva (Espagne): Physics and Chemistry of the Earth, v. 11, p. 673-682.

Debreil, J.-A., 2014, Évolution volcanologique et chimico-stratigraphique du district minier de Matagami, sous-province de l'Abitibi, Québec: Unpub. Ph.D. thesis thesis, Université du Québec Institut National de la Recherche Scientifique, 256 p.

Deditius, A. P., Utsunomiya, S., Reich, M., Kesler, S. E., Ewing, R. C., Hough, R., and Walshe, J., 2011, Trace metal nanoparticles in pyrite: Ore Geology Reviews, v. 42, p. 32-46.

Djon, M. L. N., and Barnes, S.-J., 2012, Changes in sulfides and platinum-group minerals with the degree of alteration in the Roby, Twilight, and High Grade Zones of the Lac des Iles Complex, Ontario, Canada: Mineralium Deposita, v. 47, p. 875-896.

Franchini, M., McFarlane, C., Maydagán, L., Reich, M., Lentz, D. R., Meinert, L., and Bouhier, V., in press, Trace metals in pyrite and marcasite from the Agua Rica porphyry-high sulfidation epithermal deposit, Catamarca, Argentina: textural features and metal zoning at the porphyry to epithermal transition: Ore Geology Reviews.

Franklin, J. M., Sangster, D. F., Lydon, J. W., 1981, Volcanic-associated massive sulfide deposits : Economic Geology 75th Anniversary Volume, p.485-627.

Galley, A. G., Jonasson, I. R., and Watkinson, D. H., 2000, Magnetite-rich calc-silicate alteration in relation to synvolcanic intrusion at the Ansil volcanogenic massive sulfide deposit, Rouyn–Noranda, Quebec, Canada: Mineralium Deposita, v. 35, p. 619-637.

Galley, A. G., Watkinson, D. H., Jonasson, I. R., and Riverin, G., 1995, The subsea-floor formation of volcanic-hosted massive sulfide; evidence from the Ansil Deposit, Rouyn-Noranda, Canada: Economic Geology, v. 90, p. 2006-2017.

Genna, D., Gaboury, D., and Roy, G., 2014a, Evolution of a volcanogenic hydrothermal system recorded by the behavior of LREE and Eu: Case study of the Key Tuffite at Bracemac–McLeod deposits, Matagami, Canada: Ore Geology Reviews, v. 63, p. 160-177.

Genna, D., Gaboury, D., and Roy, G., 2014b, The Key Tuffite, Matagami Camp, Abitibi Greenstone Belt, Canada: petrogenesis and implications for VMS formation and exploration: Mineralium Deposita, v. 49, p. 489-512.

Graham, G. E., Kelley, K. D., Slack, J. F., and Koenig, A. E., 2009, Trace elements in Zn–Pb–Ag deposits and related stream sediments, Brooks Range Alaska, with implications for Tl as a pathfinder element: Geochemistry: Exploration, Environment, Analysis, v. 9, p. 19-37.

Hannington, M., Herzig, P., Scott, S., Thompson, G., and Rona, P., 1991, Comparative mineralogy and geochemistry of gold-bearing sulfide deposits on the mid-ocean ridges: Marine Geology, v. 101, p. 217-248.

Hannington, M. D., de Ronde, C. D. J., and Petersen, S., 2005, Sea-floor tectonics and submarine hydrothermal systems, *in* Hedenquist, J. W., Thompson, J. F. H., Goldfarb, R. J., and Richards, J. P., eds., Economic Geology 100th anniversary volume: Littelton, Colorado, USA, Society of Economic Geologists, p. 111-141.

Hannington, M. D., Kjarsgaard, I., and Bleeker, W., 1999, Sulfide mineralogy, geochemistry and ore genesis of the Kidd Creek deposit. Part I. The North, Central, and South Orebodies: Economic Geology, Monograph 10, p. 163-224.

Hazarika, P., Mishra, B., Saravanan Chinnasamy, S., and Bernhardt, H.-J., 2013, Multi-stage growth and invisible gold distribution in pyrite from the Kundarkocha sediment-hosted gold deposit, eastern India: Ore Geology Reviews, v. 55, p. 134-145.

Huston, D. L., Sie, S. H., Suter, G. F., Cooke, D. R., and Both, R. A., 1995, Trace elements in sulfide minerals from eastern Australian volcanic-hosted massive sulfide deposits; Part I, Proton microprobe analyses of pyrite, chalcopyrite, and sphalerite, and Part II, Selenium levels in pyrite; comparison with delta 34 S values and implications for the source of sulfur in volcanogenic hydrothermal systems: Economic Geology, v. 90, p. 1167-1196.

Ikramuddin, M., Asmeron, Y., Nordstrom, P. M., Kinart, K. P., Martin, W. M., Digby, S. J. M., Elder, D. D., Nijak, W. F., and Afemari, A. A., 1983, Thallium: A potential guide to mineral deposits: Journal of Geochemical Exploration, v. 19, p. 465-490.

Ikramuddin, M., Besse, L., and Nordstrom, P. M., 1986, Thallium in the Carlin-type gold deposits: Applied Geochemistry, v. 1, p. 493-502.

Ingham, E. S., Cook, N. J., Cliff, J., Ciobanu, C. L., and Huddleston, A., 2014, A combined chemical, isotopic and microstructural study of pyrite from roll-front uranium deposits, Lake Eyre Basin, South Australia: Geochimica et Cosmochimica Acta, v. 125, p. 440-465.

Ioannou, S. E., and Spooner, E. T. C., 2007, Fracture analysis of a volcanogenic massive sulfide-related hydrothermal cracking zone, Upper Bell River Complex, Matagami, Quebec: application of permeability tensor theory: Economic Geology, v. 102, p. 667-690.

Jolly, W. T., 1978, Metamorphic history of the Archean Abitibi belt., *in* Fraser, J. A., and Heywood, W. W., eds., Metamorphism in the Canadian Shield, Geological Survey of Canada, Paper 78-10, p. 63-78.

Kristall, B., Nielsen, D., Hannington, M. D., Kelley, D. S., and Delaney, J. R., 2011, Chemical microenvironments within sulfide structures from the Mothra Hydrothermal Field: Evidence from high-resolution zoning of trace elements: Chemical Geology, v. 290, p. 12-30.

Large, R. R., 1977, Chemical evolution and zonation of massive sulfide deposits in volcanic terrains: Economic Geology, v. 72, p. 549-572.

Large, R. R., Allen, R. L., Blake, M. D., and Herrmann, W., 2001, Hydrothermal alteration and volatile element halos for the Rosebery K lens volcanic-hosted massive sulfide deposit, Western Tasmania: Economic Geology, v. 96, p. 1055-1072.

Large, R. R., Danyushevsky, L., Hollit, C., Maslennikov, V., Meffre, S., Gilbert, S., Bull, S., Scott, R., Emsbo, P., Thomas, H., Singh, B., and Foster, J., 2009, Gold and trace element zonation in pyrite using a laser imaging technique: implications for the timing of gold in orogenic and carlin-style sediment-hosted deposits: Economic Geology, v. 104, p. 635-668.

Large, R. R., Maslennikov, V. V., Robert, F., Danyushevsky, L. V., and Chang, Z., 2007, Multistage sedimentary and metamorphic origin of pyrite and gold in the giant Sukhoi Log deposit, Lena Gold Province, Russia: Economic Geology, v. 102, p. 1233-1267.

Larocque, A. C. L., Hodgson, C. J., Cabri, L. J., and Jackman, J. A., 1995, Ion-microprobe analysis of pyrite, chalcopyrite and pyrrhotite from the Mobrun VMS deposit in northwestern Quebec; evidence for metamorphic remobilization of gold: Canadian Mineralogist, v. 33, p. 373-388.

Layton-Matthews, D., Peter, J. M., Scott, S. D., and Leybourne, M. I., 2008, Distribution, mineralogy, and geochemistry of selenium in felsic volcanic-hosted massive sulfide deposits of the Finlayson Lake District, Yukon Territory, Canada: Economic Geology, v. 103, p. 61-88.

Liaghat, S., and MacLean, W. H., 1992, The Key Tuffite, Matagami mining district; origin of the tuff components and mass changes: Exploration and Mining Geology, v. 1, p. 197-207.

Loftus-Hills, G., and Solomon, M., 1967, Cobalt, nickel and selenium in sulphides as indicators of ore genesis: Mineralium Deposita, v. 2, p. 228-242.

Lydon, J. W., 1984, Ore deposit Models-8. Volcanogenic Massive Sulphide Deposits Part I: A descri^ptive model: Geoscience Canada, v. 11.

Maier, R. C., and McGoldrick, P. J., 2005, Pyrite trace element halos to northern Australian sediment-hosted Zn-Pb-Ag deposits, *in* Mao, J., and Bierlein, F. P., eds., Mineral Deposit Research: Meeting the Global Challenge, Springer Berlin Heidelberg, p. 161-163.

Maier, W. D., Barnes, S.-J., and Pellet, T., 1996, The economic significance of the Bell River Complex, Abitibi subprovince, Quebec: Canadian Journal of Earth Sciences, v. 33, p. 967-980.

Maslennikov, V. V., Maslennikova, S. P., Large, R. R., and Danyushevsky, L. V., 2009, Study of trace element zonation in vent chimneys from the Silurian Yaman-Kasy volcanic-hosted massive sulfide deposit (Southern Urals, Russia) using laser ablation-inductively coupled plasma mass spectrometry (LA-ICPMS): Economic Geology, v. 104, p. 1111-1141.

McClenaghan, S. H., Lentz, D. R., Martin, J., and Diegor, W. G., 2009, Gold in the Brunswick No. 12 volcanogenic massive sulfide deposit, Bathurst Mining Camp, Canada: Evidence from bulk ore analysis and laser ablation ICP-MS data on sulfide phases: Mineralium Deposita, v. 44, p. 523-557.

Mercier-Langevin, P., Gibson, H. L., Hannington, M. D., Goutier, J., Monecke, T., Dubé, B., and Houlé, M. G., 2014, A special issue on Archean magmatism, volcanism, and ore deposits: Part 2. Volcanogenic massive sulfide deposits preface: Economic Geology, v. 109, p. 1-9.

Metz, S., and Trefry, J. H., 2000, Chemical and mineralogical influences on concentrations of trace metals in hydrothermal fluids: Geochimica et Cosmochimica Acta, v. 64, p. 2267-2279.

Mortensen, J. K., 1993, U–Pb geochronology of the eastern Abitibi Subprovince. Part 1: Chibougamau–Matagami–Joutel region: Canadian Journal of Earth Sciences, v. 30, p. 11-28.

Murao, S., and Itoh, S., 1992, High thallium content in Kuroko-type ore: Journal of Geochemical Exploration, v. 43, p. 223-231.

Piché, M., 1991, Synthèse géologique et métallogénique du camp minier de Matagami, Québec: Unpub. Ph.D. thesis thesis, Université du Québec à Chicoutimi, 269 p.

Piché, M., Guha, J., Daigneault, R., Sullivan, J. R., and Bouchard, G., 1990, Les gisements volcanogènes du camp minier de Matagami: Structure, stratigraphie et implications métallogéniques: Canadian Institute of Mining and Metallurgy, v. Special Volume 43, p. 327-336.

Pilote, P., Debreil, J.-A., Williamson, K., Rabeau, O., and Lacoste, P., 2011, Révision géologique de la région de Matagami., Québec Exploration - Poster 276: Québec.

Piña, R., Gervilla, F., Barnes, S.-J., Ortega, L., and Lunar, R., 2012, Distribution of platinum-group and chalcophile elements in the Aguablanca Ni–Cu sulfide deposit (SW Spain): Evidence from a LA-ICP-MS study: Chemical Geology, v. 302–303, p. 61-75.

Piña, R., Gervilla, F., Barnes, S.-J., Ortega, L., and Lunar, R., 2013, Platinum-group elements-bearing pyrite from the Aguablanca Ni-Cu sulphide deposit (SW Spain): a LA-ICP-MS study: European Journal of Mineralogy, v. 25, p. 241-252.

Reich, M., Deditius, A., Chryssoulis, S., Li, J.-W., Ma, C.-Q., Parada, M. A., Barra, F., and Mittermayr, F., 2013, Pyrite as a record of hydrothermal fluid evolution in a porphyry copper system: A SIMS/EMPA trace element study: Geochimica et Cosmochimica Acta, v. 104, p. 42-62.

Revan, M. K., Genç, Y., Maslennikov, V. V., Maslennikova, S. P., Large, R. R., and Danyushevsky, L. V., 2014, Mineralogy and trace-element geochemistry of sulfide minerals in hydrothermal chimneys from the Upper-

Cretaceous VMS deposits of the eastern Pontide orogenic belt (NE Turkey): Ore Geology Reviews, v. 63, p. 129-149.

Roberts, I. F., 1982, Trace element chemistry of pyrite: A useful guide to the occurrence of sulfide base metal mineralization: Journal of Geochemical Exploration, v. 17, p. 49-62.

Rona, P. A., 1984, Hydrothermal mineralization at seafloor spreading centers: Earth Science Reviews, v. 20, p. 1-104.

Ross, P.-S., McNicoll, V. J., Debreil, J.-A., and Carr, P., 2014, Precise U-Pb geochronology of the Matagami Mining Camp, Abitibi Greenstone Belt, Quebec: stratigraphic constraints and implications for volcanogenic massive sulfide exploration: Economic Geology, v. 109, p. 89-101.

Salmon, B., Lavigne, M., and Gauthier, J., 2007, Prefeasibility Study on the Caber Deposit – Technical Report on the Caber and Caber North Deposits, Matagami, Québec. Report by Genivar and Scott Wilson Roscoe Postle Associates Inc. to Metco Resources Inc., p. 196.

Scott, R. J., Meffre, S., Woodhead, J., Gilbert, S. E., Berry, R. F., and Emsbo, P., 2009, Development of framboidal pyrite during diagenesis, low-grade regional metamorphism, and hydrothermal alteration: Economic Geology, v. 104, p. 1143-1168.

Sharman, E. R., Taylor, B. E., Minarik, W. G., Dubé, B., and Wing, B. A., 2014, Sulfur isotope and trace element data from ore sulfides in the Noranda district (Abitibi, Canada): implications for volcanogenic massive sulfide deposit genesis: Mineralium Deposita, p. 1-16.

Sharpe, J. I., 1968, Géologie et gisements de sulfures de la région de Matagami, Comté d'Abitibi-Est, Québec., Ministère des Richesses Naturelles du Québec. Rapport géologique 137, p. 122.

Sharpe, R., and Gemmell, J. B., 2002, The Archean Cu-Zn Magnetite-Rich Gossan Hill Volcanic-Hosted Massive Sulfide Deposit, Western Australia: Genesis of a Multistage Hydrothermal System: Economic Geology, v. 97, p. 517-539.

Thomas, H. V., Large, R. R., Bull, S. W., Maslennikov, V., Berry, R. F., Fraser, R., Froud, S., and Moye, R., 2011, Pyrite and pyrrhotite textures and composition in sediments, laminated quartz veins, and reefs at Bendigo

gold mine, Australia: insights for ore genesis: Economic Geology, v. 106, p. 1-31.

Vaughan, D. J., and Rosso, K. M., 2006, Chemical Bonding in Sulfide Minerals: Reviews in Mineralogy and Geochemistry, v. 61, p. 231-264.

Wagner, T., Klemd, R., Wenzel, T., and Mattsson, B., 2007, Gold upgrading in metamorphosed massive sulfide ore deposits: Direct evidence from laser-ablation–inductively coupled plasma–mass spectrometry analysis of invisible gold: Geology, v. 35, p. 775-778.

Wilson, S. A., Ridley, W. I., and Koenig, A. E., 2002, Development of sulfide calibration standards for the laser ablation inductively-coupled plasma mass spectrometry technique: Journal of Analytical Atomic Spectrometry, v. 17, p. 406-409.

Winderbaum, L., Ciobanu, C. L., Cook, N. J., Paul, M., Metcalfe, A., and Gilbert, S., 2012, Multivariate analysis of an LA-ICP-MS trace element dataset for pyrite: Mathematical Geosciences, v. 44, p. 823-842.

Xiong, Y., 2007, Hydrothermal thallium mineralization up to 300 °C: A thermodynamic approach: Ore Geology Reviews, v. 32, p. 291-313.

Zhou, T. F., Fan, Y., Yuan, F., Wu, M. A., Hou, M. J., Voicu, G., Hu, Q. H., Zhang, Q. M., and Yue, S. C., 2005, A preliminary geological and geochemical study of the Xiangquan thallium deposit, eastern China: the world's first thallium-only mine: Mineralogy and Petrology, v. 85, p. 243-251.

CHAPITRE 5

5. DISCUSSIONS

5.1. INTRODUCTION

Ce projet de recherche visaient deux buts : 1) étudier l'évolution des systèmes hydrothermaux de type SMV et 2) développer des outils géochimiques qui pourraient permettre de traduire efficacement la signature hydrothermale des tuffites dans l'optique d'assister l'exploration des SMV dans le camp de Matagami et ailleurs dans le monde. Afin d'atteindre ces buts, 4 objectifs avaient été définis :

- Comprendre l'environnement de dépôt de la Tuffite Clé.
- Établir le lien entre la Tuffite Clé et les minéralisations.
- Caractériser les différentes composantes de la Tuffite Clé.
- Développer et tester des outils pour l'exploration.

Les résultats de cette étude répondent aux objectifs fixés dans le cadre de ce projet. Un sommaire des éléments pertinents est présenté ci-dessous en fonction des différentes thématiques.

5.2. ORIGINE DE LA TUFFITE CLÉ

L'originalité du projet de recherche réside dans l'approche méthodologique pour étudier les horizons de tuffites. La formation de ces tuffites est interprétée comme le produit de deux composantes d'un même système dont les proportions sont variables : 1) une composante d'origine tuffacée et 2) une composante chimique. La vision du projet vise à scinder le pôle chimique en deux composantes : 1) la

composante précipitée et 2) la composante d'altération hydrothermale (Figure 1.2). Chacune de ces composantes a été caractérisée de manière indépendante et mène à une réinterprétation significative de l'origine de la Tuffite Clé et des minéralisations qui lui sont associées. La Tuffite Clé est maintenant interprétée comme un tuf andésitique d'affinité calco-alcaline, et représente l'équivalent explosif des laves andésitiques à la base du Groupe de Wabassee. Le volume colossal de cendre (jusqu'à 10 m d'épaisseur sur >17 km N-S et >1 km E-O) peut être expliqué par un évènement explosif catastrophique ou par une multitude de centres éruptifs. L'absence de variation latérale de faciès et les fines couches préservées dans la Tuffite Clé indiquent des conditions de dépôt calmes dans un bassin relativement profond, où une partie de la colonne d'eau est saturée de particules de cendres. L'enregistrement de cette sédimentation progressive des particules de cendre représente un hiatus du volcanisme important à l'échelle du camp et auquel a été attribuée la formation de minéralisations exhalatives. Cependant, les observations de terrain, de carottes de forage et la chimie fine de la Tuffite Clé, autour des deux gisements accessibles (Persévérance et Bracemac-McLeod), démontrent que la composante exhalative est limitée voire absente. L'alternance de lits de silice et de sulfures dans la Tuffite Clé à proximité de ces gisements était un argument fort en faveur d'une activité exhalative soutenue. Il est cependant démontré que cette alternance est attribuable au

remplacement préférentiel de couches plus poreuses et vraisemblablement de granulométrie plus grossière.

La Tuffite Clé n'est donc pas une exhalite au sens strict du terme, mais un horizon localement fortement altéré par le passage des fluides hydrothermaux. À plus grande échelle, cette altération est caractérisée par une forte chloritisation proximale (200 m) et une séricitisation distale (jusqu'à 400 m). Ces altérations se retrouvent aussi bien dans le mur (rhyolite du Lac Watson) que dans le toit (rhyolite et tuffite de Bracemac et andésite du Groupe de Wabassee) des zones minéralisées. Cette configuration de l'altération suggère, en accord avec les relations géométriques des minéralisations, que la majeure partie de l'épisode minéralisateur a eu lieu après la mise en place d'une partie des unités volcaniques du Groupe de Wabassee, par des processus remplacement de zones plus perméables (Tuffite Clé et carapace de hyaloclastite au sommet de la rhyolite du Lac Watson), sous le plancher océanique.

5.3. LIEN TUFFITE CLÉ – MINÉRALISATION

Le lien entre la Tuffite Clé et les minéralisations SMV du camp de Matagami a longtemps été débattu. Plusieurs des premiers travaux réalisés à Matagami ont proposé une origine épigénétique des minéralisations (Latulippe, 1959; Miller, 1960; Jenney, 1961; Hallam, 1964; Sharpe, 1968) alors que tous les travaux

récents ont accepté un modèle exhalatif (Roberts, 1975; Roberts and Reardon, 1978; MacGeehan and MacLean, 1980; Costa et al., 1983; Ioannou et al., 2007).

Les résultats de ce projet démontrent, sur la base d'observations de relation paragenètiques, de lithogéochimie et de chimie minérale, que les minéralisations de Bracemac-McLeod et Persévérance ont été formées principalement par des processus de remplacement par opposition à des accumulations de type exhalatif. Ces résultats impliquent une réévaluation du modèle métallogénique des SMV de Matagami. Il n'en demeure pas moins que l'origine des fluides est en grande partie l'eau de mer, mise en convection par des flux thermaux d'origine volcanique. Le lien entre les minéralisations et la Tuffite Clé est donc plus spatial que génétique. Dans l'optique d'étudier l'évolution du système hydrothermal, et en l'absence apparente de composante exhalative significative, il convient de concentrer les efforts sur la composante « altération » de la Tuffite Clé.

5.4. ÉVOLUTION DU SYSTÈME MINÉRALISATEUR ET IMPLICATIONS POUR L'EXPLORATION

Basé sur des observations détaillées, réalisées sur le terrain, en forage ou sous terre, nous avons privilégiées deux approches pour étudier l'évolution du système hydrothermal. La première repose sur les éléments des terres rares (ETR), et la deuxième sur la signature en éléments traces dans les pyrites. Dans les deux cas, les résultats ont des implications significatives pour l'exploration.

5.4.1. MOBILITE DES ETR

En combinant analyses géochimiques en roche totale et minérale (in situ), la distribution des ETR a été étudiée dans les zones d'altération du gisement de Bracemac-McLeod. Généralement considérés comme immobiles, il a été démontré que sous certaines conditions d'hydrothermalisme, les terres rares légères (TRL) et l'europium peuvent être redistribuées dans des minéraux secondaires. Les zones distales séricitisées représentent le meilleur équivalent de l'amorce du système hydrothermal (basse température). Cette zone est caractérisée par la destruction des verres volcaniques primaires et des plagioclases, minéraux réactifs aux fluides hydrothermaux. Géochimiquement, cela se traduit par une anomalie négative en Eu et une perte des TRL.

La zone chloritisée, proximale au gisement, est le produit de l'augmentation en température des fluides minéralisateurs. Cette zone est généralement caractérisée par des gains en TRL et Eu. Les observations pétrographiques indiquent que la génération d'allanite avec la chlorite explique le gain en TRL. Cependant, un calcul de bilan de masse démontre que c'est la cristallisation d'apatite (± carbonates) qui contrôle l'anomalie positive en Eu.

Ces résultats ont une implication directe pour l'exploration. La mobilité des ETR est indicatrice de conditions d'hydrothermalisme spécifiques qui semble refléter l'efficacité du système hydrothermal. La mobilité des TRL et de l'Eu peut être

utilisée comme outil de guidage (Figure 3.5). En particulier, l'Eu possède un comportement anormal qui s'étend largement en dehors des zones minéralisées, soit dans les zones d'altération hydrothermale de basse température (jusqu'à 400 m des minéralisations).

5.4.2. ÉLEMENTS TRACES DANS LES PYRITES

La distribution des éléments traces dans les pyrites de la Tuffite Clé et des minéralisations de Bracemac-McLeod a été étudiée par LA-ICP-MS. Les minéralisations de Bracemac-McLeod sont divisés en 3 zones : 1) riche en zinc, 2) riche en cuivre et 3) avec présence de magnétite. La pyrite est présente, en quantité variable, dans chacune de ces zones. L'étude chimique, texturale et paragénétique permet d'analyser les variations de la distribution des éléments traces dans la pyrite au cours de l'évolution du système hydrothermal. Spécifiquement, 5 types de pyrites ont été mis en évidence. Les pyrites nodulaires (pyrite I) présentes dans la Tuffite Clé et les pyrites sub-idiomorphes de relative basse température (250°C) associées aux zones riches en zinc (pyrite II). Elles ont des signatures chimiques similaires indiquant que ces deux types de pyrites se sont formés avec des conditions physico-chimiques et des fluides identiques. Ces pyrites sont caractérisées par la présence d'un large spectre d'éléments (Cu, Zn, Ag, Sn, Sb, Te, Au, Pb, Bi), mais surtout par un enrichissement significatif en Sb et Tl par rapport aux autres types de pyrites. Les pyrites sub-idiomorphes

associées aux zones riches en cuivre ont une signature différente, enrichies seulement en Se ± Co, In, Pb et Bi. Ces pyrites sont souvent en surcroissance aux pyrites I et II et sont associées à un fluide de plus haute température (300°C). La présence de magnétite, en remplacement de pyrite et de sphalérite, est généralement indicatrice de fluide de très haute température (>350°C). Les pyrites (pyrite IV), préservées du remplacement, sont recristallisées et sont elles aussi caractérisées par des valeurs élevées en Se, mais complètement appauvri de tout autres éléments. Cette signature se retrouve aussi dans les pyrites idiomorphes d'origine métamorphique que l'on observe à l'échelle du camp. Durant la recristallisation à haute température des pyrites IV et V, seulement les éléments en substitution directe dans la structure cristalline de la pyrite (Ni, Co, As et Se) sont préservées. En conséquence, seulement Ni, Co, As, Se, Sb et Tl ont été utiles dans la reconstruction de l'évolution hydrothermale du système SMV de Bracemac-McLeod.

Ces résultats ont des implications concrètes pour l'exploration. Le ratio Se/Tl permet de différencier les pyrites des zones minéralisées riches en Zn (Se/Tl<10), des pyrites des zones minéralisées riches en cuivre (10<Se/Tl<10000), et des pyrites associées à des zones non-économiques (remplacées par la magnétite ou pyrites d'origine métamorphique; Se/Tl>10000). L'approche innovatrice de cette méthode, basée sur la chimie des grains entiers, rend nos résultats directement applicables pour l'exploration. Des concentrés de pyrite, analysés

pour As, Tl et Se, par des méthodes plus classiques de spectrométrie de masse, ont le potentiel d'être utilisés comme outils de guidage en utilisant les diagrammes proposés.

5.5. RÉFÉRENCES

Costa, U. R., Barnett, R. L., and Kerrich, R., 1983, The Mattagami Lake Mine Archean Zn-Cu sulfide deposit, Quebec; hydrothermal coprecipitation of talc and sulfides in a sea-floor brine pool; evidence from geochemistry, 18 O/ 16 O, and mineral chemistry: Economic Geology, v. 78, p. 1144-1203.

Hallam, R., 1964, Matagami Lake Mines Ltd., some aspects of the geology and ore control: Monthly bulletin of the Canadian Institute of Mining and Metallurgy, v. 57, p. 389-396.

Ioannou, S. E., Spooner, E. T. C., and Barrie, C. T., 2007, Fluid temperature and salinity characteristics of the Matagami volcanogenic massive sulfide district, Quebec: Economic Geology, v. 102, p. 691-715.

Jenney, C. P., 1961, Geology and ore deposits of the Mattagami area, Quebec: Economic Geology, v. 56, p. 740-757.

Latulippe, M., 1959, Mattagami area of northwestern Quebec: Geol Assoc Canada Proc, v. 2, p. 45-54.

MacGeehan, P. J., and MacLean, W. H., 1980, Tholeiitic basalt-rhyolite magmatism and massive sulphide deposits at Matagami, Quebec: Nature, v. 283, p. 153-157.

Miller, R. J. M., 1960, Geology of Mattagami Lake Mines: Canadian Inst Mining Metall Bull, v. 53, p. 194.

Roberts, R. G., 1975, The geological setting of the Mattagami Lake Mine, Quebec; a volcanogenic massive sulfide deposit: Economic Geology, v. 70, p. 115-129.

Sharpe, R., and Gemmell, J. B., 2001, Alteration characteristics of the Archean Golden Grove Formation at the Gossan Hill deposit, Western Australia:

induration as a focusing mechanism for mineralizing hydrothermal fluids: Economic Geology, v. 96, p. 1239-1262.

Roberts, R. G., and Reardon, E. J., 1978, Alteration and ore-forming processes at Mattagami Lake Mine, Quebec: Canadian Journal of Earth Sciences, v. 15, p. 1-21.

CHAPITRE 6

6. CONCLUSIONS

Dans le cadre de cette thèse, nous souhaitions mieux comprendre l'évolution des systèmes hydrothermaux de type sulfures massifs volcanogènes (SMV) dans l'optique de développer des outils géochimiques qui pourraient permettre de traduire efficacement la signature hydrothermale des tuffites en vue d'assister l'exploration dans le camp de Matagami, Abitibi et ailleurs dans le monde. Les tuffites sont les unités les plus proches spatialement et génétiquement de l'évènement minéralisateur. Leur nature est complexe, résultat d'un mélange de sources détritiques et hydrothermales. Les résultats de cette étude ont fait ressortir l'importance de décortiquer chacune des composantes afin de dégager le meilleur signal hydrothermal associé aux minéralisations.

Les principales contributions du projet sont sous la forme de trois articles scientifiques publiés (2) et soumis (1). Les principaux résultats et implications sont présentés ci-dessous :

1) La Tuffite Clé n'est pas une exhalite au sens strict du terme, mais un horizon de cendre, localement fortement altéré voire même remplacé par le passage de fluides hydrothermaux. Implications : la Tuffite Clé ne devrait plus être le seul métallotecte pour l'exploration. Ce résultat ouvre de nouveaux secteurs d'exploration à l'échelle du camp.
2) Les processus hydrothermaux à l'origine des gisements de Bracemac-McLeod et Persévérance sont dominés par un remplacement des roches

plutôt que par une accumulation exhalative de sulfures sur le fond océanique. Implications : le modèle génétique des minéralisations SMV du camp de Matagami mérite d'être revisiter pour tenir compte des observations de ce projet. Basé sur les travaux réalisés à Bracemac-McLeod et Persévérance, un modèle de mise en place des minéralisations post-basculement synvolcanique du Flanc Sud est proposé (Annexe 5). Il mérite d'être testé par une étude structurale régionale, supportée par des études structurales sur les différents gisements du Flanc Sud.

3) La mobilité de certains ETR est une nouvelle fois démontrée pour des systèmes de type SMV. Implications : la mobilité des ETR reflète l'efficacité du système hydrothermal et ces éléments peuvent être utilisés en exploration. Spécifiquement l'Eu a un comportement anormal jusqu'à 400 m des zones minéralisées.
4) Les cinq générations de pyrites identifiées ont des signatures chimiques très différentes. Une suite d'éléments a été utilisée pour décortiquer l'évolution du système hydrothermal de Bracemac-McLeod. Implications : Particulièrement Se, Tl et As peuvent être utilisés en exploration pour discriminer des pyrites provenant de sulfures massifs stériles versus des sulfures massifs riches en zinc (basse température) ou cuivre (haute température).

ANNEXES

ANNEXE 1

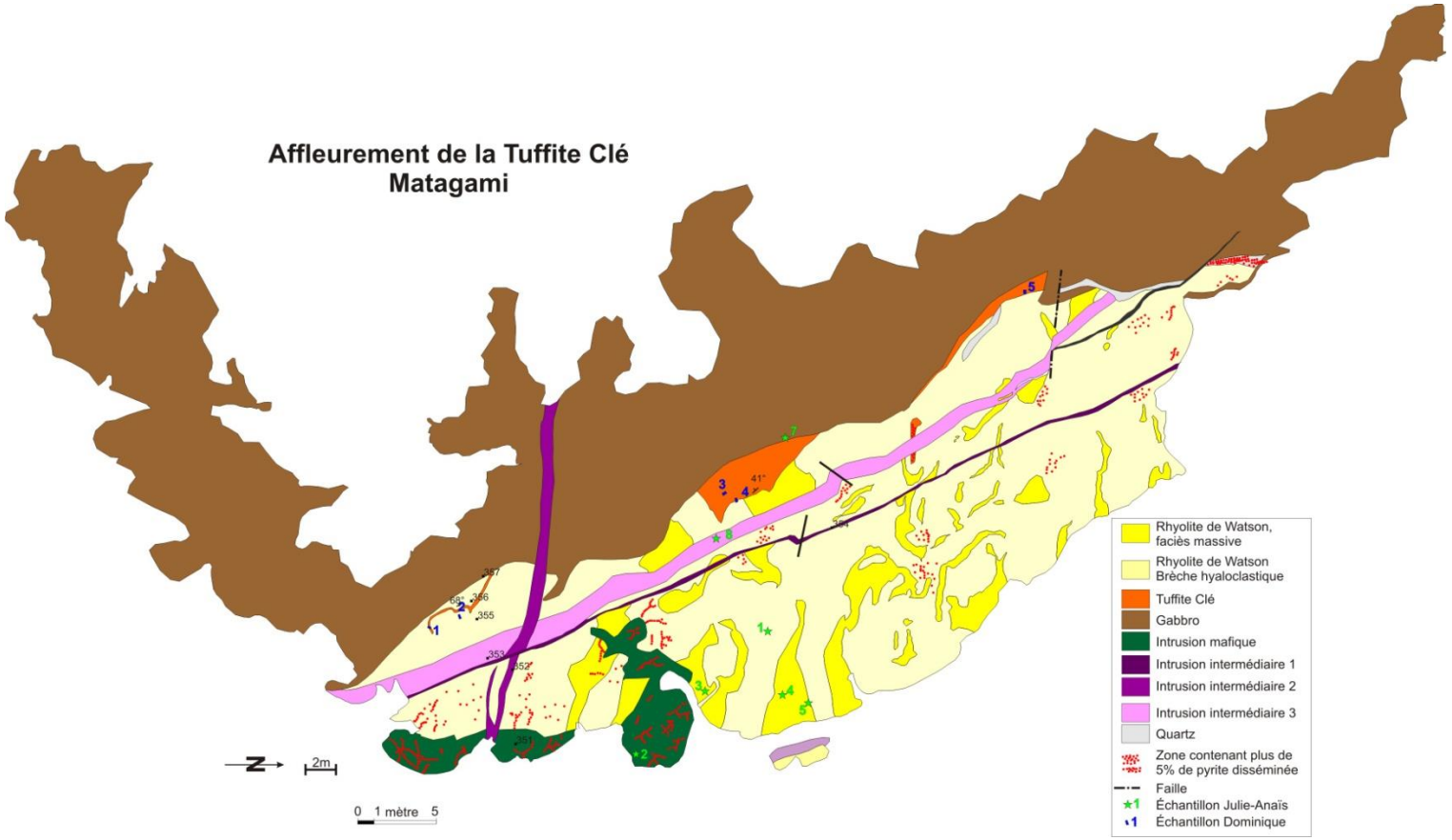

Cartographie de détail d'un affleurement de Tuffite Clé. Réalisée en collaboration avec J-A Debreil.

ANNEXE 2 : LITHOGÉOCHIMIE COMPLÈTE

BRACEMAC MCLEOD

Sample ID	UTM_X	UTM_Y	Total	LOI	Al2O3	CaO	Fe2O3	K2O	MgO	MnO	Na2O	P2O5	S	SiO2	TiO2
972167	308267.5	5504907	99.86	5.09	11.87	0.13	24.69	0.16	4.33	0.23	0.02	0.09	4.60	52.02	0.44
716495	308376.2	5504984	99.96	3.80	12.92	0.17	8.60	3.38	1.71	0.03	0.09	0.14		66.33	0.47
716493	308376.2	5504984	100.39	4.11	7.81	0.09	13.02	1.82	0.78	0.02	0.05	0.08		68.61	0.29
972161A	308137.5	5505122	98.56	7.42	10.87	0.13	17.04	1.61	4.04	0.05	0.02	0.10	8.30	54.13	0.39
972162	308137.5	5505122	99.06	4.30	9.12	0.52	17.98	0.03	4.70	0.10	0.02	0.04	1.90	60.26	0.34
716477	308372.2	5505274	99.54	5.12	13.86	0.14	11.39	3.29	2.55	0.08	0.09	0.10		61.28	0.49
716496	308376.2	5504984	100.62	7.58	12.71	0.22	15.07	3.51	1.23	0.02	0.11	0.17		52.57	0.52
716494	308376.2	5504984	100.41	5.93	7.46	0.12	15.37	1.20	2.00	0.04	0.02	0.10		63.28	0.24
972117	308376.2	5504984	99.49	4.21	13.51	0.22	8.63	2.54	5.23	0.04	0.06	0.08	4.50	63.79	0.46
972116	308376.2	5504984	98.65	7.10	4.50	5.97	11.12	0.38	5.13	0.22	0.02	0.05	0.98	60.09	0.16
972161B	308137.5	5505122	99.24	5.13	3.42	0.12	12.61	0.03	1.63	0.03	0.02	0.06	6.60	73.60	0.10
34	307478.8	5506158	100.25	3.42	12.07	0.32	13.41	1.62	3.76	0.34	0.04	0.07	0.67	63.90	0.44
716488	308267.5	5504907	98.52	5.07	0.48	2.45	17.85	0.03	0.82	0.29	0.00	0.02		69.89	0.02
716489	308267.5	5504907	97.47	9.53	2.32	4.54	19.88	0.03	2.33	0.38	0.00	0.02		55.89	0.08
35	307478.8	5506158	107.36	6.15	6.14	0.17	29.25	0.02	2.62	0.63	0.01	0.05	9.7	48.91	0.24
972166	308267.5	5504907	99.71	3.21	17.53	0.17	8.72	4.32	2.53	0.08	0.09	0.12	0.10	62.15	0.51
32	307607.9	5506094	103.52	4.80	14.83	0.13	12.68	2.70	2.95	0.10	0.59	0.08	3.1	60.93	0.51
716485	307589.2	5506098	99.83	6.65	8.08	0.11	35.36	0.66	2.62	0.09	0.02	0.09		42.72	0.41
31	307607.9	5506094	112.52	9.95	10.32	0.17	25.07	1.45	2.11	0.09	0.29	0.10	12.3	49.82	0.35
716487	307589.2	5506098	98.82	2.74	4.66	0.03	11.20	0.04	2.04	0.15	0.00	0.02		77.45	0.21
716492	307307.2	5505941	99.23	7.17	5.23	0.04	22.62	0.23	1.27	0.08	0.00	0.02		61.92	0.19
716481	308339.3	5504839	100.05	3.55	15.25	0.12	9.37	4.03	1.99	0.05	0.10	0.10		62.38	0.48
972153	308127.9	5505156	93.87	20.27	1.55	3.92	53.63	0.03	2.00	0.11	0.02	0.04	21.60	8.99	0.06
972106	308376.3	5504952	98.95	5.81	15.39	2.00	12.30	3.72	3.62	0.05	0.07	0.10	3.53	54.43	0.56
716472	307237.4	5505770	99.01	2.45	3.72	1.78	2.08	0.55	2.01	0.02	0.14	0.02		85.96	0.12
716473	307237.4	5505770	98.58	1.86	3.37	0.10	3.31	0.06	3.25	0.02	0.00	0.02		86.43	0.13
716464	308119.7	5504958	99.61	6.97	16.83	0.19	11.62	5.24	1.39	0.04	0.16	0.14		50.69	0.63
716463	308119.7	5504958	100.11	6.10	15.49	0.16	10.31	4.53	1.82	0.04	0.09	0.11		59.74	0.48
28	307514.9	5505833	110.12	5.82	7.11	0.08	19.06	0.27	1.66	0.06	0.02	0.05	7.1	65.96	0.28
27	307514.9	5505833	105.40	5.85	6.61	0.33	18.00	0.29	1.52	0.05	0.01	0.07	6.2	64.28	0.25
716478	308688.2	5505066	99.15	3.91	10.64	0.49	11.46	1.47	1.47	0.04	1.86	0.09		65.69	0.34
716479	308688.2	5505066	98.70	3.73	10.65	3.06	7.17	2.11	0.94	0.06	1.93	0.07		67.96	0.37
716474	308561.8	5504828	99.18	3.97	10.22	0.08	12.76	3.42	0.89	0.02	0.08	0.05		67.12	0.30
716475	308104.3	5505000	99.24	4.11	8.51	0.28	10.87	0.03	7.31	0.08	0.00	0.02		67.60	0.30

BRACEMAC MCLEOD

Sample ID	Zr	Nb	La	Ce	Pr	Nd	Sm	Eu	Gd	Tb	Dy	Y	Ho	Er	Tm	Yb	Lu
972167	106.38	4.30	9.12	19.30	2.59	7.80	2.39	0.78	2.64	0.28	2.05	21.69	0.42	1.50	0.21	1.42	0.24
716495	126.02	4.34	10.15	22.36	2.80	11.47	2.88	1.51	2.76	0.40	2.26	13.81	0.47	1.33	0.20	1.26	0.19
716493	79.93	4.04	8.69	19.66	2.42	9.54	2.04	0.42	1.77	0.25	1.53	10.57	0.32	0.89	0.13	0.78	0.12
972161A	115.87	4.93	11.22	24.98	3.20	11.80	2.62	0.86	2.67	0.38	2.37	19.63	0.46	1.51	0.23	1.47	0.24
972162	87.25	4.97	15.00	33.41	4.89	20.71	5.44	1.82	4.65	0.62	3.60	21.24	0.65	1.92	0.26	1.66	0.24
716477	113.42	3.98	35.94	76.85	9.35	36.67	7.73	3.59	5.40	0.65	2.85	13.91	0.49	1.22	0.17	1.08	0.16
716496	137.46	4.68	15.50	34.37	4.21	16.44	3.48	1.40	2.64	0.33	1.74	10.67	0.37	1.01	0.15	0.99	0.15
716494	73.41	2.21	11.09	24.28	2.96	11.66	2.41	1.35	1.68	0.19	0.92	5.83	0.18	0.50	0.08	0.49	0.07
972117	106.02	3.47	13.64	30.69	3.80	13.01	2.95	0.91	2.87	0.34	1.96	13.27	0.37	1.12	0.16	1.10	0.17
972116	58.35	1.79	6.42	14.51	1.77	3.77	0.84	0.93	1.11	0.14	0.79	5.34	0.12	0.38	0.05	0.35	0.04
972161B	34.72	1.92	4.67	9.58	1.25	1.00	0.74	0.72	1.18	0.09	0.75	6.71	0.10	0.47	0.04	0.37	0.06
34	113.00	4.32	3.30	7.82	1.06	4.62	1.17	0.63	1.55	0.31	2.17	15.90	0.51	1.62	0.25	1.72	0.25
716488	4.71	0.35	1.93	4.73	0.71	3.53	1.43	1.01	2.04	0.33	2.03	14.49	0.40	1.15	0.17	0.98	0.14
716489	22.48	0.84	3.84	8.94	1.22	5.34	1.75	1.05	2.52	0.43	2.73	23.46	0.61	1.79	0.26	1.62	0.25
35	60.30	2.59	7.00	15.80	2.10	9.30	2.40	0.88	2.46	0.39	2.25	15.40	0.48	1.34	0.19	1.20	0.18
972166	148.00	4.62	6.02	14.31	1.90	3.97	1.20	0.46	1.67	0.26	1.76	14.88	0.38	1.31	0.19	1.28	0.20
32	119.00	4.39	10.70	23.50	2.90	11.90	2.60	1.04	2.51	0.38	2.16	14.60	0.46	1.30	0.18	1.30	0.20
716485	80.95	3.05	13.97	29.69	3.61	14.00	2.70	1.10	1.80	0.24	1.32	8.90	0.29	0.74	0.11	0.70	0.11
31	81.60	3.61	15.50	32.70	3.90	14.70	2.70	1.32	2.30	0.30	1.61	10.70	0.32	0.89	0.12	0.78	0.12
716487	61.87	2.69	4.49	9.85	1.30	5.68	1.51	0.92	1.72	0.27	1.71	12.25	0.36	1.11	0.18	1.13	0.17
716492	49.42	1.74	7.84	16.65	2.10	8.55	2.00	0.94	1.52	0.19	0.99	6.29	0.20	0.50	0.07	0.48	0.07
716481	164.44	5.61	10.37	23.04	2.89	11.82	2.84	0.84	2.60	0.45	3.09	21.49	0.79	2.10	0.33	2.13	0.32
972153	21.37	0.83	3.30	6.73	0.86	1.11	0.87	0.84	2.01	0.29	2.07	19.32	0.39	1.25	0.17	1.16	0.18
972106	119.87	4.52	10.90	25.10	3.26	11.54	2.50	0.72	2.51	0.32	1.88	14.38	0.41	1.25	0.19	1.30	0.19
716472	27.92	1.43	4.72	9.94	1.17	4.45	0.86	0.33	0.75	0.11	0.61	3.95	0.11	0.33	0.05	0.29	0.04
716473	28.10	1.29	1.38	3.19	0.41	1.72	0.43	0.21	0.45	0.08	0.49	3.77	0.10	0.32	0.05	0.31	0.04
716464	167.17	6.25	13.08	29.37	3.66	14.71	3.12	1.03	3.05	0.49	3.15	21.33	0.69	1.89	0.27	1.70	0.25
716463	122.51	5.51	3.66	8.73	1.13	4.85	1.27	0.29	1.69	0.31	2.20	17.37	0.55	1.69	0.26	1.76	0.27
28	62.80	2.76	5.90	12.90	1.63	6.96	1.80	0.90	1.84	0.27	1.50	10.80	0.31	0.87	0.12	0.80	0.12
27	66.60	2.54	6.10	13.20	1.65	6.77	1.61	0.75	1.55	0.22	1.13	7.90	0.24	0.68	0.10	0.70	0.11
716478	88.74	3.54	27.47	60.27	7.83	33.38	8.99	1.30	9.33	1.44	8.44	51.52	1.73	4.29	0.59	3.37	0.48
716479	86.56	3.84	30.07	66.65	8.72	37.54	9.62	1.55	9.09	1.23	6.66	39.57	1.27	3.48	0.50	2.95	0.44
716474	136.64	7.69	30.12	70.46	9.56	43.09	11.46	1.87	13.05	2.21	14.58	116.28	3.45	9.12	1.29	7.51	1.06
716475	81.74	2.86	22.71	57.24	8.30	39.47	12.37	1.09	9.67	1.23	5.97	28.38	1.06	2.39	0.33	1.94	0.27

PERSEVERANCE

Sample ID	UTM_X	UTM_Y	Total	Loi	Al2O3	CaO	Fe2O3T	K2O	MgO	MnO	Na2O	P2O5	S	SiO2	TiO2
863491	307227.5	5505805	104.77	4.99	7.24	0.13	12.63	1.08	2.24	0.06	0.02	0.07	5.7	67.63	0.29
863490	307227.5	5505805	102.27	2.98	9.91	0.36	9.27	0.28	3.88	0.08	2.44	0.05	1.7	70.33	0.37
716484	307588.4	5505760	99.13	4.31	14.29	3.09	7.09	4.17	2.42	0.10	0.07	0.07		61.00	0.54
47	307754.6	5506007	111.02	11.74	7.66	1.48	22.73	1.14	2.91	0.06	0.04	0.05	13.6	47.67	0.25
972193	307754.6	5506007	98.15	5.23	7.87	1.80	12.23	1.05	2.99	0.06	0.04	0.05	5.53	64.13	0.27
716453	308381.3	5505288	99.65	3.40	8.54	0.01	11.14	0.04	5.84	0.07	0.00	0.02		70.09	0.45
716452	307362.9	5506480	100.03	3.49	15.70	0.62	8.78	3.97	2.15	0.05	1.07	0.11		61.86	0.57
716451	307362.9	5506480	99.91	4.88	13.91	1.31	12.49	4.66	1.58	0.05	0.23	0.13		56.83	0.50
972207	307281	5506442	99.61	6.60	16.79	3.01	7.31	5.61	1.39	0.10	0.33	0.12	3.14	56.79	0.61
972209	307269	5506470	99.34	5.53	13.20	2.13	6.72	4.32	1.30	0.08	0.13	0.08	2.10	64.86	0.42
716469	307879	5505678	99.12	4.23	12.54	0.67	7.09	3.59	1.73	0.04	0.07	0.07		65.71	0.42
972201	299228.4	5515377	100.45	2.99	6.25	0.16	5.24	0.04	6.05	0.02	0.03	0.01	0.05	79.40	0.20
972205	298801.9	5515449	100.36	5.16	11.65	0.02	7.83	0.04	11.25	0.05	0.03	0.01	0.05	63.91	0.39
972206	298801.9	5515449	98.93	5.74	12.81	0.02	8.59	0.04	12.52	0.05	0.03	0.01	0.05	58.59	0.51
D 972206	298801.9	5515449	100.49	5.74	13.33	0.02	8.66	0.04	12.51	0.05	0.03	0.01		59.53	0.52
972225	298905.3	5515295	101.56	5.33	16.95	0.02	5.71	1.72	11.01	0.05	0.18	0.01	0.05	59.97	0.44
972227	298905.3	5515295	100.47	6.66	15.49	0.13	10.77	0.04	14.84	0.06	0.03	0.09	0.05	51.57	0.68
972249	298868.2	5515412	101.21	1.86	3.20	0.74	3.17	0.04	3.90	0.02	0.03	0.16	0.05	87.94	0.11
972250	298868.2	5515412	101.48	4.17	7.91	0.42	7.32	0.04	9.21	0.05	0.03	0.14	0.05	71.82	0.31
972275	298802.4	5515452	100.43	5.83	13.38	0.15	8.87	0.04	12.96	0.08	0.18	0.11	0.05	58.13	0.56
D 972275	298802.4	5515452	100.17	5.83	13.23	0.15	8.88	0.04	13.01	0.08	0.17	0.11		57.98	0.55
972274	298802.4	5515452	102.39	4.49	11.92	0.02	6.00	0.12	10.40	0.06	0.67	0.01	0.05	68.16	0.39
972273	298802.4	5515452	100.27	4.95	15.36	0.18	6.06	0.04	11.70	0.07	2.73	0.01	0.05	58.64	0.43
70	299233.7	5515392	100.09	4.25	9.75	0.16	6.95	0.02	8.66	0.03	0.01	0.06	0.05	69.73	0.29
69	299233.7	5515392	99.75	5.79	13.08	0.34	9.06	0.02	11.59	0.05	0.01	0.05	0.05	59.17	0.36
71	299273.9	5515503	99.35	3.99	9.18	0.08	7.42	0.02	8.12	0.03	0.01	0.06	0.05	69.99	0.31
969354	Underground		98.68	5.62	13.55	0.06	6.91	0.32	12.07	0.04	0.04	0.05	0.05	59.38	0.42
969357	Underground		100.26	6.18	14.96	0.01	7.48	0.33	13.44	0.04	0.05	0.02	0.05	57.07	0.43
969353	Underground		99.91	6.58	16.53	0.01	7.98	0.51	14.09	0.05	0.07	0.02	0.05	53.44	0.42
969355	Underground		101.37	3.70	8.70	0.02	4.98	0.07	8.53	0.03	0.01	0.02	0.05	74.79	0.36
969352	Underground		100.21	5.13	11.62	0.10	7.64	0.02	11.23	0.03	0.01	0.03	0.05	63.76	0.42
969351	Underground		99.68	5.52	12.97	0.01	7.03	0.24	12.17	0.03	0.04	0.02	0.05	61.00	0.42
969359	Underground		101.44	3.85	9.00	0.25	4.96	0.15	8.51	0.03	0.01	0.11	0.05	74.09	0.30
79841M	298907.8	5515378	99.51	6.41	12.9	0.19	14.5	0.01	13.93	0.14	0.09	0.12		50.74	0.45
79846M	298889	5515324	98.56	0.93	2.01	0.34	1.35	0.24	1.25	0.01	0.02	0.01		92.26	0.09
85235M	298715.4	5515430	98.47	7.8	13.78	6.48	7.33	0.05	6.46	0.11	3.81	0.52		51.23	0.83
85236M	298716.1	5515432	99.11	5	12.52	0.21	9.74	0.68	8.68	0.06	0.12	0.15		61.43	0.47

PERSEVERANCE

Sample ID	Zr	Nb	La	Ce	Pr	Nd	Sm	Eu	Gd	Tb	Dy	Y	Ho	Er	Tm	Yb	Lu
863491	71.40	3.16	6.80	15.30	2.00	8.89	2.10	0.48	2.27	0.34	1.98	15.10	0.44	1.24	0.17	1.10	0.16
863490	78.00	2.85	14.40	26.60	3.10	12.40	2.70	1.32	2.72	0.38	2.06	13.40	0.41	1.11	0.15	1.00	0.15
716484	108.52	4.71	9.16	19.76	2.47	10.41	2.75	0.73	4.24	0.85	6.16	48.30	1.51	3.88	0.53	3.05	0.43
47	61.90	1.98	9.00	19.40	2.40	9.60	2.10	0.46	1.85	0.24	1.26	8.40	0.26	0.70	0.10	0.65	0.11
972193	110.57	4.44	10.42	22.35	3.28	15.96	4.51	1.05	6.04	1.02	6.92	51.01	1.47	4.58	0.67	4.31	0.69
716453	92.65	4.45	10.91	25.50	3.62	19.81	4.68	0.68	3.35	0.42	2.52	12.40	0.44	1.17	0.18	1.13	0.17
716452	171.35	4.78	14.88	35.50	4.48	18.10	3.94	1.00	3.54	0.52	3.04	18.20	0.61	1.70	0.25	1.63	0.26
716451	146.93	6.13	16.00	35.53	4.25	16.57	3.45	1.18	3.26	0.50	3.01	19.17	0.61	1.80	0.27	1.68	0.26
972207	129.00	5.81	7.70	18.70	2.30	10.00	2.10	0.81	2.06	0.29	1.97	11.80	0.41	1.24	0.18	1.32	0.20
972209	165.00	7.25	16.80	37.70	4.58	19.30	4.46	1.02	4.65	0.76	4.56	32.70	0.97	2.95	0.42	2.90	0.43
716469	108.97	4.16	10.18	23.03	2.97	12.78	3.42	0.56	4.01	0.68	4.25	27.89	0.94	2.60	0.39	2.43	0.37
972201	50.00	2.47	4.20	10.20	1.38	6.28	1.80	0.46	1.80	0.27	1.86	10.60	0.39	1.19	0.18	1.29	0.20
972205	91.00	4.78	6.40	15.50	2.10	9.40	2.80	0.79	3.52	0.65	3.98	27.40	0.77	2.16	0.29	1.81	0.25
972206	114.00	5.71	4.70	11.00	1.51	7.10	2.20	0.55	2.18	0.33	2.16	12.40	0.43	1.28	0.18	1.28	0.18
D 972206	119.00	6.11	4.60	10.90	1.46	6.92	2.20	0.56	2.28	0.37	2.38	14.40	0.46	1.39	0.20	1.38	0.19
972225	87.80	2.79	7.00	15.30	1.90	7.42	1.54	0.74	1.29	0.17	1.28	6.70	0.26	0.81	0.11	0.78	0.12
972227	158.00	7.35	20.60	46.10	5.65	23.70	4.81	1.34	3.90	0.47	2.68	15.50	0.53	1.57	0.23	1.60	0.24
972249	48.00	1.56	4.50	10.10	1.33	6.48	2.20	0.63	1.92	0.22	1.20	4.30	0.19	0.49	0.06	0.43	0.06
972250	67.10	3.32	3.00	6.90	0.92	4.47	1.59	0.69	1.70	0.22	1.36	7.60	0.27	0.82	0.12	0.86	0.13
972275	128.00	5.36	15.10	32.90	3.90	16.20	3.30	0.92	2.72	0.34	2.03	11.20	0.40	1.19	0.16	1.19	0.17
D 972275	129.00	5.23	13.90	29.90	3.60	14.80	3.00	0.89	2.57	0.33	2.02	11.10	0.39	1.16	0.17	1.17	0.17
972274	108.00	3.93	13.60	27.50	3.10	12.00	2.20	0.56	1.76	0.21	1.40	7.00	0.28	0.83	0.11	0.82	0.12
972273	96.00	3.13	13.90	27.00	3.00	11.70	2.10	0.62	1.56	0.16	1.18	5.80	0.24	0.77	0.11	0.79	0.11
70	66.80	2.02	1.19	2.99	0.40	1.79	0.59	0.22	0.72	0.13	0.81	5.90	0.20	0.59	0.10	0.68	0.11
69	76.10	2.48	3.10	7.12	0.93	4.00	1.10	0.37	1.17	0.20	1.15	7.40	0.25	0.77	0.12	0.82	0.13
71	98.00	3.99	3.00	6.91	0.93	4.07	1.28	0.20	1.78	0.33	2.13	14.00	0.46	1.37	0.21	1.45	0.22
969354	95.00	3.72	8.30	17.80	2.20	8.90	2.10	0.69	1.89	0.29	1.70	11.00	0.36	1.05	0.16	1.09	0.17
969357	80.50	2.63	6.50	12.90	1.50	5.83	1.28	0.49	1.18	0.18	1.16	7.30	0.24	0.73	0.11	0.75	0.11
969353	84.20	2.63	6.50	11.90	1.35	5.06	0.96	0.43	0.92	0.14	0.88	5.90	0.20	0.59	0.09	0.66	0.11
969355	98.00	3.99	10.90	25.20	3.20	13.10	2.80	0.79	2.10	0.25	1.32	8.70	0.29	0.87	0.14	0.95	0.15
969352	108.00	4.09	11.40	24.80	3.00	12.00	2.50	0.70	2.00	0.27	1.42	8.90	0.30	0.86	0.12	0.86	0.13
969351	99.00	3.57	11.50	24.20	2.90	11.50	2.40	0.64	1.90	0.25	1.35	8.40	0.29	0.81	0.12	0.81	0.12
969359	58.00	2.26	8.60	19.20	2.50	11.20	3.10	0.41	3.10	0.46	2.39	14.10	0.46	1.24	0.18	1.19	0.19
79841M	123	3										8					
79846M	37	2										3					
85235M	156	10										7					
85236M	116	4										9					

KT > 400m

Sample ID	UTM_X	UTM_Y	Total	Loi	Al2O3	CaO	Fe2O3T	K2O
972125	304932	5507332.59	99.4	4.03	13.06	0.31	9.28	1.94
972126	304932	5507332.59	100.0	2.45	15.68	2.15	5.17	3.77
972136	304242.81	5508501.5	100.2	8.04	16.09	4.53	11.76	2.00
972213	304664.26	5506931.05	98.5	5.03	13.28	2.26	11.92	2.58
972214	304664.26	5506931.05	98.7	5.87	13.82	2.92	11.99	3.62
972215	304664.26	5506931.05	99.2	5.17	15.13	3.77	6.68	3.42
972239	303095.28	5509856.33	101.7	10.08	15.89	6.84	9.25	3.63
972220	303850.36	5508173.1	101.0	2.24	15.95	0.92	5.15	1.04
972221	303850.36	5508173.1	99.8	4.44	18.09	1.04	13.99	2.97
PRECURSEUR			99.8	5.26	15.22	2.75	9.47	2.77

Sample ID	MgO	MnO	Na2O	P2O5	S	SiO2	TiO2	Zr	Nb	La
972125	1.53	0.04	3.44	0.13	4.53	61.39	0.47	136.73	5.14	13.46
972126	1.75	0.13	2.75	0.11	0.33	64.01	0.53	127.89	4.72	11.62
972136	0.92	0.06	4.57	0.14	6.10	45.76	0.63	150.87	12.27	21.29
972213	2.10	0.08	2.30	0.12	5.59	55.60	0.52	118.00	5.54	11.70
972214	2.10	0.08	1.76	0.10	4.78	54.78	0.49	111.00	4.12	10.20
972215	2.48	0.12	2.35	0.10	1.91	58.48	0.52	107.00	4.09	10.10
972239	2.97	0.21	1.97	0.08	1.78	49.26	0.53	132.00	5.14	11.70
972220	1.83	0.06	6.07	0.06	0.37	67.06	0.37	78.40	2.41	7.10
972221	0.93	0.05	5.41	0.08	6.33	48.77	0.55	147.00	6.89	11.10
PRECURSEUR	1.85	0.09	3.40	0.10	3.52	56.12	0.51	123.21	5.59	12.03

Sample ID	Ce	Pr	Nd	Sm	Eu	Gd	Tb	Dy	Y	Ho
972125	30.65	3.73	12.77	2.56	0.76	2.60	0.36	2.20	14.32	0.43
972126	25.38	3.12	9.69	2.04	0.72	2.36	0.30	2.00	13.34	0.35
972136	46.46	6.05	24.38	4.91	1.45	5.21	0.64	3.41	20.64	0.66
972213	26.40	3.30	13.60	2.80	0.77	2.68	0.39	2.41	14.30	0.48
972214	22.70	2.80	11.40	2.40	0.72	2.09	0.28	1.79	9.90	0.34
972215	21.90	2.70	11.00	2.10	0.73	1.96	0.25	1.65	8.90	0.33
972239	25.30	3.00	12.20	2.60	0.92	2.52	0.35	2.16	11.80	0.42
972220	16.00	1.90	7.72	1.50	0.42	1.29	0.15	1.15	6.20	0.23
972221	24.20	2.90	12.10	2.40	0.71	1.91	0.21	1.34	8.10	0.29
PRECURSEUR	26.56	3.28	12.76	2.59	0.80	2.51	0.33	2.01	11.94	0.39

Sample ID	Er	Tm	Yb	Lu
972125	1.28	0.18	1.22	0.18
972126	1.09	0.15	1.03	0.15
972136	1.80	0.27	1.73	0.24
972213	1.47	0.22	1.58	0.25
972214	1.03	0.15	1.02	0.15
972215	0.96	0.14	0.98	0.14
972239	1.22	0.18	1.21	0.18
972220	0.70	0.09	0.67	0.09
972221	0.92	0.14	1.05	0.16
PRECURSEUR	1.16	0.17	1.17	0.17

ANNEXE 3.1: ANALYSES MICRO-SONDE: APATITES

Sample	#	Drill hole	P2O5	MgO	CaO	MnO	FeO	SrO	Na2O	F	F=O	Cl	Cl=O	Total
972106	06 1_1	MC-04-09	42.4	0.0	56.6	0.0	0.0	0.0	0.0	2.9	-1.2	0.0	0.0	100.7
972106	06 1_1a	MC-04-09	43.1	0.0	56.0	0.0	0.1	0.0	0.0	4.9	-2.1	0.0	0.0	102.1
972106	06 2_1	MC-04-09	43.4	0.0	56.3	0.0	0.2	0.0	0.0	3.3	-1.4	0.0	0.0	101.8
972106	06 2_2	MC-04-09	41.8	0.0	56.3	0.0	0.1	0.0	0.0	3.7	-1.5	0.0	0.0	100.3
972106	06 2_3	MC-04-09	43.7	0.0	56.9	0.1	0.1	0.0	0.0	3.1	-1.3	0.0	0.0	102.7
972106	06 2_4	MC-04-09	43.3	0.0	56.7	0.0	0.2	0.0	0.0	3.3	-1.4	0.0	0.0	102.1
972106	06 3_1	MC-04-09	41.1	0.0	55.6	0.0	0.0	0.0	0.0	4.3	-1.8	0.0	0.0	99.3
972106	06 3_2	MC-04-09	41.6	0.1	55.0	0.0	0.3	0.0	0.1	4.9	-2.1	0.0	0.0	100.1
972106	06 3_3	MC-04-09	39.3	1.1	50.8	0.0	3.1	0.0	0.0	4.1	-1.7	0.0	0.0	96.7
972106	06 4_1	MC-04-09	40.5	0.1	54.8	0.0	0.4	0.0	0.0	3.9	-1.6	0.0	0.0	98.2
972116	16 1_1	MC-08-55	43.3	0.0	56.4	0.1	0.2	0.0	0.0	3.2	-1.3	0.0	0.0	101.9
972116	16 2_1	MC-08-55	42.3	0.0	55.5	0.2	0.1	0.0	0.1	4.3	-1.8	0.0	0.0	100.6
972116	16 4_2	MC-08-55	42.9	0.0	56.1	0.1	0.1	0.0	0.1	5.6	-2.4	0.0	0.0	102.5
972117	17 1_1	MC-08-55	42.2	0.1	55.9	0.0	0.4	0.0	0.1	3.4	-1.4	0.0	0.0	100.6
972117	17 1_2	MC-08-55	41.6	0.1	55.5	0.1	0.4	0.0	0.1	4.4	-1.9	0.0	0.0	100.4
972117	17 1_4	MC-08-55	42.8	0.1	55.7	0.1	0.3	0.0	0.1	4.2	-1.8	0.0	0.0	101.6
972117	17 2_0	MC-08-55	43.0	0.0	56.7	0.0	0.4	0.0	0.0	3.4	-1.4	0.0	0.0	102.1
972117	17 2_1	MC-08-55	42.0	0.1	55.9	0.1	0.5	0.0	0.1	2.9	-1.2	0.0	0.0	100.4
972117	17 2_2	MC-08-55	43.2	0.1	56.1	0.1	0.5	0.0	0.1	2.8	-1.2	0.0	0.0	101.6
972117	17 2_3	MC-08-55	41.3	0.0	56.2	0.0	0.3	0.0	0.0	3.6	-1.5	0.0	0.0	99.9
972117	17 2_4	MC-08-55	42.6	0.0	56.3	0.0	0.4	0.0	0.0	3.3	-1.4	0.0	0.0	101.3
972161	61 1_1	MC-08-62	41.9	0.0	55.3	0.5	0.0	0.0	0.0	4.6	-1.9	0.0	0.0	100.5
972161	61 1_2	MC-08-62	42.7	0.0	55.5	0.1	0.2	0.0	0.0	4.3	-1.8	0.0	0.0	101.1
972161	61 2_1	MC-08-62	39.7	0.0	55.3	0.1	0.6	0.0	0.1	4.2	-1.8	0.0	0.0	98.2
972161	61 2_1a	MC-08-62	42.0	0.0	56.0	0.2	0.1	0.0	0.1	3.0	-1.3	0.0	0.0	100.2
972161	61 2_2	MC-08-62	39.9	0.0	55.4	0.1	0.0	0.0	0.0	4.0	-1.7	0.0	0.0	97.7
972161	61 2_3	MC-08-62	42.8	0.0	56.1	0.1	0.0	0.0	0.0	3.0	-1.3	0.0	0.0	100.8
972161	61 3_1	MC-08-62	41.2	0.0	55.6	0.0	0.2	0.0	0.1	3.4	-1.4	0.0	0.0	99.1
716464	64 1_2	MC-05-20	42.3	0.0	55.1	0.1	0.1	0.0	0.1	4.9	-2.0	0.0	0.0	100.5
716464	64 1_3	MC-05-20	42.6	0.0	56.6	0.0	0.1	0.0	0.0	3.2	-1.3	0.0	0.0	101.3
716464	64 1_4	MC-05-20	41.0	0.0	55.4	0.1	0.3	0.0	0.1	4.5	-1.9	0.0	0.0	99.4
716464	66 1_1	MC-05-20	41.3	0.0	55.5	0.0	0.2	0.0	0.0	4.8	-2.0	0.0	0.0	99.8
972166	66 1_3	MC-07-25	41.8	0.0	55.0	0.1	0.3	0.0	0.0	4.1	-1.7	0.0	0.0	99.6
972166	66 1_4	MC-07-25	42.0	0.0	56.6	0.1	0.3	0.0	0.0	2.9	-1.2	0.0	0.0	100.7
972166	66 1_5	MC-07-25	41.2	0.0	56.6	0.0	0.3	0.0	0.0	3.3	-1.4	0.0	0.0	100.0
716474	74 1_1	MC-05-19	41.0	0.0	55.8	0.0	0.0	0.0	0.0	5.0	-2.1	0.0	0.0	99.8
716474	74 1_1a	MC-05-19	43.1	0.0	56.5	0.0	0.3	0.0	0.0	3.0	-1.3	0.0	0.0	101.7
716474	74 1_2	MC-05-19	42.3	0.0	55.6	0.0	0.1	0.0	0.0	3.6	-1.5	0.0	0.0	100.2
716474	74 2_1a	MC-05-19	42.1	0.0	55.8	0.0	0.1	0.0	0.0	5.0	-2.1	0.0	0.0	100.9
716474	74 3_1	MC-05-19	42.8	0.0	56.3	0.0	0.2	0.0	0.0	2.9	-1.2	0.0	0.0	101.0
716474	74 3_1a	MC-05-19	41.9	0.0	56.3	0.0	0.2	0.0	0.0	3.0	-1.3	0.0	0.0	100.2
716474	74 4_1	MC-05-19	40.2	0.0	55.8	0.0	0.1	0.0	0.0	4.5	-1.9	0.0	0.0	98.7
716474	74 4_1a	MC-05-19	41.0	0.0	55.6	0.1	0.1	0.0	0.0	4.0	-1.7	0.0	0.0	99.2
716477	77 1_1	MC-04-04	43.1	0.0	55.7	0.0	0.3	0.0	0.0	3.6	-1.5	0.0	0.0	101.3
716477	77 1_2	MC-04-04	42.4	0.0	55.2	0.0	0.4	0.0	0.0	3.9	-1.6	0.0	0.0	100.3
716477	77 1_3	MC-04-04	42.4	0.1	54.9	0.1	0.5	0.0	0.1	3.9	-1.6	0.0	0.0	100.3
716477	77 1_4	MC-04-04	42.4	0.0	55.1	0.1	0.3	0.0	0.1	4.2	-1.8	0.0	0.0	100.4
716477	77 1_5	MC-04-04	41.9	0.0	54.6	0.1	0.4	0.0	0.0	3.1	-1.3	0.0	0.0	98.8
716479	79 6_1	MC-05-15	42.3	0.1	55.7	0.0	0.3	0.0	0.1	3.7	-1.6	0.0	0.0	100.8
716495	95 1_1	MC-07-28	41.5	0.0	55.9	0.3	0.2	0.0	0.0	4.2	-1.8	0.0	0.0	100.5
716495	95 2_1	MC-07-28	42.9	0.0	55.9	0.2	0.0	0.0	0.0	3.6	-1.5	0.0	0.0	101.2
716495	95 2_2	MC-07-28	42.7	0.0	56.2	0.3	0.1	0.0	0.0	2.7	-1.1	0.0	0.0	100.8
716495	95 3_1	MC-07-28	42.6	0.0	55.5	0.4	0.1	0.0	0.1	3.7	-1.5	0.0	0.0	100.8
716495	95 3_2	MC-07-28	42.3	0.0	56.0	0.5	0.1	0.0	0.0	3.4	-1.4	0.0	0.0	100.9

ANNEXE 3.2 : ANALYSES LA-ICP-MS: APATITES

Sample	Line_ID	Drill Hole	La	Ce	Pr	Nd	Sm	Eu	Gd	Tb	Dy
972106	06-2-AP1.D	MC-04-09	47.2	190.0	41.8	294.4	108.0	26.1	130.0	11.6	41.7
972106	06-2-AP4.D	MC-04-09	58.0	236.0	48.0	304.0	113.2	27.2	119.2	12.0	40.4
972106	06-3-AP1.D	MC-04-09	59.6	284.0	66.8	396.0	168.0	34.6	192.0	17.2	51.2
972106	06-3-AP2.D	MC-04-09	110.8	380.0	72.4	396.0	124.8	29.6	146.0	13.4	51.6
972106	06-3-AP3.D	MC-04-09	376.0	1240.0	144.0	700.0	172.0	35.6	188.0	22.0	124.0
972106	06-3-AP3.D	MC-04-09	280.0	880.0	132.0	548.0	126.0	28.8	140.8	15.9	69.6
972106	06-4-AP1.D	MC-04-09	63.6	315.2	65.6	388.8	171.2	45.1	210.0	18.6	65.2
972116	16-2-AP3.D	MC-08-55	69.6	248.0	52.4	232.0	66.8	77.2	74.4	13.2	55.6
972117	17-1-AP1.D	MC-08-55	460.0	1444.0	192.8	624.0	90.4	18.5	73.6	9.0	40.0
972117	17-1-AP2.D	MC-08-55	508.0	1376.0	204.8	708.0	115.2	20.7	92.4	10.7	47.2
972117	17-1-AP3.D	MC-08-55	532.0	1404.0	212.0	832.0	184.0	48.8	236.0	28.8	144.0
972117	17-2-AP2.D	MC-08-55	404.0	1216.0	166.4	588.0	92.4	19.0	74.8	8.9	41.2
972117	17-2-AP3.D	MC-08-55	388.0	1020.0	142.8	536.0	90.8	20.1	84.4	10.5	39.2
972117	17-2-AP4.D	MC-08-55	416.0	1120.0	180.0	644.0	111.6	20.8	90.4	10.2	44.8
972117	17-4-AP2,D	MC-08-55	732.0	2040.0	232.8	960.0	194.8	47.7	189.2	21.3	99.2
972161	61-1-AP1.D	MC-08-62	198.8	448.0	69.2	324.0	112.8	380.0	150.0	18.1	77.2
972161	61-1-AP2.D	MC-08-62	264.0	696.0	103.2	448.0	94.0	176.0	102.8	13.6	64.0
972161	61-2-AP1.D	MC-08-62	184.0	468.0	69.6	328.0	94.4	580.0	131.2	17.6	81.2
972161	61-2-AP3.D	MC-08-62	244.0	688.0	100.4	448.0	123.6	540.0	168.0	19.2	80.8
972161	61-3-AP1.D	MC-08-62	150.4	416.0	64.0	302.0	84.8	369.2	114.8	13.3	55.2
716464	64-1-AP1.D	MC-05-20	212.0	656.0	105.6	448.0	108.4	39.2	125.2	17.5	78.8
716464	64-1-AP3.D	MC-05-20	3.2	18.8	4.1	35.8	26.8	16.6	82.8	12.8	56.4
716464	64-1-AP4.D	MC-05-20	312.0	1160.0	172.0	752.0	176.0	44.8	200.0	30.0	120.0
716464	64-1-AP4.D	MC-05-20	256.0	728.0	104.8	436.0	110.8	28.6	116.4	13.6	66.0
716464	66-1-AP1.D	MC-05-20	113.2	416.0	86.0	492.0	220.0	155.6	320.0	39.2	144.4
972166	66-1-AP3.D	MC-07-25	76.8	288.8	50.8	255.6	74.4	89.6	106.4	10.8	35.4
972166	66-1-AP4.D	MC-07-25	52.8	221.6	43.6	240.4	85.2	64.0	117.2	12.7	47.6
972166	66-1-AP5.D	MC-07-25	66.4	308.0	59.6	336.0	114.8	90.4	151.2	16.8	57.2
972166	66-1-AP6.D	MC-07-25	50.8	183.2	43.6	272.0	102.0	56.4	164.8	19.9	74.0
716474	74-1-AP1.D	MC-05-19	106.0	389.6	87.2	616.0	267.2	36.8	395.2	42.8	187.6
716474	74-1-AP2.D	MC-05-19	109.6	392.0	88.8	608.0	284.0	39.6	420.0	45.6	180.0
716474	74-2AP-1.D	MC-05-19	30.8	140.4	30.8	198.0	92.4	18.0	148.8	18.6	85.2
716474	74-2AP-3.D	MC-05-19	22.6	104.8	25.6	182.8	84.8	16.3	154.4	19.4	92.0
716474	74-2AP-3.D	MC-05-19	188.0	216.0	47.6	284.0	134.0	20.8	156.0	24.0	104.0
716474	74-3-AP1.D	MC-05-19	46.8	212.0	39.2	244.0	102.8	15.1	145.2	18.8	87.6
716477	77-1-AP1.D	MC-04-04	228.0	1100.0	209.6	1052.0	360.0	308.8	340.0	32.5	105.2
716477	77-1-AP2.D	MC-04-04	138.4	524.0	112.4	724.0	246.0	192.8	250.4	23.0	71.2
716477	77-1-AP3.D	MC-04-04	668.0	1980.0	272.0	1220.0	233.2	34.7	216.0	22.6	111.6
716477	77-1-AP4.D	MC-04-04	222.0	920.0	191.2	1176.0	436.4	330.8	466.4	43.3	134.4
716479	79-2-AP1,D	MC-05-15	468.8	1252.0	181.2	834.4	222.8	31.2	254.4	31.8	181.6
716479	79-6-AP1,D	MC-05-15	384.0	992.0	159.6	820.0	230.0	43.9	282.0	36.4	186.8
716489	89-2-AP1.D	MC-05-18	15.2	69.6	19.1	149.6	116.8	52.4	154.4	16.4	62.4
716495	95-1-AP1,D	MC-07-28	332.4	514.8	54.0	238.8	75.2	242.0	94.0	10.3	45.1
716495	95-2-AP1,D	MC-07-28	581.2	1140.0	106.0	366.0	77.2	390.8	74.0	7.6	33.8
716495	95-2-AP2,D	MC-07-28	752.0	1548.0	152.0	540.0	108.0	412.0	100.4	10.0	47.0
716495	95-3-AP1,D	MC-07-28	644.0	964.0	84.4	303.2	62.8	562.0	65.6	6.6	29.4
716495	95-3-AP2,D	MC-07-28	571.6	700.0	75.6	297.6	61.6	424.4	71.6	7.6	34.3

ANNEXE 3.2 : ANALYSES LA-ICP-MS: APATITES (SUITE)

Sample	Y	Ho	Er	Tm	Yb	Lu	ΣREE-Y	La/Yb	La/Nd	Eu/Eu
972106	120.8	5.4	6.7	0.6	1.7	0.1	1026.1	20.4	0.3	0.7
972106	110.4	4.6	5.5	0.4	2.1	0.1	1081.2	19.6	0.4	0.7
972106	116.8	6.0	7.6	0.5	1.8	0.1	1402.3	23.8	0.3	0.6
972106	158.8	7.8	13.2	1.0	3.8	0.5	1509.8	20.7	0.6	0.7
972106	316.0	20.8	46.0	3.0	22.8	4.8	3415.0	11.8	1.1	0.6
972106	250.0	11.0	20.0	1.5	12.0	1.2	2516.8	16.7	1.0	0.7
972106	138.0	6.9	9.2	0.5	1.5	0.0	1499.4	30.8	0.3	0.7
972116	244.0	9.1	22.4	2.4	8.4	1.1	1176.7	5.9	0.6	3.3
972117	185.6	7.1	17.5	2.2	10.9	2.2	3177.8	30.2	1.5	0.7
972117	232.0	9.7	24.0	2.6	12.0	2.3	3365.6	30.4	1.4	0.6
972117	592.0	22.4	52.4	6.0	34.8	6.6	4335.8	11.0	1.3	0.7
972117	162.0	6.6	15.2	2.0	10.1	1.6	2808.1	28.6	1.4	0.7
972117	190.0	8.6	18.6	2.2	8.9	1.9	2561.9	31.2	1.4	0.7
972117	224.0	8.1	20.4	2.0	10.8	1.7	2904.8	27.6	1.3	0.6
972117	364.0	15.9	40.0	4.2	24.8	3.8	4969.8	21.2	1.5	0.8
972161	344.0	11.3	22.0	2.3	7.4	0.8	2165.8	19.4	1.2	8.9
972161	420.0	13.2	28.4	3.8	15.6	2.2	2444.8	12.1	1.2	5.5
972161	332.0	12.3	21.2	1.8	6.4	0.6	2328.3	20.5	1.1	16.0
972161	320.0	12.0	19.6	2.3	9.6	0.8	2776.3	18.2	1.1	11.5
972161	195.2	7.7	13.6	1.2	3.7	0.3	1791.5	29.0	1.0	11.5
716464	256.0	11.8	19.3	1.8	8.4	1.1	2089.2	18.0	0.9	1.0
716464	197.6	8.1	16.0	1.1	5.3	0.5	485.7	0.4	0.2	1.0
716464	628.0	17.6	44.0	4.3	64.0	7.6	3732.3	3.5	0.8	0.7
716464	262.4	11.3	18.8	2.3	10.7	1.9	2167.5	17.2	1.2	0.8
716464	304.0	14.5	17.3	0.8	2.4	0.2	2325.6	34.4	0.5	1.8
972166	86.8	3.6	4.0	0.3	0.7	0.1	1084.0	79.2	0.6	3.1
972166	111.2	4.8	5.9	0.4	0.9	0.1	1008.3	42.7	0.4	2.0
972166	104.4	5.1	6.0	0.3	1.2	0.1	1317.5	41.1	0.4	2.1
972166	186.4	7.3	9.4	0.6	2.6	0.2	1173.1	14.0	0.4	1.3
716474	756.0	26.5	56.0	5.8	33.2	4.4	3010.4	2.3	0.3	0.3
716474	540.0	22.8	36.0	3.3	11.7	0.7	2782.1	6.7	0.4	0.4
716474	332.0	13.8	28.7	3.0	14.6	2.0	1157.0	1.5	0.3	0.5
716474	336.0	14.4	29.3	2.7	10.4	1.1	1096.5	1.6	0.2	0.4
716474	424.0	16.4	30.0	3.6	10.4	0.8	1659.6	13.0	1.3	0.4
716474	344.0	15.0	32.4	3.8	16.0	2.2	1324.9	2.1	0.4	0.4
716477	256.0	10.6	13.0	0.7	1.5	0.1	4017.9	110.6	0.4	2.7
716477	148.0	6.5	8.5	0.4	1.3	0.1	2446.9	78.6	0.4	2.4
716477	432.0	19.2	38.7	4.2	18.0	2.7	5272.9	26.6	1.1	0.5
716477	271.2	12.3	15.7	0.7	2.8	0.2	4223.4	57.7	0.4	2.2
716479	792.0	32.9	83.6	9.7	49.6	7.2	4433.2	6.8	1.1	0.4
716479	728.0	27.6	65.2	7.6	38.4	6.4	4007.8	7.2	0.9	0.5
716489	234.4	9.2	16.4	1.3	5.9	0.5	923.6	1.9	0.2	1.2
716495	169.6	6.0	11.0	0.9	3.7	0.4	1798.1	64.0	2.7	8.8
716495	123.2	4.9	9.9	0.9	4.0	0.5	2919.9	105.3	3.1	15.6
716495	205.2	7.1	15.4	1.5	6.8	0.9	3906.2	79.8	2.7	11.9
716495	121.6	4.3	8.5	0.9	4.2	0.5	2862.0	111.1	4.2	26.6
716495	161.6	5.4	11.3	1.1	5.8	0.7	2430.2	71.2	3.8	19.5

ANNEXE 3.3: ANALYSES MICROSONDE: CARBONATES

Sample	#	Drill Hole	Carbonate	Mg(CO3)	Ca(CO3)	Mn(CO3)	Fe(CO3)	Total
972116	16 2_2	MC-08-55	Ankerite	31.3	52.4	1.6	14.0	99.3
972116	16 3_1	MC-08-55	Ankerite	35.5	53.3	2.7	8.3	99.8
972116	16 3_2	MC-08-55	Ankerite	29.7	53.0	2.0	15.5	100.3
972166	16 3_3	MC-07-25	Ankerite	35.3	54.0	3.0	8.5	100.7
716489	89 1_1	MC-05-18	Ankerite	20.6	51.1	3.6	23.7	99.0
716489	89 2_1	MC-05-18	Ankerite	21.0	51.1	3.6	24.6	100.3
716489	89 2_2	MC-05-18	Ankerite	20.7	50.9	3.6	25.1	100.4
716489	89 3_1	MC-05-18	Ankerite	19.7	52.7	3.5	24.3	100.1
716489	89 3_2	MC-05-18	Ankerite	20.8	51.5	3.3	24.3	99.8
716489	89 3_3	MC-05-18	Ankerite	20.8	51.1	3.3	24.5	99.7
972106	06 3_1	MC-04-09	Calcite	1.1	104.0	1.2	2.5	108.7
972106	06 5_1	MC-04-09	Calcite	0.7	98.6	1.8	2.0	103.0
972106	06 5_1a	MC-04-09	Calcite	0.3	97.6	1.0	0.8	99.7
972106	06 5_2	MC-04-09	Calcite	0.8	104.5	1.5	2.1	108.8
972116	16 1_1	MC-08-55	Calcite	0.5	102.0	1.1	0.7	104.4
972116	16 1_2	MC-08-55	Calcite	0.4	104.2	1.4	0.6	106.6
972116	16 2_1	MC-08-55	Calcite	0.4	104.2	1.3	0.7	106.7
972116	16 2_2	MC-08-55	Calcite	0.1	104.8	0.5	0.2	105.5
972117	17 1_1	MC-08-55	Calcite	0.4	104.6	1.3	0.8	107.1
972117	17 1_2	MC-08-55	Calcite	0.4	100.9	1.2	0.7	103.3
972117	17 1_2a	MC-08-55	Calcite	0.2	100.0	0.5	0.0	100.7
972117	17 2_1	MC-08-55	Calcite	0.4	103.4	1.5	0.6	105.9
972117	17 3_1	MC-08-55	Calcite	0.7	102.4	1.7	0.9	105.7
972117	17 3_2	MC-08-55	Calcite	0.3	100.2	1.3	0.5	102.3
972166	66 2_1	MC-07-25	Calcite	0.0	96.8	1.5	0.1	98.4
972166	66 2_2	MC-07-25	Calcite	0.1	97.8	0.6	0.1	98.5
972166	66 3_1	MC-07-25	Calcite	0.0	98.6	2.2	0.1	100.9
716479	79 1_1	MC-05-15	Calcite	0.4	97.9	1.8	1.6	101.7
716479	79 2_1	MC-05-15	Calcite	0.5	101.5	2.0	1.4	105.3
716479	79 2_2	MC-05-15	Calcite	0.3	101.4	1.9	1.1	104.6
716479	79 3_1	MC-05-15	Calcite	0.1	101.1	3.0	0.2	104.4
716479	79 3_2	MC-05-15	Calcite	0.1	102.6	2.3	0.4	105.4
716479	79 4_1	MC-05-15	Calcite	0.1	104.1	2.1	0.9	107.1
716479	79 4_2	MC-05-15	Calcite	0.1	99.4	2.3	0.8	102.6
716479	79 5_1	MC-05-15	Calcite	0.1	98.2	2.6	0.1	101.0
716479	79 5_2	MC-05-15	Calcite	0.2	99.9	3.7	0.7	104.6
716479	79 6_1	MC-05-15	Calcite	0.1	101.3	2.2	0.6	104.2
716489	89 2_1	MC-05-18	Calcite	0.2	98.4	1.3	1.0	100.8

ANNEXE 3.4 : ANALYSES LA-ICP-MS: CARBONATES

Sample	#	Drill Hole	Carbonate	La	Ce	Pr	Nd	Sm	Eu	Gd	Tb
972116	16-1-AP1,D	MC-08-55	Ankerite	1.9	7.2	1.1	6.0	2.6	2.8	2.8	0.5
972116	16-2-AP1,D	MC-08-55	Ankerite	1.5	5.4	0.8	7.0	2.0	2.8	3.9	0.3
972116	16-2-AP3,D	MC-08-55	Ankerite	1.6	5.0	1.0	3.7	1.4	2.3	1.8	0.4
972116	16-2-AP4,D	MC-08-55	Ankerite	1.2	3.8	0.3	2.3	1.4	1.6	1.7	0.2
972116	16-2-CA2,D	MC-08-55	Ankerite	1.8	7.6	1.5	6.6	2.1	3.2	3.3	0.6
972116	16-3-CA1,D	MC-08-55	Ankerite	2.9	9.4	1.6	9.3	4.2	3.9	5.6	1.0
972116	16-3-CA2,D	MC-08-55	Ankerite	2.7	8.9	1.4	8.0	3.4	3.4	4.6	0.8
972116	16-3-CA3,D	MC-08-55	Ankerite	2.8	8.9	1.2	5.7	2.3	2.7	8.6	0.5
716489	89-1-C1B,D	MC-05-18	Ankerite	0.6	1.7	0.3	1.6	1.0	3.4	1.4	0.2
716489	89-2-C1B,D	MC-05-18	Ankerite	3.2	8.3	1.1	6.2	3.3	2.9	4.3	0.6
716489	89-2-C2B,D	MC-05-18	Ankerite	1.1	4.9	1.1	7.8	6.6	5.2	9.9	1.5
716489	89-3-C1B,D	MC-05-18	Ankerite	0.8	3.0	0.7	5.0	3.9	5.3	5.7	0.9
716489	89-3-C2B,D	MC-05-18	Ankerite	0.4	1.2	0.2	1.7	1.2	4.3	1.8	0.2
716489	89-3-C3B,D	MC-05-18	Ankerite	1.5	4.4	0.9	5.7	3.8	4.1	5.3	0.7
972106	06-3-CA1,D	MC-04-09	Calcite I	0.6	2.2	0.4	2.0	1.1	0.8	1.8	0.4
972106	06-3-CA2,D	MC-04-09	Calcite I	0.2	0.6	0.2	0.7	0.1	0.8	2.0	0.3
972106	06-5-CA1,D	MC-04-09	Calcite I	9.7	17.4	2.4	9.8	3.0	1.1	4.5	0.6
972106	06-5-CA2,D	MC-04-09	Calcite I	7.2	11.6	1.6	7.3	2.3	1.1	3.8	0.5
972106	06-5-CA3,D	MC-04-09	Calcite I	1.5	3.5	0.5	3.0	1.2	0.8	2.5	0.4
972116	16-1-CA1,D	MC-08-55	Calcite I	2.2	4.8	0.6	3.0	1.1	2.2	2.1	0.3
972116	16-1-CA2,D	MC-08-55	Calcite I	2.1	5.0	0.7	3.4	1.4	1.7	2.3	0.4
972116	16-2-CA1,D	MC-08-55	Calcite I	2.6	5.8	0.8	4.0	1.7	2.8	3.7	0.4
972116	16-2-CA2,D	MC-08-55	Calcite I	2.6	5.8	0.8	3.6	1.4	2.3	3.7	0.4
972116	16-4-AP1,D	MC-08-55	Calcite I	3.6	9.4	1.5	6.9	2.7	3.9	4.5	0.5
972117	17-1-CA1,D	MC-08-55	Calcite I	4.8	15.5	3.4	21.4	16.0	8.0	24.0	3.9
972117	17-1-CA2,D	MC-08-55	Calcite I	1.5	4.9	1.0	6.1	5.4	3.8	9.2	1.7
972117	17-2-CA1,D	MC-08-55	Calcite I	1.7	7.5	1.5	9.9	9.0	5.9	16.1	3.1
972117	17-3-CA1,D	MC-08-55	Calcite I	2.5	9.4	1.8	10.9	7.6	7.0	11.1	1.6
972117	17-3-CA2,D	MC-08-55	Calcite I	3.1	11.8	2.3	14.5	10.5	8.6	17.0	2.8
716479	79-3-C1B,D	MC-05-15	Calcite I	7.7	14.9	2.1	10.0	4.6	1.7	11.2	1.2
716479	79-4-C2B,D	MC-05-15	Calcite I	11.2	20.5	3.0	16.1	6.4	1.8	11.4	1.3
716479	79-6-CA1,D	MC-05-15	Calcite I	7.0	12.6	1.8	10.4	4.1	1.9	7.0	0.7
716489	89-2-CA1,D	MC-05-18	Calcite I	11.7	23.6	3.6	16.3	6.0	5.7	4.3	0.6
972116	16-2-CA1,D	MC-08-55	Calcite II	22.4	51.2	8.8	32.0	4.9	3.3	6.0	0.8
972116	16-4-AP2,D	MC-08-55	Calcite II	6.4	15.4	2.1	9.4	2.4	2.2	4.0	0.3
972161	61-2-CA2,D	MC-08-62	Calcite II	16.4	35.6	5.8	40.4	8.8	10.2	16.0	3.9
972166	66-2-CA1,D	MC-07-25	Calcite II	58.0	139.6	17.1	84.0	18.1	2.5	14.4	1.3
972166	66-2-CA2,D	MC-07-25	Calcite II	43.2	105.2	13.1	63.6	12.9	2.2	12.6	1.1
972166	66-3-CA1,D	MC-07-25	Calcite II	16.0	34.4	4.2	17.4	4.7	1.5	6.7	0.8
716479	79-1-C1B,D	MC-05-15	Calcite II	62.8	104.0	15.8	69.2	21.2	6.3	30.8	3.8
716479	79-1-C1B,D	MC-05-15	Calcite II	77.6	128.4	19.2	86.8	28.8	6.5	37.8	4.2
716479	79-2-C1B,D	MC-05-15	Calcite II	64.4	116.0	17.2	80.0	23.2	6.1	27.6	3.2
716479	79-2-C2B,D	MC-05-15	Calcite II	73.2	138.8	18.5	79.6	24.8	7.0	33.6	4.0
716479	79-5-C1B,D	MC-05-15	Calcite II	118.8	178.4	22.6	109.6	38.4	8.2	46.4	6.0
716479	79-5-C2B,D	MC-05-15	Calcite II	119.6	222.8	31.1	132.4	39.1	5.1	33.4	3.4

ANNEXE 3.4 : ANALYSES LA-ICP-MS: CARBONATES (SUITE)

Sample	Dy	Y	Ho	Er	Tm	Yb	Lu	ΣREE-Y	La/Yb_{PM}	La/Nd_{PM}	Eu/Eu^*_{PM}
972116	3.3	14.0	0.6	1.3	0.1	0.8	0.1	45.0	2.5	0.3	3.2
972116	1.8	11.8	0.3	0.9	0.1	0.6	0.0	39.3	2.7	0.2	3.0
972116	2.0	6.9	0.2	0.8	0.1	0.5	0.0	27.8	3.1	0.4	4.6
972116	0.8	4.6	0.1	0.1	0.0	0.1	0.0	18.1	10.2	0.5	3.1
972116	3.5	16.4	0.5	1.1	0.1	0.8	0.1	49.1	2.3	0.3	3.8
972116	4.7	16.6	0.7	1.3	0.1	0.5	0.1	61.7	6.2	0.3	2.4
972116	3.9	14.3	0.6	1.1	0.1	0.5	0.1	53.7	5.4	0.3	2.6
972116	2.7	12.5	0.5	1.1	0.1	0.7	0.1	50.4	3.8	0.5	1.6
716489	1.2	6.4	0.2	0.7	0.1	0.7	0.1	19.7	0.9	0.4	9.0
716489	3.0	16.1	0.6	1.5	0.2	1.6	0.3	53.4	1.9	0.5	2.3
716489	7.8	36.8	1.4	4.0	0.6	4.1	0.8	93.7	0.3	0.1	2.0
716489	4.9	23.6	0.8	2.3	0.3	2.0	0.4	59.6	0.4	0.2	3.4
716489	1.2	6.6	0.2	0.6	0.1	0.7	0.1	20.5	0.6	0.2	8.8
716489	4.0	18.8	0.7	1.9	0.3	1.7	0.3	54.2	0.9	0.3	2.8
972106	2.2	15.4	0.6	1.7	0.3	2.0	0.6	31.9	0.3	0.3	1.7
972106	1.5	15.3	0.6	1.5	0.3	2.2	0.4	26.5	0.1	0.3	2.7
972106	3.2	17.2	0.7	2.1	0.3	2.4	0.5	74.9	4.0	1.0	0.9
972106	3.0	17.0	0.5	1.9	0.3	2.2	0.5	60.9	3.2	1.0	1.2
972106	2.4	14.1	0.5	1.4	0.2	1.7	0.4	34.0	0.8	0.5	1.3
972116	2.2	11.7	0.4	0.9	0.1	0.6	0.1	32.3	3.8	0.7	4.4
972116	2.2	12.2	0.3	0.9	0.1	0.6	0.1	33.2	3.6	0.6	2.8
972116	2.6	14.2	0.4	1.1	0.1	0.8	0.2	41.3	3.2	0.6	3.4
972116	2.0	11.6	0.3	0.8	0.1	0.6	0.1	36.1	4.5	0.7	2.9
972116	3.4	14.2	0.5	1.0	0.1	0.7	0.1	53.0	5.5	0.5	3.4
972117	18.8	74.4	2.4	4.6	0.4	1.9	0.2	199.6	2.6	0.2	1.3
972117	7.9	34.2	1.1	2.0	0.2	0.8	0.1	79.7	1.9	0.2	1.6
972117	15.5	66.4	2.1	4.3	0.4	1.9	0.2	145.6	0.9	0.2	1.5
972117	6.9	26.5	0.8	1.4	0.1	0.4	0.0	88.2	5.7	0.2	2.3
972117	11.5	42.1	1.2	1.9	0.1	0.6	0.0	128.2	5.5	0.2	2.0
716479	7.1	34.8	1.4	4.4	0.8	7.2	1.7	110.9	1.1	0.8	0.7
716479	6.7	25.6	1.3	4.9	0.8	6.6	1.8	119.4	1.7	0.7	0.6
716479	3.8	18.5	0.8	3.0	0.5	5.4	1.5	79.0	1.3	0.7	1.0
716489	4.1	28.7	0.9	2.6	0.4	3.8	1.1	113.6	3.1	0.7	3.3
972116	4.0	19.6	0.7	1.2	0.1	0.9	0.1	155.9	24.3	0.7	1.9
972116	1.6	7.7	0.3	0.4	0.1	0.3	0.0	52.4	20.6	0.7	2.1
972161	9.6	43.2	1.6	2.3	1.0	1.5	0.5	196.8	10.8	0.4	2.6
972166	3.6	14.6	0.5	1.1	0.1	0.6	0.0	355.4	94.8	0.7	0.5
972166	2.9	15.6	0.5	1.0	0.1	1.1	0.1	275.3	38.6	0.7	0.5
972166	4.0	18.9	0.6	1.1	0.1	0.8	0.1	111.3	19.5	0.9	0.8
716479	17.7	62.0	2.2	5.1	0.5	3.0	0.4	404.7	21.2	0.9	0.8
716479	18.3	66.4	2.4	4.6	0.5	1.9	0.4	483.8	40.1	0.9	0.6
716479	14.4	44.4	2.0	4.7	0.4	3.3	0.6	407.6	19.6	0.8	0.7
716479	18.4	69.2	2.4	5.4	0.4	2.4	0.4	478.1	30.0	0.9	0.7
716479	24.9	71.6	3.0	5.4	0.6	4.0	0.6	638.4	30.0	1.1	0.6
716479	12.4	39.6	1.6	3.1	0.3	2.3	0.4	646.6	52.0	0.9	0.4

ANNEXE 3.5 : PARAMÈTRES LA-ICP-MS

Analytical details for the Laser Ablation-ICP-MS analyses of carbonates and apatite at UQAC

Laser ablation system	Excimer 193nm Resonetics Resolution M-50	
ICP-MS	Agilent 7700x	
Laser frequency	10 Hz	
Power	5 mj	
Stage speed	5 $\mu m.s^{-1}$	
Beam size	15-75 µm	
Dwell time	10ms/peak	
Analysis	single line raster (~260µm)	
	30s gas blank	
	60s of signal	
Gas flow	Helium (650 $ml.m^{-1}$)	
	Nitrogen (1 $ml.m^{-1}$)	
	Argon (0.7-0.9 $ml.m^{-1}$)	
Internal standard	Ca	using microprobe results
Reference material for calibration	GSE-1g	USGS-synthetic glass
Reference material for monitoring	NISTSRM610 for all elements	synthetic glass from National Institute of Standards and Technology
	GSD-1g	USGS-synthetic glass
Data reduction	Iolite software (IGOR pro 6.3)	

ANNEXE 3.6 : STANDARDS LA-ICP-MS

	LOD		NISTSRM610		
	Apatite	**Carbonates**			
	ppm	ppm	median (n=17)	sd	Working values
Mg	0.26	0.02	524.0	29.9	465.0
Al	1.27	0.06	10080.0	725.2	10797.0
Si	3650.72	1476.60	329700.0	22260.5	327180.0
P	5.65	1.87	360.0	35.9	343.0
K	37.72	0.83	1446.0	472.4	486.0
Ca44	72.08	18.88	85000.0	3044.3	82144.0
La	0.03	0.00	446.0	21.1	457.0
Ce	0.03	0.00	457.8	20.0	448.0
Pr	0.02	0.00	447.8	19.0	430.0
Nd	0.15	0.01	433.0	28.8	431.0
Sm	0.18	0.02	458.0	31.9	451.0
Eu	0.05	0.00	449.0	23.3	461.0
Gd	0.18	0.01	471.6	33.6	444.0
Tb	0.03	0.00	446.0	26.8	443.0
Dy	0.12	0.01	453.0	28.4	427.0
Y	0.03	0.00	477.0	26.8	450.0
Ho	0.01	0.00	469.0	30.8	449.0
Er	0.04	0.01	482.6	32.0	426.0
Tm	0.04	0.00	452.0	29.8	420.0
Yb	0.12	0.02	476.0	30.2	445.0
Lu	0.04	0.00	463.4	33.5	435.0
ΣLREE	0.40	0.05			
ΣREE-Y	1.05	0.11			

ANNEXE 3.6 : STANDARDS LA-ICP-MS (SUITE)

	GSD-1g			**GSE-1g**		
	average (n=18)	sd	Working values	average (n=19)	sd	Working values
Mg	22095.0	746.6	21709.0	21110.0	151.8	21106.0
Al	71445.0	1958.4	70921.5	68800.0	511.3	68804.0
Si	263850.0	14408.3	248656.8	251000.0	2524.2	250994.0
P	861.0	26.3	860.0	40.4	19.9	70.0
K	26455.0	2028.4	25300.0	21800.0	207.9	21800.0
Ca44	51810.0	718.4	51429.3	52860.0	278.6	52858.0
La	40.4	2.6	39.1	392.0	2.3	392.0
Ce	44.8	2.0	41.4	414.0	2.3	414.0
Pr	48.6	2.6	45.0	460.0	2.6	460.0
Nd	46.0	2.5	44.7	453.0	2.8	453.0
Sm	49.4	3.1	47.8	488.0	3.6	488.0
Eu	42.8	3.2	41.0	410.1	3.6	410.0
Gd	49.6	3.2	50.7	514.0	4.0	514.0
Tb	47.1	2.4	47.0	480.0	4.0	480.0
Dy	52.1	3.3	51.2	524.0	4.7	524.0
Y	42.1	2.5	42.0	410.0	2.8	410.0
Ho	50.7	2.6	49.0	501.0	3.7	501.0
Er	41.5	2.3	40.1	595.0	4.1	595.0
Tm	50.2	3.2	49.0	500.0	2.8	500.0
Yb	51.5	3.2	50.9	520.0	3.0	520.0
Lu	53.8	2.9	51.5	518.0	3.4	518.0
ΣLREE						
ΣREE-Y						

ANNEXE 4.1 : STANDARDS LA-ICP-MS

Isotope	MASS-1					NIST-610		
		Used for calibration		Used as monitor		Used as monitor		
	Certified value	This study n=128 average	std	This study n=64 average	std	Certificate Value	This study n=32 average	std
28Si		**221**	107	**245**	173	335000	**240063**	25374
33S	276000	**276212**	4709.4	**277939**	9517	693	**N.A.**	**N.A.**
34S	276000	**276259**	4534.2	**277788**	9304	693	**N.A.**	**N.A.**
51V	63	**63**	0.5	**63**	1	442	**525**	22
52Cr	37	**37**	1	**37**	1	405	**267**	11
55Mn	260	**260**	3	**258**	7	485	**Internal st**	
57Fe	15.6	**Internal st**		**Internal st**		458	**N.A.**	0.0
59Co	67	**67**	1	**67**	1	405	**458**	12
60Ni	160	**160**	4	**154**	9	459	**847**	113
65Cu	134000	**134191**	1832	**133511**	2984	430	**577**	68
66Zn	210000	**210018**	3023	**209620**	4868	456	**712**	177
71Ga	50	**50**	0.4	**50**	1	438	**372**	12
72Ge	50	**50**	1	**50**	1	426	**345**	11
75As	65	**65**	2	**65**	4	317	**309**	19
82Se	53	**53**	1	**53**	2	109	**122**	5
107Ag	67	**67**	1	**67**	2	239	**268**	16
111Cd	70	**70**	3	**71**	5	259	**363**	58
115In	50	**50**	1	**50**	1	441	**362**	17
118Sn	55	**55**	1	**55**	1	396	**416**	23
121Sb	55	**55**	0.5	**55**	1	369	**357**	16
125Te	33	**33**	1	**33**	1	302	**519**	23
197Au	47	**48**	3	**48**	4	23	**21**	1
205Tl	(66)	**52**	2	**52**	2	61	**52**	3
208Pb	80	**80**	2	**81**	4	426	**476**	31
209Bi	66	**66**	1	**66**	1	358	**412**	22

ANNEXE 4.2 : ANALYSES LA-ICP-MS: PYRITES

	Host	Hole ID	Distance	Type	Analysis	Size	51V	52Cr	55Mn	59Co	60Ni	65Cu	66Zn
68-1	KT	BRC-07-40	400	zoned	grain	0.5	8.6	5.3	35.0	347.0	366.6	487	1616
68-2	KT	BRC-07-40	400	zoned	grain	0.5	1.2	1.1	22.6	67.3	251.3	84	568
68-3	KT	BRC-07-40	400	zoned	grain	0.5	3.3	2.6	23.2	159.2	348.6	95	3247
68-4	KT	BRC-07-40	400	zoned	grain	0.5	bdl	0.0	1207.0	286.5	1135.0	1499	564
68-5	KT	BRC-07-40	400	zoned	grain	0.2	bdl	bdl	145.5	70.8	2268.0	689	9528
68-6	KT	BRC-07-40	400	zoned	grain	0.6	bdl	-0.1	1113.0	408.9	1482.0	461	3384
68-7	KT	BRC-07-40	400	zoned	grain	0.6	bdl	bdl	941.5	658.0	1479.0	11	12
972122-1	KT	BRC-04-22	1000	zoned	grain	0.75	bdl	0.1	33.9	326.3	400.5	734	359
972122-2	KT	BRC-04-22	1000	zoned	grain	0.75	bdl	0.2	25.6	8.7	623.0	3	5
972122-3	KT	BRC-04-22	1000	zoned	grain	0.5	bdl	-0.1	25.2	440.4	359.7	657	14
972122-4	KT	BRC-04-22	1000	zoned	L	1.75	bdl	0.3	44.9	1.6	202.9	11	213
972122-5	KT	BRC-04-22	1000	zoned	grain	1.75	1.7	0.8	81.1	6198.0	149.9	71	219
972122-6	KT	BRC-04-22	1000	zoned	grain	0.75	bdl	0.0	898.7	3485.0	218.3	644	124
972122-7	KT	BRC-04-22	1000	zoned	L	1.5	0.1	0.8	24.9	235.9	136.9	488	152
972122-8	KT	BRC-04-22	1000	zoned	grain	1.5	0.5	3.1	92.9	318.9	205.3	427	1797
972122-9	KT	BRC-04-22	1000	zoned	grain	1.5	bdl	0.5	85.3	478.6	150.5	43	959
972122-10	KT	BRC-04-22	1000	zoned	grain	0.5	0.0	0.6	203.6	323.4	371.6	383	1389
972124-1	KT	BRC-97-15	1500	zoned	L	1.75	bdl	0.5	24.8	29.7	562.3	939	294
972124-2	KT	BRC-97-15	1500	zoned	grain	1.75	3.8	1.7	62.9	52.9	343.6	56	2983
972124-3	KT	BRC-97-15	1500	zoned	grain	0.45	0.4	1.7	43.2	139.7	420.1	357	16220
972124-4	KT	BRC-97-15	1500	zoned	grain	1.75	0.7	2.0	70.1	130.0	479.6	1257	13920
972124-5	KT	BRC-97-15	1500	zoned	grain	0.6	0.6	2.3	56.6	123.9	422.8	682	6133
972124-6	KT	BRC-97-15	1500	zoned	grain	1.2	bdl	2.0	31.1	31.2	504.6	230	125
972124-7	KT	BRC-97-15	1500	zoned	grain	1	0.1	0.9	36.2	56.1	607.1	211	193
972124-8	KT	BRC-97-15	1500	zoned	grain	0.35	2.2	0.8	34.1	660.9	329.3	75	4
972124-9	KT	BRC-97-15	1500	zoned	grain	1.5	0.8	1.5	68.3	83.9	708.0	796	368
972124-10	KT	BRC-97-15	1500	zoned	grain	0.3	1.6	1.2	39.0	1268.0	497.2	88	9
972124-11	KT	BRC-97-15	1500	zoned	grain	0.5	1.0	0.8	122.9	1661.0	246.8	981	7
972124-12	KT	BRC-97-15	1500	zoned	grain	1.5	1.8	2.4	29.5	29.6	596.2	274	542
63-1	KT	MC-05-20	50	zoned	grain	1.12	bdl	0.2	2.7	175.0	362.1	5	114
63-2	KT	MC-05-20	50	zoned	S	1.12	1.9	0.6	62.7	309.5	401.7	3	12
63-3	KT	MC-05-20	50	zoned	S	1.12	bdl	0.0	1.1	214.0	266.8	2	247
63-4	KT	MC-05-20	50	zoned	grain	0.6	bdl	0.4	1.9	505.2	362.2	1	140
63-5	KT	MC-05-20	50	zoned	grain	0.45	0.1	0.3	4.1	741.7	239.8	9	7739
63-6	KT	MC-05-20	50	zoned	grain	0.8	bdl	0.2	1.4	317.1	395.8	2	68
63-7	KT	MC-05-20	50	zoned	L	1.5	bdl	0.0	3.2	774.8	495.0	685	5
63-8	KT	MC-05-20	50	zoned	L	1.5	bdl	0.2	3.3	102.0	768.9	1	2
63-9	KT	MC-05-20	50	zoned	grain	0.8	bdl	0.8	57.0	2394.0	1031.0	380	385
63-10	KT	MC-05-20	50	zoned	grain	1.1	bdl	0.4	2.1	650.5	436.3	1	1269
63-11	KT	MC-05-20	50	zoned	L	1.1	bdl	0.2	1.2	6.8	573.7	1	8
972153-1	KT	MC-07-23	12.5	5	grain	0.25	bdl	0.1	24.6	227.6	133.5	4	1

	71Ga	72Ge	75As	82Se	107Ag	111Cd	115In	118Sn	121Sb	125Te	197Au	205Tl	208Pb	209Bi
68-1	1.4	1.7	208.8	70.0	91.4	5.8	0.3	11.6	6.2	211.2	0.6	0.1	180	12.9
68-2	0.3	0.9	303.0	53.6	352.2	2.1	0.1	3.7	1.7	378.7	0.2	0.0	45	3.3
68-3	0.8	1.3	409.8	60.2	13.3	12.1	0.3	5.1	2.6	48.0	0.1	0.0	54	5.2
68-4	0.2	1.4	1343.0	165.2	30.0	3.5	0.2	2.3	2.6	69.4	0.1	0.0	73	10.2
68-5	0.1	0.7	420.0	238.0	87.9	33.7	1.1	1.1	1.9	114.3	0.1	0.0	35	7.8
68-6	0.2	1.6	2013.0	150.4	16.5	12.5	0.4	5.9	1.9	60.3	0.1	0.0	73	9.8
68-7	0.1	1.1	2811.0	95.7	6.3	0.2	0.0	0.5	1.0	34.2	0.0	0.0	20	5.1
972122-1	0.1	1.1	999.6	47.2	5.8	1.2	0.1	0.4	0.4	5.3	0.0	0.0	10	2.0
972122-2	0.2	0.9	1416.0	82.9	0.1	0.1	0.0	0.2	0.1	1.6	0.0	0.0	3	0.7
972122-3	0.2	0.9	1034.0	41.7	2.2	0.2	0.0	0.6	0.2	21.5	0.0	0.0	23	3.2
972122-4	0.1	1.1	366.1	65.9	0.5	0.8	0.0	0.5	1.3	17.1	0.0	0.0	34	7.5
972122-5	0.7	1.1	522.7	44.1	54.4	1.0	0.1	1.8	0.4	61.8	0.5	0.0	23	6.4
972122-6	0.2	0.9	985.5	38.2	4.0	0.6	0.1	3.7	0.6	15.2	0.1	0.0	21	6.1
972122-7	0.2	1.1	280.4	52.2	0.2	0.6	0.1	1.6	0.3	14.6	0.0	0.0	9	2.3
972122-8	0.5	1.2	311.0	41.6	1.3	6.3	0.3	1.3	0.6	19.7	0.0	0.0	44	10.6
972122-9	0.2	1.2	379.5	45.3	0.6	3.3	0.1	1.7	0.4	10.5	0.0	0.0	12	3.2
972122-10	0.2	1.2	391.3	42.1	12.1	5.4	0.2	1.8	1.0	62.9	0.3	0.0	176	14.3
972124-1	0.1	1.1	1270.0	74.9	6.0	1.3	0.1	0.8	1.3	20.4	0.0	0.0	1112	4.0
972124-2	0.8	1.3	1249.0	58.0	1.4	15.8	0.4	1.4	1.0	2.2	0.0	0.0	63	0.9
972124-3	0.3	1.0	914.1	68.8	6.2	88.7	2.1	1.7	1.8	8.6	0.1	0.0	561	3.7
972124-4	0.4	1.3	459.9	69.9	6.2	77.1	1.9	3.8	2.4	10.3	0.1	0.0	302	3.4
972124-5	0.3	1.2	178.7	88.8	20.9	29.8	0.9	1.5	1.0	29.3	0.2	0.0	2861	8.6
972124-6	0.2	1.2	574.7	72.5	1.7	0.4	0.0	1.6	0.4	5.7	0.0	0.0	243	1.4
972124-7	0.1	1.4	829.6	73.6	2.6	0.8	0.0	1.5	0.4	7.5	0.0	0.0	470	1.9
972124-8	0.2	1.2	1049.0	69.9	2.6	0.1	0.0	2.4	0.3	5.9	0.0	0.0	674	1.8
972124-9	0.2	2.4	158.1	69.8	25.1	1.4	0.1	1.4	0.5	16.0	0.3	0.0	328	2.0
972124-10	0.3	1.2	1288.0	75.0	0.5	0.1	0.0	1.2	0.9	2.3	0.0	0.0	17	1.1
972124-11	0.1	1.3	828.0	49.4	1.4	0.1	0.2	0.8	0.7	2.5	0.0	0.0	67	1.1
972124-12	0.4	2.5	928.9	71.2	3.6	1.8	0.1	3.4	0.6	10.3	0.0	0.0	477	1.9
63-1	0.1	2.0	1655.0	124.2	0.0	0.4	0.0	0.4	0.0	0.8	0.0	0.0	0	0.2
63-2	1.6	1.9	833.9	100.0	138.0	0.1	0.0	0.4	0.1	104.6	0.0	0.0	10	4.5
63-3	0.1	1.3	1701.0	96.2	0.2	0.7	0.0	0.8	0.3	1.3	0.0	0.0	4	2.0
63-4	0.1	1.3	1288.0	99.8	1.6	0.3	0.0	2.4	0.3	7.3	0.1	0.0	5	4.0
63-5	0.1	1.2	2033.0	143.4	5.1	20.3	1.2	2.4	0.6	11.3	0.2	0.0	10	5.7
63-6	0.2	1.7	1317.0	93.5	0.8	0.2	0.0	1.3	0.3	2.9	0.0	0.0	3	3.8
63-7	0.1	1.8	1082.0	136.1	100.5	0.1	2.8	859.4	36.0	113.3	0.5	0.1	98	40.4
63-8	0.1	1.7	1395.0	125.8	0.4	0.1	0.0	0.5	0.0	0.8	0.0	0.0	8	2.0
63-9	0.5	1.5	2094.0	149.4	283.0	1.0	0.1	1.7	1.6	354.3	7.0	19.7	552	89.6
63-10	0.1	1.9	1834.0	63.0	2.4	3.5	0.1	0.5	0.2	3.6	0.1	0.0	147	5.4
63-11	0.1	1.6	1378.0	83.0	0.0	0.2	0.0	0.3	0.0	0.7	0.0	0.0	0	0.2
972153-1	0.1	1.4	132.1	121.7	0.0	0.1	0.0	0.0	0.1	0.3	0.0	0.0	1	1.0

	Host	Hole ID	Distance	Type	Analysis	Size	51V	52Cr	55Mn	59Co	60Ni	65Cu	66Zn
972153-2	KT	MC-07-23	12.5	5	L	1.6	bdl	0.0	17.2	213.7	138.1	165	3
972153-3	KT	MC-07-23	12.5	5	L	1.6	bdl	0.0	1.8	220.2	173.4	50	1
972153-4	KT	MC-07-23	12.5	5	grain	0.35	bdl	0.2	18.5	294.4	96.5	32	3
972153-5	KT	MC-07-23	12.5	5	grain	0.35	bdl	0.0	49.7	284.0	93.2	18	1
972153-6	KT	MC-07-23	12.5	5	grain	0.6	bdl	0.0	17.5	170.2	154.4	363	14
972153-7	KT	MC-07-23	12.5	5	L	0.7	bdl	0.2	5.6	213.4	168.8	79	2
972153-8	KT	MC-07-23	12.5	5	S	0.25	bdl	bdl	8.7	425.0	98.6	90	4
972153-9	KT	MC-07-23	12.5	5	grain	0.75	bdl	0.3	8.0	121.2	182.7	223	3
972153-10	KT	MC-07-23	12.5	5	grain	1.5	bdl	0.1	4.9	125.8	162.6	252	12
972153-11	KT	MC-07-23	12.5	5	S	1.5	bdl	0.0	1.2	334.5	216.2	197	5
972153-12	KT	MC-07-23	12.5	5	S	1.5	bdl	0.1	3.2	171.7	200.5	1101	51
972153-13	KT	MC-07-23	12.5	5	S	1.5	0.0	1.1	41.6	123.5	200.9	174	14
74-1	KT	MC-05-19	225	zoned	grain	0.5	5.2	6.2	73.3	225.6	161.2	75	11
74-2	KT	MC-05-19	225	zoned	S	0.25	8.0	4.2	332.3	94.5	197.4	373	109
74-3	KT	MC-05-19	225	zoned	grain	0.25	2.7	4.5	16.5	144.3	92.0	52	4
74-4	KT	MC-05-19	225	zoned	S	0.25	bdl	0.9	7.2	34.8	427.5	67	2
74-5	KT	MC-05-19	225	zoned	grain	0.4	bdl	1.1	47.3	57.0	351.4	813	9
74-6	KT	MC-05-19	225	zoned	S	0.15	bdl	0.8	20.2	160.6	361.9	373	2
74-7	KT	MC-05-19	225	zoned	grain	0.55	5.7	11.6	65.3	439.3	154.0	24	9
89-1	KT	MC-05-18	0	zoned	grain	0.5	bdl	0.3	12.9	139.0	132.6	1335	105
89-2	KT	MC-05-18	0	zoned	grain	0.55	bdl	0.2	16.9	53.7	122.2	1040	48
89-3	KT	MC-05-18	0	zoned	grain	0.2	bdl	0.4	22.1	660.7	146.1	20	2
89-4	KT	MC-05-18	0	1	grain	0.75	bdl	0.2	241.6	1082.0	298.3	963	35
89-5	KT	MC-05-18	0	zoned	S	0.1	bdl	0.2	13.3	887.6	217.9	622	62
89-6	KT	MC-05-18	0	1	L	0.75	bdl	0.1	242.1	983.6	259.2	1121	35
89-7	KT	MC-05-18	0	zoned	grain	0.8	bdl	0.4	148.4	607.4	212.0	17	13
89-8	KT	MC-05-18	0	zoned	grain	0.7	bdl	0.9	359.9	516.0	167.0	365	39
89-9	KT	MC-05-18	0	zoned	grain	0.4	bdl	0.5	87.4	516.7	157.2	1003	59
89-10	KT	MC-05-18	0	zoned	grain	0.35	0.6	0.4	58.6	1439.0	156.1	59	10
972105-1	KT	MC-04-09	62.5	zoned	grain	2	bdl	0.2	2.1	1022.0	422.6	222	159
972105-2	KT	MC-04-09	62.5	zoned	grain	2	bdl	0.1	4.8	841.8	447.3	1270	388
972105-3	KT	MC-04-09	62.5	zoned	grain	0.75	bdl	bdl	13.2	63.8	446.0	645	2017
972105-4	KT	MC-04-09	62.5	1	grain	0.25	bdl	0.6	26.7	550.6	287.9	1412	5149
972105-5	KT	MC-04-09	62.5	zoned	S	0.25	bdl	0.1	1.6	160.4	879.5	283	1822
972105-6	KT	MC-04-09	62.5	zoned	grain	0.45	bdl	0.1	6.4	1439.0	225.1	1116	1539
972105-7	KT	MC-04-09	62.5	zoned	grain	0.3	0.2	0.2	6.5	379.2	677.4	549	756
972105-8	KT	MC-04-09	62.5	zoned	grain	0.4	bdl	0.3	11.3	570.1	794.9	774	3758
972105-9	KT	MC-04-09	62.5	zoned	grain	0.45	bdl	-0.1	3.6	993.2	532.2	390	3296
972117-1	KT	MC-08-55	0	zoned	grain	0.9	1.7	1.6	6.7	594.6	383.8	42	108
972117-2	KT	MC-08-55	0	zoned	S	0.9	bdl	0.6	2.5	295.2	338.2	11	7
972117-3	KT	MC-08-55	0	zoned	grain	0.3	1.1	1.0	9.7	272.9	348.1	90	6061

	71Ga	72Ge	75As	82Se	107Ag	111Cd	115In	118Sn	121Sb	125Te	197Au	205Tl	208Pb	209Bi
972153-2	0.5	1.4	5.0	416.6	0.7	0.1	0.1	0.4	0.3	2.9	0.1	0.0	29	18.6
972153-3	0.1	1.5	6.1	408.9	0.4	0.1	0.2	0.3	0.1	0.6	0.0	0.0	30	2.6
972153-4	0.1	1.1	3.0	494.1	0.7	0.1	0.1	0.4	0.1	0.4	0.0	0.0	44	1.5
972153-5	0.3	0.9	37.2	352.2	0.5	0.1	0.4	0.4	0.2	2.1	0.0	0.0	36	10.8
972153-6	0.5	1.2	9.4	344.1	1.1	0.1	0.3	0.4	0.5	3.1	0.0	0.1	27	16.7
972153-7	0.1	1.5	21.3	351.9	0.7	0.1	0.1	0.4	0.4	3.6	0.1	0.0	63	18.5
972153-8	0.2	1.0	124.4	311.6	0.3	0.1	0.1	0.1	0.2	1.0	0.0	0.0	22	5.8
972153-9	0.5	1.4	5.0	259.5	0.6	0.1	0.2	0.4	0.2	2.6	0.1	0.0	64	10.8
972153-10	0.3	1.3	18.4	130.5	0.6	0.1	0.4	0.5	0.3	1.9	0.0	0.0	40	8.2
972153-11	0.1	1.5	1.5	1059.0	1.7	0.2	0.3	0.7	0.1	0.4	0.0	0.0	138	1.1
972153-12	0.1	1.1	4.9	324.7	1.2	0.3	1.4	1.1	0.3	3.2	0.1	0.0	52	12.6
972153-13	2.1	1.4	16.0	296.5	0.6	0.2	0.2	0.7	0.4	5.1	0.1	0.0	48	20.3
74-1	2.1	1.6	234.1	259.7	6.9	0.1	0.0	1.5	1.2	147.7	0.4	0.1	64	34.9
74-2	5.7	2.7	251.1	141.6	2.0	0.4	0.3	0.5	1.2	83.5	0.1	0.0	90	45.4
74-3	1.4	1.3	205.7	123.9	0.4	0.2	0.0	1.3	3.1	23.9	0.1	0.1	66	12.3
74-4	0.1	1.1	1233.0	238.1	21.0	0.1	0.0	0.4	0.1	230.7	0.5	0.0	143	53.0
74-5	0.4	1.4	516.1	203.0	14.1	0.3	0.1	0.6	0.8	330.6	0.1	0.1	300	61.3
74-6	0.3	1.4	985.5	186.2	12.7	0.1	0.0	0.3	0.4	175.5	0.3	0.0	90	66.0
74-7	4.1	2.0	468.7	270.9	2.0	0.2	0.1	3.4	4.1	183.0	0.2	0.1	163	47.3
89-1	4.4	1.7	818.5	53.5	6.4	0.6	12.7	392.7	0.8	10.9	0.2	0.0	25	52.2
89-2	1.0	1.4	477.4	64.6	7.3	0.3	1.1	41.3	1.0	14.8	0.5	0.0	89	48.8
89-3	0.8	1.3	424.0	60.6	5.2	0.0	0.0	0.7	1.2	10.2	0.2	0.0	127	46.6
89-4	0.2	1.2	481.1	117.1	160.0	0.3	2.3	12.5	5.1	102.0	0.3	6.0	1109	1065.0
89-5	0.1	1.1	709.0	29.0	7.2	0.3	0.9	3.8	0.7	6.7	0.1	0.0	23	72.3
89-6	0.1	1.0	403.8	93.2	103.2	0.4	1.9	7.9	5.3	69.5	0.4	5.8	828	892.9
89-7	0.2	1.1	418.1	29.3	0.5	0.1	0.1	1.1	0.2	1.6	0.0	0.0	3	8.6
89-8	1.2	1.3	222.5	25.5	3.3	0.2	0.6	4.1	0.5	4.0	0.1	0.0	23	39.1
89-9	0.1	0.9	305.4	28.4	4.6	0.4	1.2	1.2	0.5	4.9	0.1	0.0	13	104.2
89-10	0.6	1.3	460.1	34.8	2.4	0.1	0.2	1.1	0.3	6.8	0.1	0.0	19	84.4
972105-1	0.1	1.3	293.2	110.7	3.8	0.6	0.2	5.6	0.4	3.6	0.0	0.1	4	4.9
972105-2	0.2	1.0	603.5	121.4	6.4	1.5	0.5	1.9	4.3	18.0	0.2	3.1	52	50.6
972105-3	0.1	0.9	356.7	87.4	2.5	7.7	1.2	26.1	0.8	6.5	0.3	0.0	11	11.6
972105-4	1.2	1.7	842.9	43.3	37.2	22.3	5.3	44.2	60.3	77.9	0.5	13.2	304	210.3
972105-5	0.1	1.1	502.0	120.7	0.7	6.2	1.1	1.1	0.2	6.5	0.1	0.0	6	6.0
972105-6	0.1	0.9	339.5	135.7	3.6	7.6	1.0	2.0	0.9	7.4	0.1	0.0	14	15.4
972105-7	3.1	1.3	612.8	221.7	1.9	2.7	0.5	3.9	0.6	12.4	0.1	0.0	15	14.9
972105-8	1.8	1.7	791.3	232.4	6.7	15.8	2.1	3.3	1.9	15.6	0.2	0.1	23	24.3
972105-9	0.4	1.3	405.3	194.0	16.1	12.9	1.3	3.0	0.7	20.7	0.1	0.0	11	15.3
972117-1	1.0	1.6	1401.0	102.7	6.0	0.5	0.0	2.3	3.1	67.4	0.3	0.1	42	14.9
972117-2	0.3	1.3	1408.0	233.9	0.8	0.1	0.0	0.8	1.4	79.0	0.1	0.0	19	5.9
972117-3	0.8	1.1	919.8	84.8	13.0	27.1	2.1	2.1	2.3	54.4	0.2	0.1	47	17.3

	Host	Hole ID	Distance	Type	Analysis	Size	51V	52Cr	55Mn	59Co	60Ni	65Cu	66Zn
972117-4	KT	MC-08-55	0	zoned	grain	0.6	bdl	106.9	1.7	30.0	218.1	91	98
972117-5	KT	MC-08-55	0	zoned	grain	1.1	bdl	1.0	4.3	344.9	281.7	32	4510
972117-6	KT	MC-08-55	0	zoned	grain	0.6	3.3	2.8	5.5	621.0	341.3	137	1011
972117-7	KT	MC-08-55	0	zoned	grain	0.6	bdl	0.4	1.3	356.5	261.4	47	3
972117-8	KT	MC-08-55	0	zoned	grain	0.6	4.3	4.0	4.4	813.9	201.0	31	62
972127-1	KT	BRC-97-15	1500	zoned	grain	0.8	bdl	0.3	16.3	5075.0	122.8	7	303
972127-2	KT	BRC-97-15	1500	zoned	grain	1.5	bdl	0.5	29.2	3783.0	236.4	8	1528
972127-3	KT	BRC-97-15	1500	zoned	grain	0.5	4.6	1.8	561.9	1032.0	181.2	13	47
972127-4	KT	BRC-97-15	1500	zoned	grain	1.6	bdl	0.6	2328.0	1359.0	298.0	28	900
972127-5	KT	BRC-97-15	1500	zoned	grain	0.6	bdl	0.3	24.0	3155.0	181.2	28	16840
972127-6	KT	BRC-97-15	1500	zoned	grain	2	0.0	bdl	388.8	216.6	256.7	1	15
972127-7	KT	BRC-97-15	1500	zoned	grain	2	0.7	1.2	54.6	1346.0	365.5	3	5503
972127-8	KT	BRC-97-15	1500	zoned	grain	2	bdl	0.5	15.5	1345.0	274.0	2	1845
96-1	KT	MC-07-28	0	1	grain	1	0.3	0.9	108.6	654.4	506.3	2313	3082
96-2	KT	MC-07-28	0	1	S	1	0.0	0.3	255.0	602.3	495.1	2953	363
96-3	KT	MC-07-28	0	1	grain	0.5	0.2	0.3	227.3	796.3	645.0	4185	420
96-4	KT	MC-07-28	0	1	grain	0.5	0.3	0.3	142.0	667.2	539.1	3996	5278
96-5	KT	MC-07-28	0	1	grain	0.3	0.4	0.3	136.8	794.5	587.5	1135	423
96-6	KT	MC-07-28	0	1	S	0.9	bdl	0.4	609.1	1050.0	919.0	5788	550
96-7	KT	MC-07-28	0	1	S	2.12	3.3	0.5	38.7	677.1	290.4	4203	13640
96-8	KT	MC-07-28	0	1	S	2.12	4.5	0.5	32.5	668.2	249.2	6305	3975
96-9	KT	MC-07-28	0	1	S	2.12	2.7	0.3	6.0	648.5	176.0	832	9857
96-10	KT	MC-07-28	0	1	?	?	4.7	0.8	19.7	744.8	286.0	2923	8581
972167-1	KT	MC-07-25	0	5	grain	1.6	bdl	bdl	5.8	154.0	273.2	40	5
972167-2	KT	MC-07-25	0	5	L	1.6	bdl	bdl	0.3	24.2	204.9	1	1
972167-3	KT	MC-07-25	0	5	grain	1.75	0.2	bdl	202.9	44.5	257.7	122	35
972167-4	KT	MC-07-25	0	5	grain	1.75	0.1	bdl	18.7	66.1	227.8	2	7
972167-5	KT	MC-07-25	0	5	grain	0.75	bdl	bdl	0.5	257.4	314.6	99	804
972167-6	KT	MC-07-25	0	5	grain	0.7	bdl	bdl	5.8	1390.0	170.0	12	3241
972167-7	KT	MC-07-25	0	5	grain	0.4	bdl	0.2	5.0	796.9	305.8	30	18470
972167-8	KT	MC-07-25	0	5	grain	0.3	bdl	bdl	77.9	1177.0	207.8	6	756
77-1	KT	MC-04-04	0	zoned	grain	0.5	2.5	2.9	43.1	1775.0	440.1	20	9
77-2	KT	MC-04-04	0	zoned	grain	0.6	2.0	3.0	13.3	2305.0	700.1	9	80
77-3	KT	MC-04-04	0	zoned	grain	0.5	2.1	2.2	2.6	6220.0	975.1	15	180
77-4	KT	MC-04-04	0	zoned	grain	0.25	0.4	1.4	0.6	1172.0	2410.0	2	1
77-5	KT	MC-04-04	0	zoned	grain	1	0.4	0.2	1.0	1754.0	540.1	9	2
77-6	KT	MC-04-04	0	zoned	grain	0.55	3.3	2.9	18.9	1629.0	376.1	19	5
77-7	KT	MC-04-04	0	zoned	grain	0.4	2.1	1.3	14.6	1197.0	1184.0	5	4
87-1	KT	BRC-07-51	12.5	zoned	grain	2.75	bdl	bdl	41.5	121.1	232.3	544	25
87-2	KT	BRC-07-51	12.5	zoned	grain	2.75	bdl	bdl	1526.0	248.9	183.8	164	59
87-3	KT	BRC-07-51	12.5	zoned	L	2.75	3.7	bdl	17.3	65.9	154.8	52	5

	71Ga	72Ge	75As	82Se	107Ag	111Cd	115In	118Sn	121Sb	125Te	197Au	205Tl	208Pb	209Bi
972117-4	0.1	0.9	635.9	194.0	220.9	0.5	0.0	0.3	1.5	320.4	0.1	0.0	199	28.0
972117-5	0.2	1.5	968.5	289.0	1.8	15.8	1.3	0.7	1.0	78.2	0.1	0.0	28	7.2
972117-6	0.9	1.3	1527.0	101.9	2.7	4.2	0.3	1.7	1.9	43.9	0.1	0.1	19	5.8
972117-7	0.1	1.0	927.6	334.0	0.6	0.1	0.0	0.5	0.9	100.0	0.1	0.0	18	5.5
972117-8	1.4	1.3	1699.0	99.0	1.4	0.3	0.0	2.3	2.5	60.6	0.2	0.1	20	4.8
972127-1	0.3	1.5	510.7	89.1	19.8	1.0	0.1	0.3	0.4	83.8	2.0	0.0	74	3.6
972127-2	0.1	1.8	485.2	106.0	108.0	5.3	0.2	0.7	0.5	2925	1.9	0.0	2731	179.1
972127-3	4.1	2.4	7.1	169.4	4.0	0.1	0.0	0.5	1.4	168.2	0.1	0.0	799	17.7
972127-4	1.1	2.2	162.6	154.2	28.6	2.8	0.1	1.4	0.7	91.9	1.1	0.0	424	11.3
972127-5	0.2	1.3	337.3	508.5	4791.0	58.4	1.9	0.8	2.8	72770	0.3	0.8	61640	4221.0
972127-6	0.3	1.7	72.0	145.5	0.1	0.1	0.0	0.3	0.1	15.4	0.0	0.0	4	0.7
972127-7	0.9	2.6	223.1	64.7	0.3	18.6	0.7	2.4	0.2	4.9	0.0	0.0	8	1.3
972127-8	0.2	2.1	236.5	62.8	0.1	6.5	0.2	0.7	0.0	1.2	0.0	0.0	2	0.2
96-1	0.5	1.9	1715.0	61.0	102.4	11.0	0.8	8.1	88.1	134.3	1.6	121.9	364	127.1
96-2	0.2	1.6	1401.0	55.2	137.5	1.1	0.4	9.4	95.6	176.2	2.9	95.5	304	140.5
96-3	0.5	1.5	1999.0	84.5	566.1	1.3	0.7	21.8	148.2	563.1	1.6	70.2	704	233.1
96-4	0.5	1.6	1512.0	76.8	250.1	16.8	1.2	17.5	93.4	225.8	1.9	68.1	397	142.0
96-5	0.6	1.6	1550.0	85.8	660.2	1.0	0.3	59.4	127.7	520.0	1.5	14.7	540	213.8
96-6	0.3	1.3	2296.0	98.4	577.8	1.6	0.8	28.8	243.5	562.5	3.0	12.0	1050	376.8
96-7	1.5	1.5	2922.0	98.0	135.1	51.2	3.1	20.0	91.7	151.0	1.4	27.0	576	99.3
96-8	1.9	1.7	2382.0	76.8	102.7	13.3	1.2	14.1	66.8	124.0	0.9	18.2	406	69.3
96-9	1.3	1.3	874.0	33.0	52.9	35.9	1.5	7.1	39.4	51.5	0.4	4.5	135	34.4
96-10	2.1	1.5	1909.0	73.4	143.3	30.7	1.8	16.2	64.7	128.8	1.5	19.1	359	70.2
972167-1	0.1	2.0	671.3	165.3	239.9	0.1	0.0	0.3	0.2	292.4	5.0	0.0	66	4.9
972167-2	0.0	1.1	622.9	164.1	0.0	0.1	0.0	0.1	0.0	0.1	0.0	0.0	0	0.0
972167-3	0.3	1.6	557.4	123.8	0.9	0.1	0.1	1.0	0.3	2.2	0.0	0.0	4	1.1
972167-4	0.2	1.2	679.7	156.1	0.8	0.0	0.0	0.2	0.1	1.4	0.0	0.0	1	0.2
972167-5	0.0	1.3	1082.0	139.8	1.3	2.8	0.3	0.2	0.2	2.5	0.0	0.0	1	1.2
972167-6	0.1	1.0	884.1	68.6	42.8	13.3	1.7	53.8	0.8	53.1	0.1	0.0	5	6.7
972167-7	0.0	1.2	1015.0	136.4	1302.0	58.4	5.0	0.3	1.9	1328.0	0.7	0.0	32	22.1
972167-8	0.1	1.4	852.2	74.9	371.3	2.1	0.2	3.4	1.1	609.1	6.2	0.0	54	23.0
77-1	0.7	1.5	1870.0	150.2	35.6	0.1	0.0	3.6	9.9	48.4	0.9	0.1	76	21.0
77-2	0.4	1.0	2526.0	119.1	4.8	0.2	0.0	2.4	7.7	12.4	0.1	0.1	49	12.8
77-3	0.3	1.3	5415.0	117.4	81.9	0.5	0.1	5.2	9.5	85.8	0.5	0.1	58	13.5
77-4	0.0	0.9	4481.0	109.7	3.1	0.0	0.0	3.0	1.2	4.1	0.0	0.0	14	3.4
77-5	0.1	1.4	2071.0	138.8	44.7	0.1	0.0	4.0	1.8	42.6	0.5	0.0	22	5.4
77-6	0.7	1.1	1692.0	98.8	24.9	0.0	0.0	3.3	8.7	32.4	0.3	0.2	130	23.9
77-7	0.4	0.9	2427.0	104.0	1.1	0.1	0.0	2.1	8.6	9.3	0.0	0.1	38	7.5
87-1	0.1	1.2	26.0	285.5	9.4	0.2	0.1	0.4	0.5	31.1	0.1	0.0	5	11.1
87-2	0.0	1.1	16.6	237.7	11.3	0.3	0.0	0.4	0.1	19.9	0.1	0.0	2	5.8
87-3	0.1	0.8	10.5	276.0	21.8	0.0	0.0	0.2	0.1	29.5	0.5	0.0	1	1.0

	Host	Hole ID	Distance	Type	Analysis	Size	51V	52Cr	55Mn	59Co	60Ni	65Cu	66Zn
87-4	KT	BRC-07-51	12.5	zoned	grain	0.8	2.9	bdl	333.2	649.7	166.8	58	8
87-5	KT	BRC-07-51	12.5	zoned	grain	0.8	bdl	bdl	5.2	451.0	393.5	4	2
87-6	KT	BRC-07-51	12.5	zoned	grain	0.75	bdl	bdl	179.9	377.5	331.7	70	3
87-7	KT	BRC-07-51	12.5	1	grain	0.5	bdl	bdl	4.2	62.2	286.2	1404	4
87-8	KT	BRC-07-51	12.5	1	S	0.25	bdl	bdl	3.9	53.7	256.8	1437	3
92-1	KT	BRC-08-73	25	zoned	grain	0.3	bdl	bdl	11.4	7646.0	543.3	437	12
92-2	KT	BRC-08-73	25	zoned	grain	1.1	0.0	bdl	14.8	14870.0	188.2	879	17
92-3	KT	BRC-08-73	25	zoned	grain	0.5	0.4	bdl	22.5	7043.0	573.2	887	47
92-4	KT	BRC-08-73	25	zoned	grain	0.12	7.9	3.7	377.5	409.0	349.4	1054	558
92-5	KT	BRC-08-73	25	zoned	grain	0.5	4.7	1.5	52.8	219.1	91.6	365	23
92-6	KT	BRC-08-73	25	zoned	L	2	0.7	0.1	11.4	162.1	883.0	3621	43
92-7	KT	BRC-08-73	25	zoned	grain	2	1.0	0.8	12.5	177.9	108.4	404	4
92-8	KT	BRC-08-73	25	zoned	grain	0.9	2.5	0.5	42.9	57.0	216.0	211	30
92-9	KT	BRC-08-73	25	zoned	grain	0.9	3.7	0.3	80.7	121.0	650.0	34	23
92-10	KT	BRC-08-73	25	zoned	grain	0.9	4.0	bdl	84.3	58.4	71.4	4913	24
972110-1	KT	MC-07-24	93.75	5	grain	0.4	bdl	bdl	8.1	176.4	115.4	114	497
972110-2	KT	MC-07-24	93.75	5	grain	1.25	0.3	bdl	44.9	92.3	104.4	306	985
972110-3	KT	MC-07-24	93.75	5	grain	1.9	bdl	bdl	49.1	59.2	145.6	1285	18
972110-4	KT	MC-07-24	93.75	5	grain	0.6	bdl	bdl	27.9	172.2	166.6	258	227
972110-5	KT	MC-07-24	93.75	5	grain	0.3	0.5	0.1	33.3	187.1	89.3	416	1205
972110-6	KT	MC-07-24	93.75	5	grain	2.4	bdl	bdl	44.9	87.4	223.8	641	33
972110-7	KT	MC-07-24	93.75	5	grain	0.3	bdl	bdl	21.2	119.3	95.5	114	431
972110-8	KT	MC-07-24	93.75	5	grain	1.1	0.3	bdl	60.0	179.8	170.5	789	31
972110-9	KT	MC-07-24	93.75	5	grain	0.45	0.5	0.3	142.5	90.5	61.8	775	2120
MAT-07-31-1	KT	BRC-07-57	12.5	zoned	L	3.5	1.7	bdl	8.5	412.2	164.2	1024	1
MAT-07-31-2	KT	BRC-07-57	12.5	zoned	L	3.5	bdl	bdl	1.0	454.0	144.9	215	1339
MAT-07-31-3	KT	BRC-07-57	12.5	zoned	L	3.5	1.1	bdl	52.9	1082.0	228.9	983	23
MAT-07-31-4	KT	BRC-07-57	12.5	zoned	grain	0.5	12.5	10.1	140.2	544.3	308.5	12	284
MAT-07-31-5	KT	BRC-07-57	12.5	zoned	grain	1.1	0.0	bdl	12.5	375.9	547.9	84	2598
MAT-07-31-6	KT	BRC-07-57	12.5	zoned	grain	0.5	0.2	0.2	17.1	382.4	1447.0	4	13
MAT-07-31-7	KT	BRC-07-57	12.5	zoned	grain	1	bdl	-0.1	1.0	453.8	499.8	9	8
MAT-07-31-8	KT	BRC-07-57	12.5	zoned	grain	0.25	1.1	bdl	20.6	278.8	231.9	4	551
972116-1	KT	MC-08-55	0	1	grain	1.25	bdl	1.1	959.7	382.4	431.0	82320	7121
972116-2	KT	MC-08-55	0	1	S	1.25	bdl	0.1	95.3	568.6	328.6	1673	1450
972116-3	KT	MC-08-55	0	1	S	1.25	bdl	0.4	71.4	389.8	313.7	353	242
972116-4	KT	MC-08-55	0	1	S	0.1	5.8	0.3	28.8	260.4	331.5	45	1213
972116-5	KT	MC-08-55	0	1	grain	1	bdl	0.2	44.5	505.2	352.9	463	191
972116-6	KT	MC-08-55	0	1	S	1	1.3	0.1	76.9	554.1	365.0	531	331
972116-7	KT	MC-08-55	0	1	S	1	0.8	0.6	47.3	631.9	321.8	2789	118
972116-8	KT	MC-08-55	0	1	S	1	bdl	0.4	140.1	473.2	379.2	1487	1591
972116-9	KT	MC-08-55	0	1	S	1	bdl	0.4	308.1	581.7	331.5	239	1950

	71Ga	72Ge	75As	82Se	107Ag	111Cd	115In	118Sn	121Sb	125Te	197Au	205Tl	208Pb	209Bi
87-4	3.0	2.4	42.0	313.2	142.3	0.1	0.0	0.3	0.8	255.1	4.7	0.0	48	63.6
87-5	0.1	0.8	112.4	419.3	18.2	0.1	0.0	0.2	0.2	50.4	0.1	0.0	3	1.9
87-6	0.1	1.0	117.1	453.6	280.6	0.0	0.1	0.2	0.5	377.6	25.9	0.0	5	4.0
87-7	0.0	0.9	0.4	188.3	86.7	0.5	0.1	0.7	6.9	1.7	0.0	125.9	724	2.0
87-8	0.1	1.3	0.9	547.1	150.8	0.3	0.9	338.7	9.3	0.9	0.0	66.6	1634	9.3
92-1	0.1	1.3	626.5	85.6	1.5	0.1	0.1	0.7	0.4	10.1	0.1	0.0	9	6.4
92-2	0.2	1.2	201.0	82.7	7.9	0.1	0.1	0.7	0.7	33.1	0.1	0.0	16	26.0
92-3	0.5	1.3	404.3	74.1	7.4	0.4	0.2	1.9	0.9	28.0	0.2	0.0	27	24.1
92-4	5.5	1.4	765.3	68.2	4.7	2.4	0.4	5.4	1.2	16.2	0.1	0.1	27	15.4
92-5	1.4	1.1	3259.0	65.1	0.6	0.1	0.0	1.4	0.7	7.3	0.5	0.0	19	6.1
92-6	0.4	1.4	1879.0	89.2	8.3	0.4	0.2	0.9	0.6	15.6	0.3	0.0	33	13.7
92-7	0.4	1.2	2404.0	64.5	0.6	0.0	0.0	0.8	0.5	10.5	0.3	0.0	12	5.3
92-8	1.0	1.4	245.2	80.4	4.7	0.2	0.1	0.4	0.7	17.1	0.1	0.0	19	10.0
92-9	1.2	1.4	306.6	83.0	6.4	0.1	0.1	0.7	1.5	30.4	0.1	0.0	37	17.8
92-10	1.3	0.9	413.4	75.6	0.7	0.0	0.5	2.2	0.3	27.7	0.1	0.0	15	5.5
972110-1	0.2	1.2	37.8	67.5	0.1	1.9	0.0	0.2	0.0	0.2	0.0	0.0	1	0.2
972110-2	0.6	1.1	17.1	26.1	3.1	4.4	0.1	2.3	0.6	4.1	0.0	0.4	34	4.7
972110-3	0.3	1.5	15.3	46.0	5.5	0.1	0.0	1.5	1.2	0.4	0.0	8.1	33	0.5
972110-4	0.2	1.3	25.7	177.0	1.1	0.8	0.0	2.9	1.4	0.5	0.0	0.3	32	1.7
972110-5	0.7	1.0	30.3	146.3	4.0	4.7	0.2	4.1	1.9	0.7	0.0	1.6	85	2.2
972110-6	0.2	1.9	22.0	105.9	2.4	0.2	0.0	2.4	1.1	0.7	0.0	1.6	41	1.1
972110-7	0.1	1.0	15.6	70.8	1.4	1.7	0.1	1.5	0.2	1.1	0.0	0.5	26	3.6
972110-8	0.5	1.5	20.9	75.9	3.9	0.2	0.0	4.3	1.0	8.0	0.0	0.3	64	9.8
972110-9	0.8	0.6	41.9	80.0	1.6	9.9	0.3	1.3	0.2	1.0	0.0	0.1	11	2.2
MAT-07-31-1	0.6	1.5	2129.0	142.0	4.5	0.0	0.3	6.4	0.8	112.4	0.2	0.0	13	8.1
MAT-07-31-2	0.1	1.0	2062.0	189.9	2.7	6.1	0.5	0.4	0.8	307.2	0.1	0.0	138	6.2
MAT-07-31-3	0.8	1.3	2356.0	172.6	29.4	0.1	0.2	1.1	3.8	195.0	0.3	0.0	222	24.6
MAT-07-31-4	3.8	1.4	525.2	75.4	4.4	0.0	0.1	24.5	1.4	35.3	0.6	0.1	21	51.0
MAT-07-31-5	0.2	1.4	3556.0	117.0	8.3	12.1	0.8	0.8	1.1	85.7	2.5	0.0	62	11.8
MAT-07-31-6	0.1	0.9	479.8	136.8	1.3	0.0	0.0	0.4	0.3	333.7	0.1	0.0	1	250.5
MAT-07-31-7	0.1	1.2	7439.0	158.7	0.8	0.1	0.0	0.2	0.2	127.1	7.2	0.0	8	3.1
MAT-07-31-8	0.6	1.2	4.1	28.1	1.5	2.1	0.3	1.4	0.2	2.7	0.1	0.0	2	2.0
972116-1	0.9	2.9	885.2	104.0	39.4	20.8	14.8	1213.0	88.6	148.9	1.1	35.0	421	85.3
972116-2	0.4	2.2	1485.0	52.3	22.3	5.0	0.7	105.1	60.7	125.0	0.8	182.5	258	57.4
972116-3	0.2	1.6	1116.0	41.5	27.7	1.2	0.8	227.1	56.8	118.2	0.7	179.1	255	57.8
972116-4	2.7	1.0	715.9	99.4	8.7	3.9	0.3	25.7	3.5	11.0	0.2	1.3	37	4.6
972116-5	0.7	1.6	1771.0	33.3	17.9	0.7	0.1	6.3	80.3	143.5	1.0	149.0	419	83.2
972116-6	1.1	1.4	1620.0	28.2	24.2	1.7	0.2	6.7	104.1	202.9	1.2	163.8	547	109.6
972116-7	1.0	1.2	2457.0	43.2	15.0	0.4	0.3	11.9	43.4	65.0	0.7	110.3	238	42.4
972116-8	0.6	3.4	1333.0	43.6	52.4	6.2	0.4	16.1	67.5	161.3	1.4	156.7	294	65.1
972116-9	0.8	3.8	1220.0	51.9	51.5	7.1	0.3	4.9	43.6	107.8	0.6	56.1	221	43.3

	Host	Hole ID	Distance	Type	Analysis	Size	51V	52Cr	55Mn	59Co	60Ni	65Cu	66Zn
972116-10	KT	MC-08-55	0	1	grain	1	bdl	0.34	878.00	392.10	516.40	14180	90920
972116-11	KT	MC-08-55	0	1	grain	0.5	bdl	0.45	54.42	644.60	414.80	1001	1712
972165-1	MS	MC-07-25	0	2	grain	0.25	bdl	0.14	115.10	27.47	134.90	6883	532
972165-2	MS	MC-07-25	0	2	grain	0.5	bdl	0.04	45.75	11.35	150.60	4887	2124
972165-3	MS	MC-07-25	0	2	S	0.12	bdl	0.01	52.83	122.20	125.50	1184	12960
972165-4	MS	MC-07-25	0	2	S	0.25	bdl	0.21	37.27	6.25	134.80	3179	779
972165-5	MS	MC-07-25	0	2	grain	0.5	bdl	bdl	309.30	8.20	207.60	1405	80
972165-6	MS	MC-07-25	0	2	grain	1.1	bdl	0.07	220.30	10.80	196.90	4846	48
972165-7	MS	MC-07-25	0	2	S	0.5	bdl	0.33	122.50	6.49	172.00	154	24
972165-8	MS	MC-07-25	0	2	S	0.3	bdl	bdl	296.60	2.40	146.60	36	16
972165-9	MS	MC-07-25	0	2	S	0.2	bdl	0.34	362.80	21.83	213.90	501	50
972165-10	MS	MC-07-25	0	2	grain	0.5	bdl	0.05	783.60	13.80	241.40	363	74
972165-11	MS	MC-07-25	0	2	S	0.25	bdl	0.62	75.40	610.60	302.60	87	122000
972165-12	MS	MC-07-25	0	2	S	0.5	bdl	0.25	260.80	68.58	219.20	1491	725
95b-1	MS	MC-07-28	0	2	grain	1	bdl	-0.01	48.49	54.64	159.00	2047	1903
95b-2	MS	MC-07-28	0	2	S	1	bdl	bdl	118.70	12.72	122.30	165	3508
95b-3	MS	MC-07-28	0	2	grain	0.5	0.08	0.42	74.83	72.13	160.30	2721	12870
95b-4	MS	MC-07-28	0	2	grain	0.8	bdl	0.44	22.90	165.10	269.00	2691	4032
95b-6	MS	MC-07-28	0	2	grain	0.12	bdl	0.42	10.61	208.30	195.50	1279	1892
95b-7	MS	MC-07-28	0	2	grain	0.5	bdl	0.45	60.96	188.10	314.10	12300	417
95b-8	MS	MC-07-28	0	2	S	0.4	bdl	0.33	45.32	120.00	244.20	450	127
95b-9	MS	MC-07-28	0	2	grain	0.8	bdl	0.20	10.60	52.84	150.80	1676	296
95b-10	MS	MC-07-28	0	2	S	0.8	bdl	0.39	14.33	60.89	204.50	11140	82
95b-11	MS	MC-07-28	0	2	S	0.3	bdl	0.34	61.36	243.20	360.50	5238	799
95b-12	MS	MC-07-28	0	2	S	0.2	bdl	0.26	4.20	24.82	180.80	1168	1276
972160-1	MS	MC-08-62	0	3	grain	1.75	bdl	bdl	32.73	312.40	86.01	787	641
972160-2	MS	MC-08-62	0	3	S	0.55	bdl	bdl	6.82	577.60	49.44	78	158
972160-3	MS	MC-08-62	0	3	S	0.55	bdl	bdl	114.70	296.90	63.63	1076	2
972160-4	MS	MC-08-62	0	3	grain	0.6	bdl	bdl	64.82	973.30	89.00	1850	13930
972160-5	MS	MC-08-62	0	3	grain	0.5	bdl	bdl	5.29	213.40	49.71	2425	233
972160-6	MS	MC-08-62	0	3	grain	0.7	bdl	bdl	4.33	229.90	44.37	493	496
972160-7	MS	MC-08-62	0	3	grain	0.2	bdl	bdl	35.06	267.80	102.70	896	1962
972160-8	MS	MC-08-62	0	3	S	0.15	bdl	bdl	9.40	525.90	100.60	1105	5713
972160-9	MS	MC-08-62	0	3	grain	0.5	bdl	bdl	3.16	238.70	47.54	757	3702
972160-10	MS	MC-08-62	0	3	grain	0.6	bdl	bdl	2.52	225.70	98.86	3	1725
972160-11	MS	MC-08-62	0	3	grain	0.5	bdl	bdl	0.46	112.70	97.59	2	164
972160-12	MS	MC-08-62	0	3	grain	0.4	bdl	bdl	20.07	205.30	52.72	19	17000
972160-13	MS	MC-08-62	0	3	grain	0.5	bdl	-0.08	0.36	438.10	103.70	22	62
972162-1	WLR	MC-08-62	0	zoned	grain	2.9	bdl	0.16	47.15	250.30	320.60	154	465
972162-2	WLR	MC-08-62	0	zoned	L	2.9	bdl	0.16	1.74	12.69	248.40	1	2
972162-3	WLR	MC-08-62	0	zoned	S	2.9	bdl	0.18	5.57	504.40	203.70	91	157

	71Ga	72Ge	75As	82Se	107Ag	111Cd	115In	118Sn	121Sb	125Te	197Au	205Tl	208Pb	209Bi
972116-10	0.6	2.6	1067.0	83.3	51.9	298.4	14.0	248.5	95.2	166.7	1.4	39.4	513	99.2
972116-11	0.7	3.6	1651.0	65.5	25.9	6.4	0.8	161.4	66.9	145.1	0.9	195.8	331	70.8
972165-1	1.4	2.5	876.8	6.8	17.6	1.4	0.0	1.4	9.8	6.3	0.5	89.8	88	0.5
972165-2	0.4	1.5	823.9	5.0	20.9	5.7	0.0	1.7	7.9	4.0	0.2	53.7	96	0.4
972165-3	2.8	4.8	555.1	15.8	8.5	30.9	0.0	2.5	6.0	1.9	0.3	62.4	62	0.1
972165-4	0.2	1.2	1003.0	3.1	22.0	2.1	0.0	0.6	6.6	3.7	0.2	71.5	53	0.3
972165-5	0.1	2.4	283.1	2.1	15.0	0.2	0.0	0.7	14.3	14.1	0.7	102.4	75	1.0
972165-6	0.3	2.5	277.7	3.4	16.0	0.2	0.0	1.9	15.7	13.5	0.7	80.8	75	1.1
972165-7	0.0	3.2	326.3	2.2	7.8	0.0	0.0	0.3	12.9	15.8	0.4	74.4	59	1.0
972165-8	0.1	1.8	114.9	1.8	0.7	0.1	0.0	0.2	1.8	1.4	0.1	29.7	3	0.1
972165-9	0.1	3.9	357.5	2.3	4.6	0.1	0.0	0.5	10.0	5.2	0.5	366.1	47	0.5
972165-10	0.1	4.3	381.9	2.8	5.0	0.2	0.0	0.5	8.3	5.0	0.2	410.3	45	0.5
972165-11	0.6	1.9	329.3	29.3	13.1	291.9	0.3	1.4	6.7	3.4	0.0	11.7	28	0.5
972165-12	0.1	2.2	807.0	3.9	31.0	1.3	0.0	1.6	30.7	24.2	0.7	79.3	274	1.9
95b-1	2.5	1.5	259.9	3.4	18.6	4.9	0.1	5.7	40.5	12.3	0.4	61.2	301	23.9
95b-2	0.0	1.2	498.2	2.2	3.5	10.6	0.1	2.4	5.7	1.6	0.3	430.9	73	2.4
95b-3	2.9	3.5	245.7	6.0	35.1	35.2	0.3	31.7	32.3	10.2	0.4	64.7	257	19.3
95b-4	0.8	1.3	453.5	4.7	22.7	9.6	0.6	175.5	73.1	18.9	0.6	332.6	426	49.0
95b-6	0.3	1.4	669.1	22.5	22.1	5.1	0.1	3.9	35.6	3.2	0.3	322.8	235	8.6
95b-7	0.1	2.1	640.6	9.7	46.1	1.1	0.5	105.4	97.8	27.9	0.6	469.3	324	68.8
95b-8	0.1	2.8	681.4	3.0	22.3	0.2	0.1	30.3	58.2	16.8	0.5	619.9	189	41.1
95b-9	0.3	0.9	568.4	3.2	12.7	0.8	0.0	7.2	10.7	3.7	0.8	11.7	178	7.7
95b-10	5.4	1.0	485.1	8.3	19.3	0.4	0.3	72.1	19.8	8.7	0.5	14.4	160	16.6
95b-11	3.0	1.3	695.5	8.3	63.8	2.2	1.7	536.0	161.1	36.8	0.9	265.4	538	101.2
95b-12	0.1	1.0	405.7	2.8	5.1	4.0	0.0	3.4	10.0	4.0	0.4	15.5	53	7.6
972160-1	0.4	1.5	78.7	116.5	13.0	2.1	0.6	16.8	4.7	2.0	0.2	5.4	246	16.7
972160-2	0.7	0.8	396.4	289.0	1766.0	13.1	0.4	71.8	800.3	9.5	0.2	0.5	91540	2077.0
972160-3	0.2	1.3	26.7	143.6	11.5	0.0	0.1	0.5	1.9	0.6	0.0	2.3	273	11.8
972160-4	14.7	1.8	673.4	292.4	108.9	49.2	6.5	21.3	19.1	11.2	0.4	0.1	20460	383.7
972160-5	1.0	1.3	83.8	19.4	20.0	0.9	1.1	28.0	5.8	1.9	0.1	1.3	949	34.0
972160-6	1.1	2.0	323.1	11.0	16.6	1.7	0.3	2.5	12.9	0.8	0.2	0.6	1287	23.3
972160-7	0.5	1.7	146.7	45.3	35.3	6.5	1.0	19.7	10.7	2.3	0.2	0.2	4733	83.1
972160-8	21.7	2.6	316.9	19.0	36.0	20.0	2.5	12.1	15.4	1.4	0.1	0.2	3106	48.4
972160-9	0.4	1.4	105.7	16.8	22.9	11.7	1.6	11.9	8.7	1.9	0.1	0.3	1963	48.9
972160-10	0.3	1.3	684.6	12.4	0.8	4.9	0.6	0.2	0.7	0.1	0.0	bdl	43	1.0
972160-11	0.1	1.3	846.6	14.6	0.3	0.5	0.1	0.2	0.8	0.1	0.0	0.1	9	0.9
972160-12	2.9	1.1	547.4	68.8	624.2	48.2	6.8	24.4	326.1	0.2	0.1	0.1	26080	607.7
972160-13	0.0	1.4	1413.0	16.4	0.2	0.3	0.0	1.1	0.1	0.2	0.0	bdl	1	0.1
972162-1	0.2	2.2	74.9	120.9	4.7	2.1	0.3	2.1	2.6	5.4	0.1	0.1	28	1.7
972162-2	0.0	1.2	663.2	99.3	0.0	0.1	0.0	0.3	0.0	0.5	0.0	0.0	1	0.3
972162-3	0.1	1.2	8.5	288.9	7.5	0.6	0.0	3.4	4.1	9.9	0.2	0.3	63	2.8

	Host	Hole ID	Distance	Type	Analysis	Size	51V	52Cr	55Mn	59Co	60Ni	65Cu	66Zn
972162-4	WLR	MC-08-62	0	zoned	S	2.9	bdl	bdl	1.90	196.10	172.70	41	49
972162-5	WLR	MC-08-62	0	1	grain	0.5	1.81	0.42	179.40	313.80	306.70	1427	19400
972162-6	WLR	MC-08-62	0	1	grain	1.5	0.45	0.20	410.00	351.90	305.40	1171	14340
972162-7	WLR	MC-08-62	0	1	S	1	1.53	0.71	321.80	322.40	233.30	1142	30810
972162-8	WLR	MC-08-62	0	zoned	grain	0.25	0.28	0.54	29.48	165.30	130.00	1350	1008
972162-9	WLR	MC-08-62	0	zoned	grain	0.3	bdl	0.50	57.97	445.00	310.00	565	6495
972162-10	WLR	MC-08-62	0	zoned	grain	0.45	0.71	0.73	78.28	148.80	468.20	1655	2878
972168-1	WLR	MC-07-25	0	3	grain	1.5	bdl	0.12	6.35	151.80	150.30	167	8
972168-2	WLR	MC-07-25	0	3	grain	0.4	bdl	bdl	20.38	248.80	142.30	460	18
972168-3	WLR	MC-07-25	0	3	grain	1.5	bdl	0.13	15.80	648.10	258.80	672	85
972168-4	WLR	MC-07-25	0	3	grain	0.4	bdl	0.27	45.34	149.50	134.20	1605	69
972168-5	WLR	MC-07-25	0	3	grain	2	bdl	0.24	4.61	471.20	203.80	413	50
972168-6	WLR	MC-07-25	0	3	grain	3.4	bdl	bdl	7.59	926.10	402.20	1446	322
972168-7	WLR	MC-07-25	0	3	grain	1.1	bdl	0.48	3.14	764.30	193.50	351	54
972168-8	WLR	MC-07-25	0	3	grain	2	bdl	0.55	22.79	904.90	324.30	1921	514
972168-9	WLR	MC-07-25	0	3	grain	1.1	bdl	0.21	13.64	1025.00	133.40	1550	264
972168-10	WLR	MC-07-25	0	3	grain	0.6	bdl	0.36	54.35	604.80	193.50	3977	14
972168-11	WLR	MC-07-25	0	3	grain	1.3	bdl	0.44	49.96	1022.00	162.30	1518	252
972101-1	WLR	MC-07-28	25	zoned	grain	0.75	bdl	bdl	7.24	73.86	41.57	174	2
972101-2	WLR	MC-07-28	25	zoned	L	1.25	bdl	bdl	3.58	59.61	38.85	187	1
972101-3	WLR	MC-07-28	25	zoned	L	1.25	bdl	bdl	54.05	220.60	44.45	48	11
972101-4	WLR	MC-07-28	25	zoned	L	1.25	bdl	bdl	0.35	78.49	40.54	2	0
972101-5	WLR	MC-07-28	25	zoned	grain	0.4	bdl	bdl	31.65	1270.00	57.42	2	7
972101-6	WLR	MC-07-28	25	zoned	grain	0.5	bdl	bdl	0.89	167.90	34.36	7	1
972101-7	WLR	MC-07-28	25	zoned	grain	1.25	bdl	bdl	3.89	236.80	56.84	124	2
972101-8	WLR	MC-07-28	25	zoned	grain	0.25	bdl	bdl	5.27	820.30	42.50	33	2
972101-9	WLR	MC-07-28	25	zoned	grain	0.7	bdl	bdl	0.61	237.40	226.10	103	1
972101-10	WLR	MC-07-28	25	zoned	grain	0.5	bdl	bdl	39.44	51.54	236.50	587	1373
972101-11	WLR	MC-07-28	25	zoned	grain	1	bdl	bdl	0.48	102.90	247.70	803	5
972130-1	FLT	BRC-95-11	1200	4	grain	0.25	bdl	0.34	5.80	252.50	916.50	6	3822
972130-2	FLT	BRC-95-11	1200	4	S	0.6	bdl	0.16	1.07	289.10	1264.00	53	5
972130-3	FLT	BRC-95-11	1200	4	grain	0.75	bdl	0.52	1.73	7429.00	929.10	15	68
972130-4	FLT	BRC-95-11	1200	4	S	0.5	bdl	0.40	1.10	801.30	1871.00	2	0
972130-5	FLT	BRC-95-11	1200	4	grain	0.6	bdl	0.51	1.90	1156.00	744.10	10	2
972130-6	FLT	BRC-95-11	1200	4	grain	0.75	bdl	0.32	32.95	#######	362.20	179	146
972130-7	FLT	BRC-95-11	1200	4	grain	0.5	bdl	0.70	1.75	#######	491.80	203	182
972120-1	FLT	MC-08-39	125	4	grain	0.5	bdl	bdl	1.57	2173.00	256.60	96	3893
972120-2	FLT	MC-08-39	125	4	grain	0.6	bdl	bdl	2.25	3788.00	266.20	169	518
972120-3	FLT	MC-08-39	125	4	S	0.2	bdl	0.01	2.26	5146.00	261.50	3	1028

	71Ga	72Ge	75As	82Se	107Ag	111Cd	115In	118Sn	121Sb	125Te	197Au	205Tl	208Pb	209Bi
972162-4	0.1	1.1	3.7	120.4	1.8	0.2	0.0	2.1	2.5	0.7	0.0	0.1	32	0.0
972162-5	1.8	5.7	1228.0	49.2	82.3	97.8	11.2	5.7	18.3	142.8	1.1	80.5	296	64.9
972162-6	0.9	3.2	1060.0	61.5	251.5	71.8	10.0	10.8	17.3	281.4	1.3	66.0	429	107.9
972162-7	1.6	4.1	834.6	60.8	147.3	158.9	18.3	21.3	20.3	204.5	1.8	21.0	238	87.5
972162-8	0.3	0.7	222.9	114.5	27.5	4.0	0.9	3.1	6.8	34.7	0.3	0.0	76	2.8
972162-9	0.3	1.5	337.1	128.1	8.7	21.1	3.7	2.3	2.8	13.3	0.2	0.6	35	5.2
972162-10	0.8	1.9	519.5	172.3	45.6	12.4	2.5	14.3	5.2	41.0	0.2	0.0	55	5.7
972168-1	0.5	2.5	44.7	21.2	14.4	0.1	0.2	0.6	2.1	1.9	0.2	22.7	33	73.0
972168-2	2.1	2.1	106.5	37.5	8.0	0.1	0.9	0.7	4.7	3.2	0.5	24.1	59	181.5
972168-3	1.6	2.4	108.0	93.9	9.8	0.4	1.2	1.1	15.5	3.9	0.6	58.7	100	210.5
972168-4	6.2	1.7	85.4	33.5	7.7	0.3	2.7	2.9	5.0	2.2	0.5	35.2	59	136.0
972168-5	0.5	1.7	62.9	99.9	5.2	0.5	0.9	1.1	1.7	2.0	0.2	0.0	50	89.4
972168-6	0.7	3.2	46.4	343.9	10.8	1.0	2.8	2.6	2.0	1.7	0.3	5.1	86	70.2
972168-7	0.4	1.7	70.8	155.9	9.3	0.3	1.0	1.0	2.0	2.5	0.4	0.3	121	102.5
972168-8	1.6	3.1	190.5	164.0	24.8	1.5	4.7	4.7	8.1	6.7	1.6	0.6	178	382.2
972168-9	1.1	1.7	55.8	224.2	8.0	0.6	3.3	7.3	1.4	1.5	0.3	0.5	51	75.2
972168-10	2.8	2.1	200.7	83.6	10.7	0.2	6.6	0.9	37.2	1.7	0.1	4.5	63	92.7
972168-11	5.6	2.5	126.0	142.9	9.9	0.8	3.3	7.1	14.1	2.2	0.3	3.3	68	124.6
972101-1	0.0	0.9	576.2	19.0	0.3	0.1	0.0	0.1	0.4	5.8	0.0	0.0	6	3.6
972101-2	0.0	0.8	506.7	38.3	0.4	0.0	0.0	0.1	0.3	3.5	0.0	0.0	5	3.2
972101-3	1.1	0.8	410.1	24.8	0.3	0.0	0.0	0.1	0.8	10.2	0.0	0.0	12	6.6
972101-4	0.0	0.8	516.5	20.8	0.1	0.0	0.0	0.1	0.4	6.2	0.0	0.0	5	0.3
972101-5	0.6	0.8	368.1	31.5	0.1	0.1	0.0	0.1	0.2	9.4	0.0	0.0	1	1.0
972101-6	0.0	0.7	187.2	29.4	0.2	0.1	0.0	0.1	0.5	6.8	0.0	0.0	4	1.6
972101-7	0.1	1.0	343.4	37.5	0.4	0.0	0.0	0.1	1.0	14.9	0.0	0.0	4	3.2
972101-8	0.1	0.9	301.5	28.7	0.6	0.0	0.0	0.1	3.3	4.0	0.0	0.0	8	3.7
972101-9	0.0	0.8	140.3	84.9	0.1	0.1	0.0	0.1	0.2	0.8	0.0	0.0	1	0.3
972101-10	0.7	0.7	180.9	69.9	1.1	22.7	3.6	0.3	1.0	1.7	0.0	0.0	6	4.8
972101-11	0.0	1.1	150.5	79.0	3.0	0.1	0.3	0.2	0.6	1.2	0.1	0.0	3	2.9
972130-1	0.1	1.5	532.3	226.1	1.8	10.9	0.5	0.2	0.2	8.6	0.0	0.0	4	0.7
972130-2	0.1	1.6	1742.0	204.3	8.9	0.2	0.0	0.3	0.1	18.3	0.2	0.0	32	0.4
972130-3	0.1	1.8	6833.0	179.5	61.2	0.3	0.0	0.4	0.2	73.7	0.1	0.0	84	1.2
972130-4	0.1	1.6	2593.0	276.2	0.0	0.1	0.0	0.3	0.0	3.1	0.0	0.0	0	0.1
972130-5	0.1	1.4	1216.0	180.4	3.7	0.2	0.0	0.2	0.2	9.1	0.0	0.0	881	2.6
972130-6	0.1	2.0	11530.0	109.8	780.0	0.6	0.1	0.4	1.2	883.2	36.0	0.1	34	3.8
972130-7	0.1	1.7	10950.0	148.2	314.8	0.7	0.0	0.3	0.3	407.3	24.7	0.0	57	2.0
972120-1	0.1	1.1	615.4	171.6	2.4	17.2	3.6	0.3	1.7	14.0	0.3	0.0	15	17.5
972120-2	0.1	0.9	1115.0	179.0	2.6	4.8	1.6	92.4	2.2	34.7	0.5	0.0	16	29.3
972120-3	0.1	0.9	2133.0	169.7	0.1	3.9	0.9	0.3	1.1	9.4	0.0	0.0	4	4.4

	Host	Hole ID	Distance	Type	Analysis	Size	51V	52Cr	55Mn	59Co	60Ni	65Cu	66Zn
972120-5	FLT	MC-08-39	125	4	grain	0.2	bdl	0.02	1.09	9681.00	118.90	2	1
972120-6	FLT	MC-08-39	125	4	grain	0.35	bdl	bdl	1.49	211.20	317.90	3	1
972120-7	FLT	MC-08-39	125	4	grain	1.2	bdl	bdl	99.95	4729.00	617.60	925	209
972120-8	FLT	MC-08-39	125	4	grain	1.2	bdl	0.05	32.81	3536.00	570.40	1593	1218
972120-9	FLT	MC-08-39	125	4	grain	0.12	bdl	0.22	5.12	2225.00	533.20	71	19
972120-10	FLT	MC-08-39	125	4	grain	0.35	bdl	bdl	4.40	6003.00	430.60	2796	1774

	71Ga	72Ge	75As	82Se	107Ag	111Cd	115In	118Sn	121Sb	125Te	197Au	205Tl	208Pb	209Bi
972120-5	0.0	0.8	2245.0	81.2	1.8	0.1	0.0	0.2	0.0	12.3	0.4	0.0	1	8.3
972120-6	0.1	1.0	181.6	164.5	1.2	0.0	0.0	0.2	0.0	6.1	0.2	0.0	2	5.1
972120-7	0.3	1.3	911.0	161.0	20.5	1.3	0.6	2.0	0.3	31.4	0.1	0.0	5	4.7
972120-8	0.8	1.0	657.5	184.7	13.7	7.8	5.0	51.6	0.5	122.4	2.1	0.0	9	103.0
972120-9	0.3	1.2	991.8	169.4	2.6	0.3	0.0	0.9	6.8	68.8	0.4	0.0	44	56.4
972120-10	0.2	0.9	2242.0	97.7	21.4	8.2	3.0	0.3	0.2	26.3	2.0	0.0	4.9	8.8

KT = Key Tuffite; MS = Massive sulfides; WLR = Watson Lake rhyolite; FLT = fault; L = line; S = spot

ANNEXE 4.3 : MATRICES DE CORRÉLATION : PYRITES

PyI	Mn	Co	Ni	Cu	Zn	As	Se	Ag	Cd	In	Sn	Sb	Te	Au	Tl	Pb
Co	0.0															
Ni	0.4	0.4														
Cu	0.7	-0.1	0.1													
Zn	0.5	-0.2	0.0	0.1												
As	-0.1	0.5	0.4	-0.1	-0.1											
Se	-0.1	-0.4	-0.1	0.0	-0.1	-0.4										
Ag	0.2	0.4	0.7	-0.1	-0.1	0.2	0.1									
Cd	0.5	-0.3	0.0	0.1	**1.0**	-0.1	-0.1	-0.1								
In	0.6	-0.3	-0.1	0.5	**0.7**	-0.2	-0.1	-0.1	0.8							
Sn	0.6	-0.3	0.1	**0.9**	0.1	-0.2	0.2	-0.1	0.1	0.4						
Sb	0.3	0.5	**0.9**	0.2	0.0	0.6	-0.2	0.6	-0.1	-0.2	0.1					
Te	0.3	0.5	**0.8**	0.0	0.0	0.4	-0.2	**0.9**	0.0	0.0	-0.1	**0.8**				
Au	0.4	0.3	0.7	0.1	0.2	0.5	-0.3	0.5	0.2	0.2	-0.1	0.7	0.7			
Tl	-0.3	-0.3	0.0	-0.2	-0.2	0.1	-0.1	-0.3	-0.2	-0.3	0.0	0.0	-0.1	0.0		
Pb	0.1	0.1	0.2	0.0	-0.1	-0.3	**0.8**	0.4	-0.1	-0.1	0.1	0.1	0.2	-0.1	-0.2	
Bi	0.2	0.7	0.1	-0.1	-0.1	-0.2	0.0	0.2	-0.1	-0.1	-0.1	0.0	0.1	0.0	-0.4	0.5

PyII	Mn	Co	Ni	Cu	Zn	As	Se	Ag	Cd	In	Sn	Sb	Te	Au	Tl	Pb
Co	-0.3															
Ni	0.1	0.6														
Cu	-0.3	0.0	0.3													
Zn	-0.1	**0.8**	0.3	-0.2												
As	-0.3	0.0	0.0	0.3	-0.2											
Se	-0.3	**0.9**	0.3	0.0	**0.7**	0.1										
Ag	-0.3	0.3	0.6	0.5	-0.1	0.4	0.1									
Cd	-0.1	**0.8**	0.3	-0.2	**1.0**	-0.2	**0.7**	-0.1								
In	-0.2	0.4	**0.7**	0.3	0.1	0.1	0.2	**0.8**	0.1							
Sn	-0.2	0.3	0.7	0.3	-0.1	0.2	0.0	**0.8**	-0.1	**1.0**						
Sb	-0.2	0.3	**0.7**	0.4	-0.1	0.2	0.1	**0.9**	-0.1	**0.9**	**0.9**					
Te	-0.1	0.2	**0.7**	0.4	-0.2	0.2	-0.1	**0.8**	-0.2	**0.7**	**0.7**	**0.9**				
Au	-0.1	-0.1	0.4	0.3	-0.4	0.1	-0.3	0.5	-0.4	0.4	0.5	0.6	**0.7**			
Tl	0.2	0.1	0.4	0.0	-0.2	0.2	-0.1	0.2	-0.2	0.2	0.2	0.4	0.3	0.1		
Pb	-0.3	0.3	0.6	0.3	-0.2	0.2	0.0	**0.8**	-0.2	**0.8**	**0.8**	**0.9**	**0.8**	0.6	0.3	
Bi	-0.3	0.3	0.7	0.4	-0.1	0.2	0.0	**0.8**	-0.1	**0.9**	**0.9**	**1.0**	**0.8**	0.5	0.4	**0.9**

PyIII	Mn	Co	Ni	Cu	Zn	As	Se	Ag	Cd	In	Sn	Sb	Te	Au	Tl	Pb
Co	0.1															
Ni	-0.1	0.6														
Cu	0.4	0.4	0.3													
Zn	0.1	0.0	-0.3	-0.1												
As	-0.2	-0.1	-0.3	-0.3	0.3											
Se	0.2	**0.8**	0.4	0.2	0.1	-0.2										
Ag	-0.1	0.0	-0.3	-0.3	0.2	0.1	0.4									
Cd	0.1	0.1	-0.3	-0.1	**1.0**	0.3	0.2	0.3								
In	0.3	0.5	0.2	0.6	0.6	0.0	0.3	0.0	0.6							
Sn	-0.1	0.0	-0.4	-0.1	0.3	0.1	0.4	**0.9**	0.4	0.1						
Sb	-0.1	0.0	-0.3	-0.2	0.2	0.1	0.3	1.0	0.3	0.1	**0.9**					
Te	0.2	0.5	0.1	0.2	0.2	0.0	0.6	0.5	0.4	0.3	0.6	0.4				
Au	0.0	0.4	0.6	0.2	-0.1	-0.3	0.3	-0.1	-0.1	0.3	-0.1	-0.1	0.5			
Tl	0.0	-0.1	0.3	0.0	-0.2	-0.3	-0.2	-0.1	-0.2	-0.1	-0.2	-0.1	0.1	0.3		
Pb	-0.1	0.1	-0.3	-0.2	0.2	0.2	0.4	**1.0**	0.4	0.1	**0.9**	**1.0**	0.6	-0.1	-0.2	
Bi	-0.1	0.1	-0.1	-0.2	0.2	0.1	0.5	**1.0**	0.3	0.1	**0.9**	**1.0**	0.6	0.1	-0.1	**1.0**

PyIV	Mn	Co	Ni	Cu	Zn	As	Se	Ag	Cd	In	Sn	Sb	Te	Au	Tl	Pb
Co	-0.1															
Ni	-0.1	0.1														
Cu	0.2	-0.3	-0.2													
Zn	-0.1	0.4	0.3	-0.1												
As	0.0	0.5	**0.7**	-0.4	0.5											
Se	-0.3	0.0	0.0	-0.2	-0.2	-0.3										
Ag	-0.1	0.5	0.5	-0.2	**0.9**	0.5	-0.1									
Cd	-0.1	0.5	0.3	-0.1	1.0	0.5	-0.2	0.9								
In	-0.2	0.5	0.4	-0.1	**0.9**	0.5	0.0	0.9	**0.9**							
Sn	-0.1	**0.7**	0.0	-0.1	0.1	0.3	-0.2	0.0	0.2	0.2						
Sb	0.1	0.3	0.1	0.3	0.5	0.1	-0.3	0.5	0.5	0.4	0.2					
Te	0.0	0.5	0.5	-0.2	**0.9**	0.6	-0.1	**1.0**	**0.9**	**0.8**	0.0	0.5				
Au	0.1	0.4	0.3	-0.2	0.0	0.4	-0.1	0.3	0.0	0.0	0.0	0.1	0.5			
Tl	0.1	-0.2	-0.1	0.6	-0.1	-0.2	-0.2	-0.1	-0.1	-0.1	0.0	0.4	-0.1	-0.1		
Pb	-0.2	0.0	0.0	0.2	-0.1	-0.3	0.6	0.0	-0.1	0.0	-0.2	0.2	0.1	0.2	0.0	
Bi	-0.1	0.4	0.2	-0.1	0.4	0.1	0.1	0.5	0.3	0.4	0.0	0.2	0.5	0.3	-0.2	0.2

PyV	Mn	Co	Ni	Cu	Zn	As	Se	Ag	Cd	In	Sn	Sb	Te	Au	Tl	Pb
Co	0.1															
Ni	-0.1	-0.4														
Cu	0.3	0.1	-0.1													
Zn	-0.1	-0.3	-0.1	0.2												
As	0.0	**0.9**	0.0	-0.1	-0.3											
Se	-0.1	-0.7	**0.7**	-0.4	0.1	-0.4										
Ag	0.2	**0.8**	-0.2	-0.1	-0.2	**0.9**	-0.4									
Cd	-0.1	-0.3	-0.2	0.3	**1.0**	-0.3	0.1	-0.2								
In	0.1	-0.2	-0.3	0.6	0.6	-0.3	0.0	-0.2	**0.8**							
Sn	0.0	-0.1	-0.2	0.2	0.0	-0.2	0.0	-0.1	0.2	0.4						
Sb	-0.1	-0.1	-0.2	-0.1	0.0	-0.1	-0.1	0.0	0.0	0.0	0.2					
Te	0.2	**0.8**	-0.2	0.0	-0.2	**0.8**	-0.4	**1.0**	-0.2	-0.1	-0.1	0.0				
Au	0.1	**0.8**	-0.2	0.0	-0.2	**0.9**	-0.4	**1.0**	-0.2	-0.2	-0.1	0.0	1.0			
Tl	0.2	0.5	-0.3	-0.1	-0.1	0.5	-0.3	**0.8**	-0.1	0.0	0.0	0.0	**0.8**	**0.7**		
Pb	-0.1	-0.1	0.1	-0.1	-0.2	0.0	0.0	-0.1	-0.2	-0.2	-0.1	-0.1	-0.1	-0.1	-0.1	
Bi	0.1	-0.1	-0.2	0.3	0.1	-0.3	0.0	-0.2	0.2	0.7	0.5	0.4	0.0	-0.1	0.0	-0.1

Zoned	Mn	Co	Ni	Cu	Zn	As	Se	Ag	Cd	In	Sn	Sb	Te	Au	Tl	Pb
Co	0.0															
Ni	0.2	0.1														
Cu	0.3	0.0	0.0													
Zn	0.1	0.0	0.0	0.1												
As	0.0	0.6	0.3	0.0	0.0											
Se	0.0	0.0	0.1	-0.1	-0.1	-0.1										
Ag	0.0	0.1	0.0	0.0	0.1	0.1	0.2									
Cd	0.1	0.0	0.0	0.1	**1.0**	0.0	-0.1	0.1								
In	0.2	0.0	0.0	0.4	0.4	0.0	0.0	0.1	0.6							
Sn	0.2	0.0	0.0	**0.7**	0.1	0.0	0.0	0.0	0.1	0.4						
Sb	0.1	0.0	0.0	0.1	0.1	0.0	0.0	0.3	0.1	0.1	0.2					
Te	0.0	0.1	0.0	0.0	0.1	0.0	0.2	**0.9**	0.1	0.0	0.0	0.0				
Au	0.0	0.5	0.0	0.0	0.0	0.6	0.1	0.2	0.0	0.0	0.0	0.0	0.0			
Tl	0.1	-0.1	0.0	0.1	0.0	0.0	-0.2	0.0	0.0	0.0	0.2	0.2	0.0	0.0		
Pb	0.0	0.0	-0.1	0.0	0.1	0.0	0.2	**0.7**	0.1	0.1	0.0	**0.7**	0.5	0.0	0.0	
Bi	0.0	0.1	0.0	0.0	0.1	0.0	0.2	**0.9**	0.1	0.1	0.0	0.4	**0.8**	0.0	0.0	**0.8**

ANNEXE 4.4 : MODÉLISATION DE L'ÉVOLUTION DES CONDITIONS PHYSICO-CHIMIQUES ASSOCIÉES À LA PRÉCIPITATION DES DIFFÉRENTS TYPES DE PYRITES (MODIFIÉ DE LARGE, 1977)

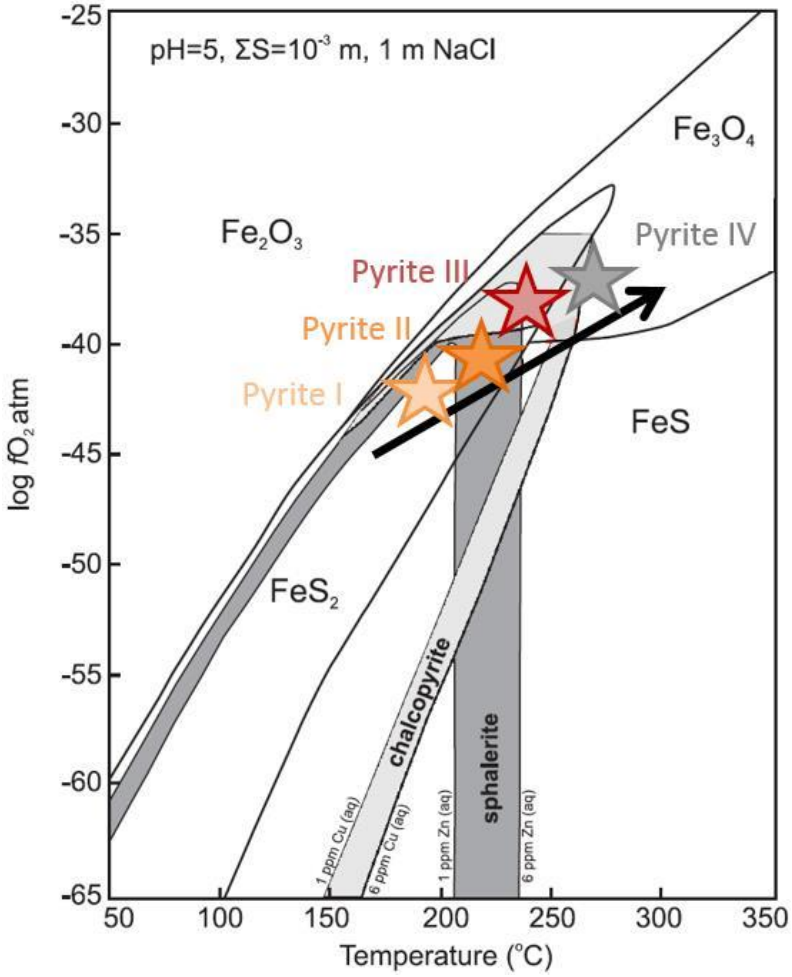

ANNEXE 5

HYPOTHÈSE D'UN BASCULEMENT POUR EXPLIQUER LA GEOMETRIE DES GISEMENTS

Les deux gisements accessibles étudiés dans ce projet ne représentent pas seulement l'extrémité Sud et Nord du Flanc Sud, mais aussi deux géométries diamétralement opposés en ce qui concerne la forme des amas minéralisés : des amas discordants sub-verticaux pour Persévérance, et des lentilles tabulaires concordantes pour Bracemac-McLeod. En dépit de ces différences, leur formation peut être intégrée au sein d'un modèle unique à l'échelle du Flanc Sud du camp minier de Matagami.

La Figure 5.1 représente une série de sections des six autres gisements connus le long du Flanc Sud : Mattagami Lake, Bell Allard, Bell Allard Sud, Isle-Dieu, Orchan et Orchan Ouest. Faure (2010) a mis en évidence qu'en dépit de la variation du pendage de la séquence stratigraphique du Flanc Sud, la zone de filonnets (*stringers*) et le halo d'altération demeurait sub-verticaux pour tous les gisements considérés. Le Tableau 5.1 est une compilation de plusieurs paramètres géométriques des minéralisations, des zones d'altération et de la Tuffite Clé pour tous les gisements connus le long du Flanc Sud. Indépendamment du tonnage, il y a une corrélation positive significative entre le pendage du Flanc Sud et l'épaisseur (Fig. 5.2a) ou l'extension (Fig. 5.2b) des

corps minéralisés : plus le pendage est fort, moins les minéralisations sont épaisses, mais plus étendues. Ces relations indiquent que le pendage contrôle la géométrie des gisements et suggèrent que l'évènement minéralisateur a eu lieu pendant ou après le basculement synvolcanique du Flanc Sud.

Plusieurs pourraient attribuer ces relations géométriques à l'effet de la déformation régionale ductile: comme la transposition des zones de *stringers* et la remobilisation des sulfures. Cependant, l'imprégnation de la déformation ductile le long du Flanc Sud est relativement faible (Jolly, 1978; Lavallière et al., 1994), hétérogène et confiné à des corridors de cisaillement ductile-cassant étroits. Aucune fabrique pénétrative n'est visible dans les roches en dehors des zones influencées par les failles majeures, les corridors de déformation et les zones fortement chloritisées (Sharpe, 1968; Piché et al., 1993), qui sont des zones fortement altérées et donc affaiblies ce qui facilite la concentration de la déformation ductile.

Le Complexe de la Rivière Bell sous-jacent aurait pu jouer un rôle clé dans la faible déformation qui caractérise le Flanc Sud. Le complexe igné étant compétant a probablement agi comme un bloc rigide, fournissant une protection pour les roches volcaniques sus-jacentes, durant l'épisode de déformation régional. La déformation a été concentrée sur la périphérie et plus particulièrement le long du Flanc Nord, où les lithologies sont verticalisées et

foliées. Une telle hétérogénéité de la déformation est commune, telle que documentée pour le dome de Noranda (Dimroth et al., 1983; Goutier, 1997) et le Pluton de Misema en Abitibi (Pearson et Daigneault, 2009). Malgré la déformation régionale, les relations géométriques primaires des structures synvolcaniques semblent préservées le long du Flanc Sud. En conséquence, la distribution et l'orientation des dykes mafiques et des filons-couches, qui sont contrôlés par des structures synvolcaniques, sont d'importance pour déchiffrer la géométrie originale du système hydrothermal.

Les sections verticales présentées pour Persévérance (Fig. 2.3) et Bracemac-McLeod (Fig. 2.4) mettent en évidences des différences majeures de la géométrie des roches intrusives. À Persévérance, les intrusions sont dominées par des dykes sub-verticaux, et les filons-couches sont mineurs. À Bracemac-McLeod, c'est l'opposé : les roches intrusives sont dominées par des filons- couches qui ont gonflé l'empilement volcanique. Basé sur des observations de terrain et sur des analyses géochimiques, la plupart des intrusions le long du Flanc Sud sont interprétées comme des apophyses du Complexe de la Rivière Bell et se sont donc mis en place avant la déformation et le métamorphisme régional (Jenney, 1961; Roberts, 1975; MacGeehan and MacLean, 1980).

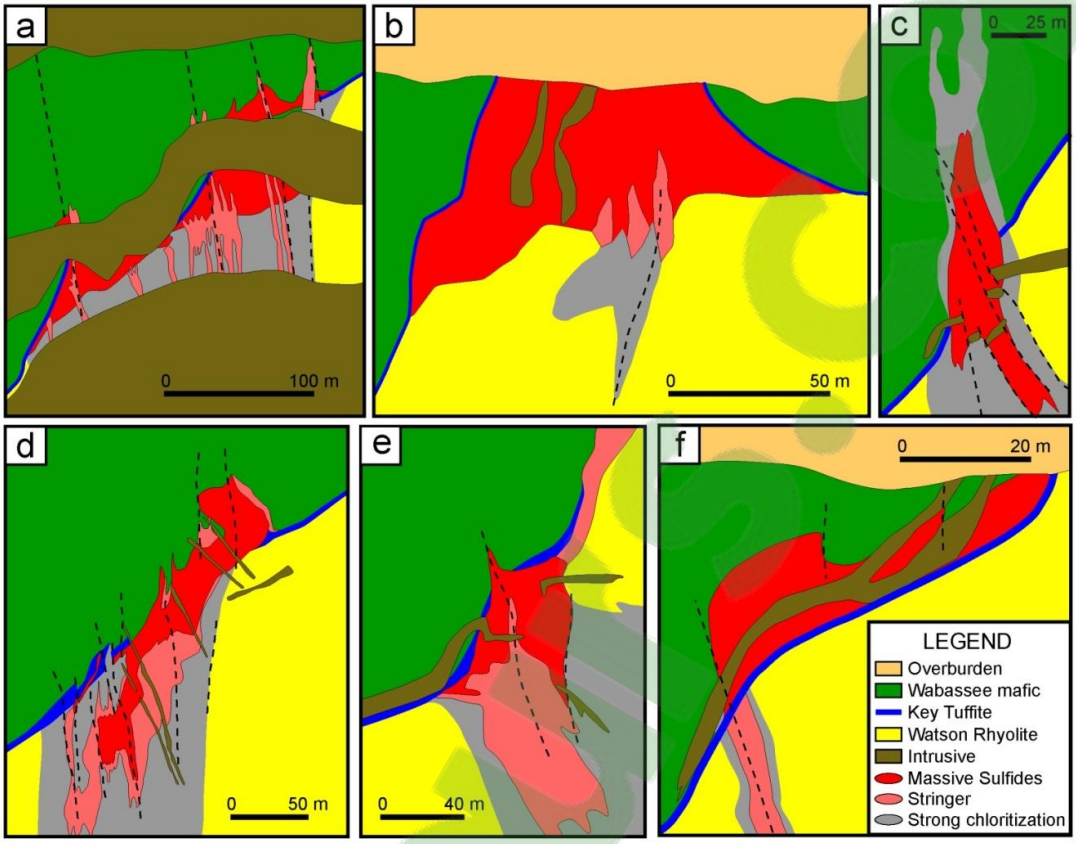

Figure 5.1 Sections représentatives des gisements découverts le long du Flanc Sud du camp de Matagami. a) Isle Dieu (modifiée de Noranda); b) Mattagami Lake (modifiée de Mattagami Mines LTD); c) Orchan Ouest (modifiée de Orchan Mines LTD); d) Bell Allard (modifiée de Noranda, 1999); e) Orchan (modifiée de Large, 1977); f) Bell Allard Sud (modifiée de Orchan Mines LTD, 1965).

	Gisements	Angle *stockwork* et Tuffite Clé	Pendage de la Tuffite Clé	Axe long X	Axe court Y	Épaisseur Z
Perseverance	P main	90	10	180	55	210
	Equinox	90	10	300	140	170
	P West	90	10	125	90	160
Isle Dieu		55	35	360	255	50
Mattagami Lake		65	0	525	240	290
Orchan Ouest#1		20	35	180	45	80
Orchan #5		45	35	170	120	160
Bell Allard		45	50	355	220	60
Bell Allard Sud		55	50	170	70	15
Bracemac		35	55	520	255	30
McLeod		0	65	1140	290	20

Tableau 5.1 Compilation des paramètres géométriques de tous les gisements connus le long du Flanc Sud du camp de Matagami.

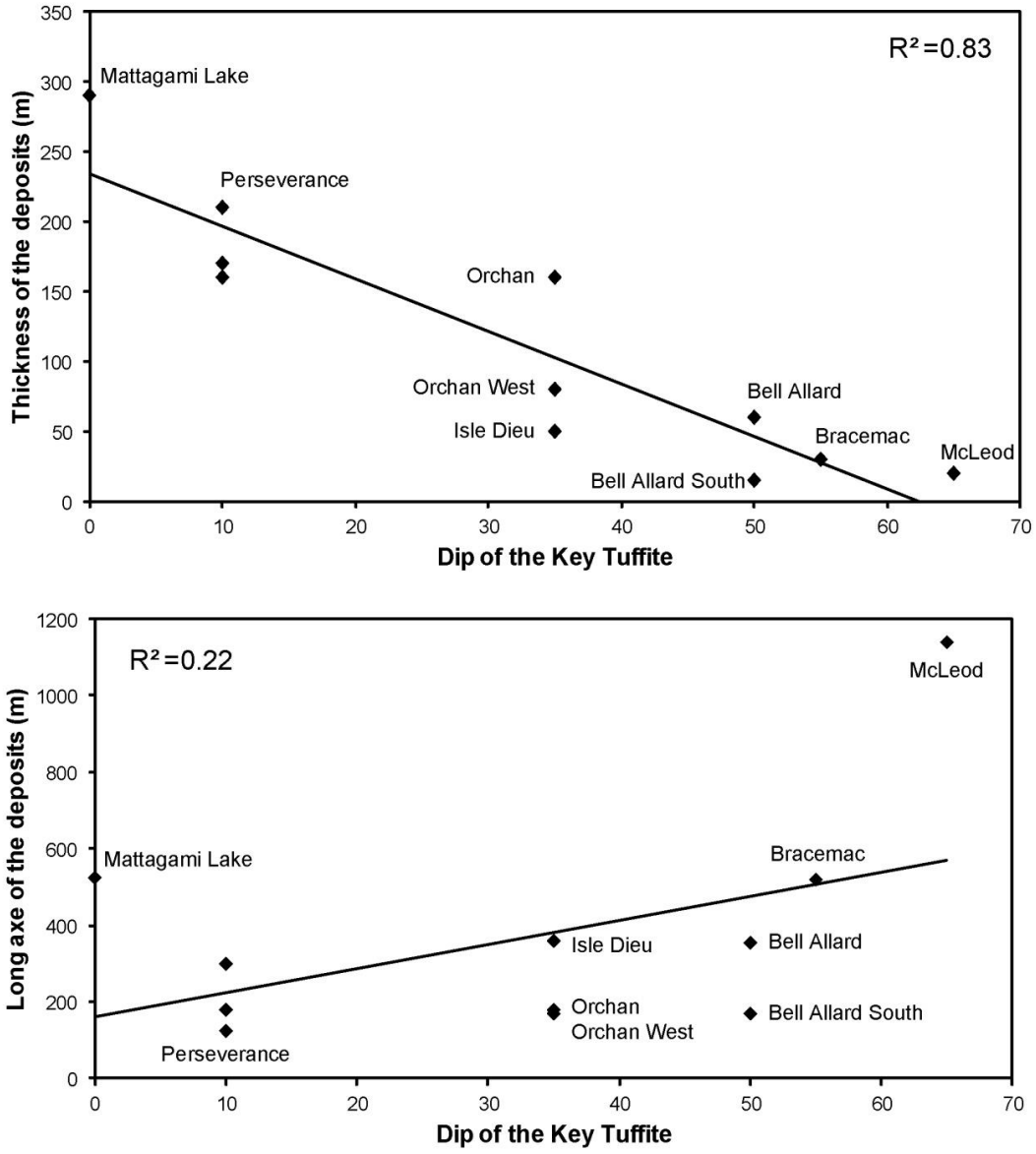

Figure 5.2 Lien entre la géométrie des gisements et le pendage du Flanc Sud. a. Épaisseur des gisements versus pendage de la séquence stratigraphique. b. Axe long des gisements versus pendage de la Tuffite Clé.

L'épaisseur de la Tuffite Clé (2 m en moyenne), et qui est relativement homogène à l'échelle du camp, implique que le dépôt de cendre sur le plancher océanique s'est fait sur une paléo-surface sub-horizontale. En présumant que les dykes et les filons-couches se sont introduits dans un même intervalle de temps à Persévérance et à Bracemac-McLeod, il est surprenant d'observer des géométries aussi différentes. Une hypothèse logique est que le Flanc Sud était déjà basculé au moment de l'injection des dykes et des filons-couches. Le basculement synvolcanique progressif et asymétrique vers le Sud-Est pourrait être expliqué par une inflation significative du Complexe de la Rivière Bell. Des données séismiques de Calvert et al. (1995) indiquent que le Complexe de la Rivière Bell s'enracine en profondeur jusqu'à un minimum de 5 km. La mise en place d'un tel volume de magma, vraisemblablement en plusieurs pulses, a inévitablement provoqué une inflation significative de la séquence volcanique sus-jacente.

UN MODELE DE FORMATION EPIGENETIQUE POUR LES SMV DU CAMP DE MATAGAMI

Le pendage du Flanc Sud a joué un rôle important dans la géométrie des gisements (Fig. 5.1). Dans les cas de Persévérance et Bracemac-McLeod, les fluides hydrothermaux ascendants ont été canalisés en profondeur par des structures synvolcaniques. Cependant, dans le cas d'une séquence volcanique

sub-horizontale à Persévérance, la minéralisation est limitée aux structures synvolcaniques seulement. La Tuffite Clé, qui surmonte la minéralisation, est fortement altérée (Fig. 2.8a) mais complètement stérile de sulfures (Fig. 2.8a). La silicification pervasive de la Tuffite Clé (Fig. 2.8b) et de la rhyodacite de Dumagami (Fig. 2.7a) a pu se produire de manière précoce par les fluides hydrothermaux de basse température qui ont colmaté toutes les espaces ouverts. Dans ce scénario, la Tuffite Clé représente une barrière imperméable qui a scellé le système. Ce processus est courant dans les SMV de type remplacement (Jones et al., 2006; Schardt and Large, 2009) car il concentre la minéralisation en dessous d'horizon imperméable (e.g. Gibson and Kerr, 1993; Galley et al., 1995; Doucet et al., 1998; Sharpe and Gemmell, 2001) et accentue les processus de raffinage (Franklin, 1995; Hannington et al., 1998).

À Bracemac-McLeod, la minéralisation est mise en place à l'intersection de structures synvolcaniques et de la Tuffite Clé. Les fluides hydrothermaux ascendants sont dispersés lorsqu'ils atteignent la Tuffite Clé qui est poreuse, pour produire une altération concordante importante. Le style tabulaire des corps minéralisés de Bracemac-McLeod suggère un remplacement progressif induit par la percolation de fluides le long de la Tuffite Clé mais aussi le long de la carapace de hyaloclastite au sommet de la Rhyolite du Lac Watson. Ce processus a déjà été documenté à la mine du Lac Mattagami (Roberts, 1975; Roberts and Reardon, 1978). Avec un pendage élevé du Flanc Sud, les fluides de basse température

ont permis la silicification d'une partie de la Tuffite Clé (Fig. 2.8c) et de la rhyolite de Bracemac (Fig. 2.7b). La formation de cette barrière imperméable a accentué la migration latérale des fluides hydrothermaux (Kerr and Gibson, 1993), entrainant l'échappée des fluides vers des zones de plus basse pression (en amont-pendage) en utilisant la porosité résiduelle de la Tuffite Clé. La migration latérale des fluides dans la Tuffite Clé a été testée géochimiquement en utilisant les calculs de gains et pertes de masses en fonction de l'éloignement des minéralisations. Les résultats (Fig. 2.14) montrent un patron d'altération cohérent autour de la mine Bracemac-McLeod: une chloritisation proximale importante (<230 m) comprise dans un halo de séricitisation plus large (230 à 400 m). Le halo d'altération présent dans la rhyolite du Lac Watson est identique en chimie et en taille à celui de la Tuffite Clé. Il s'agit de la première documentation, dans la Tuffite Clé, d'une organisation géochimique cohérente qui évolue en fonction de la distance des minéralisations et est d'intérêt pour l'exploration.

La migration des fluides vers la surface, après un basculement synvolcanique, implique des profils asymétriques des altérations et des minéralisations, avec la majorité des minéralisations concordantes localisées en amont-pendage des zones de stringer. Cette géométrie est particulièrement bien observée à Bell Allard Sud (Fig. 5.1f) et Bell Allard (Fig. 5.1d). La lentille No. 3 de Orchan illustre aussi très bien la migration des fluides minéralisateurs en amont-pendage (Fig.1 dans Large, 1977). Bien que 60 à 70% de la minéralisation est en remplacement

dans la rhyolite du Lac Watson, la Tuffite Clé est particulièrement enrichie en sphalérite, sur plus de 90 m en amont-pendage de la structure synvolcanique (Large, 1977).

Les gisements de SMV du camp de Matagami sont parmi les plus riches en zinc dans le monde. Des processus de minéralisation par remplacement, sous le plancher océanique sont un mécanisme de piégeage bien plus efficace en comparaison de processus exhalatifs où une grande partie des métaux est dispersée dans l'océan (Doyle and Allen, 2003). La précipitation de sphalérite est contrôlée par une augmentation du pH (Bourcier and Barnes, 1987), mais aussi par une baisse de température en dessous de 175°C (Hannington et al., 1995). Un mélange des fluides hydrothermaux avec l'eau de mer froide entraîne une baisse efficace du pH et de la température. Ceci suggère que lorsque les fluides minéralisateurs ont atteins la Tuffite Clé, cette dernière était probablement saturée en eau de mer froide et dense drainée en profondeur par la porosité de la Tuffite Clé ou par des structures synvolcaniques.

RÉFÉRENCES

Bourcier, W. L., and Barnes, H. L., 1987, Ore solution chemistry; VII, Stabilities of chloride and bisulfide complexes of zinc to 350 degrees C: Economic Geology, v. 82, p. 1839-1863.

Calvert, A. J., Sawyer, E. W., Davis, W. J., and Ludden, J. N., 1995, Archaean subduction inferred from seismic images of a mantle suture in the Superior Province: Nature, v. 375, p. 670-674.

Dimroth, E., Imreh, L., Goulet, N., and Rocheleau, M., 1983, Evolution of the south-central segment of the Archean Abitibi Belt, Quebec. Part II: Tectonic evolution and geomechanical model: Canadian Journal of Earth Sciences, v. 20, p. 1355-1373.

Doucet, P., Mueller, W., and Chartrand, F., 1998, Alteration and ore mineral characteristics of the Archean Coniagas massive sulfide deposit, Abitibi belt, Quebec: Canadian Journal of Earth Sciences, v. 35, p. 620-636.

Doyle, M. G., and Allen, R. L., 2003, Subsea-floor replacement in volcanic-hosted massive sulfide deposits: Ore Geology Reviews, v. 23, p. 183-222.

Faure, S., 2010, Reconnaissance de structures synvolcaniques majeures dans les environnements de sulfures massifs volcanogènes, nord-ouest de la Sous-province d'Abitbi., Rapport, Projet CONSOREM 2009-04, p. 34.

Franklin, J. M., 1995, Volcanic-associated massive sulphide base metals: Geological Survey of Canada, Geology of Canada, v. 8, p. 158-183.

Galley, A. G., Watkinson, D. H., Jonasson, I. R., and Riverin, G., 1995, The subsea-floor formation of volcanic-hosted massive sulfide; evidence from the Ansil Deposit, Rouyn-Noranda, Canada: Economic Geology, v. 90, p. 2006-2017.

Gibson, H. L., and Kerr, D. J., 1993, Giant volcanic-associated massive sulphide deposits: with emphasis on Archean examples: Economic Geology Special Publication 2, p. 319-348.

Goutier, J., 1997, Géologie de la région de Destor. Ministère des ressources naturelles (Québec), Report RG 96-13. 37 p.

Hannington, M. D., Galley, A. G., Herzig, P. M., and Petersen, S., 1998, Comparison of the TAG mound and stockwork complex with Cyprus-type massive sulfide deposits.: Proceedings of the Ocean Drilling Program, Scientific results, v. 158, p. 389-415.

Hannington, M. D., Jonasson, I. R., Herzig, P. M., and Petersen, S., 1995, Physical and chemical processes of seafloor mineralization at mid-ocean ridges: Geophysical Monograph Series, v. 91, p. 115-157.

Jolly, W. T., 1978, Metamorphic history of the Archean Abitibi belt., *in* Fraser, J. A., and Heywood, W. W., eds., Metamorphism in the Canadian Shield, Geological Survey of Canada, Paper 78-10, p. 63-78.

Jones, S., Gemmell, J. B., and Davidson, G. J., 2006, Petrographic, geochemical, and fluid inclusion evidence for the origin of siliceous cap rocks above volcanic-hosted massive sulfide deposits at Myra Falls, Vancouver Island, British Columbia, Canada: Economic Geology, v. 101, p. 555-584.

Kerr, D. J., and Gibson, H. L., 1993, A comparison of the Horne volcanogenic massive sulfide deposit and intracauldron deposits of the Mine Sequence, Noranda, Quebec: Economic Geology, v. 88, p. 1419-1442.

Large, R. R., 1977, Chemical evolution and zonation of massive sulfide deposits in volcanic terrains: Economic Geology, v. 72, p. 549-572.

Lavallière, G., Guha, J., and Daigneault, R., 1994, Cheminées de sulfures massifs atypiques du gisement d'Isle-Dieu, Matagami, Québec; implications pour l'exploration: Exploration and Mining Geology, v. 3, p. 109-129.

Pearson, V., and Daigneault, R., 2009, An Archean megacaldera complex: The Blake River Group, Abitibi greenstone belt: Precambrian Research, v. 168, p. 66-82.

Piché, M., Guha, J., and Daigneault, R., 1993, Stratigraphic and structural aspects of the volcanic rocks of the Matagami mining camp, Quebec; implications for the Norita ore deposit: Economic Geology, v. 88, p. 1542-1558.

Schardt, C., and Large, R. R., 2009, New insights into the genesis of volcanic-hosted massive sulfide deposits on the seafloor from numerical modeling studies: Ore Geology Reviews, v. 35, p. 333-351.

Sharpe, J. I., 1968, Géologie et gisements de sulfures de la région de Matagami, Comté d'Abitibi-Est, Québec., Ministère des Richesses Naturelles du Québec. Rapport géologique 137, p. 122.

ANNEXE 6

Behaviour of Europium in the Key Tuffite around the Bracemac-McLeod deposit: A new geochemical tool to assist VMS exploration in the Matagami mining camp, Quebec, Canada.

Dominique Genna, Damien Gaboury

LAMEQ - Experimental and Quantitative Metallogeny Research Laboratory at University of Quebec at Chicoutimi (UQAC), 555 boul. de l'Université, Chicoutimi, G7H 2B1, Canada

Gilles Roy

Xstrata Zinc Canada, Matagami Exploration office C.P.819. Matagami, QC, J0Y 2A0, Canada

Introduction

Tuffaceous exhalites commonly display a spatial and genetic link with volcanogenic massive sulfide (VMS) deposits and, by consequence, represent an important guide for exploration of this type of mineralization (e.g. Ridler, 1971; Kalogeropoulos and Scott, 1989). Because of this strategic significance, numerous successful geochemical tools were developed to assist exploration in the Bathurst mining camp, Canada (Peter and Goodfellow, 2003) or in the Hokuroku District, Japan (Kalogeropoulos and Scott, 1983) for example.

Scott et al. (1983) proposed two components in the formation of tuffaceous exhalites: 1) a detrital component from the settling of volcanic particles (ash, lapilli, blocks); and 2) a seafloor precipitate component generated from hydrothermal fluid vents (exhalite sensu stricto). These two poles imply a hiatus in the volcanism which allows an efficient hydrothermal system to be established. However, most ancient VMS deposits have undergone a regional metamorphism or a late-stage episode of hydrothermal alteration (or both) after the syngenetic mineralization event on the seafloor (Franklin et al. 1981; Large, 1992). These processes underline the importance of a third component in the characterization of the tuffaceous exhalites: epigenetic hydrothermal alteration. These "late" fluids have the potential to significantly change the initial exhalite composition and must be well constrained in order to address meaningful interpretation and develop efficient vectoring tools for exploration.

The Key Tuffite (KT; Miller, 1960), in the Matagami mining camp of the Abitibi (Quebec, Canada), is historically known as one such exhalative horizon. With an average thickness of 2m and ~17 km in lateral continuity, the KT has been used as the main guide for VMS exploration in the camp for the last 50 years. All exploited deposits are located along this tuffaceous and locally cherty horizon. Despite its economic importance and numerous studies (e.g. Davidson, 1977; Liaghat

and MacLean, 1992), attempts to develop geochemical vectoring tools for exploration were mostly inconclusive because of the complex chemical nature of the unit. An aggressive exploration drilling program by Xstrata Zinc and Donner Metals around the new Bracemac-McLeod VMS deposits provided an exceptional opportunity to sample the KT both proximal and distal to the mineralization. This study investigates the petrogenesis of the KT and its link with the mineralizing event in order to develop geochemical vectors towards the massive sulfide lenses.

Geological setting

The Archean Abitibi greenstone belt in Canada is the largest (300 x 700 km) and also one of the richest VMS-bearing (>80 deposits) greenstone belts in the world (Card, 1990; Allen et al., 2002). The 2.7 Ga (Mortensen, 1993; Ross et al. submitted) Matagami mining camp (Fig. 1) is located in the northern part of the Abitibi belt. With more than 50 Mt of zinc-rich ore (9% Zn on average) extracted and in reserve since the 1960's and 20 known deposits, this mining camp constitutes an important zinc district in the world. The camp stratigraphy established by Sharpe (1968) and validated by Piché et al. (1990) is divided into two groups (Fig. 2): 1) the Watson Group, which is composed of dacite and rhyolite, overlain by 2) the Wabassee Group, which comprises mostly basalt and andesite flows with subordinate rhyolite and dacite. The KT is located at the interface between the Watson and the Wabassee Groups. Sulfide mineralization is located at, or in close stratigraphic proximity to, the KT. Mineralization in the camp is typically associated with chlorite alteration in the immediate footwall which can obliterate primary rock textures and significantly impact geochemical characteristics. The Watson Group is crosscut at the base by the Bell River Complex, a large gabbro-anorthosite layered intrusion interpreted to be the thermal source for the VMS formation (Piché et al., 1990; Maier et al., 1996; Ioannou and Spooner, 2007; Carr et al., 2008).

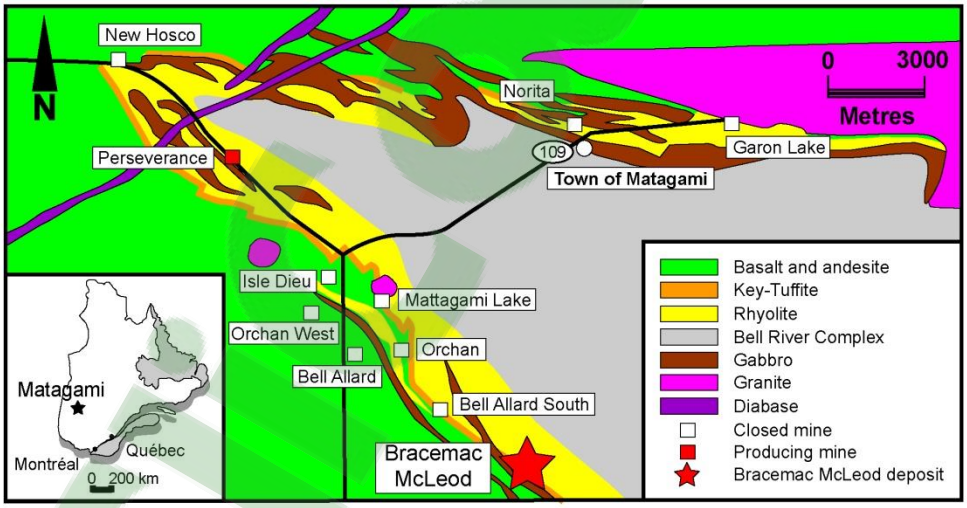

Fig1. Geological map of the Matagami Mining Camp. Modified from Xstrata Zinc.

Bracemac-McLeod geology

The Bracemac-McLeod geology is shown in the cross sections in Figure 2. The volcanic units trend north-west to south-east and are dipping between 60° to 70° towards the southwest. The

Watson rhyolite is directly overlain by the KT which marks the abrupt transition into the Wabassee Group. A thin rhyolitic unit known as the Bracemac Rhyolite was emplaced at the base of the Wabassee Group and directly overlays the KT in the deposit area. It in turn is overlain by a thin exhalative unit: the Bracemac Tuffite (BT) that marks the transition into andesitic rocks. Approximately 300 metres above the KT, there is a marked change to rocks of basaltic composition. The entire stratigraphic sequence has been intruded by gabbroic sills and lesser dykes that have inflated the stratigraphic sequence.

The Bracemac-McLeod deposits consist of two main mineralized zones comprised of seven mineralized lenses spatially controlled by synvolcanic faults and separated by a horizontal distance of 800m. Together they contain measured and indicated mineral resources of 3.6 million tonnes grading 10.62% Zn and 1.45% Cu, 32.3g/t Ag, 0.48g/t Au (Côté and Lavigne, 2010). Additional inferred mineral resources of 2.6 million tonnes grading 8.79% Zn, 1.31% Cu, 38.84g/t Ag and 1.06g/t Au are present in and around the McLeod zone, including the McLeod Deep lens discovered in 2010 (Côté and Lavigne, 2010). The mineralogy of the lenses is dominated by sphalerite and pyrite with lesser amounts of chalcopyrite (± magnetite and minor galena). Most of the mineralization occurs at the KT contact, however two of the Bracemac lenses were deposited in the mafic rocks above the KT, forming a stacked sequence interpreted as resulting from reactivation of a hydrothermal system along a synvolcanic structure following the deposition of the Wabassee Group (Côté and Lavigne, 2010). It is the first occurrence of stacking found in the Matagami Camp.

With a strong proximal chloritisation (± talc), a moderate intermediate chloritisation and distal sericitisation, typical facies of VMS alterations are encountered around the mineralisation and represent the primary exploration tool. The proximal alteration, named Pipe, is sub-concordant to the mineralization (Fig. 2a).

The Key Tuffite ("KT")

The KT is a thick (2 to 6m on average) and continuous (~17km) unit which is thinly layered. It can be mapped on surface and in the subsurface by drilling and mine operations at the district scale (Fig. 1). The geometry of the KT differs from other exhalites known in the Abitibi which are typically much thinner (10s of cm) and discontinuous, e.g. the Main Contact, Millenbach mine (Kalogeropoulos and Scott, 1989). Previous studies concluded that the KT was the result of the mixing of at least 2 components in varying proportions: 1) a detrital component (ash), now represented mostly by chlorite which is the dominant mineral at the district scale; and 2) a seafloor precipitate component, represented by silica and sulfides (Davidson 1977) resulting from hydrothermal venting of metallic and siliceous plumes on the seafloor. This last component was thought to be related to the mineralizing event (Liaghat and MacLean, 1992). However the epigenetic hydrothermal alteration component has never been previously considered.

The KT is well developed in the Bracemac-McLeod area. Its thickness ranges between 0.1 - 10 m and in some places it is absent. Such variations can occur over short distances and make correlation of specific beds impossible. In addition, no systematic increase of the thickness is recorded by the KT closer to the Bracemac-McLeod deposits, as previously documented around the Bell Allard South deposit (Davidson, 1977), located 2.2km northwest of the study area (Fig. 1). At the megascopic scale, the KT is highly variable (Fig. 3) and composed mainly of quartz, sulfides (mostly pyrite), sericite, chlorite, and carbonates. The modal percentage of these minerals is also highly variable even along the same drill core. In the chert-rich portions, the delicate

lamination features are extremely well preserved, whereas the bedding appears coarser when chlorite is dominant.

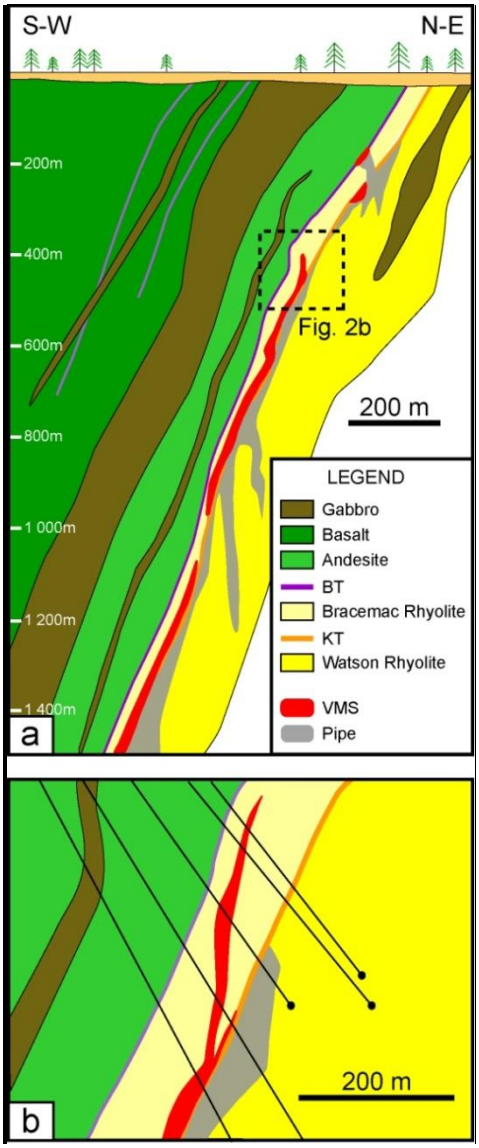

Fig.2: a – Geological section of the McLeod deposit (13425±50m). Modified from Xstrata Zinc and Donner Metals. b – Zoom in the upper part of the McLeod deposit.

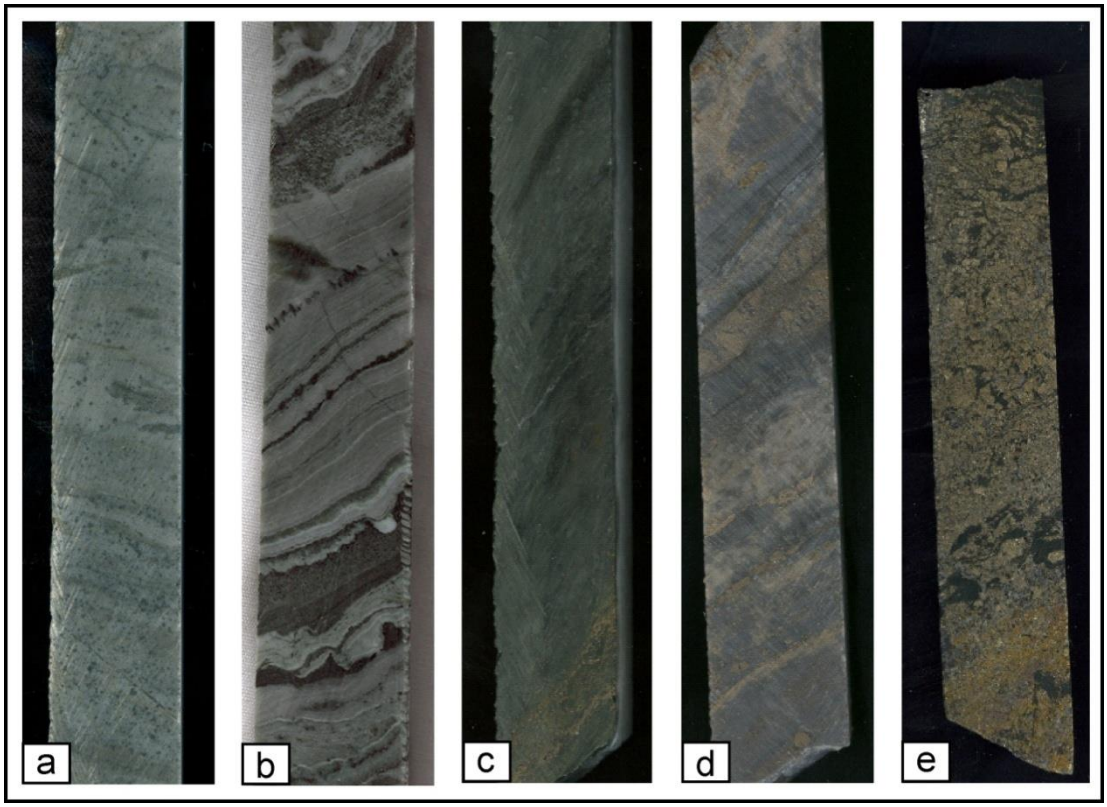

Fig.3: Facies variability of the KT around Bracemac-McLeod. Width of the core: 2cm.

Link between Key Tuffite and mineralization

Geometrically, the extensive (~1km x ~250m) and thin (<20m) stratiform mineralization of the McLeod lens along the KT unit (Fig. 2) is different to the classic mound-shaped lenses of exhalative VMS systems (e.g. Ohmoto, 1996). Drill core observations of the Bracemac-McLeod deposits clearly demonstrate that a significant portion of the mineralization crosscuts and locally replaces: 1) the KT unit (Fig. 4a), 2) the hyaloclastic deposits in the uppermost portion of the footwall Watson rhyolite (Fig. 4b) and 3) the Bracemac rhyolite hanging wall (Fig. 2b). In the upper part of the McLeod zone, the majority of the massive sulfide lens is hosted in the Bracemac rhyolite hanging wall whereas at depth, it is associated with or immediately below the KT unit. Genetically, these relationships are not easily reconcilable with an exhalative origin of the mineralization on the seafloor; although it can still be argued that the mineralizing event continued after the seafloor was covered by the Bracemac rhyolite, in particular since we know that there is stacking at Bracemac. Within the KT unit, both the relative position and textures of the mineralization are highly variable. Observations demonstrate that mineralization commonly crosscuts and replaces the KT bedding and can occur at any stratigraphic level within the KT, from the upper to the lower contact. These features are not typical of exhalative systems but more consistent with a replacement origin (Doyle and Allen, 2003). Based on all the crosscutting, replacement and geometrical relationships, it is considered that mineralization at Bracemac-McLeod was mainly formed by hydrothermal replacement along the permeable KT unit.

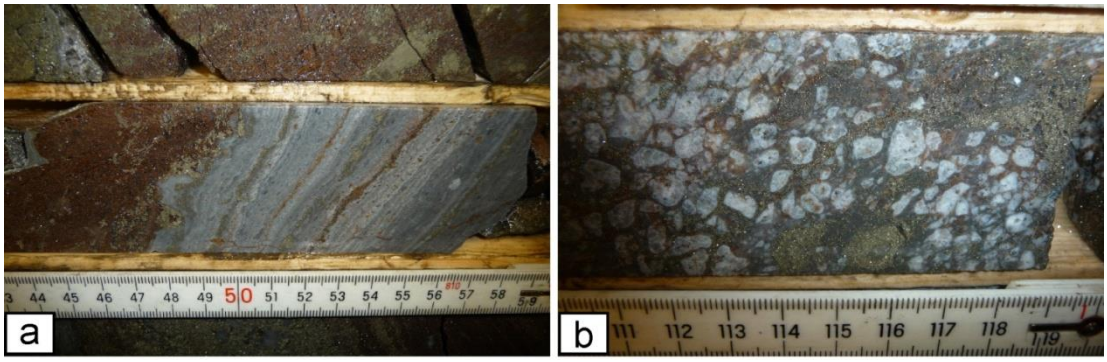

Fig.4: Evidence of late mineralization: a – Silicified KT preserved in the middle of the mineralization of the McLeod deposit. b – Hyaloclastite of the Watson rhyolite summit. The fragments are silicified and the matrix is replaced by pyrite and sphalerite.

Methodology

Twenty three drill-cores were selected from more than 400 holes in an area 2.6 km long by 1.4 km wide. Whole-rock geochemistry was carried out on 42 samples for major, trace and rare earth elements (REE) at the Institut National de la Recherche Scientifique (INRS) laboratory in Quebec City, Canada, using Inductively Coupled Plasma-Atomic Emission Spectrometry (ICP-AES) and Mass Spectrometry (ICP-MS). Samples were generally 20 cm in length and located, when it was possible, systematically at the base of the unit.

Geochemical results

Most of the major and many of the trace elements are mobile during hydrothermal alteration associated with the formation of VMS (Barrett and MacLean, 1999). Only TiO_2 and Zr are considered immobile even during extreme alteration (Finlow-Bates and Stumpfl, 1981). Thus, the ratio of these two elements is commonly used to classify altered rocks in volcanic terranes (e.g. MacLean and Kranidiotis, 1987; Barrett et al., 2005). This approach was used to identify the detrital source of the KT.

Figure 5a represents a plot of immobile elements for all the volcanic rocks around the Bracemac-McLeod area. Although the absolute TiO_2 and Zr values are highly variable, their ratios remain constant for each lithology and plot along different alteration lines through the origin with positive correlation values. The KT unit is clearly different in composition from the underlying and overlying rhyolites. With a correlation value (R^2) of immobile elements of 0.78, the composition of the detrital component was most likely homogeneous prior to mass gain and loss induced by hydrothermal alteration. A plot of Nb/Y versus Zr/TiO_2 (Fig. 5b) indicates an andesitic composition for the KT as suggested already by the similarity of the alteration lines of the KT and the andesitic unit of the hanging-wall Wabassee Group (Fig.5a).

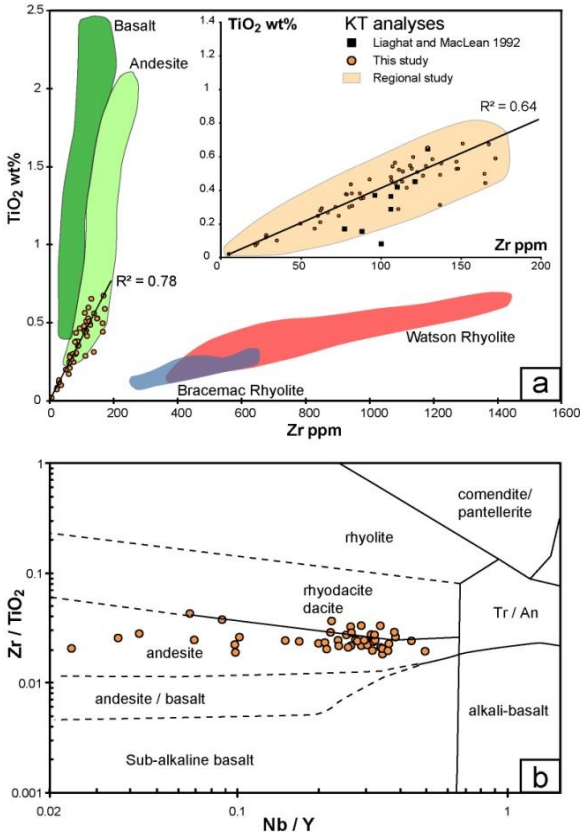

Fig.5: a- TiO_2 vs Zr plot for all volcanic rocks. Data from Xstrata Zinc. Inset graph – TiO_2 vs Zr plot for KT only. Black squares represent Liaghat and MacLean (1992) samples. Circles are samples from this study. The orange field represents 300 samples from the PhD regional study. b – Nb/Y vs Zr/TiO_2x10000 plot for the KT samples (Winchester and Floyd, 1977)

For the purpose of VMS vectoring, single element and ratio element plots were tested for coherent variation towards mineralization. No significant variation, in agreement with previous work, was established, except for europium which shows a systematic increase towards the deposit (Fig. 6a). In order to quantify this increase, the europium anomaly was calculated by comparing the measured concentration (Eu) to an expected concentration (Eu*) calculated by straight-line interpolation between Sm and Gd (Rollinson, 1993). In this study the europium anomaly has been calculated as followed: $(Eu/Eu^*)_{pm} = 2 \times Eu_{pm} / (Sm_{pm} \times Gd_{pm})$, where pm (Primitive Mantle) are the normalization values from Sun and McDonough (1989).

Figure 6b illustrates the spatial distribution of the europium anomaly around the mineralization of Bracemac-McLeod. Away from the deposit, the anomaly is negative with a value of <0.5. Progressively towards the deposit, the anomaly becomes positive and reaches a maximum value of 1.95 in the lens. This positive Eu signature is persistent up to 200m from the deposit.

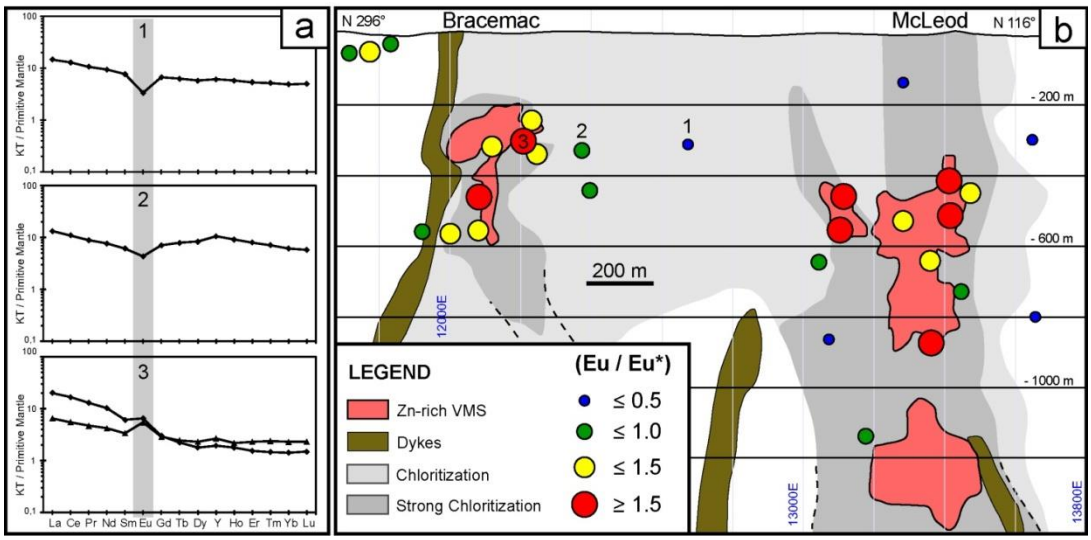

Fig.6: A- Primitive Mantle normalized REE-Y patterns and Eu variation with varying distances from the Bracemac orebody (labelled 1-3). B – Composite longitudinal section along the Bracemac-McLeod deposits. The Eu anomaly (Eu/Eu*) systematically increases towards the mineralized lenses. Normalization values from Sun and McDonough, 1989.

Origin of the Key Tuffite

The KT unit was previously considered as the result of mixing volcanic ash and chemical precipitation on the seafloor (Davidson, 1977). These 2 components are addressed below with the aim of solving the KT unit origin. Liaghat and MacLean (1992) proposed, with a limited number of samples (Fig. 5a), that the detrital component resulted from a mix of andesitic and rhyolitic ash in variable proportions. Our data indicates that the KT unit is andesitic in composition only (Fig. 5) and that the composition prior to hydrothermal alteration was very homogeneous as indicated by value R^2 of 0.78 for the immobile elements (Fig. 5a). Furthermore, data from Liaghat and MacLean (1992) also yield a R^2 of 0.67 indicating, in combination with our data, that the KT unit is not the result of ash mixing. This is confirmed by our regional study on more than 300 samples from the whole mining camp (Fig. 5a). Moreover, the similarity between the alteration lines of the KT with the andesitic unit at the base of the Wabassee Group suggests that the KT represents the first explosive activity of the Wabassee Group.

At Bracemac-McLeod, drill-core observations suggest that the mineralization formed mainly by replacement processes. As a consequence, the seafloor chemical precipitate component was most likely negligible. This can be geochemically tested by a plot of Y/Ho versus Eu/Eu* (Fig. 7) which is useful to discriminate chemical precipitation processes versus replacement processes based on three end-members: 1) high temperature fluid (Douville et al, 1999); 2) archean seawater, represented by Strelley Pool stromatolites (Van Kranendonk et al, 2003); and 3) crust (Rollinson, 1993). This graph shows that most of the samples plot near the crust pole, indicating that replacement processes are dominant and that chemical precipitate component from high temperature fluids or seawater is negligible. However, a discrete trend towards the high temperature fluids can be observed and seems to represent an increase of hydrothermal alteration. It is thus interpreted that the seafloor precipitate component is weak and even lacking for the KT unit. This may account for the fact that previous attempts to develop geochemical tools to assist exploration were inconclusive. Nevertheless, the degree of hydrothermal alteration along the KT increases towards the lenses and it is best manifested by europium (e.g., Fig. 6).

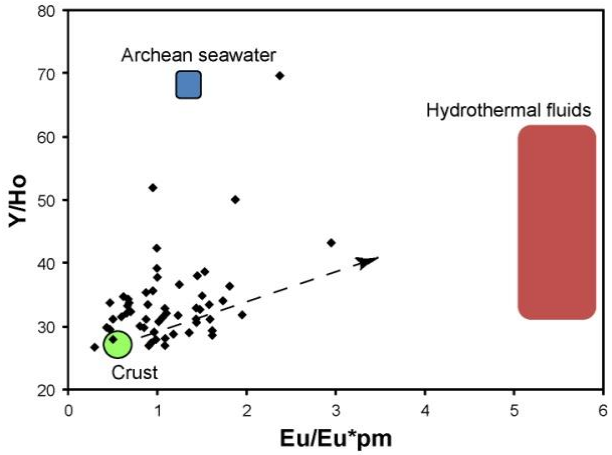

Fig.7: Eu anomaly normalized to Primitive Mantle (Sun and MacDonough, 1989) versus Y/Ho plot. Modified from Pinti et al. 2009. See text for end-member references.

Behaviour of europium in hydrothermal fluids

Europium enrichment in VMS settings is a well-known process induced by hydrothermal fluid flow (e.g. Michard and Albarède, 1986, Douville et al. 1999). Unlike the other REE which have only a +3 valence and are relatively immobile, Eu has two valences (+2 and +3) of which only the +2 species can be transported by hot and reducing Cl-rich fluids. Plagioclase is an important host of Eu^{2+}, because of the substitution with Ca^{2+}, and is easily altered by hot hydrothermal fluids. In the accepted model, Eu is leached from plagioclase in the alteration area and then precipitated, under favourable conditions, in the vicinity of the mineralized bodies (e.g. Lottermoser, 1992; Douville et al. 1999). At Bracemac-McLeod, this study proposes that the hydrothermal fluids leached Eu from the underlying Watson rhyolite and were focussed upward along synvolcanic faults up to the stratigraphic level of the KT where the mineralizing fluids dispersed laterally because of the porosity of this tuffaceous layer. Progressively, with the formation of Ca-(Eu)-rich alteration mineral/s (such as apatite, Fe-carbonates, scheelite) the Eu content decreased in the fluids resulting in a zonation of Eu (Fig. 6).

Conclusions

In the KT unit in close proximity to the Bracemac-McLeod deposits, the tuffaceous component is dominant whereas the exhalative seafloor precipitate appears to be negligible. The mineralization formed by the replacement of the tuffaceous KT by fluid percolation along this permeable unit or by replacement of the Watson and Bracemac rhyolites. As a result the hydrothermal component of the KT is dominated by epigenetic hydrothermal alteration. This process is geochemically demonstrated by the behaviour of Y and REE. In particular, Eu^{2+}, which is soluble in hydrothermal fluids, preserves the hydrothermal alteration halo around the mineralized lenses. The Eu anomaly increases systematically towards the sulfide deposits, showing a positive signature persistent up to 200m from the orebodies. This Eu signature constitutes the first efficient geochemical tool to assist VMS exploration in the Matagami camp.

Acknowledgements

This PhD project is a part of a larger research program on the Matagami mining camp, including a volcanology PhD (INRS-Quebec) and a geophysics PhD (École Polytechnique-Montreal). Financial support for this study was provided by NSERC, CONSOREM, DIVEX, Geological Survey of Canada, Xstrata Zinc, Donner Metals, SOQUEM, and Breakwater Resources. We thank the companies for the authorization to diffuse these results. R. Adair (Donner Metals) is additionally thanked for his informal review of a preliminary version of the document. Finally, thanks are given to Sarah Dare, post-doctoral fellow at UQAC, for proof reading the English.

References

Allen RL, Weihed P, Blandell D, Crawford T, Davidson G, Galley A, Gibson H, Hannington M, Herrington R, Herzig P, Large R, Lentz D, Maslennikov V, McCutcheon S, Peter J, Tornos F. (2002). Global comparisons of volcanic-associated massive sulphide districts. Geological Society Special Publication 204, 13-37.

Barrett TJ, MacLean WH, Årebäck H. (2005) The Palaeoproterozoic Kristineberg VMS deposit, Skellefte district, northern Sweden. Part II: chemostratigraphy and alteration. Mineralium Deposita 40, 368-395.

Barrett TJ, MacLean WH. (1999) Volcanic sequences, lithogeochemistry, and hydrothermal alteration in some bimodal volcanic-associated massive sulfide systems. In: Barrie CT, Hannington MD (eds) Reviews in Economic Geology, vol 8. Society of Economic Geologists, pp 101-131.

Card KD, (1990). A review of the Superior Province of the Canadian Shield, a product of Archean accretion. Precambrian Research. 48, 99-156.

Carr PM, Cathles LM, Barrie CT. (2008). On the size and spacing of volcanogenic massive sulfide deposits within a district with application to the Matagami district Quebec. Economic Geology **103**, 1395-1409.

Coté A, Lavigne M. (2010) Technical Report and Feasibility Study for the Bracemac-McLeod Project Matagami Area Quebec (Xstrata Zinc and Genivar Limited Partnership). 315 p.

Davidson AJ. (1977) Petrography and chemistry of the Key Tuffite at Bell Allard, Matagami, Quebec. Unpublished M.Sc. thesis, McGill University, Montreal, Quebec, 131 p.

Douville E, Bienvenu P, Charlou JL, Donval JP, Fouquet Y, Appriou P, Gamo T. (1999) Yttrium and rare earth elements in fluids from various deep-sea hydrothermal systems. Geochimica et Cosmochimica Acta 63: 627-643.

Doyle MG, Allen RL. (2003) Subsea-floor replacement in volcanic-hosted massive sulfide deposit. Ore Geology Reviews 23: 183-222.

Finlow-Bates T, Stumpfl EF. (1981) The behaviour of so-called immobile elements in hydrothermally altered rocks associated with volcanogenic submarine-exhalative ore deposits. Mineralium Deposita 16: 319-328.

Franklin JM, Sangster DM, Lydon JW. (1981) Volcanic-associated massive sulfide deposits. Economic Geology - 75th Anniversary Volume, 485-627.

Ioannou SE, Spooner ETC. (2007) Fracture Analysis of a Volcanogenic Massive Sulfide-Related Hydrothermal Cracking Zone, Upper Bell River Complex, Matagami, Quebec: Application of Permeability Tensor Theory. Economic Geology 102: 667-690.

Kalogeropoulos SI, Scott SD. (1983) Mineralogy and geochemistry of tuffaceous exhalites (Tetsusekiei) of the Fukazawa Mine, Hokuroku District, Japan. Economic Geology, Monograph 5: 412-432.

Kalogeropoulos SI, Scott SD. (1989) Mineralogy and geochemistry of an Archean tuffaceous exhalite: the Main Contact Tuff, Millenbach mine area, Noranda, Quebec. Canadian Journal of Earth Sciences 26: 88-105.

Large RR. (1992) Australian volcanic-hosted massive sulfide deposits: features, styles, and genetic models. Economic Geology 87: 471-510.

Liaghat S, MacLean WH. (1992) The Key Tuffite, Matagami mining district: Origin of the tuff components and mass changes. Exploration and Mining Geology 1: 197-207.

Lottermoser BG. (1992) Rare earth elements and hydrothermal ore formation processes. Ore Geology Reviews 7: 25-41.

MacLean WH, Kranidiotis P. (1987). Immobile elements as monitors of mass transfer in hydrothermal alteration: Phelps Dodge massive sulfide deposit, Matagami, Quebec. Economic Geology 82, 951-962.

Maier WD, Barnes SJ, Pellet T. (1996). The economic significance of the Bell River Complex, Abitibi subprovince, Quebec. Canadian Journal of Earth Science 33, 967-980.

Michard A, Albarède F. (1986) The REE content of some hydrothermal fluids. Chemical Geology 55: 51-60.

Miller RJM. (1960) Geology of Mattagami Lake Mines [abs.]: Canadian Inst. Mining Metall. Bull 53: 194.

Mortensen, J.K., 1993. U-Pb geochronology of the eastern Abitibi Subprovince. Part 1: Chibougamau-Matagami-Joutel region. Canadian Journal of Earth Science 30, 11-28.

Ohmoto H. (1996) Formation of volcanogenic massive sulfide deposits: The Kuroko perspective. Ore Geology Reviews 10: 135-177.

Peter JM, Goodfellow WD. (2003). Hydrothermal sedimentary rocks of Heath Steele belt, Bathurst mining camp, New Brunswick : Part 3. Application of mineralogy and mineral and Bulk compositions to Massive Sulfide Exploration. Economic Geology, Monograph 11: 417-433.

Piché M, Guha J, Daigneault R, Sullivan JR, Bouchard G. (1990) Les gisements volcanogènes du camp minier de Matagami: structure, stratigraphie et implications métallogeniques. Canadian Institute of Mining and Metallurgy Special Volume 43: 327-336.

Pintì DL, Hashizume K, Sugihara A, Massault M, Philippot P. (2009) Isotopic fractionation of nitrogen and carbon in Paleoarchean cherts from Pilbara craton, Western Australia: origin of ^{15}N-depleted nitrogen. Geochimica et Cosmochimica Acta 73: 3819-3848.

Ridler RH. (1971) Analysis of Archean volcanic basins in the Canadian Shield using exhalite concept. [abs.] Bulletin of Canadian Institute of Mining and Metallurgy 64: 20.

Rollinson HR. (1993) Using Geochemical Data: Evaluation, Presentation, Interpretation, Longman, UK. 352 pp.

Ross PS, McNicoll V, Debreil J, Carr P. (submitted) Precise U-Pb geochronology of the Matagami mining camp, Abitibi Greenstone Belt, Quebec: stratigraphic constraints and implications for VMS exploration. Economic Geology.

Sharpe JI. (1968). Geology and sulfide deposits of the Matagami area, Abitibi-East County. Quebec Department of Natural Resources Geological Report 137, 122 p.

Sun SS, McDonough WF. (1989). Chemical and isotopic systematics of oceanic basalts: implications for mantle composition and processus. In Fitton, J.G., Upton, B.G.J. (Eds.), Magmatism in the Ocean Basins. Geological Society of America, Special Publication 42: 399-444.

Van Kranendonk MJ, Webb GE, Kamber BS. (2003) Geological and trace element evidence for a marine sedimentary environment of deposition and biogenicity of 3.45 Ga stromatolitic carbonates in the Pilbara Craton, and support for a reducing Archaean ocean. Geobiology 1, 91-108.

Winchester JA, Floyd PA. (1977) Geochemical discrimination of different magma series and their differentiation products using immobile elements. Chemical Geology 20: 325-343.